



Pathways of toxicity after inhalation of nanoparticles

**The influence of physicochemical properties on the
biodistribution, molecular pathways and toxicity**

Susan Dekkers

Pathways of toxicity after inhalation of nanoparticles

The influence of physicochemical properties on the
biodistribution, molecular pathways and toxicity.

Susan Dekkers

© 2021 Susan Dekkers
Thesis Utrecht University
ISBN: 978-90-393-7364-4

Layout by: Dennis Hendriks / ProefschriftMaken.nl
Cover design by: Susan Dekkers
Print: ProefschriftMaken, The Netherlands

Pathways of toxicity after inhalation of nanoparticles

The influence of physicochemical properties on the
biodistribution, molecular pathways and toxicity.

Toxicologische werkingsmechanismen van nanodeeltjes na inhalatie

De invloed van fysisch-chemische eigenschappen op de biodistributie,
moleculaire mechanismen en toxiciteit
(met een samenvatting in het Nederlands)

Proefschrift

ter verkrijging van de graad van doctor aan de
Universiteit Utrecht
op gezag van de
rector magnificus, prof.dr. H.R.B.M. Kummeling,
ingevolge het besluit van het college voor promoties
in het openbaar te verdedigen op

donderdag 18 maart 2021 des middags te 12.45 uur

door

Susan Dekkers

geboren op 5 mei 1975
te Utrecht

Promotoren:

Prof. dr. F.R. Cassee

Prof. dr. ir. B. Brunekreef

Copromotoren:

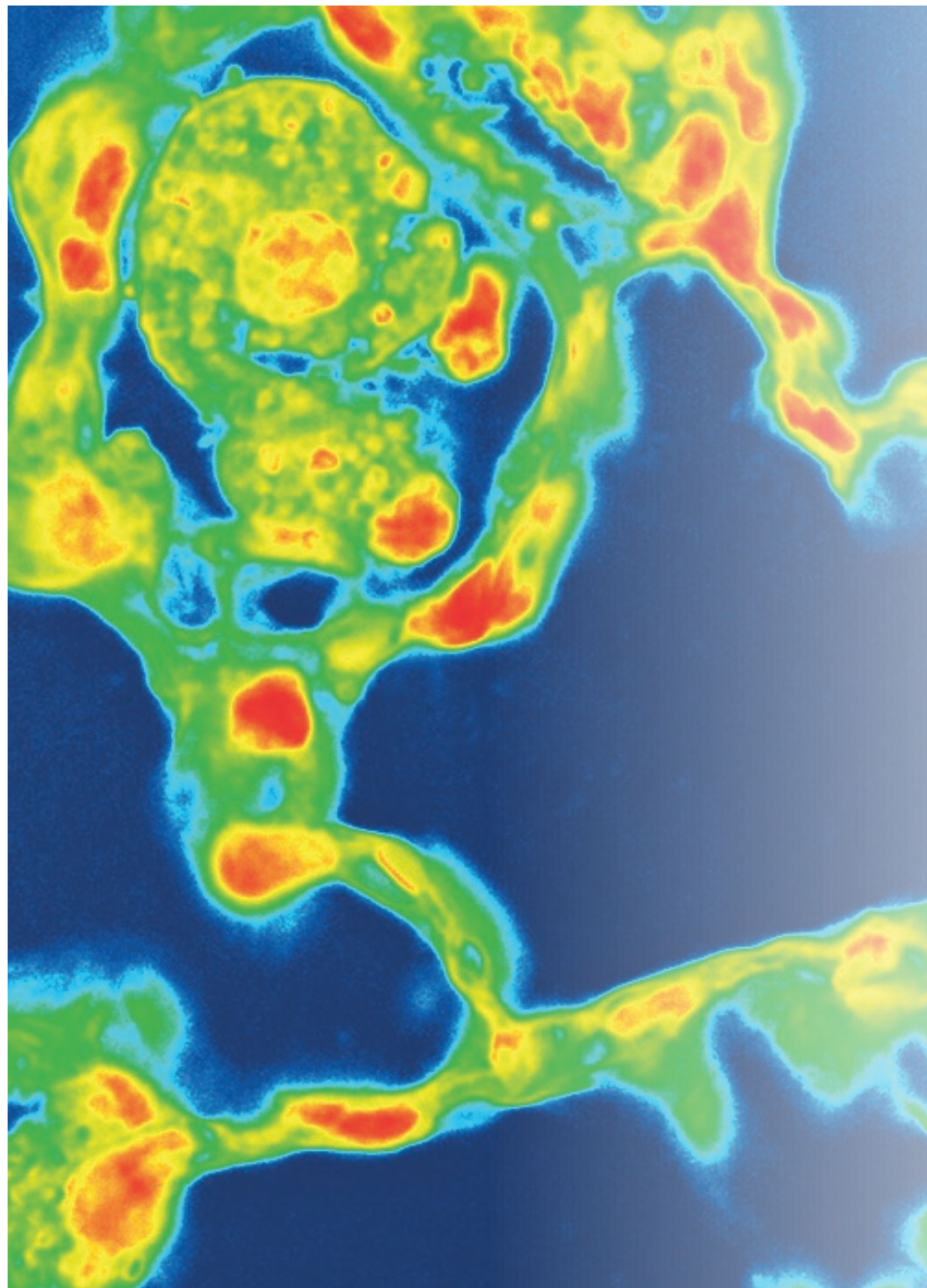
Dr. R.J. Vandebriel

Dr. W.H. de Jong

This research was financially supported by the European Union's Seventh Framework Programme for research, technology development and demonstration under grant agreement n° 310451 (NanoMILE) and the Netherlands Food and Consumer Product Safety Authority (V090016) (NVWA).

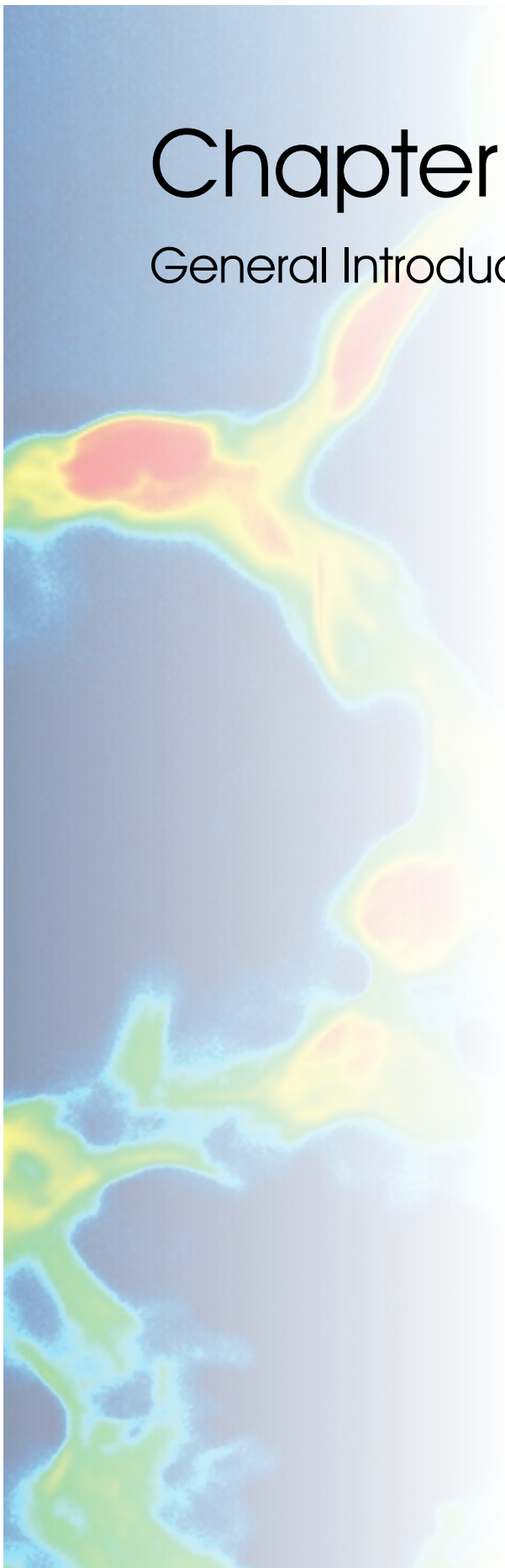
Contents

Chapter 1	General introduction	7
Chapter 2	The effect of zirconium doping of cerium dioxide nanoparticles on pulmonary and cardiovascular toxicity and biodistribution in mice after inhalation (Dekkers et al., 2017)	19
Chapter 3	Differences in the toxicity of cerium dioxide nanomaterials after inhalation can be explained by lung deposition, animal species and nanoforms (Dekkers et al., 2018a)	57
Chapter 4	Multi-omics approaches confirm metal ions mediate the main toxicological pathways of metal-bearing nanoparticles in lung epithelial A549 cells (Dekkers et al., 2018b)	95
Chapter 5	Role of chemical composition and redox modification of poorly soluble nanomaterials on their ability to enhance allergic airway sensitisation in mice (Dekkers et al., 2019)	129
Chapter 6	The influence of chemical composition and redox activity of nanomaterials on in vitro inflammasome activation and dendritic cell maturation	169
Chapter 7	General discussion	195
	Summary	207
	Samenvatting	212
	Curriculum Vitae	218
	List of publications	219
	Dankwoord	223



Chapter 1

General Introduction



the 1990s, the number of people with a mental health problem has increased in the UK (Mental Health Act 1983, 1990).

There is a growing awareness of the need to improve the lives of people with mental health problems. The UK Government has set out a strategy for mental health care (Department of Health 1999). The strategy is based on the following principles:

- (i) People with mental health problems should be treated as individuals, with their own needs and wishes.
- (ii) People with mental health problems should be given the opportunity to participate in decisions about their care and treatment.
- (iii) People with mental health problems should be given the opportunity to live in their own homes and communities.

The strategy also states that people with mental health problems should be given the opportunity to live in their own homes and communities.

The strategy also states that people with mental health problems should be given the opportunity to live in their own homes and communities. This is a key principle of the strategy and is reflected in the following objectives:

- (i) To reduce the number of people with mental health problems who are in hospital.
- (ii) To improve the quality of life of people with mental health problems.
- (iii) To improve the effectiveness of mental health services.

The strategy also states that people with mental health problems should be given the opportunity to live in their own homes and communities.

The strategy also states that people with mental health problems should be given the opportunity to live in their own homes and communities. This is a key principle of the strategy and is reflected in the following objectives:

- (i) To reduce the number of people with mental health problems who are in hospital.
- (ii) To improve the quality of life of people with mental health problems.
- (iii) To improve the effectiveness of mental health services.

The strategy also states that people with mental health problems should be given the opportunity to live in their own homes and communities.

The strategy also states that people with mental health problems should be given the opportunity to live in their own homes and communities. This is a key principle of the strategy and is reflected in the following objectives:

- (i) To reduce the number of people with mental health problems who are in hospital.
- (ii) To improve the quality of life of people with mental health problems.
- (iii) To improve the effectiveness of mental health services.

The strategy also states that people with mental health problems should be given the opportunity to live in their own homes and communities.

General Introduction

The influence of physicochemical properties of nanomaterials

The most appealing feature of nanomaterials is that their properties can be manipulated in such a way they can exhibit the most amazing functionalities. At the same time, this is also the most alarming aspect of nanomaterials, since we don't know exactly yet how manipulating their properties might affect their ability to cause adverse human health effects. Knowing how the different properties of nanomaterials influence their ability to cause human health effects may enable us to design nanomaterials with amazing functionalities without increasing human health risks.

The aim of the research described in this thesis is to investigate how several physicochemical properties of nanoparticles (NPs) influence their biodistribution, molecular pathways and toxicity after inhalation. The focus is on inhalation, as this route of exposure is currently regarded as the main route of concern for human health effects (Kuhlbusch et al., 2018). In this thesis the results of several *in vivo* and *in vitro* toxicity studies on the influence of several physicochemical properties on various biological effects are described. The studies examined the following physicochemical properties: redox activity, dissolution, chemical composition and size. The investigated biological effects included *in vivo* lung deposition, biodistribution and inflammation, *in vitro* multi-omics responses in alveolar epithelial cells, *in vivo* adjuvant activity, *in vitro* inflammasome activation and *in vitro* dendritic cell maturation.

Towards predictive toxicology of nanoparticles

That particles may cause severe human health effects after inhalation has been known for centuries. The history and current knowledge on the toxicity of inhaled particles has been reviewed in several publications (Donaldson and Seaton, 2012; Riediker et al., 2019). Adverse health effects of inhaled particles were first observed among workers exposed to asbestos, crystalline silica and coal dust. The scientific attention for the toxicology of inhaled particles further increased when adverse health effects were also observed in the general population that were associated with poor air quality such as during the 'great smog' episode of 1952 in London (Bell et al., 2004). The publication of the report of the Royal Academy of Engineering and the Royal Society on the opportunities and uncertainties of nanoscience and nanotechnologies in 2004 (Royal Society and Royal Academy of Engineering, 2004) broadened the scientific attention to also include the potential adverse health effects of manufactured NPs.

Nanotechnology makes it possible to manufacture NPs with an unlimited amount of variations in physicochemical properties, such as size, shape and surface modifications. This endless amount of variations makes it practically impossible to test each individual variation or nanoform of each type of NP (Dekkers et al., 2016). Therefore, knowledge on the relation

between certain physicochemical properties of NPs and their ability to cause adverse effects becomes increasingly important. This knowledge will improve the ability to predict the toxicity of new nanomaterials without extensive toxicity testing of each individual nanoform. Over the last 15 years a number of papers have been published dedicated to predictive toxicity, grouping, and read-across (Arts et al., 2015; Banares et al., 2017; Singh et al., 2019; Stone et al., 2020; Winkler, 2016). Several reviews have appeared in which various mechanisms of toxicity of (nano)particles and their connection to various physicochemical properties are described (Bakand et al., 2012; Bierkandt et al., 2018; Nel et al., 2006). Some mechanisms of toxicity, such as the release of ions or the ability to induce oxidative stress, are quite generic and relevant for multiple adverse effects and routes of exposure. Other mechanisms of toxicity, such as frustrated phagocytosis after translocation to the pleural cavity, are more specific for one adverse effects and one route of exposure, in this case mesothelioma after inhalation of asbestos-like nanomaterials. In reviews on the toxicity of NPs after inhalation, generally a distinction is made between mechanisms and physicochemical properties that determine the biokinetics, including airway and lung deposition, uptake and translocation to secondary organs and mechanisms and physicochemical properties that determine or influence the biological effects of NPs, such as redox activity and the capacity to generate of reactive oxygen species (ROS), the release of ions, cationic toxicity due to mitochondrial perturbation, inflammasome activation, photoactivation, protein and DNA damage, altered cell cycle regulation, phagocytosis impairment, endothelial dysfunction and adjuvant effects (Bakand et al., 2012; Bakand et al., 2005; Braakhuis et al., 2014; Nel et al., 2013).

Linking physicochemical properties to mechanisms of toxicity

A detailed description and explanation on all the different mechanisms and physicochemical properties is beyond the scope of this thesis. The following paragraph provides a brief review of the mechanisms and properties investigated in this thesis. The focus is on two relations between physicochemical properties and mechanisms of toxicity: 1) redox activity and the capacity of generating ROS and 2) dissolution and the release of ions. Another important mechanisms by which NPs can induce toxicity is via the interaction with the immune system. The immune system is prone to react to foreign intrusions, including particles. Some of these reactions are normal immunological responses to facilitate clearance of the NPs from the body and recovery of the homeostasis, while others may lead to undesired adverse effects (Boraschi et al., 2017). Therefore, also several immunological mechanisms, including the adjuvant activity of NPs, inflammasome activation and dendritic cell maturation have been investigated.

Redox activity and the generation of reactive oxygen species

One of the most investigated and well established mechanisms by which NPs can induce toxicity is via the generation of reactive oxygen species, which may lead to oxidative stress and subsequent cellular injury and pro-inflammatory signaling (Hsieh et al., 2013; Nel et al.,

2013). The ability of NPs to generate ROS is influenced by several physicochemical properties, including their size or rather their relatively large surface area which makes them more reactive, their shape and their surface characteristics, such as the surface charge, surface-treatment and redox activity (Fu et al., 2014). Also changes of the NPs due to interaction with their surrounding environment, such as aggregation, UV light activation, dissolution and the release of metal ions can affect their ability to generate ROS. Metal oxides, in particular in the nanosized range, are known to facilitate the formation of ROS by depleting electrons from cellular redox species (cellular components able to release electrons) or by serving as catalysts in ROS production through Fenton reactions or Haber-Weiss cycle reactions (Fu et al., 2014). Additionally, NPs can stimulate free radical generation from cellular enzymes. Metal oxides with a conduction band energy (E_c) level that overlaps with the cellular redox potential (-4.12 to -4.84 eV) have been shown to have the ability to induce oxygen radicals, oxidative stress, and acute pulmonary inflammation (Zhang et al., 2012). The generation of ROS does not always cause cellular injury, because biological fluids (e.g. epithelial lining fluid) and cells also contain antioxidants and numerous compensatory mechanisms. Only an overproduction of ROS can lead to failure of cells to maintain their normal physiological redox-regulated functions, resulting in oxidative stress, cellular injury and inflammatory responses (Fu et al., 2014).

Dissolution and the release of ions

Another well-known mechanism of toxicity by which NPs can induce toxicity, is by the release of ions (ion shedding) (Gebel et al., 2014; Nel et al., 2013). The toxicity of for example Ag, Cu and ZnO NPs is in part due to a delayed dissolution and subsequent release of ions which often takes place after cellular uptake of the NPs. The similarity and differences of ion versus solid particle toxicity has been investigated in several studies (Cronholm et al., 2013; Liu et al., 2016). However, the different molecular responses within the various pathways leading to toxicity are not yet fully understood. Physicochemical properties that influence NP dissolution and release of ions include chemical composition, size, surface area and surface chemistry. Next to these intrinsic properties, also environmental conditions, such as pH, temperature and the presence of proteins influence the dissolution of NPs (Shi et al., 2017; Sohal et al., 2018).

Adjuvant activity

Other important mechanisms by which NPs can induce toxicity is via the interaction with the immune system. Particles are known to be able to induce and to enhance lung inflammation and allergic responses after inhalation (Meldrum et al., 2017). Nano-sized silica and titanium dioxide particles have been shown to enhance allergic airways sensitization in mice (Brandenberger et al., 2013; Vandebriel et al., 2018). There is limited understanding of the different physicochemical properties of NPs which influence their adjuvant properties. Due to the variabilities in the models used and the often limited extend of NM characterization

in the different studies, no reliable comparison could be made between adverse effects of NMs with different characteristics across different studies (Meldrum et al., 2017). Comparisons within studies indicate that NP composition, size, agglomeration size, surface area, shape, solubility, surface charge and surface coating are all potentially important factors determining the immune responses (Meldrum et al., 2017). However to what extent these properties influence which mechanistic pathways remains to be determined.

Inflammasome activation and dendritic cell maturation

The first types of immune cells that recognize and respond to inhaled NPs are often macrophages and dendritic cells (DCs) (Boraschi et al., 2017). However, the response of macrophages and DCs to NPs is different. Macrophages usually produce inflammatory chemokines and cytokines to recruit neutrophils and monocytes, while DCs usually respond by maturation and migration to the lymph nodes, the production cytokines and initiation of T-cell proliferation and differentiation. One of the mechanisms by which inflammatory responses of macrophages and DCs can be initiated is inflammasome activation.

Inflammasomes are intracellular protein complexes that upon sensing danger signals can initiate inflammatory responses, including the production of IL-1 β and IL-18 (Vandebriel et al., 2016). Inflammasomes can respond to a wide range of danger signals, including pathogen-associated molecular patterns (PAMPs), such as lipopolysaccharide, damage-associated molecular patterns (DAMPs), such as extracellular ATP, UV radiation, chemical sensitizers, asbestos and NPs. Secretion of IL-1 β and IL-18 leads to an influx of other immune cells, including neutrophils and dendritic cells to the affected tissues to facilitate clearance of nanomaterials (Sun et al., 2013b). The mechanisms of inflammasome activation induced by NPs are not fully understood. Several studies are suggesting that the physicochemical properties of NPs including the ability to generate ROS, aspect ratio, dispersion state, size and surface chemistry could play major roles in NLRP3 inflammasome activation (Sun et al., 2013b; Vandebriel et al., 2016). Inflammasome activation has been suggested to be one of the mechanisms involved in the adjuvant activity of NPs (Meldrum et al., 2017; Sun et al., 2013a; Vandebriel et al., 2016).

DC are cells of the innate immune system that link the innate to the adaptive immunity. Immature DCs can engulf foreign materials, including NPs, but also apoptotic or necrotic cells. DC maturation is a process in which immature DC become active antigen presenting cells by acquire several properties fundamental properties, including antigen processing and presentation, migration and ability to activate antigen-specific naïve T-cells in secondary lymphoid organs (Feraý et al., 2020). Depending on the chemical composition, surface chemistry, shape and dose, NPs may promote DCs' capability to induce an IL-12 induced Th1 response, an IL-4 induced Th2 response and/or an IL-6 induced Th17 response (Ihrie and Bonner, 2018; Jia et al., 2018). The DC maturation assay has been suggested as a promising

in vitro screen predictive for adjuvant activity of NPs *in vivo* (Feray et al., 2020; Vandebriel et al., 2018).

Aim, objectives and outline of this thesis

Although there are several mechanisms of toxicity identified by which NMs may cause adverse effects after inhalation, there are still a lot of knowledge gaps on the precise molecular mechanisms and the influence of the various physicochemical properties of NMs on these mechanisms within the different pathways (gaps). In this thesis research on the influence of several physicochemical properties on some mechanisms of toxicity is further described. Combining the knowledge on the influence and interrelationships between the different physicochemical properties and mechanisms of toxicity will enable us to better predict the toxicity of newly developed NPs or NPs for which limited toxicity data is available. This will facilitate implementation of Safe-by-Design and risk assessment of NPs using predictive toxicity, grouping, and read-across.

The research described in this thesis was performed within the European NanoMILE project¹. The NanoMILE project included investigations on the biological mechanisms and pathways underlying toxic effects of nanomaterials related to their physicochemical properties. The overarching objective of NanoMile was to formulate an intelligent and powerful paradigm for the mode(s) of interaction between manufactured nanomaterials and organisms or the environment to allow the development of a single framework for the categorization of nanomaterial safety and to create a universally applicable framework for nanosafety.

The main aim of the research described in this thesis is to investigate the influence of physicochemical properties of nanomaterials on assumed pathways of toxicity after inhalation. This was done using a carefully selected range of *in vivo* and *in vitro* toxicity assays in combination with a carefully selected set NPs with specific properties that were synthesized within this NanoMILE project, translating into the following research objectives:

1. Assess the influence of size and redox activity of undoped and Zr-doped CeO₂ NPs on their deposition, biodistribution and pulmonary (and cardiovascular) effects in mice and rats following inhalation. (chapter 2+3)
2. Investigate the influence of dissolution and redox activity of Ag, ZnO and undoped and Zr-doped CeO₂ NPs on the molecular pathways by which these NPs induce toxicity in A549 lung cell *in vitro* (chapter 4).
3. Evaluate the influence of chemical composition and redox activity of undoped and Zr-doped CeO₂ and undoped and Fe-doped Co₃O₄ NPs on their adjuvant properties in an *in vivo* model for airway allergy (chapter 5).

¹ Grand agreement number 310451 (NanoMILE) of the European Union Seventh Framework Programme for research, technology development and demonstration.

4. Study the influence of chemical composition and redox activity of undoped and Zr-doped CeO_2 and undoped and Fe-doped Co_3O_4 NPs on *in vitro* inflammasome activation and dendritic cell maturation (chapter 6).

We hypothesized that redox modification through Zr-doping of CeO_2 and Fe-doping of Co_3O_4 NPs would lead to a decreased *in vitro* and *in vivo* toxicity and adjuvant activity of the NPs.

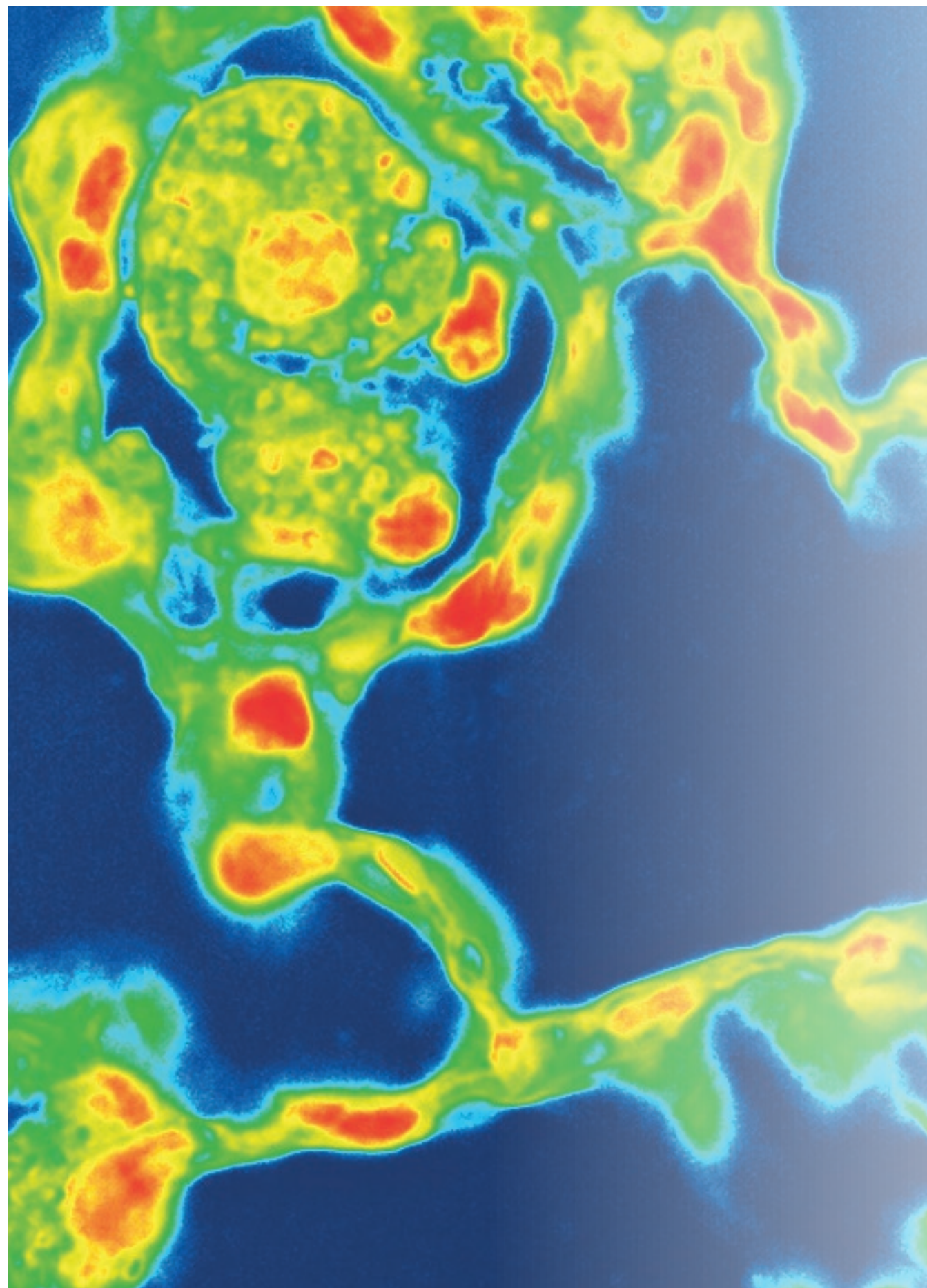
More knowledge on the influence of the physicochemical properties of nanomaterials on the pathways of toxicity is needed to predict the toxicity of nanomaterials and to enable safety assessment of new nanomaterials without extensive toxicity testing of each individual nanoform. The influence of various physicochemical properties of several NPs on the biodistribution, molecular pathways and toxicity after inhalation will be discussed in the following chapters. In chapter 2 and 3 of this thesis, the results of several studies on the influence of the size and redox activity on the deposition, biodistribution and toxicity of CeO_2 NPs after inhalation are described. Chapter 4 contains the results of a study on the influence of dissolution and redox activity of Ag, ZnO and CeO_2 NPs on the molecular mechanisms causing *in vitro* toxicity in lung epithelial cells. In chapter 5 the influence of the chemical composition and redox modification of CeO_2 and Co_3O_4 NPs on their ability to enhance allergic airway sensitization *in vivo* is discussed, while chapter 6 concerns the investigation on ability of the same NPs to induce *in vitro* inflammasome activation and dendritic cell maturation and compares the *in vitro* results with the immune responses observed in the *in vivo* study. A general discussion reflection on the key findings, implications and future perspectives can be found in chapter 7.

References

- Arts JH, Hadi M, Irfan MA, Keene AM, Kreiling R, Lyon D, Maier M, Michel K, Petry T, Sauer UG, Warheit D, Wiench K, Wohlleben W and Landsiedel R (2015) A decision-making framework for the grouping and testing of nanomaterials (DF4nanoGrouping). *Regul Toxicol Pharmacol* **71**:S1-27.
- Bakand S, Hayes A and Dechsakulthorn F (2012) Nanoparticles: a review of particle toxicology following inhalation exposure. *Inhal Toxicol* **24**:125-135.
- Bakand S, Winder C, Khalil C and Hayes A (2005) Toxicity assessment of industrial chemicals and airborne contaminants: transition from in vivo to in vitro test methods: a review. *Inhal Toxicol* **17**.
- Banares MA, Haase A, Tran L, Lobaskin V, Oberdorster G, Rallo R, Leszczynski J, Hoet P, Korenstein R, Hardy B and Puzyn T (2017) CompNanoTox2015: novel perspectives from a European conference on computational nanotoxicology on predictive nanotoxicology. *Nanotoxicology* **11**:839-845.
- Bell ML, Davis DL and Fletcher T (2004) A retrospective assessment of mortality from the London smog episode of 1952: the role of influenza and pollution. *Environ Health Perspect* **112**:6-8.
- Bierkandt FS, Leibrock L, Wagener S, Laux P and Luch A (2018) The impact of nanomaterial characteristics on inhalation toxicity. *Toxicol Res (Camb)* **7**:321-346.
- Boraschi D, Italiani P, Palomba R, Decuzzi P, Duschi A, Fadeel B and Moghimi SM (2017) Nanoparticles and innate immunity: new perspectives on host defence. *Semin Immunol* **34**:33-51.
- Braakhuis HM, Park MV, Gosens I, De Jong WH and Cassee FR (2014) Physicochemical characteristics of nanomaterials that affect pulmonary inflammation. *Part Fibre Toxicol* **11**:18.
- Brandenberger C, Rowley NL, Jackson-Humbles DN, Zhang Q, Bramble LA, Lewandowski RP, Wagner JG, Chen W, Kaplan BL, Kaminski NE, Baker GL, Worden RM and Harkema JR (2013) Engineered silica nanoparticles act as adjuvants to enhance allergic airway disease in mice. *Part Fibre Toxicol* **10**:26.
- Cronholm P, Karlsson HL, Hedberg J, Lowe TA, Winnberg L, Elihn K, Wallinder IO and Möller L (2013) Intracellular uptake and toxicity of Ag and CuO nanoparticles: a comparison between nanoparticles and their corresponding metal ions. *Small* **9**:970-982.
- Dekkers S, Ma-Hock L, Lynch I, Russ M, Miller MR, Schins RPF, Keller J, Romer I, Kuttler K, Strauss V, De Jong WH, Landsiedel R and Cassee FR (2018a) Differences in the toxicity of cerium dioxide nanomaterials after inhalation can be explained by lung deposition, animal species and nanoforms. *Inhal Toxicol*:1-14.
- Dekkers S, Miller MR, Schins RPF, Romer I, Russ M, Vandebriel RJ, Lynch I, Belinga-Desaunay MF, Valsami-Jones E, Connell SP, Smith IP, Duffin R, Boere JAF, Heusinkveld HJ, Albrecht C, de Jong WH and Cassee FR (2017) The effect of zirconium doping of cerium dioxide nanoparticles on pulmonary and cardiovascular toxicity and biodistribution in mice after inhalation. *Nanotoxicology* **11**:794-808.
- Dekkers S, Oomen AG, Bleeker EA, Vandebriel RJ, Micheletti C, Cabellos J, Janer G, Fuentes N, Vazquez-Campos S, Borges T, Silva MJ, Prina-Mello A, Movia D, Nesslany F, Ribeiro AR, Leite PE, Groenewold M, Cassee FR, Sips AJ, Dijkzeul A, van Teunenbroek T and Wijnhoven SW (2016) Towards a nanospecific approach for risk assessment. *Regul Toxicol Pharmacol* **80**:46-59.

- Dekkers S, Wagner JG, Vandebriel RJ, Eldridge EA, Tang SVY, Miller MR, Römer I, de Jong WH, Harkema JR and Cassee FR (2019) Role of chemical composition and redox modification of poorly soluble nanomaterials on their ability to enhance allergic airway sensitisation in mice. *Particle and Fibre Toxicology* **16**:39.
- Dekkers S, Williams TD, Zhang J, Zhou J, Vandebriel RJ, De La Fonteyne LJJ, Gremmer ER, He S, Guggenheim EJ, Lynch I, Cassee FR, De Jong WH and Viant MR (2018b) Multi-omics approaches confirm metal ions mediate the main toxicological pathways of metal-bearing nanoparticles in lung epithelial A549 cells. *Environmental Science: Nano* **5**:1506-1517.
- Donaldson K and Seaton A (2012) A short history of the toxicology of inhaled particles. *Part Fibre Toxicol* **9**:13.
- Feray A, Szely N, Guillet E, Hullo M, Legrand FX, Brun E, Pallardy M and Biola-Vidamment A (2020) How to Address the Adjuvant Effects of Nanoparticles on the Immune System. *Nanomaterials (Basel)* **10**.
- Fu PP, Xia Q, Hwang HM, Ray PC and Yu H (2014) Mechanisms of nanotoxicity: generation of reactive oxygen species. *J Food Drug Anal* **22**:64-75.
- Gebel T, Foth H, Damm G, Freyberger A, Kramer PJ, Lilienblum W, Rohl C, Schupp T, Weiss C, Wollin KM and Hengstler JG (2014) Manufactured nanomaterials: categorization and approaches to hazard assessment. *Arch Toxicol* **88**:2191-2211.
- Hsieh SF, Bello D, Schmidt DF, Pal AK, Stella A, Isaacs JA and Rogers EJ (2013) Mapping the biological oxidative damage of engineered nanomaterials. *Small* **9**:1853-1865.
- Ihrie MD and Bonner JC (2018) The Toxicology of Engineered Nanomaterials in Asthma. *Curr Environ Health Rep* **5**:100-109.
- Jia J, Zhang Y, Xin Y, Jiang C, Yan B and Zhai S (2018) Interactions Between Nanoparticles and Dendritic Cells: From the Perspective of Cancer Immunotherapy. *Front Oncol* **8**:404.
- Kuhlbusch TAJ, Wijnhoven SWP and Haase A (2018) Nanomaterial exposures for worker, consumer and the general public. *NanoImpact* **10**:11-25.
- Liu J, Feng X, Wei L, Chen L, Song B and Shao L (2016) The toxicology of ion-shedding zinc oxide nanoparticles. *Crit Rev Toxicol* **46**:348-384.
- Meldrum K, Guo C, Marczylo EL, Gant TW, Smith R and Leonard MO (2017) Mechanistic insight into the impact of nanomaterials on asthma and allergic airway disease. *Part Fibre Toxicol* **14**:45.
- Nel A, Xia T, Madler L and Li N (2006) Toxic potential of materials at the nanolevel. *Science* **311**:622-627.
- Nel AE, Xia T, Meng H, Wang X, Lin S, Ji Z and Zhang H (2013) Nanomaterial toxicity testing in the 21st century: use of a predictive toxicological approach and highthroughput screening. *Acc Chem Res* **46**.
- Riediker M, Zink D, Kreyling W, Oberdorster G, Elder A, Graham U, Lynch I, Duschl A, Ichihara G, Ichihara S, Kobayashi T, Hisanaga N, Umezawa M, Cheng TJ, Handy R, Gulumian M, Tinkle S and Cassee F (2019) Particle toxicology and health - where are we? *Part Fibre Toxicol* **16**:19.

- Royal Society and Royal Academy of Engineering (2004) Nanoscience and Nanotechnologies: Opportunities and Uncertainties. , in *RS policy document*, Royal Society and Royal Academy of Engineering, London.
- Shi M, de Mesy Bentley KL, Palui G, Mattoussi H, Elder A and Yang H (2017) The roles of surface chemistry, dissolution rate, and delivered dose in the cytotoxicity of copper nanoparticles. *Nanoscale* **9**:4739-4750.
- Singh AV, Laux P, Luch A, Sudrik C, Wiehr S, Wild AM, Santomauro G, Bill J and Sitti M (2019) Review of emerging concepts in nanotoxicology: opportunities and challenges for safer nanomaterial design. *Toxicol Mech Methods* **29**:378-387.
- Sohal IS, O'Fallon KS, Gaines P, Demokritou P and Bello D (2018) Ingested engineered nanomaterials: state of science in nanotoxicity testing and future research needs. *Part Fibre Toxicol* **15**:29.
- Stone V, Gottardo S, Bleeker EAJ, Braakhuis H, Dekkers S, Fernandes T, Haase A, Hunt N, Hristozov D, Jantunen P, Jeliazkova N, Johnston H, Lamon L, Murphy F, Rasmussen K, Rauscher H, Jiménez AS, Svendsen C, Spurgeon D, Vázquez-Campos S, Wohlleben W and Oomen AG (2020) A framework for grouping and read-across of nanomaterials- supporting innovation and risk assessment. *Nano Today* **35**:100941.
- Sun B, Ji Z, Liao YP, Wang M, Wang X, Dong J, Chang CH, Li R, Zhang H, Nel AE and Xia T (2013a) Engineering an effective immune adjuvant by designed control of shape and crystallinity of aluminum oxyhydroxide nanoparticles. *ACS Nano* **7**:10834-10849.
- Sun B, Wang X, Ji Z, Li R and Xia T (2013b) NLRP3 inflammasome activation induced by engineered nanomaterials. *Small* **9**:1595-1607.
- Vandebriel RJ, Dekkers S, de Jong WH and Cassee FR (2016) An Update on NLRP3 Inflammasome Activation by Engineered Nanomaterials. *Current Bionanotechnology* **2**:40-46.
- Vandebriel RJ, Vermeulen JP, van Engelen LB, de Jong B, Verhagen LM, de la Fonteyne-Blankestijn LJ, Hoonakker ME and de Jong WH (2018) The crystal structure of titanium dioxide nanoparticles influences immune activity in vitro and in vivo. *Part Fibre Toxicol* **15**:9.
- Winkler DA (2016) Recent advances, and unresolved issues, in the application of computational modelling to the prediction of the biological effects of nanomaterials. *Toxicology and Applied Pharmacology* **299**:96-100.
- Zhang H, Ji Z, Xia T, Meng H, Low-Kam C, Liu R, Pokhrel S, Lin S, Wang X, Liao YP, Wang M, Li L, Rallo R, Damoiseaux R, Telesca D, Madler L, Cohen Y, Zink JI and Nel AE (2012) Use of metal oxide nanoparticle band gap to develop a predictive paradigm for oxidative stress and acute pulmonary inflammation. *ACS Nano* **6**:4349-4368.



Chapter 2

The effect of zirconium doping of cerium dioxide nanoparticles on pulmonary and cardiovascular toxicity and biodistribution in mice after inhalation

Susan Dekkers¹, Mark R. Miller², Roel P.F. Schins³, Isabella Römer⁴, Mike Russ⁵, Rob J. Vandebriel¹, Iseult Lynch⁴, Marie-France Belinga-Desaunay⁴, Eugenia Valsami-Jones⁴, Shea P. Connell², Ian P. Smith², Rodger Duffin², John A.F. Boere¹, Harm J. Heusinkveld^{1,3}, Catrin Albrecht³, Wim H. de Jong¹, Flemming R. Cassee^{1,6}

Nanotoxicology 11(6):794-808 (2017)

¹ National Institute for Public Health and the Environment, Bilthoven, the Netherlands,

² Centre for Cardiovascular Science & Centre for Inflammation Research, University of Edinburgh, Edinburgh, United Kingdom,

³ IUF- Leibniz Research Institute for Environmental Medicine, Düsseldorf, Germany,

⁴ School of Geography, Earth and Environmental Sciences, University of Birmingham, Birmingham, United Kingdom,

⁵ Promethean Particles Ltd, Nottingham, United Kingdom,

⁶ Institute for Risk Assessment Sciences, Utrecht University, Utrecht, the Netherlands

Abstract

Development and manufacture of nanomaterials is growing at an exponential rate, despite an incomplete understanding of how their physicochemical characteristics affect their potential toxicity. Redox activity has been suggested to be an important physicochemical property of nanomaterials to predict their biological activity. This study assessed the influence of redox activity by modification of cerium dioxide nanoparticles (CeO₂ NPs) via zirconium (Zr) doping on the biodistribution, pulmonary and cardiovascular effects in mice following inhalation.

Healthy mice (C57BL/6J), mice prone to cardiovascular disease (ApoE^{-/-}, western-diet fed) and a mouse model of neurological disease (5xFAD) were exposed via nose-only inhalation to CeO₂ NPs with varying amounts of Zr-doping (0%, 27% or 78% Zr), or clean air, over a 4-week period (4 mg/m³ for 3 h/day, 5 days/week). Effects were assessed 4 weeks post exposure.

In all three mouse models CeO₂ NP exposure had no major toxicological effects apart from some modest inflammatory histopathology in the lung, which was not related to the amount of Zr-doping. In ApoE^{-/-} mice CeO₂ did not change the size of atherosclerotic plaques, but there was a trend towards increased inflammatory cell content in relation to the Zr content of the CeO₂ NPs.

These findings show that subacute inhalation of CeO₂ NPs causes minimal pulmonary and cardiovascular effects 4 weeks post exposure and that Zr-doping of CeO₂ NPs has limited effect on these responses. Further studies with nanomaterials with a higher inherent toxicity or a broader range of redox activities are needed to fully assess the influence of redox activity on the toxicity of nanomaterials.

Introduction

The amount and variety of nanomaterials developed, manufactured and used in different applications and commercial products is growing rapidly. Nanomaterials are of great interest because their physicochemical properties can be optimized to enhance their functionality in many different applications. However, the physicochemical properties that make nanomaterials so interesting may also lead to unexpected behavior and possible harmful effects in the environment and humans. To be able to better assess the potential risk of nanomaterials, more knowledge is needed on the possible toxicological consequences of their different (physicochemical) properties and their mechanisms of toxicity.

One of the key mechanisms of toxicity for nanomaterials is believed to be their ability to generate reactive oxygen species (ROS) (Unfried *et al.*, 2007, Miller *et al.*, 2012). After saturation of compensatory mechanisms, excessive cellular ROS can lead to oxidative stress, resulting in detrimental effects on cell function. In addition, amplification of inflammatory responses may occur that can exacerbate a number of diseases, such as cancer, cardiovascular diseases, neurodegenerative diseases and diabetes (Pisoschi and Pop, 2015). Nano-sized metal oxides are known to facilitate the formation of ROS by depleting electrons from cellular redox species (cellular components able to release electrons) or by serving as catalysts in ROS production through the Fenton reactions, Fenton-like reactions, or the Haber-Weiss cycle reaction (Fu *et al.*, 2014).

While there are clear associations between ROS generation and the toxicity of nanomaterials, comparisons between nanomaterials are complicated by the use of different core chemistries that will manifest as differences in other physicochemical properties in addition to redox activity. In the current study we applied chemical doping (intentional substitution of one element by another while maintaining the lattice structure and arrangement) of a single type of nanoparticle to specifically investigate the influence of redox activity on ROS formation, and associated induction of oxidative stress responses in mice *in vivo* after inhalation exposure. CeO₂ was selected as a nanomaterial that could be chemically modified appropriately and for which acute and subacute toxicity data from inhalation exposure was available (Srinivas *et al.*, 2011, Demokritou *et al.*, 2013, Aalapati *et al.*, 2014, Gosens *et al.*, 2014, Keller *et al.*, 2014, Morimoto *et al.*, 2015).

CeO₂ NPs are used in variety of applications, such as electrochemical sensors, fuel cells, reforming catalysts, as well as a diesel fuel additive used to increase engine efficiency and reduce particulate exhaust emissions (Cassee *et al.*, 2011, Cassee *et al.*, 2012, Dunnick *et al.*, 2016). Previous *in vitro* studies using pure CeO₂ NPs have shown contradicting results in terms of the oxidative stress impacts of CeO₂ NPs (Dunnick *et al.*, 2015, Leung *et al.*, 2015, Pesic *et al.*, 2015). Some studies have found CeO₂ NPs to induce ROS and oxidative stress

(Lin *et al.*, 2006, Park *et al.*, 2008, Eom and Choi, 2009), while others show protective effects against oxidant-induced apoptosis (Xia *et al.*, 2008, Celardo *et al.*, 2011). Differences in the CeO₂ NPs valence state in terms of the 3⁺:4⁺ ratio, or the proportion of the valence state at the NP surface, could account for some of these inconsistencies. Ce has the ability to shift between a 3⁺ and 4⁺ valence state. The antioxidant properties of CeO₂ NPs are due to its ability to scavenge free radicals, which is accomplished through its ability to switch from the 3⁺ to the 4⁺ valence state (Hirst *et al.*, 2009). The antioxidant efficacy of CeO₂ NPs can be enhanced by incorporation of Zr in the CeO₂ lattice (Tsai *et al.*, 2008).

In this study different quantities of Zr were incorporated into the crystalline structure of the CeO₂ NPs in an attempt to generate CeO₂ NPs with different antioxidant potentials. The Zr-doped CeO₂ NPs were produced through an industrial collaboration and therefore had a real-life application. Furthermore, the CeO₂ structure could tolerate Zr substitution at a range of concentrations, allowing for a precise control of the particle redox state. The aim of our study was to investigate if the modification of the redox activity of CeO₂ NPs by Zr-doping influences their pulmonary and cardiovascular effects in mice following subacute inhalation exposure. We hypothesized that the adverse biological effects of CeO₂ NPs can be diminished by Zr-doping, due to an increased antioxidant potential of the doped nanoparticles.

The study was conducted in three different mouse models to explore the (patho)physiological effects of nanoparticle exposure on multiple organ systems. This paper describes the biodistribution, pulmonary and cardiovascular findings whereas the neurological data will be published in a separate paper.

Materials and methods

Study design

To explore the (patho)physiological effects of nanoparticle on multiple organ systems, three different mouse models were exposed.

Atherosclerosis-prone apolipoprotein E-deficient (ApoE^{-/-}) mice are a well-established model for the study of the vascular disease atherosclerosis (Coleman *et al.*, 2006), a disease characterized by the build-up of lipid- and inflammatory cell-rich plaques within arteries, which underlies the majority of cardiovascular diseases. The 4-week exposure protocol was integrated into an 8-week high-fat feeding regime that has been shown to generate complex atherosclerotic plaques with many of the hallmarks of the human disease in specific arterial locations (Cassee *et al.*, 2012, Miller *et al.*, 2013). ApoE^{-/-} mice were used to study hematology, pulmonary and cardiovascular effects.

The 5xFAD mice are an Alzheimer's disease mouse model. Although these mice were included to study neurological effects that will be published in a separate paper, the hematology and pulmonary effects were also studied within the same animals and reported in this paper.

C57BL/6J mice were used as the background (non-genetically modified) strain of the disease mouse models and used to study biodistribution, hematology and pulmonary effects.

Hematology, pulmonary and cardiovascular effects were assessed 4 weeks post exposure. This period was included, firstly, to provide the extra four weeks necessary for mice to develop sufficient plaque formation in arteries and secondly, to investigate the persistency of the pulmonary and cardiovascular effects.

Three groups of each mouse model were exposed to CeO₂ NPs with different amounts of Zr-doping and one control group to clean air. The number of animals per group was different for each of the mouse models, to provide sufficient statistical power to detect differences between exposed and control animals in the most important effect parameter of each mouse model. Based on previous experiments, 8 ApoE^{-/-} mice per group were expected to be sufficient to detect statistically significant differences in atherosclerotic plaque size and 5 C57BL/6J mice per group were expected to be sufficient to detect statistically significant differences in the number of neutrophils in the bronchoalveolar lavage fluid (BALF). However, 10 C57BL/6J mice per group were included, since 10 C57BL/6J mice per group and 16 5xFAD mice per group were needed to provide sufficient statistical power in the neurological study. Mice were exposed nose-only for four weeks to 4 mg/m³ NP for 5 days/week for 3 hours/day. This dose was primarily based on another 4-week inhalation study in which inflammatory responses in the lungs of CD-1 mice were observed after exposed to 2 mg/m³ CeO₂ NPs for 5 days/week for 6 hours/day (Aalapati *et al.*, 2014). Effects were assessed 4 weeks post the final exposure (56 days after the initial exposure). A schematic overview of the experimental design is presented in Figure 1.

C57BL/6	4 weeks air or CeO ₂ NP exposure	Autopsy
	D1 D28 D57	
ApoE ^{-/-}	8 weeks Western diet	Autopsy
	4 weeks air or CeO ₂ NP exposure	
5xFAD	4 weeks air or CeO ₂ NP exposure	Autopsy
	D1 D28 D57	

Figure 1: Schematic overview of the study design. D = day. D1-D28 = exposure period and D29-D57 = recovery period.

Nanomaterial production and characterization

To modify the redox activity, CeO₂ NPs were doped with different amounts of Zr (as per Table 1, Zr contents in the doped NPs were 27 mol% and 78 mol%). Addition of Zr into the crystalline structure of CeO₂ NPs is expected to enhance the antioxidant efficacy of CeO₂ NPs (Tsai *et al.*, 2008).

CeO₂ NPs and Zr-doped CeO₂ NPs were produced using supercritical water hydrothermal synthesis (Cabanas *et al.*, 2000). Briefly, H₂O was pumped through a pre-heating coil, heated to approximately 400 °C, brought into contact with a concurrently flowing solution of metal salts at room temperature (RT), while maintaining the flow rates, temperature and pressure constant. The mixture was cooled immediately after the mixing point and passed through a 7-µm filter to remove large aggregates. The solids in the aqueous suspensions were recovered by allowing the suspension to settle and drying at approximately 100°C. The NPs were tested for endotoxin contamination using a Limulus Amoebocyte Lysate (LAL) test. No endotoxin was detected in any of the NP suspensions.

Table 1: Physicochemical characteristics of the nanoparticles.

Characteristic	Method	Nanoparticle		
		CeO ₂	27% Zr-doped CeO ₂	78% Zr-doped CeO ₂
Primary particle size (Mean ± SD) (nm)	STEM-EELS	4.7 + 1.4	4.6 + 1.4	4.7 + 1.4
Ce ³⁺ /Ce ⁴⁺ ratio	UV-vis	0.87	0.98	1.4
Scavenging capacity ROS (Mean ± SD) (% reduction compared to signal without NPs)	ESR	46 ± 26	44 ± 21	56 ± 23
Median particle diameter at 128 µg/ml in water (Mean ± SD)(nm)	DCS	39	40	41
Median particle diameter at 20 µg/ml in water (Mean ± SD)(nm)	DLS	54 ± 9	45 ± 5	52 ± 6
Median particle diameter at 1 mg/ml in water (Mean ± SD)(nm)	DLS	172 ± 2 PDI: 0.27 ± 0.01	297 ± 4 PDI: 0.47 ± 0.01	358 ± 6 PDI: 0.49 ± 0.03
zeta potential at 1 mg/ml in water (mV ± SD)	DLS	50.3 ± 0.7	45.9 ± 3	44.1 ± 2
EC ₂₀ cytotoxicity in A549 (Mean ± 90% CI) (µg/cm ²)	WST-1	0.2 (0.0-23)	9 (0.0-38)	33 (0.1-68)

STEM-EELS: Scanning Transmission Electron Microscope (STEM) Electron Energy Loss Spectroscopy (EELS) analysis; UV-vis: Ultraviolet-Visible spectrophotometry; ESR: Electron-Spin Resonance; DCS: Differential Centrifugal Sedimentation; DLS: Dynamic Light Scattering; WST-1: Water-Soluble Tetrazolium-1; EC₂₀: Effective Concentration resulting in 20% cytotoxicity.

To determine the Ce³⁺/Ce⁴⁺ ratio of the different NPs, ultraviolet-visible spectrophotometry (UV-vis) analysis was performed on 200 mg/L particle solutions, diluted in MilliQ water, with a 6800 Jenway double beam UV-Vis spectrophotometer, with long path UV-Vis cell cuvettes. The UV-Vis absorption spectra were collected over a wavelength range of 200-700nm. Both valence states of Ce strongly absorb ultraviolet light and each one has a characteristic

spectrophotometric absorbance peak, with Ce^{3+} absorbing in the 230 to 260 nm range and Ce^{4+} absorbing in the 300 to 400 nm range.

Zr-doping of CeO_2 NPs might also cause differences in other characteristics than redox activity which can also influence the toxicity of the NPs, such as particle size distribution, aggregation, agglomeration and corona formation. Therefore the hydrodynamic size distributions and zeta potential were assessed using differential centrifugal sedimentation (DCS) and dynamic light scattering (DLS) analyzes. In addition, the effect of Zr-doping on the scavenging capacity of the CeO_2 NPs was investigated with Electron-spin resonance (ESR). Before testing the NPs *in vivo*, the effect Zr-doping of CeO_2 NPs on the *in vitro* cytotoxicity was investigated in lung epithelial cells.

The scavenging capacity of ROS was investigated with ESR analysis using a cell free system with a 5,5-dimethyl-1-pyrroline N-oxide (DMPO) spin trap (He *et al.*, 2014) in combination with hydrogen peroxide (H_2O_2) and copper sulfate (CuSO_4). The nanoparticle suspensions were thoroughly vortexed and sonicated for 5 minutes at RT in a sonication bath to re-disperse any agglomerates. A sample was made of 12.5 μL nanoparticle suspension (1.28 mg/mL), 12.5 μL CuSO_4 (20 μM), 25 μL H_2O_2 (0.5 M) and 50 μL DMPO (0.05 M). This sample was incubated in a shaker water bath at 37 °C for 15 minutes at 100 rpm, vortexed and taken up in a capillary tube which was then sealed at the bottom with hematocrit and measured with the ESR Spectroscope (Miniscope MS 400, MT MagnetTech GmbH).

The effect of Zr-doping on *in vitro* cytotoxicity was tested in human lung epithelial carcinoma cells (A549) cells obtained from ATCC (VA, USA). A549 cells were cultured in tissue culture flasks in RPMI 1640 medium with Glutamax (Gibco, ThermoFisher Scientific Inc., Landsmeer, the Netherlands) supplemented with 10% Fetal Bovine Serum (FBS, Greiner BioOne BV, Alphen aan de Rijn, the Netherlands) and 1% penicillin/streptomycin (Gibco). Cells were cultured at 37°C in a humidified atmosphere of 5% CO_2 in air. Twenty-four hours before exposure, the cells were harvested by a short incubation with 0.5% ethylenediaminetetraacetic acid (EDTA) trypsin in Ca/Mg free Dulbecco's Phosphate Buffered Saline (Gibco) and counted. Fifty thousand (5×10^4) cells were seeded in 96-well plates in 200 μL cell culture medium per well. After 24 h of incubation a semi confluent monolayer of cells was obtained and the cells were exposed to 0, 1.25, 2.5, 5, 10, 20, 40 or 80 $\mu\text{g}/\text{cm}^2$ of the various NPs in cell culture medium. Additional wells with the same concentrations of NPs in cell culture medium, but no A549 cells were included to measure possible interference of the materials with the viability assay. Cell viability (i.e. cytotoxicity) was determined after 24 h of exposure by a colorimetric assay using cell proliferation reagent WST-1 (water-soluble tetrazolium-1) (Roche, Sigma-Aldrich Chemie). Dose-response modelling and derivations of the EC_{20} (effective concentration resulting in 20% cytotoxicity) were performed using PROAST software (Slob, 2002) version 63.5.

Animals

Specific pathogen free (SPF) female ApoE^{-/-} mice (N=32; Taconic, Denmark) were obtained at age 10–12 weeks at the beginning of the study. The 5xFAD and C57BL/6J mice originated from Jackson Laboratories. For this study, female 5xFAD mice (N=64) and female wild type (WT) cross breed C57BL/6J littermates (N = 40) were used at the age of 8-11 weeks. The mice were barrier maintained and housed in a single room in macrolon cages. The temperature and the relative humidity were controlled at 22±2°C and at 40-70%, respectively. Lighting was artificial with a sequence of 12 hours light and 12 hours dark (at night). Feed and drinking water was provided *ad libitum* from the arrival of the mice until the end of the study, except during exposure. The ApoE^{-/-} mice were fed a commercially available rodent Western (high fat) diet (Purified Diet Western 4021.06, ABdiets, Woerden, The Netherlands), starting at the first day of the exposure period until the end of the experiment. The other mice were fed a standard commercially available rodent diet (SMR-A, ABdiets, Woerden, The Netherlands). Animals were monitored by cage-side observations and, if necessary, handled to detect signs of compromised health. The body weight of each animal was recorded one day before the start of exposure (day -1), prior to exposure on the first day and weekly thereafter. Experiments were conducted at Intravacc (Bilthoven, The Netherlands) under a protocol approved by the Ethics Committee for Animal Experiments of the RIVM and performed according to applicable national and EU regulations.

Inhalation exposure

Approximately one week before the 4-week exposure period, 20 samples of each nanoparticle (one for each day) with a concentration of 1 mg/mL were prepared from the stock dispersions (20, 20 or 29 mg/mL for 0%, 27% and 78% Zr-doped CeO₂ NPs, respectively) by diluting with ultrapure water to the desired concentration. Stock and sample dispersions were sonicated for 5 minutes in an ultrasonic bath (Branson CPX2800, 40 kHz, 110W) before use to re-disperse any possible agglomerates. Freshly generated aerosols of NPs were generated using a spray nozzle technique, diluted with pressurized clean particle-free air, and heated to 24-25°C. Exposure was controlled based on stable particle number counts, mass concentrations, temperature and relative humidity, measured continuously using a condensation particle counter (CPC 3022A from TSI Inc., St. Paul, MN, USA), a tempered element oscillating microbalance (TEOM series1400A from Rupprecht & Patashnick, NY, USA) and M-170 Measurement Indicator (Vaisala M170, Vaisala Oyj, Helsinki, Sweden), respectively, during each exposure period. In addition, the test atmosphere is characterized at least twice during each exposure session using an optical particle sizer (OPS 3330, TSI Inc., St. Paul, MN, USA) and a scanning mobility particle sizer (SMPS 3936 from TSI Inc., St. Paul, MN, USA). The total mass concentration generated over the 3-hour exposure period was determined by gravimetric analysis of pre-weighed and post-weighed polytetrafluoroethylene (PTFE) filters (Teflo R2PJO47, Pall corporation, Port Washington, New York, USA) using a micro-balance (Mettler MC or ME-5 microbalance, Mettler-Toledo LLC, Columbus, OH, USA). The Count

Median Diameter (CMD) and the Mass Median Diameter (MMD) were estimated using the Aerosol Instrument Manager Software (Release Version 9.0.0.0, 15:32:53, Nov 11 2010 from TSI Inc., St Pauls, MN, USA), assuming spherical aggregation around primary particles of 4.7 ± 1.4 nm. In addition, aerosols were collected on polycarbonate filters for scanning electron microscopy (SEM) analysis. The SEM samples were prepared by placing a small piece of the filter on the SEM stub and coating it with platinum, and visualizing with an XL30 Environmental SEM-FEG microscope (Philips XL30 ESEM-FEG). During the 3 hour exposure periods to the different nanoparticles, the control groups were exposed to filtered air under the same conditions (nose-only tubes) for the same amount of time.

Estimated deposited dose in lungs

To estimate the deposited dose in the lungs, the multiple path particle dosimetry model (MPPD v3.04 © 2016 by Applied Research Associates, Inc., Albuquerque, NM, USA) was used. Default parameters for the B6C3F1 mouse were applied (forced respiratory capacity: 0.3 mL, upper respiratory tract volume: 0.0322 mL, nasal breathing, breathing frequency: 353/min, tidal volume: 0.20 mL, inspiration fraction: 0.5, no pause fraction). Calculations were performed using the count median diameter, geometric standard deviation and mass concentration of the exposure characterization and a density of 7.215 g/cm^3 for CeO_2 , 6.801 g/cm^3 for 27% Zr-doped CeO_2 and 6.018 g/cm^3 for 78% Zr-doped CeO_2 NPs.

Quantification of Ce and Zr in tissues

During necropsy, organs from half of the C57BL/6J mice per group were obtained to evaluate the distribution of the NPs throughout the body. Liver, spleen, kidneys, heart and right (exposed mice) or left (control mice) lung, were weighed and immediately frozen in liquid nitrogen for determination of the Ce and Zr concentrations. To allow measurement of multiple parameters within the same animal, different parts of the lungs were selected for the exposed compared to the control animals. From the exposed groups the right lung was used for quantification of Ce and Zr, because the left lung was needed for histopathological examination. From the control group the left lung was used for quantification of Ce and Zr, because the right lung was needed for bronchoalveolar lavage. The organs were digested by acidification of each sample with 2 mL nitric acid for 12h. Hydrogen fluoride (0.2 mL) was added, followed by microwave heating for 45 min up to 185°C , and maintained for a further 20 min. Boric acid (2 mL) was added to neutralize the hydrogen fluoride, and the samples were re-heated for 20 min to 160°C , and maintained for 10 min. Once cooled, samples were filtered with a 450 nm syringe filter, diluted with 10 mL deionized water and stored at room temperature (RT). The presence of Ce and Zr in the lungs, liver, spleen, kidneys and heart was determined by inductively coupled plasma mass spectrometry (ICP-MS) using a Perkin Elmer NexION 300X instrument operated in standard mode for Ce and Zr. The isotopes measured were ^{90}Zr and ^{140}Ce using ^{115}In and ^{159}Tb as internal standards. Calibration standards (0 – 100

µg/L) were prepared from VWR 1000 mg/L stock solutions. Quantities are expressed as µg/g organ tissue.

Necropsy

Hematology

Animals were anaesthetized with a mixture of ketamine and xylazine. Two blood samples were taken by eye extraction. The first sample was collected in a K3-EDTA tube (Minicollect K3EDTA, 1 mL, 450474 Greiner Bio-One) for hematological parameters as determined in a blood auto analyzer (ADVIA 2120 Hematology System, Siemens Healthineers) within 3 hours after collection. The second sample was collected in a serum tube, which was kept for at least 30 minutes at RT before centrifugation at 2000g for 10 min at 20°C. Serum was divided into separate aliquots of 50 µL and stored at -20°C for further analysis.

Bronchoalveolar lavage

Lung lavage was performed at necropsy. A cannula was placed in the trachea and the diaphragm opened to decrease the amount of air inside the lungs. For the control animals and all ApoE^{-/-} animals, the right lung half was rinsed twice with approximately 0.5 mL (26.7 mL per kg body weight) of physiological saline solution, after ligation of the left lung. The injected volume was inserted and recovered 3 times, after which the lavage liquid was collected and stored on ice for less than 2 hours. To allow necropsy of the planned number of animals within one day, both lungs were lavaged for 10 of the 16 exposed 5xFAD mice and 5 of the 10 exposed C57BL/6J mice, using the same procedure, but approximately 0.8 mL (40 mL per kg body weight) of physiological saline solution. BALF was centrifuged at 400g for 10 minutes at 4°C. The supernatant was divided into two separate aliquots of 125 µL for total protein (TP; an indicator for acute lung injury), lactate dehydrogenase (LDH; an indicator of cytotoxicity), gamma-glutamyl transferase (GGT; an indicator of lung cell damage) and alkaline phosphatase (ALP; an indicator of type II cell damage) measurements using an autoanalyser (LX20-Pro, Beckman-Coulter, Woerden, the Netherlands). The cell pellet was scored for the presence of erythrocytes, re-suspended in 500 µL phosphate-buffered saline (PBS) and kept on ice. Cell counts were determined in the re-suspended pellet using a Coulter counter (Beckman-Coulter, Live Sciences, Woerden, the Netherlands). Cell concentrations were determined using a single sample using at least 150 µL of the re-suspended cells. Cytospins (Cytospin 3, Thermo-Shandon, Runcorn, UK) were prepared and stained using May-Grunwald and Giemsa stain, and cell differentiation was performed by counting 400 cells per slide.

Histopathology

Lung tissue. For the majority of the animals, the right lung was removed after the collection of the BALF and immediately frozen in liquid nitrogen and stored at - 80°C for further analysis. The left lung was removed and, after weighing, cannulated and infused with formaldehyde for 1 hour at a pressure of 20 cm H₂O. Lungs were processed for histopathology; embedded in paraffin wax, sectioned at a thickness of 2-4 µm and stained with hematoxylin and eosin for histopathological examination. Histopathological changes were described according to distribution, severity and morphological characteristics. The morphological characteristics of chronic inflammation include for example the presence of lymphocytes and macrophages in the lung tissue, while acute inflammation is characterized by the presence of polymorphonuclear neutrophils (PMNs). Severity scores were assigned as follows: Grade 1 minimal/very few/very small; Grade 2 slight/few/small; Grade 3 moderate/moderate number/moderate size; Grade 4 marked/many/large; Grade 5 massive/extensive number/extensive size.

To allow necropsy of the planned number of animals within one day, both lungs were lavaged for 10 of the 16 exposed 5xFAD mice and 5 of the 10 exposed C57BL/6J mice. For the remaining six of the 16 exposed 5xFAD mice both lungs were infused with formaldehyde and embedded in paraffin wax for histopathological examination. For the remaining five of the 10 exposed C57BL/6J mice the right lung was weighed and immediately frozen in liquid nitrogen for determination of the Ce and Zr concentrations and the left lung was infused with formaldehyde and embedded in paraffin wax for histopathological examination. For five of the 10 control C57BL/6J mice the right lung was lavaged and stored at - 80°C and the left lung was weighed and immediately frozen in liquid nitrogen for determination of the Ce and Zr concentrations.

Assessment of atherosclerosis. Arteries (brachiocephalic, aortic arch, thoracic aorta) were isolated from ApoE^{-/-} mice. Atherosclerosis was quantified, as previously published (Miller *et al.*, 2013). Briefly, brachiocephalic arteries were fixed in formalin and histological sections were taken in triplicate at 100 µm intervals, beginning at the first section of the artery with a fully intact media. Sections were stained with Masson's Trichrome. The cross-sectional area of the plaque was measured and standardized to the medial area. A single mean value for atherosclerotic burden for each animal was calculated from the plaque size from each complete serial section throughout the brachiocephalic artery. A single section from each artery (the section exhibiting the largest plaque in cross-section) was chosen for mac-2 immunohistochemistry for macrophage-derived cells. A rat anti-mouse primary antibody was used (1/12000; CL8942AP, VH Bio, Gateshead, UK) with rat IgG (1/12000; I-400, Vector Labs, Peterborough, UK) as a negative control, followed by a goat anti-rat IgG biotinylated secondary antibody (BA-9400, Vector Labs). The area of positive staining was expressed as a proportion of the total plaque area.

Other organs. The spleen, liver, heart and kidneys were removed, weighed and stored in 4% formaldehyde for pathological analysis if required based on macroscopic findings.

Statistical analyses

Statistical analyses were performed using GraphPad Prism v7.00 (GraphPad Software, San Diego, California, USA). Ordinary one-way analysis of variance (ANOVA) analyses including all experimental groups were performed followed by a Tukey's post-hoc multiple comparisons test. A p-value ≤ 0.05 was considered statistically significant. If the group means indicated an increase or decrease with increasing amounts of Zr-doping, a linear trend analysis (alpha 0.1) was performed between the groups exposed to 0%, 27% and 78% Zr-doped CeO_2 NPs, to investigate if observed effects could be related to the amount of Zr doping of the particles .

Results

Nanoparticle characterization

UV-vis analysis showed a clear trend of increasing $\text{Ce}^{3+}/\text{Ce}^{4+}$ ratio with increasing Zr content (see Figure 2 and Table 1). The DCS and DLS analysis both showed no significant differences in hydrodynamic size distributions (data not shown) or median particles size (see Table 1) of the different NPs, indicating the Zr-doping did not cause major differences in particle size distribution, aggregation or agglomeration. As expected, the zeta potential showed a small decrease with increasing amounts of Zr-doping.

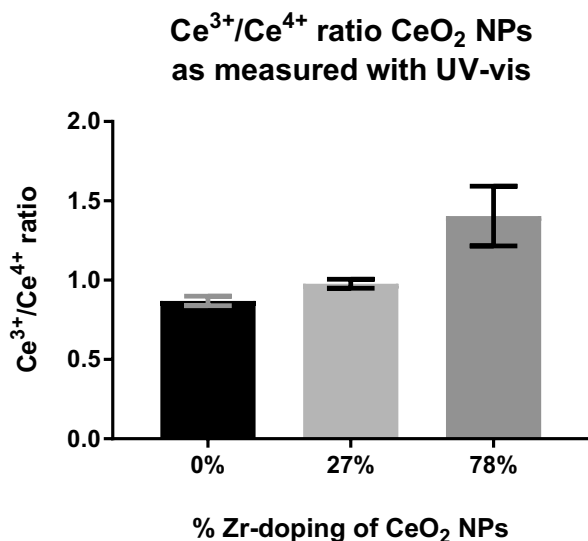


Figure 2: $\text{Ce}^{3+}/\text{Ce}^{4+}$ ratio measured with UV-vis of undoped CeO_2 , 27% Zr-doped CeO_2 and 78% Zr-doped CeO_2 NPs, showing an increasing $\text{Ce}^{3+}/\text{Ce}^{4+}$ ratio with increasing Zr-content of CeO_2 NPs.

ESR analysis showed a slight, but not statistically significant increased scavenging capacity of the CeO₂ NPs with the highest % of Zr-doping compared to the undoped CeO₂ NPs (see Figure 3 and Table 1).

In A549 cells, a decrease in cytotoxicity with increasing amounts of Zr-doping was shown. Dose response modelling resulted in increasing EC₂₀ values with increasing amounts of Zr doping (see Figure 4 and Table 1).

ESR measurements of the scavenging capacity of CeO₂ and Zr-doped CeO₂ NPs

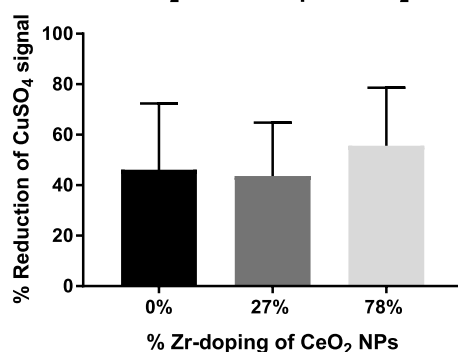
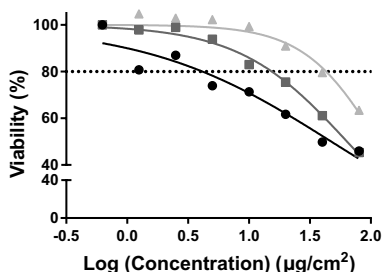


Figure 3: Percentage reduction of the Electron-spin resonance (ESR) signal of CuSO₄ and CeO₂ NPs compared to CuSO₄ alone using a cell free system with a 5,5-dimethyl-1-pyrroline N-oxide (DMPD) spin trap in combination with H₂O₂. The slightly larger % reduction of the 78% Zr-doped NPs indicates a slight but not statistically significant increase in scavenging capacity of reactive oxygen species (ROS) of 78% Zr-doped compared to the undoped and 27% Zr-doped CeO₂ NPs.

a Cell viability A549 after 24 h exposure



b EC₂₀ A549 after 24 h exposure

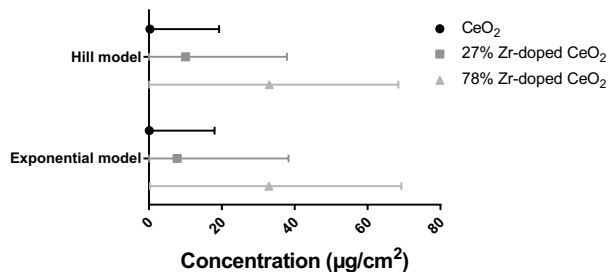


Figure 4: Percentage reduction in viability of A549 cells after exposure to 0, 1.25 2.5, 5, 10, 20, 40 or 80 µg/cm² CeO₂, 27% Zr-doped CeO₂ and 78% Zr-doped CeO₂ NPs compared to the controls (a) and the effective concentrations resulting in 20% cytotoxicity (EC₂₀) mean ± 90% confidence interval (b).

Exposure characterization

The combined SMPS-OPS particle size measurements showed that almost the entire particle size distribution was within the size range measurable with the SMPS (2.5 - 1000 nm), confirming that the SMPS data can be used to estimate the CMD and MMD. A representative SMPS and OPS size distribution of each of the different CeO₂ NPs are shown in Figure 5.

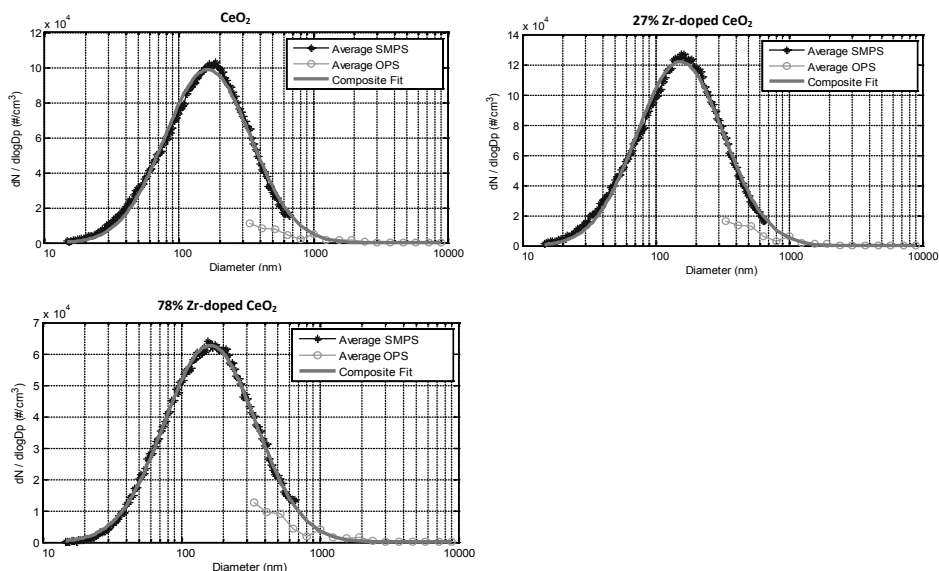


Figure 5: Combined size distributions measured with the scanning mobility particle sizer (SMPS) and the optical particle sizer (OPS) for representative samples of CeO₂, 27% Zr-doped CeO₂ and 78% Zr-doped CeO₂ NPs. The OPS distributions overlap with the composited fit of the SMPS distributions for the largest particles of the distributions, indicating that the SMPS measurements can be used to determine the count median diameter (CMD) and mass median diameter (MMD).

The physical characteristics of the different CeO₂ NP aerosols are summarized in Table 2. The primary particle size of the different CeO₂ NPs was $\sim 4.7 \pm 1.4$ nm. CMD and MMD, as measured by SMPS, were slightly larger for the 78% Zr-doped CeO₂ particles, compared to the CeO₂ and 27% Zr-doped CeO₂ particles. Mass concentration measurements determined the exposure concentration, thus, the particle number concentrations of the 78% Zr-doped CeO₂ exposure were lower than the particle number concentrations of the CeO₂ and 27% Zr-doped CeO₂ exposures.

SEM images of the NPs from aerosols collected on polycarbonate filters showed the presence of particles and agglomerates, when collected on the filter (see Figure 6). Most particles were around 300 to 500 nm, but there were also infrequent very large particles (around 1000 to 2000 nm).

Table 2: Average particle number concentration, size distribution and mass concentration of the CeO₂, 27% Zr-doped CeO₂ and 78% Zr-doped CeO₂ NP exposure (n=20).

			CeO ₂	27% Zr-doped CeO ₂	78% Zr-doped CeO ₂
STEM	Primary particle size*	nm	4.7 ± 1.4	4.6 ± 1.4	4.7 ± 1.4
CPC	Number concentration	#/cm ³	14624 ± 3709	16962 ± 5145	10785 ± 894
SMPS	Count Median Diameter (CMD)	nm	182 ± 10	183 ± 9	202 ± 7
	Geometric Standard Deviation		1.88	1.88	1.86
	Mass Median Diameter (MMD)**	nm	280 ± 12	288 ± 9	316 ± 14
	Geometric Standard Deviation		1.55	1.56	1.57
	Number concentration	#/cm ³	75620 ± 28184	70828 ± 46924	58716 ± 20693
	Filter	Gravimetric mass concentration	mg/m ³	3.98 ± 0.23	4.04 ± 0.30

*Primary particle size was determined by Scanning Transmission Electron Microscope (STEM) Electron Energy Loss Spectroscopy (EELS) analysis.

**MMD was estimated based on the particle size distributions of the SMPS measurements, assuming spherical aggregation around primary particles of 4.7 nm.

CPC: Condensation Particle Counter; SMSP: Scanning Mobility Particle Sizer.

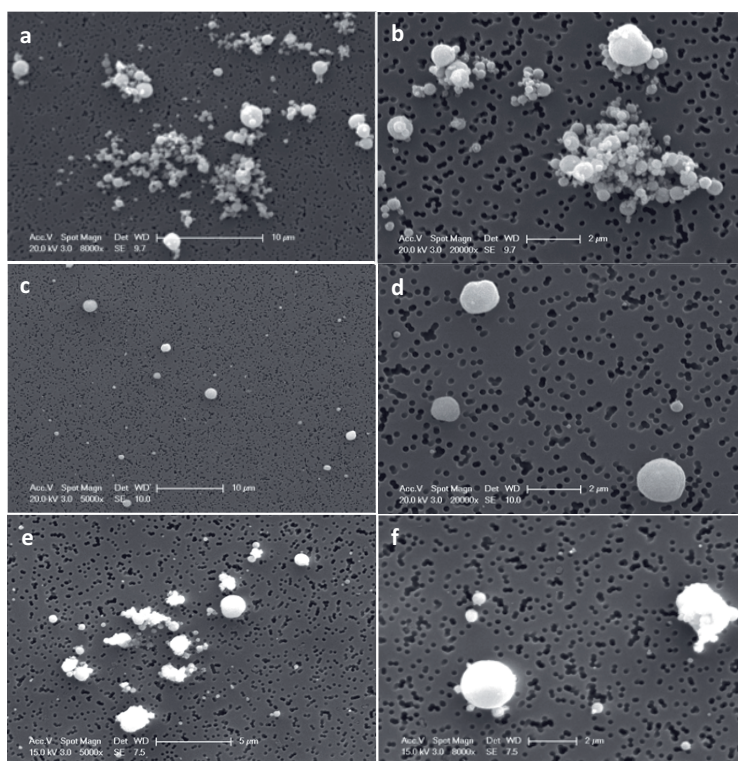


Figure 6: Scanning Electron Microscopy (SEM) image of CeO₂ particles from aerosols collected on polycarbonate filters. Undoped CeO₂ NPs (a and b) showed the presence of agglomerates mostly around 300 to 400 nm, but also some infrequent very large particles around 2000 nm. 27% Zr-doped CeO₂ NPs (c and d) showed no agglomerates and particles were mostly around 500 nm. 78% Zr-doped CeO₂ NPs showed the presence of agglomerates, mostly around 400 nm, but also some very large particles around 1000 nm and a significant amount of smaller particles of approximately 200 nm or smaller (e and f).

Estimated deposited dose in lungs

The estimated deposited dose in the lung and head was similar for CeO₂, 27% Zr-doped CeO₂ and 78% Zr-doped CeO₂ NPs, ranging from 618 to 639 ng (approximately 60% of the inhaled dose). The deposition pattern in the different regions of the lungs was also similar for the different types of CeO₂ NPs, with approximately 8% of the dose reaching the alveoli (see Table 3).

Table 3: Estimated deposition of inhaled CeO₂, 27% Zr-doped CeO₂ and 78% Zr-doped CeO₂ NPs in different regions of the lungs.

	Total inhaled dose (µg)*	Total deposited dose (µg)**	Deposited fraction per region (% of inhaled dose) **			Retained dose in lung (µg)***
			Head (%)	Tracheobronchial region (%)	Alveolar region (%)	
CeO ₂ NPs	1027	618	48.8	3.5	8.0	16.2
27% Zr-doped CeO ₂ NPs	1043	625	48.8	3.4	7.9	16.2
75% Zr-doped CeO ₂ NPs	1056	639	49.8	3.3	7.5	15.6

* Total amount inhaled = estimated as tidal volume (0.203 mL) x breathing frequency (353 min⁻¹) x exposure concentration ($\approx 4 \times 10^{-3}$ µg/mL) x exposure duration (3600 min).

** Estimated using the MPPD model

*** Retained dose in the tracheobronchial and alveolar region 4 weeks post-exposure, estimated using the MPPD model.

Quantification of Ce and Zr in tissues

The highest concentrations of Ce and Zr were found in the lung, followed by much lower concentrations in the heart, spleen, kidneys and liver, respectively (Figure 7). As would be expected, significantly higher levels of Ce and Zr were observed in the lungs of exposed mice compared to the controls. Increasing amounts of Zr-doping in the NP exposure did not result in decreasing Ce concentrations or increasing Zr concentrations in the lung. In most of the other organs, the Ce and Zr concentrations were not statistically significantly different from the background concentrations measured in the controls. A few exceptions were observed, for example, the Ce concentration in the hearts of mice exposed to 78% Zr-doped CeO₂.

Hematology

ApoE^{-/-} mice had more neutrophils compared to exposed and control C57BL/6J and 5xFAD mice (p<0.05 in Tukey's post-hoc test following one-way ANOVA). No statistically significant differences were observed in the total white blood cell counts (data not shown) or differential white blood cell counts (Figure 8) of the exposed groups compared to the controls in blood from all strains of mice, except for a small decrease in neutrophils in ApoE^{-/-} mice exposed to 78%-doped CeO₂ NPs (Tukey's post-hoc test following one-way ANOVA with p=0.02). In addition, there was a decrease (post-hoc test for linear trend following one-way ANOVA with p=0.002) in neutrophils in ApoE^{-/-} mice with increasing amounts of Zr-doping.

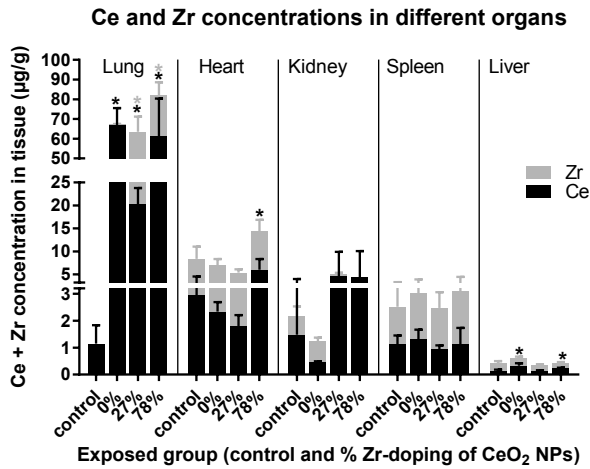


Figure 7: Ce and Zr concentrations in organs 4 weeks after exposure to clean air (control) or 0%, 27% or 78% Zr-doped CeO₂ NPs (exposed). Mean ± SD, n=4-6, *=Ce or Zr concentration is statistical significantly different from the control in Tukey's post-hoc test following one-way ANOVA with p<0.05. The bar graphs are stacked and represent the sum of the Ce concentration (bottom black colored part of each bar) and Zr concentration (upper gray colored part of each bar) in the different organs. With a few exceptions (e.g. the lung), the Ce and Zr concentrations of the exposed animals were not statistical significantly different from the control animals in most organs. The Zr concentration in the lungs of the control group and in the kidneys of the group exposed to 78% Zr-doped CeO₂ NPs was below the detection limit.

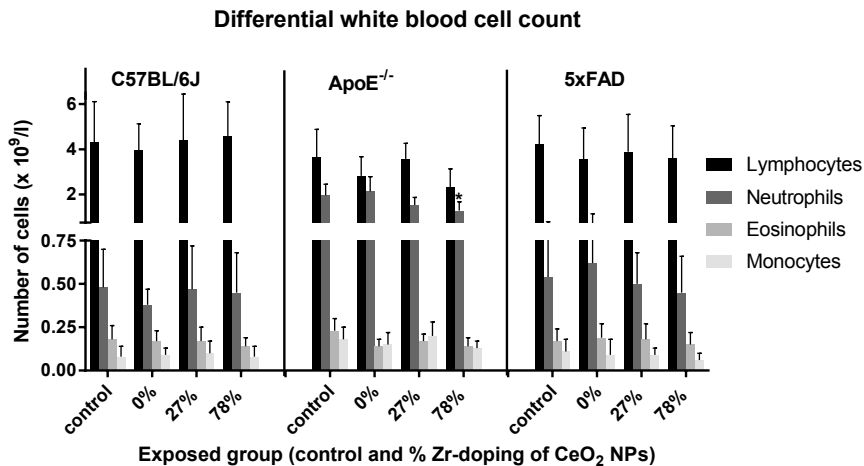


Figure 8: Differential white blood cell count 4 weeks after exposure to clean air (control) or 0%, 27% or 78% Zr-doped CeO₂ NPs (exposed). Mean ± SD, n=8-16, *=statistical significantly different from the control in Tukey's post-hoc test following one-way ANOVA with p<0.05. No statistically significant differences between the different types of white blood cells were observed between control and exposed animals, except for the neutrophils in ApoE^{-/-} mice exposed to 78% Zr-doped CeO₂ NPs. The number of basophils and large unstained cells were very small and are thus not depicted.

Bronchoalveolar lavage

The number of lymphocytes in the control C57BL/6J mice was relatively high (7.7%), but this was due to an outlier and did not represent an inflammatory response. No statistically significant differences were observed in the total cell counts (data not shown) or differential cell counts in BALF of the exposed groups compared to the controls for any strain of mouse (Figure 9), except for the total cell count in 5xFAD mice exposed to 27% Zr-doped CeO₂ NPs, which was lower than that of the control 5xFAD mice. There was a decrease ($p < 0.1$; post-hoc test for linear trend following one-way ANOVA) in total cell counts ($p = 0.075$), % macrophages ($p = 0.014$), and % neutrophils ($p = 0.05$) in ApoE^{-/-} mice with increasing amounts of Zr-doping. However, no such trends were observed in C57BL/6J or 5xFAD mice. Similarly, no statistically significant differences were observed for LDH, ALP or GGT protein levels between the exposed and control groups (Figure 10). No constitutive differences in differential cell counts or protein levels were observed between the different mice strains.

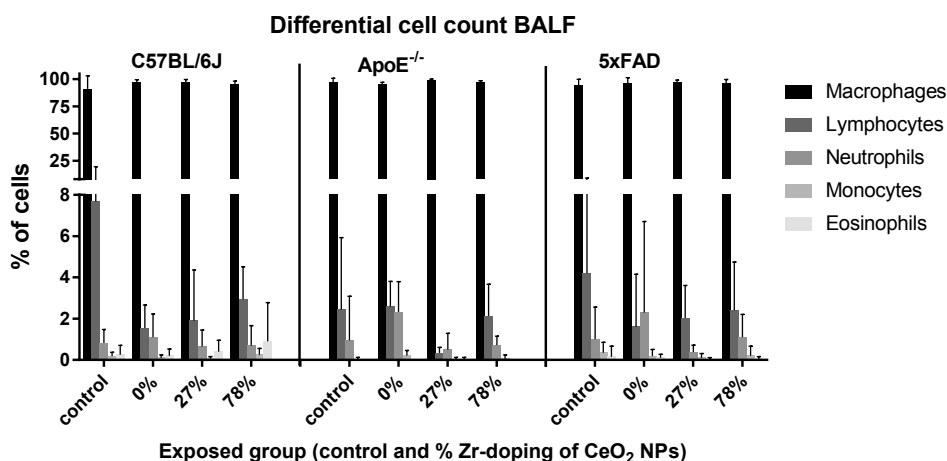


Figure 9: Differential cell count in bronchoalveolar lavage fluid (BALF) 4 weeks after exposure to clean air (control) or CeO₂, 27% Zr-doped CeO₂ or 78% Zr-doped CeO₂ NPs (exposed). Mean \pm SD, n=5-16, *=statistical significantly different from the control in Tukey's post-hoc test following one-way ANOVA with $p < 0.05$. No statistically significant differences in the different types of cells were observed between control and exposed animals, except for the number of macrophages in 5xFAD mice exposed to 27% Zr-doped CeO₂ NPs.

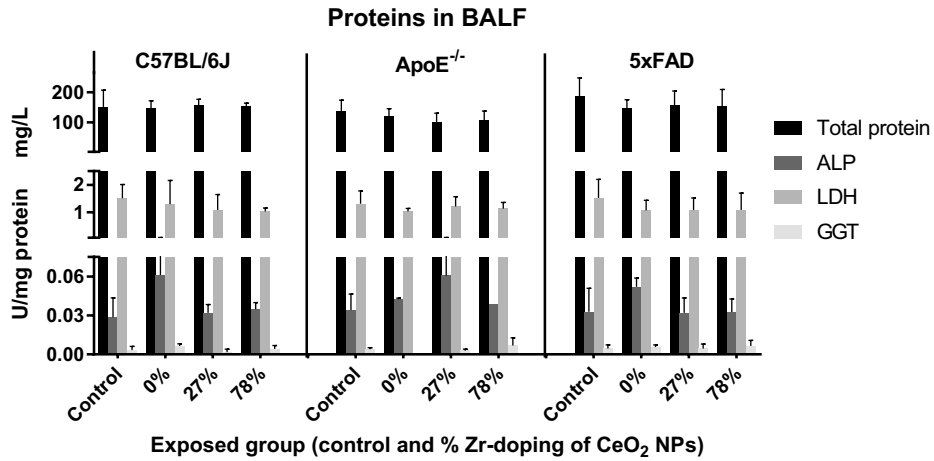


Figure 10: Total protein, Lactate Dehydrogenase (LDH), Alkaline Phosphatase (ALP) and Gamma-Glutamyl Transpeptidase (GGT) levels in bronchoalveolar lavage fluid (BALF) 4 weeks after exposure to clean air (control) or CeO₂ and 27% Zr-doped CeO₂ or 78% Zr-doped CeO₂ NPs (exposed). Mean \pm SD, n=5-16. No statistically significant differences in the total protein, LDH, ALP or GGT were observed between control and exposed animals (Tukey's post-hoc test following one-way ANOVA with $p < 0.05$).

Histopathology

Lung

While modest, an increased incidence in minimal chronic bronchoalveolar or alveolar inflammation was observed in the exposed animals compared to the control mice (see Figure 11a, b and c). The increase did not appear to be related to the percentage Zr-doping (Table 4).

Table 4: Histopathological findings in lung of C57BL/6J, ApoE^{-/-} and 5xFAD mice.

Histopathological finding →		Chronic bronchoalveolar or alveolar inflammation		Alveolar macrophages	Particle loaded alveolar macrophages	
Strain ↓	Treatment ↓	Minimal	Slight	Minimal	Minimal	Slight
C57BL/6J	Control	60% (3/5) ^a	-	-	-	-
	Total exposed	67% (10/15)	-	13% (2/15)	-	-
	CeO ₂	80% (4/5)	-	20% (1/5)	-	-
	27% Zr-doped CeO ₂	40% (2/5)	-	20% (1/5)	-	-
	78% Zr-doped CeO ₂	80% (4/5)	-	-	-	-
ApoE ^{-/-}	Control	25% (2/8)	-	-	-	-
	Total exposed	42% (10/24)	-	-	4% (1/24)	25% (6/24)
	CeO ₂	38% (3/8)	-	-	13% (1/8)	75% (6/8)
	27% Zr-doped CeO ₂	38% (3/8)	13% (1/8)	-	-	-
	78% Zr-doped CeO ₂	50% (4/8)	-	-	-	-
5xFAD	Control	69% (11/16)	-	6% (1/16)	-	-
	Total exposed	72% (13/18)	-	17% (3/18)	-	-
	CeO ₂	83% (5/6)	-	17% (1/6)	-	-
	27% Zr-doped CeO ₂	67% (4/6)	-	-	-	-
	78% Zr-doped CeO ₂	67% (4/6)	-	33% (2/6)	-	-

a Percentage of animals affected. Within brackets the number of animals with histopathological findings versus number of animals evaluated.

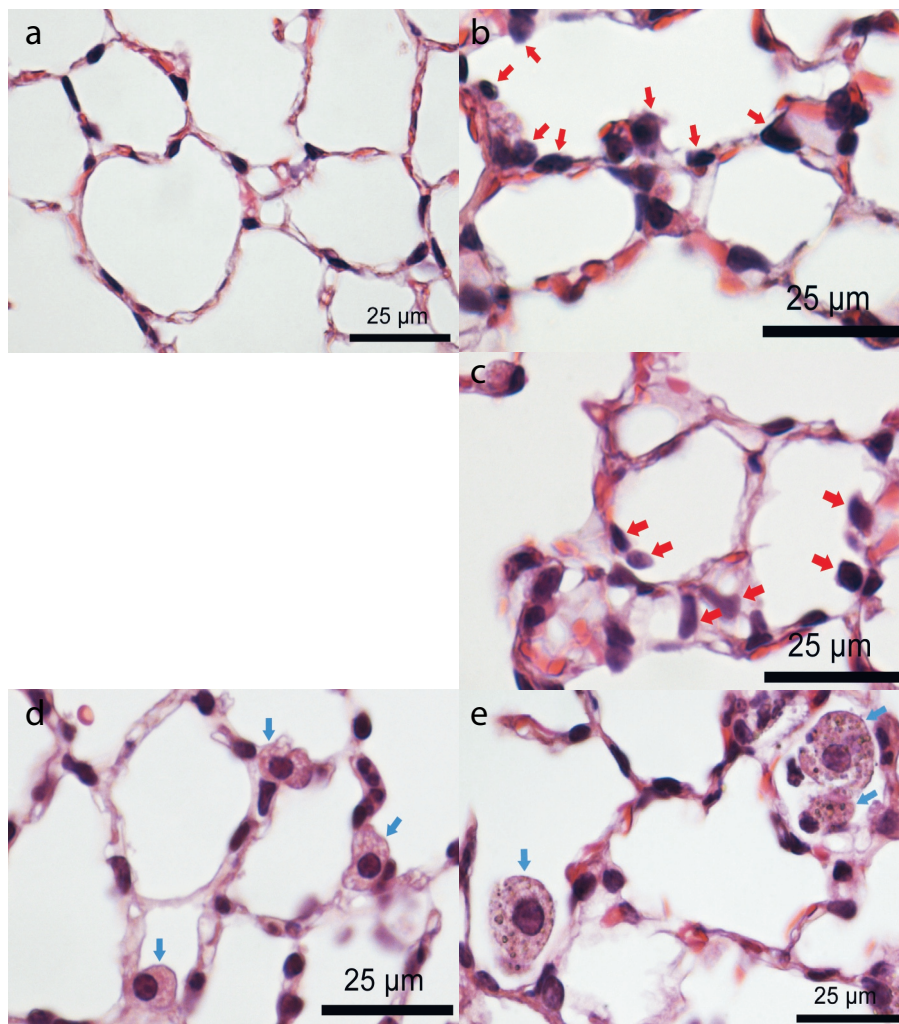


Figure 11: Lung sections showing minimal chronic bronchoalveolar inflammation, alveolar inflammation and particle loaded alveolar macrophages in mice exposed to doped and undoped CeO_2 NP exposure. Lung sections of C57BL/6J mice exposed to clean air (a) and 78% Zr-doped CeO_2 NPs (b and c) and of ApoE^{-/-} mice exposed to 27% Zr-doped CeO_2 NPs (d) and undoped CeO_2 NPs (e). Red arrows indicate mononuclear inflammatory cells on the septa of the alveoli, indicating minimal chronic bronchoalveolar inflammation (b) or inside the alveoli, indicating minimal alveolar inflammation (c). Lung sections of mice with chronic and alveolar inflammation were similar across the different mouse models and experimental groups. Blue arrows indicate empty (d) or particle loaded (e) alveolar macrophages.

Particle loaded alveolar macrophages (Figure 11 e) were observed in seven of the eight ApoE^{-/-} mice exposed to undoped CeO_2 NPs. This effect was not observed in ApoE^{-/-} mice exposed to 27% or 78% Zr-doped CeO_2 NPs or any other exposure or the control group of the other mouse models (Table 4), indicating Zr-doping may influence particle loading of alveolar macrophages in ApoE^{-/-} mice. In the bronchoalveolar lavage fluid particle loaded macrophages were seen in all the NP exposed animals but not in the control groups.

Cardiovascular Effects

ApoE^{-/-} mice exhibited regions of dense plaques in the aortic arch and branch points of large arteries. Plaques were composed of fibroblastic matrix, smooth muscle cells, lipid cavities and cholesterol crystals (Figure 12a). Atherosclerotic burden was quantified in the brachiocephalic artery, with control (air-exposed) mice having a mean plaque size of 94 ± 9% (standardized to the area of the vascular media). Exposure to undoped or Zr-doped CeO₂ NPs did not have a significant effect on the atherosclerotic burden (mean plaque size) of these arteries (p=0.62; One-way ANOVA; Figure 12b). However, there was an increase (post-hoc test for linear trend following one-way ANOVA with p=0.09) in the proportion of plaque staining positive for mac-2 (i.e. macrophage-derived foam cells; Figure 12c) with increasing Zr content of the CeO₂ NP exposure (Figure 12d).

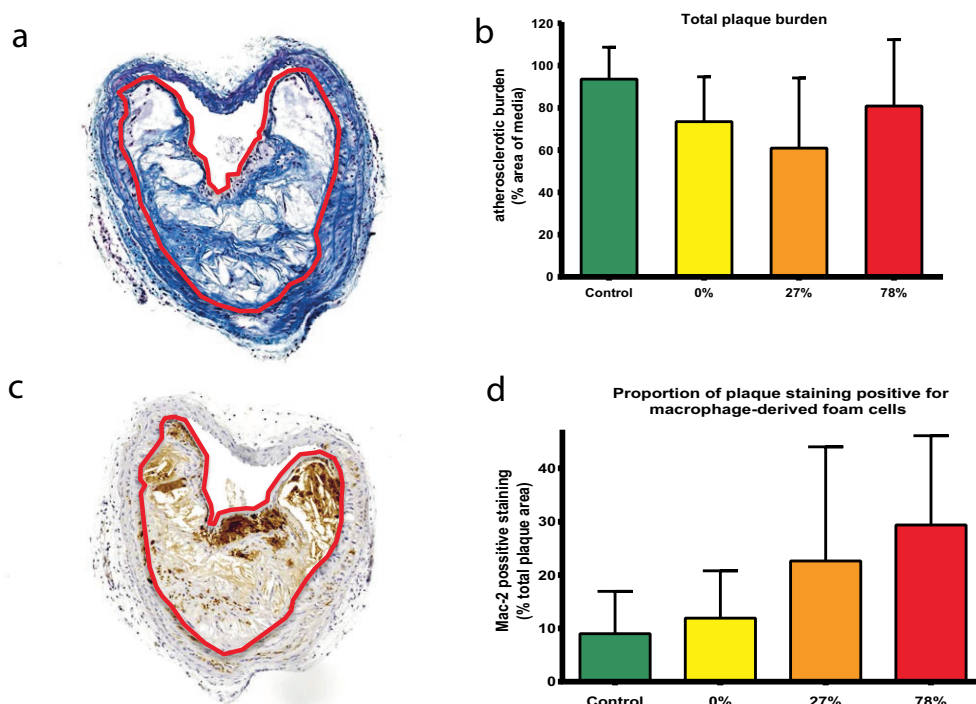


Figure 12: Effect of Zr-doped CeO₂ NPs on atherosclerosis in the brachiocephalic artery of ApoE^{-/-} mice after inhalation. (a) Representative section of brachiocephalic artery showing a large plaque on the intimal surface of the artery. The red outline highlights the area of the plaque. (b) Quantification of atherosclerotic burden throughout the brachiocephalic artery. Mean ± SEM (n=3-7). Undoped (0%) or Zr-doped (27% and 78%) CeO₂ NP exposure did not significantly affect plaque size compared to clean air exposure (controls). (c) Immunohistochemical staining for mac-2 (brown stain, showing macrophage-derived foam cells). The red outline highlights the area of the plaque. (d) Proportion of plaque staining positive for mac-2 following exposure to clean air (control), undoped (0%) and Zr-doped (27% and 78%) CeO₂ NPs. Mean ± SEM (n=4-7). No statistically significant differences were observed between control and exposed animals (Tukey's post-hoc test, following one-way ANOVA with p<0.05).

Other organs

No treatment related effects on organ weights or macroscopic findings (data not shown) were observed and thus no histopathological analysis was performed on the other organs.

Discussion

In this subacute inhalation study, only modest biological effects were observed after exposure to CeO₂ NPs or Zr-doped CeO₂ NPs in healthy mice and mouse models of atherosclerosis and Alzheimer's disease. Accordingly, altering the redox activity of nanomaterials by Zr-doping had a limited impact on the bioactivity, in the absence of any overt toxicity of the CeO₂ parent material.

Zr-doping of CeO₂ NPs

Zr-doping of CeO₂ NPs was expected to increase the antioxidant potential of CeO₂ NPs by shifting the Ce valence state towards 3⁺, increasing its capacity to shift from 3⁺ to 4⁺ and thus increasing its antioxidant potential and thereby reducing adverse pulmonary and cardiovascular effects. Our UV-vis analyses confirmed that Zr-doping does shift the valence state towards 3⁺ (see Figure 2). Furthermore, ESR analysis using a DMPO spin trap in combination with H₂O₂ showed that high concentrations of Zr-doping increased the scavenging capacity for ROS by CeO₂ NPs in a cell-free system (see Figure 3). In addition, *in vitro* tests indicated that Zr-doping decreased the cytotoxicity of CeO₂ NPs in human alveolar cells (A549) (see Figure 4). However, *in vivo* Zr-doping had a limited impact on the pulmonary and cardiovascular effects.

Previous studies investigated the effect of samarium (Sm) or gadolinium (Gd) doping of CeO₂ NPs (Celardo *et al.*, 2011, Dunnick *et al.*, 2015, Dunnick *et al.*, 2016). Sm-doping decreased the Ce³⁺/Ce⁴⁺ ratio and thereby the ability to shift from 3⁺ to 4⁺, decreasing the antioxidant properties of CeO₂ NPs in leukocyte (U937 and Jurkat) cell lines (Celardo *et al.*, 2011). Gd-doping increased the Ce³⁺/Ce⁴⁺ ratio, but also decreased the ability to shift from 3⁺ to 4⁺ and the antioxidant properties, suggesting that differences in reactivity of CeO₂ NPs are due to the ability of Ce to transition between the two valence states rather than dependent on a specific valence state (Dunnick *et al.*, 2015, Dunnick *et al.*, 2016). Although Zr-doping increased the Ce³⁺/Ce⁴⁺ ratio of the CeO₂ NPs, the ability to shift from 3⁺ to 4⁺ may be reduced instead of enhanced due to Zr-doping, because the Zr-atoms occupy some of the 4⁺ sites.

In addition, the antioxidant activity of CeO₂ NPs can also be affected by the external environment, especially the anions (Xue *et al.*, 2012). Xue *et al.* (2012) showed that CeO₂ NPs scavenge hydroxyl radicals (\cdot OH) in Tris hydrochloride (Tris-HCl) and sulfate systems, but lose their scavenging capacity in PBS. Their explanation for this is that the antioxidant activity of CeO₂ NPs is not only determined by its ability to convert Ce³⁺ into Ce⁴⁺, but also

by regeneration of Ce^{3+} by reduction of Ce^{4+} on the surface of the nanoparticles. According to Xue *et al.* (2012) in PBS cerium phosphate is formed on the surface of the NPs, which prevents the regeneration of Ce^{3+} from Ce^{4+} during the redox cycling preventing the CeO_2 NPs to scavenge $\cdot\text{OH}$. Although the aerosols of the Zr-doped CeO_2 NPs were prepared using ultrapure water instead of PBS, the antioxidant potential of the CeO_2 NPs may be similarly altered once deposited in the lungs of the mice.

Particle deposition and distribution to other organs

The deposition along different regions of the respiratory tract of mice, calculated with the MPPD model (v3.04), was similar for the different types of undoped and Zr-doped CeO_2 NPs. In all cases, the estimated fraction of particle deposition in the lung (tracheobronchial and alveolar region) was approximately 11% of the inhaled mass dose.

As expected, the highest cerium (Ce) and zirconium (Zr) concentrations, as measured by ICP-MS analysis of tissues, were found in the lung. The MPPD model can be used to predict the Ce dose in the lung 4 weeks post-exposure if it is assumed there is an even distribution of the CeO_2 NPs in the lungs. Based on the estimated retained dose of CeO_2 NPs (with 0% Zr-doping) in the lung (16.2 μg , see Table 3) and the average lung weight (158 mg), the expected Ce concentration in the lung is approximately 103 $\mu\text{g/g}$. The measured Ce concentration in the right lungs of the undoped CeO_2 NP exposed mice was slightly lower (67 $\mu\text{g/g}$) but in the same order of magnitude. The difference between the predicted and measured concentrations may reflect the lung clearance rate used by the MPPD model compared to the actual lung clearance rate *in vivo*.

Background levels of Ce and Zr were detected in various organs of animals exposed to clean air (controls). This might be caused by Ce and Zr contamination of the drinking water, food and/or bedding of the animals. Although Ce and Zr concentrations are not routinely measured in drinking water, food or bedding, Ce was detected in rat chow in a concentration of 0.22 mg Ce/kg food (Yokel *et al.*, 2012) and in tap water in concentrations of ~ 0.0009 $\mu\text{g/L}$ in the US (Donovan *et al.*, 2016) and 0.018 – 0.084 $\mu\text{g/L}$ in Croatia (Fiket *et al.*, 2015). In addition, Ce has been detected in various organs of control animals in previous *in vivo* studies (Yokel *et al.*, 2012, Yokel *et al.*, 2013).

The Ce and Zr concentrations in the lung did not reflect the different percentages of Zr-doping of the NPs, as would have been expected. Increasing amounts of Zr-doping did not lead to higher Zr concentrations or lower Ce concentrations. Moreover, surprisingly low Ce concentrations were found in the lungs of mice exposed to 27% Zr-doped CeO_2 NPs compared to mice exposed to 78% Zr-doped CeO_2 . These findings are unlikely to be due to the differences in exposure or deposition of the NPs, since the gravimetric mass concentrations and size distribution of the aerosols were almost identical (Table 2). These unexpected

findings might reflect differences in clearance, de-agglomeration or dissolution of the different CeO₂ NPs types in the lung, based on, for example, differences in agglomeration size and surface specific uptake by macrophages. We speculate that Zr-doping may increase the clearance of the NPs, since a previous study showed that the decrease in lung burden during the post-exposure period of 21 days was markedly higher for ZrO₂ NPs (42-75% decrease) compared to CeO₂ NPs (5-7% decrease) (Landsiedel *et al.*, 2014). Alternatively, it is possible that the particles may have had different effective densities that might have affected the distribution pattern.

The concentrations of Ce and Zr in heart, spleen, kidneys and liver were much lower than what was measured in the lung. Similar distribution patterns have been found in other studies after inhalation of CeO₂ NPs (Geraets *et al.*, 2012, Aalapati *et al.*, 2014, Keller *et al.*, 2014).

Pulmonary effects

CeO₂ NP exposure had no statistically significant effects on total and differential cell counts, LDH, ALP, GGT or total protein levels in the BALF of any of the tested mouse strains 4 weeks post-exposure, irrespective the Zr content. Only modest inflammatory lesions were found by histopathological analysis of lung sections of CeO₂ NPs exposed mice. As these findings were not related to the amount of Zr-doping, the observed pulmonary effects are likely to be caused by the physical interaction between the alveolar surface and the large reactive surface area of the particles, an observation not uncommon with poorly-soluble nanoparticles (Greim and Ziegler-Skylakakis, 2007). One exception to these findings were the particle-loaded alveolar macrophages in histological lung sections of ApoE^{-/-} mice that were only observed after exposure to CeO₂ NPs without Zr-doping, indicating Zr-doping may influence the occurrence of particle loaded alveolar macrophages. Interestingly, in the BALF, particle-loaded macrophages were seen in all the exposed groups (all mouse models and all CeO₂ NP types). This observation might reflect differences in the dynamics of macrophages of the ApoE^{-/-} mice; for example the inherently higher number of macrophages in the lungs of this strain of mouse (Grainger *et al.*, 2004), which can be further increased by a high fat diet (Naura *et al.*, 2009). Differences in the ability of the undoped and the Zr-doped CeO₂ NP types to influence the NP uptake, damage and turnover of macrophages in the lung may result in differences in the release of the NPs from macrophages in the lung, resulting in the observed Zr-doping related differences in the occurrence of particle-loaded alveolar macrophages in the histological lung sections 4 weeks post-exposure.

Other inhalation studies have reported more prominent effects of CeO₂ NPs than those observed in our study, including increased neutrophils and lymphocytes in BALF, increased concentrations of biochemical markers of inflammation in BALF (LDH, ALP, GGT, N-acetyl beta-d-glucosaminidase (NAG) and cytokine-induced neutrophil chemoattractant-1

(CINC-1)), increased lung weight, inflammatory lung lesions (e.g. severe alveolitis, particle loaded macrophages and granulomas, lung fibrosis) and accumulation of particle-loaded macrophages in lymph nodes and liver (Srinivas *et al.*, 2011, Demokritou *et al.*, 2013, Aalapati *et al.*, 2014, Gosens *et al.*, 2014, Keller *et al.*, 2014) (See Tables S1). It is notable that most of these studies were performed in rats, which tend to be more susceptible to pulmonary inflammation induced by poorly soluble particles than mice (Borm *et al.*, 2015). Some of the effects observed in previous studies only occurred at higher exposure concentrations (e.g. 5, 10, 25 or 50 mg/m³ for 6h/day, 5 d/w for 4 weeks), compared to the exposure of 4 mg/m³ for 3h/day, 5d/w for 4 weeks we used in our study. Additionally, our study focused on the presence of persistent toxicity 4 weeks post-exposure, when inflammation induced directly after exposure will have gradually diminished to a level that does not manifest in the BALF or histopathology. The prolonged recovery time in our study provides an opportunity to assess whether the biological effects lead to persistent adverse outcomes. Nevertheless, we acknowledge that several prior studies have demonstrated long-lasting pulmonary effects, including raised neutrophils and lymphocytes in BALF and accumulation of particle-loaded macrophages and granulomas in the lung (Aalapati *et al.*, 2014, Keller *et al.*, 2014, Morimoto *et al.*, 2015). A 4-week inhalation exposure to similar levels of CeO₂ NPs in CD-1 mice caused inflammation-induced responses in the lung characterized by necrosis, fibrosis and granulomas 4 weeks post-exposure (Aalapati *et al.*, 2014). Differences in the CeO₂ NPs and exposure characteristics could explain these diverging results. In our study, CeO₂ NPs were produced by hydrothermal synthesis, with primary particle size of ~4.7 nm, and aerosols with a mass median diameter (MMD) of 280 nm with a geometric standard deviation (GSD) of 1.56. Aalapati *et al.* (2014) used CeO₂ NPs produced via the sol-gel method, with a primary diameter of 15–30 nm and aerosols with a mass median aerodynamic diameter (MMAD) of 1.4 μm (GSD 2.4). Both the cumulative external dose, (i.e. concentration x exposure duration) and the dose rate were very similar for both studies, however, differences in particle size distribution will have led to different biological effective pulmonary doses. The measured Ce concentration in the lung 4 weeks post-exposure reported by Aalapati *et al.* was much higher (approximately 500 μg/g tissue compared to 67 μg/g in our study). The higher Ce concentration is likely to have contributed to the greater pulmonary toxicity in the Aalapati study. Other possible explanations are that CeO₂ NPs generated via sol-gel method have a different redox activity, surface structure or other properties that make them more toxic than CeO₂ NPs generated by hydrothermal synthesis. Furthermore, the strain (CD-1 mice), gender (male) and/or age (7-8 weeks) of the mice used by Aalapati *et al.* might be more sensitive to the effects of particle inhalation than the strain (C57BL/6J mice), gender (female) and/or age (9 weeks) of the mice used in our study.

The modest inflammatory lung lesions observed in this study were not related to the amount of Zr-doping of the CeO₂ NPs, with the exception of the particle-loaded alveolar macrophages in histological lung sections of ApoE^{-/-} mice that were only observed after

exposure to CeO₂ NPs without Zr-doping. Recently, another *in vivo* study (Dunnick *et al.*, 2016) investigated the influence of Gd-doping of CeO₂ NPs after inhalation exposure. In this study, Sprague Dawley rats were exposed to 0.5 or 1.0 mg/kg pure CeO₂ NPs and 10 or 20 % Gd-doped CeO₂ NPs via intratracheal instillation. Gd-doping was expected to increase the pulmonary toxicity, but no major effect of doping on the pulmonary toxicity was observed 1, 7 and 84 days after exposure of CeO₂ NPs in rats. Our study used a post-exposure period of 4 weeks and an exposure concentration that caused pronounced pulmonary toxicity in a previous study (Aalapati *et al.*, 2014). However, because only minimal pulmonary effects were observed after exposure to the CeO₂ NPs without Zr-doping in our study, most of the hypothesized ameliorative effects resulting from the Zr-doping may not have been visible under the present conditions.

Cardiovascular effects

There was no significant effect of CeO₂ NP exposure, or of the Zr-doped variants, on atherosclerotic burden. Previous studies using this mouse model showed that pulmonary exposure to nano-sized carbon black (Niwa *et al.*, 2007), carbon nanotubes (Li *et al.*, 2007, Cao *et al.*, 2014), nickel nanoparticles (Kang *et al.*, 2011) and nano-titanium dioxide (Mikkelsen *et al.*, 2011, Chen *et al.*, 2013) promoted the development of atherosclerosis. There is also a large body of literature showing that inhalation of ultrafine particles in air pollution promotes atherosclerosis in man (Kunzli *et al.*, 2011) and animal models (Moller *et al.*, 2011, Miller *et al.*, 2013). Environmental nanoparticles have a very varied composition, however, the ability of chemicals and metals on the particle surface to generate reactive oxygen species is believed to be a key determinant of their ability to induce cardiovascular effects (Miller *et al.*, 2012). Thus, we envisioned that inhalation of nanomaterials with different amounts of Zr-doping would also induce varying degrees of cardiovascular dysfunction. The lack of effect of Zr-doping of CeO₂ NPs may reflect the low reactivity of the parent compound, or potentially the small degree of deposition in the alveoli, leading to limited lung inflammation or particle translocation to the bloodstream. Interestingly, though, the composition of atherosclerotic plaques tended to be altered by subacute exposure to CeO₂ NPs with increasing Zr content. In particular, there was an increase in the plaque content of macrophage-derived foam cells with an increased proportion of Zr in the CeO₂ NPs. In man, plaques with a greater degree of inflammation are more instable and prone to rupture; the result of which can lead to thrombotic occlusion of the vessel causing a cardiovascular event e.g. heart attack or stroke (Williams *et al.*, 2002). These findings suggest that alterations in chemical composition of CeO₂ may have the potential to increase the susceptibility of plaques to rupture without necessarily increasing overall plaque size. At present, given the low biological activity of the parent material and the direction of the association between plaque macrophages and Ce:Zr ratio, it is not possible to state with any confidence that this is due to differences in redox activity. Nevertheless, this observation merits further investigation with other types of redox-modified nanomaterials in experiments with larger groups of ApoE^{-/-} mice or extended periods of exposure.

Future directions

The use of a systematic series of NPs of a single compound is desirable; however, further studies with more inherently toxic nanomaterials are required to fully address the role of redox activity. Because of the minimal pulmonary and cardiovascular effects observed with the parent material (CeO₂ NPs without Zr-doping), alteration of the redox activity of these CeO₂ NPs may have a limited capacity to subsequently alter toxicity. Metals and metal oxides that have a conduction band energy (Ec) level that overlaps with the cellular redox potential (-4.12 to -4.84 eV) were shown to have the ability to induce oxygen radicals, oxidative stress, and inflammation *in vitro* and *in vivo* (Zhang *et al.*, 2012). Ongoing work in our laboratories will investigate this hypothesis, using a newly synthesized series of metal doped nanoparticles with a conduction band energy that overlaps the cellular redox potential.

Conclusions

This study investigated the pulmonary and cardiovascular effects of redox modification of metal oxide nanoparticles using varying levels of metal doping of a structurally reproducible material. CeO₂ NPs had minimal pulmonary and cardiovascular effects following subacute inhalation at 4 weeks post-exposure. Zr-doping of CeO₂ NPs had limited effects on these responses, although indications that Zr-doping could potentially alter particle loading of alveolar macrophages and increase the inflammatory cell content in atherosclerosis plaques merit further investigation. Future studies with other types of redox-modified nanomaterials of greater inherent toxicity and a wider range of redox activities are required to fully assess the influence of redox-modification on the toxicity of nanomaterials.

Acknowledgements

The authors would like to thank Paul H.B. Fokkens, Daan L.A.C. Leseman, Liset J.J. de la Fonteyne, Piet K. Beekhof, Christine M.R. Sopotan, Hans J.C. Strootman, Jolanda Rigters, Ron F. Vlug, Karin M.P. van den Hurk, Julia Kolling, Geert B. van der Horst, Rory Verhagen, Dirk J. Elberts, Pieter W. Dissel and Angéla Gomersbach-de Ridder for their help during the conduction of the animal experiment and valuable technical assistance. In addition, Geert B. van de Horst is acknowledged for his contribution to the generation of the cytotoxicity in A549 cells and Joost Lensen of Will Research for the histopathology.

Funding

The work leading to these results has received funding from the European Union's Seventh Framework Programme for research, technology development and demonstration under grant agreement n° 310451 (NanoMILE) and the Netherlands Food and Consumer Product Safety Authority (NVWA).

References

- Aalapati, S., Ganapathy, S., Manapuram, S., Anumolu, G. & Prakya, B.M., 2014. Toxicity and bio-accumulation of inhaled cerium oxide nanoparticles in CD1 mice. *Nanotoxicology*, 8, 786-98.
- Borm, P., Cassee, F.R. & Oberdorster, G., 2015. Lung particle overload: old school -new insights? *Part Fibre Toxicol*, 12, 10.
- Cabanas, A., Darr, J.A., E., L. & Poliakoff, M., 2000. A continuous and clean one-step synthesis of nanoparticulate $Ce_{1-x}Zr_xO_2$ solid solutions in near-critical water. *Chem Comm*, 2000, 901-902.
- Cao, Y., Jacobsen, N.R., Danielsen, P.H., Lenz, A.G., Stoeger, T., Loft, S., Wallin, H., Roursgaard, M., Mikkelsen, L. & Moller, P., 2014. Vascular effects of multiwalled carbon nanotubes in dyslipidemic ApoE^{-/-} mice and cultured endothelial cells. *Toxicol Sci*, 138, 104-16.
- Cassee, F.R., Campbell, A., Boere, A.J., Mclean, S.G., Duffin, R., Krystek, P., Gosens, I. & Miller, M.R., 2012. The biological effects of subacute inhalation of diesel exhaust following addition of cerium oxide nanoparticles in atherosclerosis-prone mice. *Environ Res*, 115, 1-10.
- Cassee, F.R., Van Balen, E.C., Singh, C., Green, D., Muijser, H., Weinstein, J. & Dreher, K., 2011. Exposure, health and ecological effects review of engineered nanoscale cerium and cerium oxide associated with its use as a fuel additive. *Crit Rev Toxicol*, 41, 213-29.
- Celardo, I., De Nicola, M., Mandoli, C., Pedersen, J.Z., Traversa, E. & Ghibelli, L., 2011. Ce(3)+ ions determine redox-dependent anti-apoptotic effect of cerium oxide nanoparticles. *ACS Nano*, 5, 4537-49.
- Chen, T., Hu, J., Chen, C., Pu, J., Cui, X. & Jia, G., 2013. Cardiovascular effects of pulmonary exposure to titanium dioxide nanoparticles in ApoE knockout mice. *J Nanosci Nanotechnol*, 13, 3214-22.
- Coleman, R., Hayek, T., Keidar, S. & Aviram, M., 2006. A mouse model for human atherosclerosis: long-term histopathological study of lesion development in the aortic arch of apolipoprotein E-deficient (E0) mice. *Acta Histochem*, 108, 415-24.
- Demokritou, P., Gass, S., Pyrgiotakis, G., Cohen, J.M., Goldsmith, W., McKinney, W., Frazer, D., Ma, J., Schwegler-Berry, D., Brain, J. & Castranova, V., 2013. An in vivo and in vitro toxicological characterisation of realistic nanoscale CeO₂ inhalation exposures. *Nanotoxicology*, 7, 1338-50.
- Donovan, A.R., Adams, C.D., Ma, Y., Stephan, C., Eichholz, T. & Shi, H., 2016. Detection of zinc oxide and cerium dioxide nanoparticles during drinking water treatment by rapid single particle ICP-MS methods. *Anal Bioanal Chem*, 408, 5137-45.
- Dunnick, K.M., Morris, A.M., Badding, M.A., Barger, M., Stefaniak, A.B., Sabolsky, E.M. & Leonard, S.S., 2016. Evaluation of the effect of valence state on cerium oxide nanoparticle toxicity following intratracheal instillation in rats. *Nanotoxicology*, 10, 992-1000.
- Dunnick, K.M., Pillai, R., Pisane, K.L., Stefaniak, A.B., Sabolsky, E.M. & Leonard, S.S., 2015. The Effect of Cerium Oxide Nanoparticle Valence State on Reactive Oxygen Species and Toxicity. *Biol Trace Elem Res*, 166, 96-107.
- Eom, H.J. & Choi, J., 2009. Oxidative stress of CeO₂ nanoparticles via p38-Nrf-2 signaling pathway in human bronchial epithelial cell, Beas-2B. *Toxicol Lett*, 187, 77-83.

- Fiket, Z., Rozmaric, M., Krmpotic, M. & Benedik, L., 2015. Levels of major and trace elements, including rare earth elements, and (2)(3)(8)U in Croatian tap waters. *Environ Sci Pollut Res Int*, 22, 6789-99.
- Fu, P.P., Xia, Q., Hwang, H.M., Ray, P.C. & Yu, H., 2014. Mechanisms of nanotoxicity: generation of reactive oxygen species. *J Food Drug Anal*, 22, 64-75.
- Geraets, L., Oomen, A.G., Schroeter, J.D., Coleman, V.A. & Cassee, F.R., 2012. Tissue distribution of inhaled micro- and nano-sized cerium oxide particles in rats: results from a 28-day exposure study. *Toxicol Sci*, 127, 463-73.
- Gosens, I., Mathijssen, L.E., Bokkers, B.G., Muijser, H. & Cassee, F.R., 2014. Comparative hazard identification of nano- and micro-sized cerium oxide particles based on 28-day inhalation studies in rats. *Nanotoxicology*, 8, 643-53.
- Grainger, D.J., Reckless, J. & Mckilligin, E., 2004. Apolipoprotein E modulates clearance of apoptotic bodies in vitro and in vivo, resulting in a systemic proinflammatory state in apolipoprotein E-deficient mice. *J Immunol*, 173, 6366-75.
- Greim, H. & Ziegler-Skylakakis, K., 2007. Risk assessment for biopersistent granular particles. *Inhal Toxicol*, 19 Suppl 1, 199-204.
- He, W., Liu, Y., Wamer, W.G. & Yin, J.J., 2014. Electron spin resonance spectroscopy for the study of nanomaterial-mediated generation of reactive oxygen species. *J Food Drug Anal*, 22, 49-63.
- Hirst, S.M., Karakoti, A.S., Tyler, R.D., Sriranganathan, N., Seal, S. & Reilly, C.M., 2009. Anti-inflammatory properties of cerium oxide nanoparticles. *Small*, 5, 2848-56.
- Kang, G.S., Gillespie, P.A., Gunnison, A., Moreira, A.L., Tchou-Wong, K.M. & Chen, L.C., 2011. Long-term inhalation exposure to nickel nanoparticles exacerbated atherosclerosis in a susceptible mouse model. *Environ Health Perspect*, 119, 176-81.
- Keller, J., Wohlleben, W., Ma-Hock, L., Strauss, V., Groters, S., Kuttler, K., Wiench, K., Herden, C., Oberdorster, G., Van Ravenzwaay, B. & Landsiedel, R., 2014. Time course of lung retention and toxicity of inhaled particles: short-term exposure to nano-Ceria. *Arch Toxicol*, 88, 2033-59.
- Kunzli, N., Perez, L., Von Klot, S., Baldassarre, D., Bauer, M., Basagana, X., Breton, C., Dratva, J., Elosua, R., De Faire, U., Fuks, K., De Groot, E., Marrugat, J., Penell, J., Seissler, J., Peters, A. & Hoffmann, B., 2011. Investigating air pollution and atherosclerosis in humans: concepts and outlook. *Prog Cardiovasc Dis*, 53, 334-43.
- Landsiedel, R., Sauer, U.G., Ma-Hock, L., Schnekenburger, J. & Wiemann, M., 2014. Pulmonary toxicity of nanomaterials: a critical comparison of published in vitro assays and in vivo inhalation or instillation studies. *Nanomedicine (Lond)*, 9, 2557-85.
- Leung, Y.H., Yung, M.M., Ng, A.M., Ma, A.P., Wong, S.W., Chan, C.M., Ng, Y.H., Djurisic, A.B., Guo, M., Wong, M.T., Leung, F.C., Chan, W.K., Leung, K.M. & Lee, H.K., 2015. Toxicity of CeO₂ nanoparticles - the effect of nanoparticle properties. *J Photochem Photobiol B*, 145, 48-59.
- Li, Z., Hulderman, T., Salmen, R., Chapman, R., Leonard, S.S., Young, S.H., Shvedova, A., Luster, M.I. & Simeonova, P.P., 2007. Cardiovascular effects of pulmonary exposure to single-wall carbon nanotubes. *Environ Health Perspect*, 115, 377-82.
- Lin, W., Huang, Y.W., Zhou, X.D. & Ma, Y., 2006. Toxicity of cerium oxide nanoparticles in human lung cancer cells. *Int J Toxicol*, 25, 451-7.

- Mikkelsen, L., Sheykhzade, M., Jensen, K.A., Saber, A.T., Jacobsen, N.R., Vogel, U., Wallin, H., Loft, S. & Moller, P., 2011. Modest effect on plaque progression and vasodilatory function in atherosclerosis-prone mice exposed to nanosized TiO₂. *Part Fibre Toxicol*, 8, 32.
- Miller, M.R., Mclean, S.G., Duffin, R., Lawal, A.O., Araujo, J.A., Shaw, C.A., Mills, N.L., Donaldson, K., Newby, D.E. & Hadoke, P.W., 2013. Diesel exhaust particulate increases the size and complexity of lesions in atherosclerotic mice. *Part Fibre Toxicol*, 10, 61.
- Miller, M.R., Shaw, C.A. & Langrish, J.P., 2012. From particles to patients: oxidative stress and the cardiovascular effects of air pollution. *Future Cardiol*, 8, 577-602.
- Moller, P., Mikkelsen, L., Vesterdal, L.K., Folkmann, J.K., Forchhammer, L., Roursgaard, M., Danielsen, P.H. & Loft, S., 2011. Hazard identification of particulate matter on vasomotor dysfunction and progression of atherosclerosis. *Crit Rev Toxicol*, 41, 339-68.
- Morimoto, Y., Izumi, H., Yoshiura, Y., Tomonaga, T., Oyabu, T., Myojo, T., Kawai, K., Yatera, K., Shimada, M., Kubo, M., Yamamoto, K., Kitajima, S., Kuroda, E., Kawaguchi, K. & Sasaki, T., 2015. Pulmonary toxicity of well-dispersed cerium oxide nanoparticles following intratracheal instillation and inhalation. *J Nanopart Res*, 17, 442.
- Naura, A.S., Hans, C.P., Zerfaoui, M., Errami, Y., Ju, J., Kim, H., Matrougui, K., Kim, J.G. & Boulares, A.H., 2009. High-fat diet induces lung remodeling in ApoE-deficient mice: an association with an increase in circulatory and lung inflammatory factors. *Lab Invest*, 89, 1243-51.
- Niwa, Y., Hiura, Y., Murayama, T., Yokode, M. & Iwai, N., 2007. Nano-sized carbon black exposure exacerbates atherosclerosis in LDL-receptor knockout mice. *Circ J*, 71, 1157-61.
- Park, E.J., Choi, J., Park, Y.K. & Park, K., 2008. Oxidative stress induced by cerium oxide nanoparticles in cultured BEAS-2B cells. *Toxicology*, 245, 90-100.
- Pesic, M., Podolski-Renic, A., Stojkovic, S., Matovic, B., Zmejkoski, D., Kojic, V., Bogdanovic, G., Pavicevic, A., Mojovic, M., Savic, A., Milenkovic, I., Kalauzi, A. & Radotic, K., 2015. Anti-cancer effects of cerium oxide nanoparticles and its intracellular redox activity. *Chem Biol Interact*, 232, 85-93.
- Pisoschi, A.M. & Pop, A., 2015. The role of antioxidants in the chemistry of oxidative stress: A review. *Eur J Med Chem*, 97, 55-74.
- Slob, W., 2002. Dose-response modeling of continuous endpoints. *Toxicol Sci*, 66, 298-312.
- Srinivas, A., Rao, P.J., Selvam, G., Murthy, P.B. & Reddy, P.N., 2011. Acute inhalation toxicity of cerium oxide nanoparticles in rats. *Toxicol Lett*, 205, 105-15.
- Tsai, Y.Y., Oca-Cossio, J., Lin, S.M., Woan, K., Yu, P.C. & Sigmund, W., 2008. Reactive oxygen species scavenging properties of ZrO₂-CeO₂ solid solution nanoparticles. *Nanomedicine (Lond)*, 3, 637-45.
- Unfried, K.A., Catrin; Klotz, Lars-Oliver; Von Mikecz, Anna; Grether-Beck, Susanne; Schins, Roel P.F., 2007. Cellular responses to nanoparticles: Target structures and mechanisms. *Nanotoxicology*, 1, 52-71.
- Williams, H., Johnson, J.L., Carson, K.G. & Jackson, C.L., 2002. Characteristics of intact and ruptured atherosclerotic plaques in brachiocephalic arteries of apolipoprotein E knockout mice. *Arterioscler Thromb Vasc Biol*, 22, 788-92.

- Xia, T., Kovochich, M., Liong, M., Madler, L., Gilbert, B., Shi, H., Yeh, J.I., Zink, J.I. & Nel, A.E., 2008. Comparison of the mechanism of toxicity of zinc oxide and cerium oxide nanoparticles based on dissolution and oxidative stress properties. *ACS Nano*, 2, 2121-34.
- Xue, Y., Zhai, Y., Zhou, K., Wang, L., Tan, H., Luan, Q. & Yao, X., 2012. The vital role of buffer anions in the antioxidant activity of CeO₂ nanoparticles. *Chemistry*, 18, 11115-22.
- Yokel, R.A., Au, T.C., Macphail, R., Hardas, S.S., Butterfield, D.A., Sultana, R., Goodman, M., Tseng, M.T., Dan, M., Haghazari, H., Unrine, J.M., Graham, U.M., Wu, P. & Grulke, E.A., 2012. Distribution, elimination, and biopersistence to 90 days of a systemically introduced 30 nm ceria-engineered nanomaterial in rats. *Toxicol Sci*, 127, 256-68.
- Yokel, R.A., Tseng, M.T., Dan, M., Unrine, J.M., Graham, U.M., Wu, P. & Grulke, E.A., 2013. Biodistribution and biopersistence of ceria engineered nanomaterials: size dependence. *Nanomedicine*, 9, 398-407.
- Zhang, H., Ji, Z., Xia, T., Meng, H., Low-Kam, C., Liu, R., Pokhrel, S., Lin, S., Wang, X., Liao, Y.P., Wang, M., Li, L., Rallo, R., Damoiseaux, R., Telesca, D., Madler, L., Cohen, Y., Zink, J.I. & Nel, A.E., 2012. Use of metal oxide nanoparticle band gap to develop a predictive paradigm for oxidative stress and acute pulmonary inflammation. *ACS Nano*, 6, 4349-68.

Supplementary information

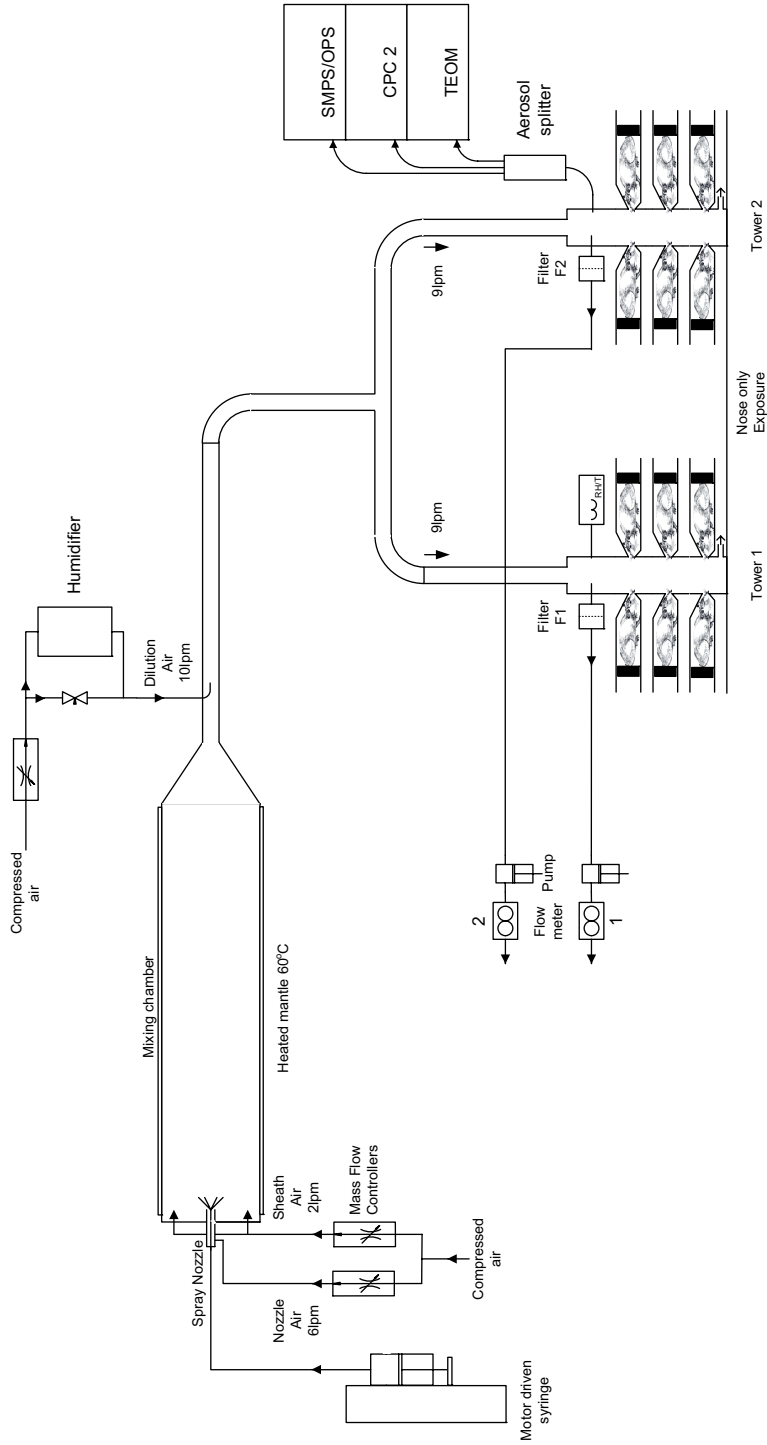


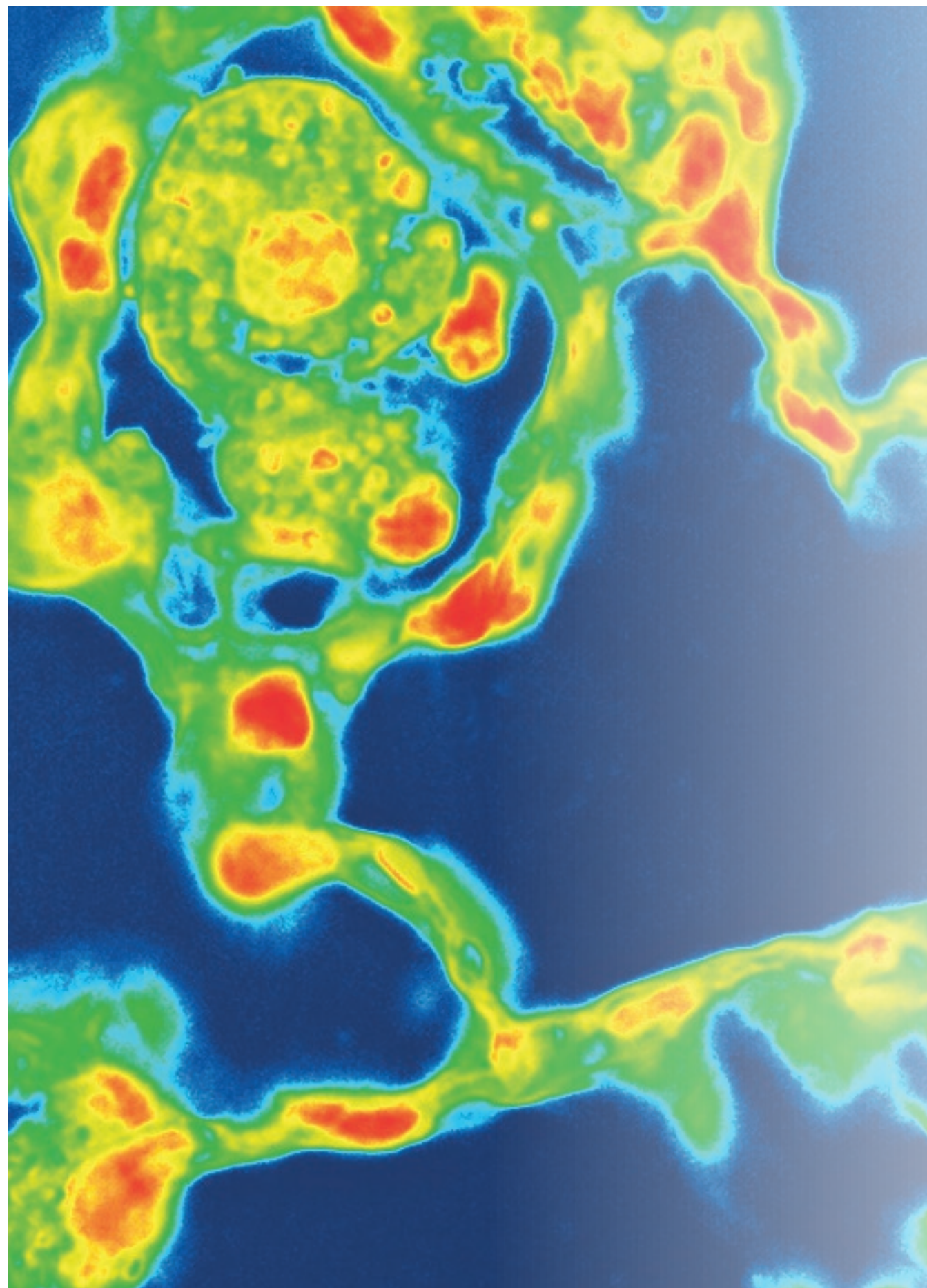
Figure S1: Schematic overview of the exposure set up.

Table S1: Overview of studies performing inhalation of CeO₂ NPs.

Reference	Species and strain	Exposure concentration (mg/m ³)	Exposure duration	Description CeO ₂ NP	Effects ²	Effects observed (days after exposure)
Srinivas <i>et al.</i> , 2011	rat	641 mg/m ³	4h	sol-gel CeO ₂ , 15-30 nm	increased total cell count, neutrophils and lymphocytes, total protein, LDH, ALP, IL-1 β , TNF- α , IL-6 in BAL and decrease cell viability and macrophages in BAL, increase in IL-1 β , TNF- α in blood, increase in MDA and GSA in lung homogenate, particles loaded alveolar macrophages and neutrophils, severe alveolitis, multifocal pulmonary granulomas	1
					increased total cell count, neutrophils and lymphocytes, total protein, LDH, IL-1 β , TNF- α , IL-6 in BAL and decrease cell viability and macrophages in BAL, increase in IL-1 β , TNF- α in blood, increase in MDA in lung homogenate, particles loaded alveolar macrophages and neutrophils in lung and tracheobronchial lymph nodes, severe alveolitis, multifocal pulmonary granulomas	14
					no increased ALP in BALF or GSH in lung homogenate	
Demokritou <i>et al.</i> , 2013	SD rat	2.7 mg/m ³	2h/d for 4d	CeO ₂	increase in polymorphonuclear neutrophils (PMNs), lactate dehydrogenase (LDH) in BAL	1
				CeO ₂ + SiO ₂ coating	no increase in albumin in BAL	1
					no increase in PMNs, LDH or albumin in BAL	
Aalapati <i>et al.</i> , 2014	CD-1 mouse	2 mg/m ³	6h/d 5d/w, 4 wk	sol-gel CeO ₂ , 15-30 nm	increase in BUN and creatinine and neutrophils and decrease in lymphocytes in blood, increased total cell count, macrophages, neutrophils, lymphocytes, total protein, LDH, TNF- α , IL-1 β and IL-6 in BAL, increased levels of MDA and GSH in lung, dark golden brown agglomerations in alveolar space, particle laden macrophages and neutrophils, inflammation, fibrosis and granulomas in the lung, aggregates of particle laden macrophages in mediastinal lymph nodes, lymphoid hyperplasia, enlarged mediastinal lymph nodes, particle laden Kuepfer cells in liver, and renal tubular necrosis	1
					no significant differences in ALP or MIP-2 in BAL compared to controls	
Aalapati <i>et al.</i> , 2014 (continued)	CD-1 mouse	2 mg/m ³	6h/d 5d/w, 4 wk	sol-gel CeO ₂ , 15-30 nm	increase in BUN and neutrophils in blood, increased macrophages, neutrophils, lymphocytes, total protein, TNF- α and IL-1 β in BALF, increased levels in MDA and GSH in lung, although MDA levels were partly recovered, dark golden brown agglomerations in alveolar space, particle laden macrophages and neutrophils, inflammation, fibrosis and granulomas in the lung, aggregates of particle laden macrophages in mediastinal lymph nodes, lymphoid hyperplasia, enlarged mediastinal lymph nodes, particle laden Kuepfer cells in liver, and renal tubular necrosis	28
					no significant differences in creatinine or lymphocytes in blood or total cell count, LDH, ALP, IL-6 and MIP-2 in BAL compared to controls	

Table S1: continued

Reference	Species and strain	Exposure concentration (mg/m ³)	Exposure duration	Description CeO ₂ NP	Effects ²	Effects observed (days after exposure)
		2 mg/m ³			increase in total cell count, lymphocytes, neutrophils, macrophages, LDH, CINC-1, CINC-2 and HO-1 in BAL and macrophage infiltration in alveolar space no neutrophil infiltration in alveolar space or interstitial area, no fibrosis	3
Morimoto <i>et al.</i> , 2015	F344 rat	_____	6h/d, 5d/w, 4wk	Wako, 7.8 nm	increase in neutrophils, LDH, CINC-1, CINC-2 and HO-1 in BAL and macrophage infiltration in alveolar space no increase in total cell count, lymphocytes or macrophages in BAL and no neutrophil infiltration in alveolar space or interstitial area, no fibrosis	1 months
		10 mg/m ³			increase in total cell count, lymphocytes, neutrophils, macrophages, LDH, CINC-1, CINC-2 and HO-1 in BAL and macrophage infiltration in alveolar space no neutrophil infiltration in alveolar space or interstitial area, no fibrosis	3
					increase in neutrophils, LDH, CINC-1, CINC-2 and HO-1 in BAL and macrophage and neutrophil infiltration in alveolar space no increase in total cell count, lymphocytes, macrophages in BAL and no infiltration in interstitial area, no fibrosis	1 months



Chapter 3

Differences in the toxicity of cerium dioxide nanomaterials after inhalation can be explained by lung deposition, animal species and nanoforms

Susan Dekkers¹, Lan Ma-Hock², Iseult Lynch³, Mike Russ⁴, Mark R. Miller⁵, Roel P.F. Schins⁶, Jana Keller², Isabella Römer³, Karin Küttler², Volker Strauss², Wim H. De Jong¹, Robert Landsiedel², Flemming R. Cassee^{1,7}.

Inhalation Toxicology 30(7-8):273-286 (2018)

¹ National Institute for Public Health and the Environment, Bilthoven, The Netherlands,

² Experimental Toxicology and Ecology, BASF SE, Ludwigshafen, Germany,

³ School of Geography, Earth and Environmental Sciences, University of Birmingham, Edgbaston, UK,

⁴ Promethean Particles Ltd., Nottingham, UK,

⁵ Centre for Cardiovascular Science, University of Edinburgh, Edinburgh, UK,

⁶ IUF – Leibniz Research Institute for Environmental Medicine, Düsseldorf, Germany,

⁷ Institute for Risk Assessment Sciences, Utrecht University, Utrecht, The Netherlands

Abstract

Considerable differences in pulmonary responses have been observed in animals exposed to cerium dioxide nanoparticles via inhalation. These differences in pulmonary toxicity might be explained by differences in lung deposition, species susceptibility or physicochemical characteristics of the tested cerium dioxide nanoforms (i.e. same chemical substance, different size, shape, surface area or surface chemistry). In order to distinguish the relative importance of these different influencing factors, we performed a detailed analysis of the data from several inhalation studies with different exposure durations, species and nanoforms, namely published data on NM211 and NM212 (JRC repository), NanoAmor (commercially available) and our published and unpublished data on PROM (industry provided). Data were analyzed by comparing the observed pulmonary responses at similar external and internal dose levels. Our analyses confirm that rats are more sensitive to developing pulmonary inflammation compared to mice. The observed differences in responses do not result purely from differences in the delivered and retained doses (expressed in particle mass as well as surface area). In addition, the different nanoforms assessed showed differences in toxic potency likely due to differences in their physicochemical parameters. Primary particle and aggregate/agglomerate size distributions have a substantial impact on the deposited dose and consequently on the pulmonary response. However, in our evaluation size could not fully explain the difference observed in the analyzed studies indicating that the pulmonary response also depends on other physicochemical characteristics of the particles. It remains to be determined to what extent these findings can be generalized to other poorly soluble nanomaterials.

Introduction

The number and variety of nanomaterials is expected to continue to increase because of the adaptability of their physicochemical properties to enhance their functionality for many different applications. However, manipulating the physicochemical properties of nanomaterials may also lead to undesirable behavior and, possibly, harmful effects in those exposed. A challenge for health risk assessment is the rapidly growing variety of nanomaterials and nanoforms (nanomaterials of the same chemical substance, but with different physicochemical characteristics such as size, shape, surface area and surface chemistry (EC 2017; ECHA 2017)). Thus, in recent years there is an increasing interest in strategies to compare assessments across different nanoforms, including (Quantitative) Structure Activity Relationships, grouping and read-across (Zhang et al. 2012; Stone et al. 2014; Arts et al. 2015; Oomen et al. 2015). A fuller understanding of the influence of basic (physicochemical) properties of nanomaterials on their potential toxicity is needed for further development, validation and specifically implementation of new or revised approaches in health risk assessment (Dekkers et al. 2016).

Recently, we have investigated the influence of zirconium doping of cerium dioxide nanoparticles (CeO_2 NPs) on their biodistribution, pulmonary and cardiovascular effects in mice following inhalation (Dekkers et al. 2017). Sub-acute (4 weeks) inhalation of the undoped CeO_2 NPs (4 mg/m^3 , 3 h/d, 5d/w) resulted in minimal pulmonary and cardiovascular effects in mice 4 weeks post-exposure. Other toxicity studies showed more pronounced effects after exposure to CeO_2 NPs under similar exposure conditions in rats (Geraets et al. 2012; Gosens et al. 2014; Keller et al. 2014; Arts et al. 2016) and mice (Aalapati et al. 2014). Possible explanations for the observed differences in toxicity of CeO_2 NPs after inhalation are: a) differences in kinetics (deposition and clearance) of the CeO_2 NPs, b) differences in the susceptibility of mice compared to rats or c) differences in the toxicity of the different nanoforms of CeO_2 , due to differences in certain physicochemical characteristics such as size, shape and surface chemistry. The objective of the analysis described in this paper is to investigate which of these possible explanations could explain the relatively mild toxicity of the undoped CeO_2 NPs observed in Dekkers et al. (2017) compared to the more pronounced toxicity observed in other inhalation studies.

The importance of toxicokinetics in interpreting pulmonary responses to inhaled NPs has been highlighted by several researchers (Kreyling et al. 2013; Kuempel et al. 2015; Pauluhn 2017). Previous studies, such as Braakhuis et al. (2016), indicate that the internal dose is more predictive of the toxicity of inhaled NPs than the external dose, suggesting that the deposition pattern (i.e. the regions of the respiratory tract in which NPs deposit) determines its interaction with the lung (e.g. lung lining fluid, cellular membranes and fluids), and the subsequent lung clearance and toxicity.

Differences in the susceptibility of different species have been observed in several studies, showing rats to be more susceptible than mice to inhaled TiO₂ NPs and carbon black (Bermudez et al. 2004; Elder et al. 2005; Warheit et al. 2016). This difference has been attributed to differences in the deposition as well as the pulmonary response, especially at concentrations where macrophage-mediated clearance is impaired (pulmonary overload conditions) (Bermudez et al. 2004; Warheit et al. 2016). Since the occurrence of lung tumors under pulmonary overload conditions in rats may not be representative for humans, the use of rats for particle toxicology has been criticized (Warheit et al. 2016). Although pulmonary overload generally occurs at higher exposure concentrations in mice and other experimental animals, there is no consensus as to the most appropriate species to predict particle induced lung toxicity in humans. One major advantage of using mice is the availability of many disease models and relative ease of genetic modification to provide mechanistic insight.

Toxicokinetics and toxicodynamics of inhaled NPs are greatly influenced by their physical characteristics, such as the size and density of the primary particles, aggregates or agglomerates, as well as by their chemical composition, dissolution rate, surface reactivity, shape, charge and hydrophobicity (Nel et al. 2006; Braakhuis et al. 2014; Bakand and Hayes 2016).

To investigate the possible explanation(s) for the discrepancies between the findings of different CeO₂ NP inhalation studies, we have compared the results of exposure to undoped CeO₂ NPs (herein referred to as PROM) from our recent study (Dekkers et al., 2017) to the results of other 4 week inhalation studies with various nanoforms of CeO₂ (referred to as NM212, NM211 and NanoAmor in the subsequent tables and figures) in rats and mice (Geraets et al. 2012; Aalapati et al. 2014; Gosens et al. 2014; Keller et al. 2014). To investigate species differences in the susceptibility to CeO₂ NPs, two additional 5 day inhalation studies using the same undoped CeO₂ NPs as used in Dekkers et al. (2017) (PROM) were performed; one in rats and one in mice to bridge the results from the various studies. These additional studies are not presently published in peer-reviewed journals, but were performed within the NanoMILE project (<http://nanomile.eu-vri.eu/>) under GLP according a short term inhalation study (STIS) protocol, and were included in Deliverable D7.2 (NanoMILE 2017) which is available upon request. The STIS has been specifically designed for the testing of toxicity and kinetics of nanomaterials and has previously been applied for hazard assessment of 13 metal oxide nanomaterials, including the CeO₂ nanoforms NM211 and NM212 (Keller et al. 2014; Landsiedel et al. 2014).

To investigate the origin of the differences in toxicity of the different CeO₂ nanoforms, the results of these 5-day inhalation studies with the PROM CeO₂ NPs were compared to the results of previous 5 day inhalation studies with other nanoforms of CeO₂ (NM212 and NM211) in rats (Keller et al. 2014).

This paper describes the analysis of data from the aforementioned CeO₂ NP inhalation studies to investigate to what extent the observed differences in toxicity between various studies can be explained by differences in kinetics, species susceptibility and/or physicochemical characteristics of the nanoforms.

We hypothesized that a lower internal dose and higher clearance of the CeO₂ NPs might explain the relatively mild effects observed 4 weeks post-exposure in our recent study (Dekkers et al. 2017). We also hypothesized that, similar to other poorly soluble particles (such as TiO₂ NPs and carbon black), rats would be more susceptible to exposure to CeO₂ NPs than mice. Lastly, based on the mild toxicity of PROM CeO₂ NPs observed in mice, we hypothesized that PROM CeO₂ NPs would also be less toxic compared to other nanoforms of CeO₂ NPs in rats.

Materials and methods

Selection of the Studies

The selected studies were limited to those where rats or mice were exposed via inhalation (either whole body or nose only) and in which the pulmonary toxicity as well as pulmonary dose (i.e. lung burden) were determined. Studies in which rats and mice were exposed for 4 weeks as well as for 5 days were selected because not all nanoforms of CeO₂ were tested in 4 week inhalation studies in both species. An overview of the inhalation studies that were analyzed can be found in Table 1. A summary of the pulmonary findings of these inhalation studies can be found in Table S1 of the supplementary information, and further details on the 5-day inhalation studies with the PROM CeO₂ NPs can be found in Table 4 and Annex S2.

From External Concentration to Internal Lung or Pulmonary Burden

To investigate the role of kinetics in pulmonary toxicity of CeO₂ NPs, toxicity data of the studies was compared using a) the external exposure concentration, b) the internal retained dose in the lung (i.e. the measured lung burden) and c) the predicted internal retained dose in the pulmonary or alveolar regions of the lung (i.e. the expected pulmonary burden). In all studies, the rats or mice were exposed to CeO₂ NPs at concentrations between 0.5 and 25 mg/m³ with similar particle size distributions (mass median aerodynamic diameter (MMAD) between 0.9 to 2.2 μm).

The measured lung burden (LB) was calculated from the measured Ce concentrations in the lung tissue (typically determined by ICP-MS) and total lung weight. For those studies in which no lung and body weights were reported (Aalapati et al. 2014; Keller et al. 2014), an estimation of the lung weight was made based on the lung weights of animals of the same strain and similar ages.

Table 1: Overview of the selected CeO₂ NP inhalation toxicity studies.

Reference	Strain, species and sex of animals	Nanoform	Aerosol conc. (mg/m ³) ^a	MMAD ± GSD (µm)	Exposure method ^b	Exposure duration (h/d)	Exposure duration (days)	Post-exposure period (weeks)
Keller et al., 2014	Wistar rats, female	NM211	0.45	1.9 ± 2.9	WB	6	5	3
			25.8	2.2 ± 2.4				
Keller et al., 2014	Wistar rats, female	NM212	0.5	1.4 ± 2.3	WB	6	5	3
			5.3	1.2 ± 2.1				
NanoMILE, 2017	Wistar rats, male	PROM	25.9	1.0 ± 2.5	NO	6	5	3
			0.57	1.3 ± 2.2				
Keller et al., 2014	Wistar rats, male	NM212	2.04	1.2 ± 2.4	WB	6	20	5
			4.85	1.1 ± 1.3				
Geraerts et al., 2012	Wistar rats, male + female	NM211	0.48	1.6 ± 2.1	NO	6	20	4
			5.2	1.3 ± 2.1				
Geraerts et al., 2012	Wistar rats, male + female	NM212	25.6	0.9 ± 2.5	NO	6	20	4
			10.8	1.0 ± 1.8				
NanoMILE, 2017	C57BL/6 J mice, male	PROM	19.95	1.2 ± 2.1	NO	6	20	4
			0.54	1.1 ± 2.5				
Dekkers et al., 2017	C57BL/6 J mice, female	PROM	2.04	1.1 ± 2.4	NO	3	20	4
			5.04	0.9 ± 3.0				
Aalipati et al., 2014	CD-1 mice, male	NanoA-mor	3.98	0.3 ± 1.6c	NO	6	20	2 and 4

^a These aerosol concentrations are rounded to 0.5, 2, 5, 10, 20 and 25 mg/m³ in the main text.

^b WB = whole body. NO = nose only.

^c Mass median diameter (MMD) instead of MMAD, estimated based on the particle size distributions of the scanning mobility particle sizer (SMPS) measurements, assuming spherical aggregation around primary particles of 4.7 nm. MMAD=mass median aerodynamic diameter. GSD=geometric standard deviation.

To verify if the different methods used to measure the LB resulted in comparable results, the anticipated LB was also estimated using the Multiple-Path Particle Dosimetry Model (MPPD V3.04, Applied Research Associates, Inc., <https://www.ara.com/products/multiple-path-particle-dosimetry-model-mppd-v-304>). The chosen MPPD airway morphometry model and input data used to estimate the retained dose in the lung of the studies can be found in Table S3 of the supplementary information. For all studies the “deposition and clearance” option of the MPPD model was used to estimate the tracheobronchial retention (TBR) and the alveolar retention (AR). The density of the bulk material of CeO₂ (7.215 g/m³) was used

as input parameter as no information is available of the density of CeO₂ nanoforms occurring in the aerosols. Default settings were used unless stated otherwise.

The estimated LB was calculated using the following formula:

$$\text{Estimated LB } (\mu\text{g/g}) = \frac{\text{TBR}(\mu\text{g}) + \text{AR}(\mu\text{g})}{\text{Lung weight (g)}}$$

The expected pulmonary burden (PB) was expressed as the surface area of the NPs per surface area of the pulmonary region of the lung (mm² NP/cm² lung) instead of μg NP/g lung, based on the findings of Braakhuis et al. (2016). PB was calculated using the measured LB, the fraction of deposition in the alveolar region of the lung (AD), the total deposition in the lung (alveolar deposition + tracheobronchial deposition; AD+TBD) (as estimated with the MPPD model), the surface area of the NPs (SA_{NP}; estimated using the reported BET measurement or calculated based on primary particle size) and the surface area of the pulmonary region of the lung (SA_{PR}; estimated with the MPPD model). The data used to calculate the PB of the selected studies can be found in Table S4 of the supplementary information. The PB was calculated using the following formula:

$$\text{PB (mm}^2/\text{nm}^2) = \frac{\text{LB (\#)} \times \frac{\text{AD (\%)}}{(\text{AD(\%)} + \text{TBD(\%)})} \times \text{SA}_{\text{NP}} (\text{m}^2)}{\text{SA}_{\text{PR}} (\text{cm}^2)}$$

To investigate if differences in LB or PB might explain the differences in toxicity, bronchoalveolar lavage fluid (BALF) and histopathological analyses of the studies were quantitatively compared using the measured exposure concentration (mg NP/m³ air), LB (μg NP/g lung) and PB (mm² NP/cm² lung). A quantitative comparison of the effects on the BALF analyses among the studies was considered appropriate, since all studies used a similar method for lung lavage (2 lavages with a similar volume of saline solution). Alveolar histiocytosis (accumulation and infiltration of monocytes and macrophages in the pulmonary tissues) and increased neutrophil counts in BALF were also plotted against the exposure concentration, LB and PB to further examine dose response relationships, as these parameters were observed in most studies and are frequently identified as first evidence of adversity (Pauluhn 2017).

Differences in Susceptibility

To investigate species differences in susceptibility to the inflammatory effects induced by CeO₂ NPs, and differences in toxicity between PROM CeO₂ NPs and NM212, data from the two additional 5-day inhalation studies with the PROM CeO₂ NPs in rats and mice (see Table 4 and Annex S2) were compared.

Statistical Analyses

GraphPad Prism v7.00 (GraphPad Software, San Diego, California, USA) was used to visualize and to analyze the data using linear regression analysis of the measured versus the estimated LB and non-linear regression analysis (curve-fitting) of the dose response curves using the various dose metrics.

Results and Discussion

Internal Lung and Pulmonary Burden

An overview of the measured and estimated LB and expected PB from the selected CeO₂ NP inhalation studies can be found in Table 2. Expressing the LB relative to the total lung weight and PB relative to the total surface area of the lung might lead to an underestimation of the LB and PB if exposure to the CeO₂ NPs also significantly increase the lung weight and/or the lung surface area. However, expressing the absolute LB and PB levels does not allow comparison of LB and PB levels of different studies, due to species, strain, age and bodyweight differences of the animals. Approximately 9 to 18% of the inhaled (mass) dose was predicted to deposit in the lungs, of which between 50 and 70% was expected to deposit in the pulmonary region of the lung (see Table S4 in the supplementary information). The measured LB was lower than the estimated LB at nearly all exposure concentrations. This overestimation of the LB by the MPPD models might be due to an underestimation of the clearance rates or an overestimation of the deposition. The clearance rates of the MPPD model are based on LB measurements from studies in which various strains of rats (F344) and mice (BALB/C and B6C3F1) were exposed to various micro- and nanosized particles (TiO₂, C60-fullerenes and Fe_xO_y) at various concentrations (0.5, 2, 10 and 20 mg/m³), exposure durations (4 h and 13 weeks) and recovery periods (0 and 6 h, 1 day, and 2, 4, 8, 13, 26 and 52 weeks). The animal strains (Wistar rats, C57Bl/6 J and CD-1 mice), NPs (CeO₂ NPs), concentrations (0.5, 2, 5, 10, 20 and 25 mg/m³), exposure duration (5 days and 4 weeks) and recovery periods (0 days and 3-5 weeks) of the selected studies only partly overlap with those on which the clearance rates of the MPPD model are based. Therefore, the high LBs estimated by the MPPD model indicate that the clearance rates might have been underestimated by the MPPD model, especially for the mice. Additionally, the deposition may have been overestimated. Next to differences in strains, concentrations and exposure durations between the selected studies and the studies on which the deposition in the MPPD model is based, also other assumptions may have led to an overestimation of deposition. For example, the model assumes spherical aerosols, while aerosols of NPs generally consist of non-spherical agglomerates of (spherical or nearly-spherical) primary particles, which tend to have a lower density than (solid) spherical particles of the same diameter. An overestimation of the density might lead to an overestimation of the amount deposited in the lungs.

Differences due to Deposition and Clearance

To investigate to what extent the differences in toxicity may be explained by differences in pulmonary deposition and clearance of the CeO₂ NPs, the LB and PB of several 4 week inhalation studies with various nanoforms of CeO₂ (NM211, NM212, PROM and NanoAmor) in rats and mice are compared. A comparison of the measured and estimated LB in rats and mice after 4 weeks of exposure to CeO₂ is presented in Figure 1.

Table 2: Measured and estimated lung burden and expected pulmonary burden of the selected inhalation studies.

Reference	Species	CeO ₂ nanoform	Exposure concentration (mg/m ³) ^a	Exposure duration	Estimated fraction of inhaled dose deposited in the lung (%)	Lung burden 0 days after exposure (µg/g lung)			Expected pulmonary burden 0 days after exposure (mm ³ /cm ³ lung) ^d	Lung burden 3 to 5 weeks after exposure (µg/g lung)		Expected pulmonary burden 3-5 weeks after exposure (mm ³ /cm ³ lung) ^d
						Estimated ^b	Estimated ^c	Measured		Estimated ^c	Measured	
Keller et al., 2014	rats	NM211	0.45	5 days	9.8	17	11	6	0.07	5	3	0.04
			25.8	5 days	9.4	942	522	269	2.8	327	206	2.6
Keller et al., 2014	rats	NM212	0.5	5 days	11.6	23	13	11	0.06	7	5	0.03
			5.3	5 days	14.3	295	170	96	0.54	96	70	0.47
			25.9	5 days	16.2	1640	997	510	3.0	647	317	2.3
NanoMILE, 2017	rats	PROM	0.57	5 days	10.3	32	17	11	0.38	8	7	0.3
			2.04	5 days	10.8	120	71	36	1.4	44	30	1.3
			4.85	5 days	12.0	310	179	79	2.9	94	63	3.5
Keller et al., 2014	rats	NM212	0.48	4 weeks	10.7	76	33	37	0.22	15	18	0.12
			5.2	4 weeks	13.1	1005	508	473	2.8	319	444	3.0
			25.6	4 weeks	17.8	6735	4053	2382	15	3033	1960	14
Geraerts et al., 2012	rats	NM211	10.8	4 weeks	14.8	3281	1494	639	6.8	1177	x	x
Geraerts et al., 2012	rats	NM212	19.9	4 weeks	13.0	5592	2776	1260	4.9	2334	x	x
NanoMILE, 2017	mice	PROM	0.54	5 days	10.7	46	29	6	0.23	12	4	0.14
			2.04	5 days	10.6	183	116	18	0.61	44	9	0.32
			5.04	5 days	12.8	522	338	60 ^e	2.1 ^e	144	29	0.94
Dekkers et al., 2017	mice	PROM	3.98	4 weeks	11.5	749	341	x	x	103	82	3.4
Aalipati et al., 2014	mice	NanoAmor	2.0	4 weeks	9.3	405	171	1353	17	52	615	7.9

^a These aerosol concentrations are rounded to 0.5, 2, 5, 10, 20 and 25 mg/m³ in the main text.

^b Estimated with the MPPD model V3.04 (deposition only).

^c Estimated with the MPPD model V3.04 (deposition and clearance).

^d Calculated using the measured lung burden, estimated pulmonary deposition fractions and estimated surface area of the pulmonary region of the lung, as described in the materials and methods section.

^e Estimated using the measured lung burden 21 days after exposure and the expected clearance (≈50%). The measured lung burden 0 days after exposure (of 495 µg/g lung) was considered unreliable, and was probably a preparation artefact (e.g. big bronchus included in the sample). x=no data available.

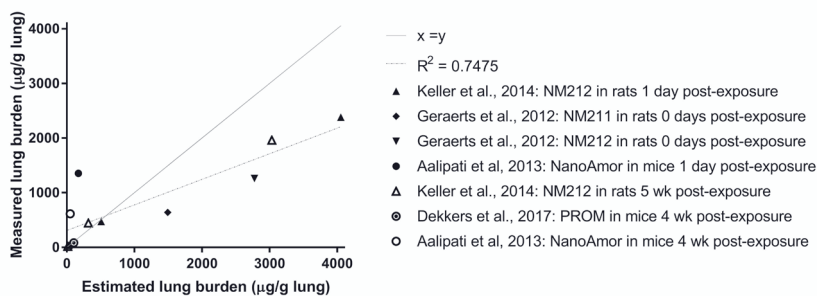


Figure 1: Measured lung burden plotted against the estimated lung burden in rats and mice after 4 weeks of exposure to various CeO₂ NPs (NM211, NM212, PROM and NanoAmor). The estimated lung burden was assessed using the MPPD V3.04 model.

The measured LB correlated well ($R^2=0.75$) with the estimated LB (Figure 1), although this correlation was dominated by studies in rats. The measured LB was mostly lower or similar than the estimated LB, except for mice exposed to 2 mg/mm³ NanoAmor for which the measured LB was approximately 10 times higher than estimated (see black and white dot in Figure 1). There was no consistent relationship between the exposure concentration or particle diameter and the percentage of clearance ($R^2<0.5$; data not shown).

Subsequently, it was investigated whether the differences in toxicity observed in the different 4 week inhalation studies with various nanoforms of CeO₂ in rats and mice can be explained by differences in toxicokinetics (LB and PB). Therefore, a quantitative comparison was performed of the markers for toxicity (BALF and histopathological analyses) using external as well as internal concentrations expressed in two different dose metrics (Table 3 and Figure 2). All but one study found aggregates of particles and macrophages in the lungs, whereas only one study (in which rats were exposed to NM212) demonstrated an increase in the presence of eosinophilic material, interpreted to be indicative of cell damage. Granulomatous inflammation, indicative of macrophage mediated inflammation, was noted in only two studies (in which rats were exposed to NM212 and mice to NanoAmor). More importantly, neutrophilic inflammation was observed in all studies. The severity of the pulmonary toxicity (alveolar histiocytosis in 20% of the animals) observed in mice 4 weeks post-exposure to PROM CeO₂ NPs (Dekkers et al. 2017) was remarkably less than the severity of the pulmonary toxicity (increase in neutrophils and lymphocytes in BALF, alveolar histiocytosis in 100% of the animals and the occurrence of eosinophilic granular material, macrophage aggregates with particles and granulomatous inflammation) observed in the other 4 week inhalation studies at similar or even lower external and internal concentrations (i.e. in rats exposed to NM211 and NM212 and mice exposed to NanoAmor). These findings indicate that differences in toxicity cannot be explained by differences in toxicokinetics alone.

When the toxicological effects were expressed as percentages of neutrophils in the BALF at each exposure concentration, non-linear curve fitting did not provide a suitable fit ($R^2=0.57$

and 0.48; Figure 2a). Non-linear curve fitting was improved by plotting % neutrophils against internal dose, for the measured LB ($R^2= 0.70$ and 0.96 ; Figure 2c) but not for the PB ($R^2=0.55$ and 0.56 ; Figure 2e). However, since the LB of the Aalapati study was approximately 10 times higher than the estimated LB (Figure 1 and Table 2), the LB and PB of this study could be considered as outliers. Without the data of the Aalapati study, the non-linear curve fitting led to better goodness of fit values for both the LB ($R^2=0.71$ and 0.97) and PB ($R^2=0.75$ and 0.71) compared to the exposure concentration ($R^2=0.66$ and 0.52). Although these curve fitting analyses did not indicate whether LB ($\mu\text{g/g}$ lung) or PB (mm^2/cm^2) is a better predictor for the observed toxicity, they are in line with previous studies that indicated that the internal dose was more predictive of the toxicity of inhaled NPs than the external dose (Kreyling et al. 2013; Kuempel et al. 2015; Braakhuis et al. 2016; Pauluhn 2017). Nevertheless, the differences in toxicity may to some extent also be explained by differences in susceptibility between mice and rats exposed to similar internal dose levels and/or differences in toxicity between the various nanoforms of CeO_2 .

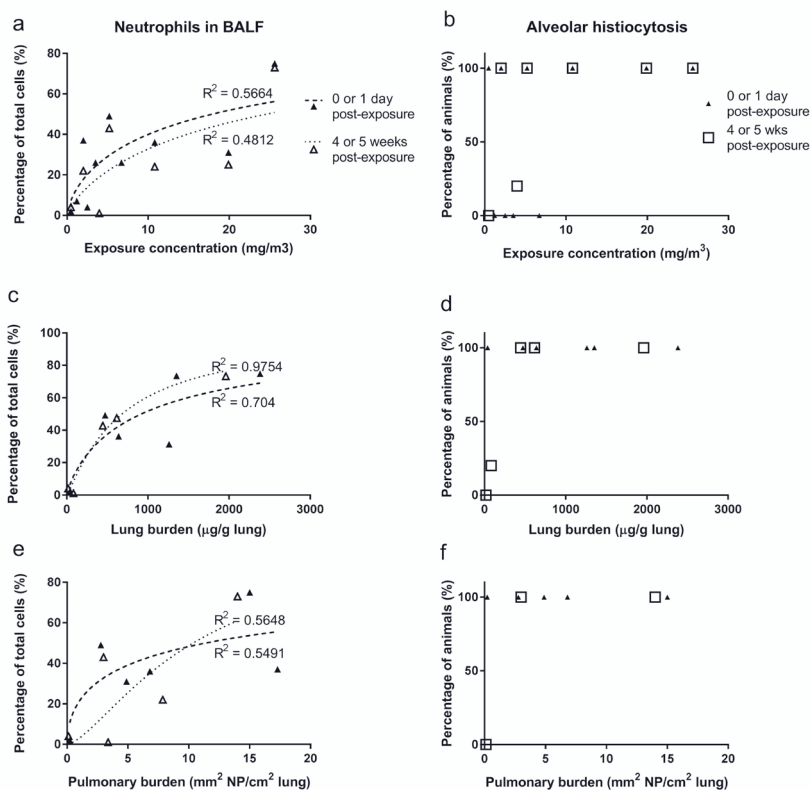


Figure 2: The percentage of neutrophils in the BALF (a, c, and e) and the percentage of animals with alveolar histiocytosis (b, d, and f) after 4 weeks of exposure to various CeO_2 NPs plotted against the measured exposure concentration ($\text{mg NP}/\text{m}^3$ air) (a and b), lung burden ($\mu\text{g NP}/\text{g}$ lung) (c and d) and expected pulmonary burden ($\text{mm}^2 \text{NP}/\text{cm}^2$ lung) (e and f). Data from all 4 week inhalation studies in rats and mice with various nanoforms of CeO_2 (NM211, NM212, PROM and NanoAmor, as described in Table 3) were used.

Table 3: Comparison of pulmonary effects in rats and mice after 4 weeks of exposure to various CeO₂ NPs (NM211, NM212, NanoAmor and PROM).

Reference	Nanoform of CeO ₂ NP	Species	Measured exposure concentration (mg/m ³) ^a	Lung burden (µg/g lung)	Pulmonary burden (mm ² /cm ² lung) ^b	BALF analysis (statistically significant difference compared to the controls)	Neutrophils in BALF (% total cells)	Alveolar histiocytosis (% of animals)	Eosinophilic granular material	Macrophage aggregates with particles	Granulomatous inflammation
0-1 days after exposure											
Keller et al. (2014)	NM-212	rats	0.48	37	0.22	-	2.3%	100%	-	+	-
	NM-212	rats	5.2	473	2.8	increased TC, NEU, LYM and MON	49%	100%	+	+	-
	NM-212	rats	25.6	2382	15	increased TC, NEU, LYM and MON	75%	100%	+	+	-
Gerearts et al. (2012) Gosens et al. (2014)	NM-211	rats	10.8	639	6.8	increased TC, NEU, LYM and MAC	36%	100%	-	+	-
	NM-212	rats	19.9	1260	4.9	increased TC, NEU, LYM and MAC	31%	100%	-	+	-
Aalapati et al. (2014)	NanoAmor	mice	2.0	1353	17	increased TC, NEU, LYM and MAC	74%	100%	-	+	+
3-5 weeks post-exposure											
Keller et al. (2014)	NM-212	rats	0.48	18	0.12	-	4%	0%	-	+	-
	NM-212	rats	5.2	444	3.0	increased NEU, LYM and MON	43%	100%	+	+	-
	NM-212	rats	25.6	1960	14	increased TC, NEU, LYM and MON	73%	100%	+	+	+
Dekkers et al. (2017)	PROM	mice	4.0	82	3.4	-	1.1%	20%	-	-	-
Aalapati et al. (2014)	NanoAmor	mice	2.0	615	7.9	increased NEU, LYM and MAC	48%	100%	-	+	+

^a These aerosol concentrations are rounded to 0.5, 2, 5, 10, 20 and 25 mg/m³ in the main text. ^b Calculated using the measured lung burden, estimated pulmonary deposition fractions and an estimated surface area of the pulmonary region of the lung, as described in the materials and methods section. TC=total cell count, NEU=neutrophils, LYM=lymphocytes, MON=monocytes, MAC=macrophages, +=increased incidence compared to the controls, -=no increased incidence compared to the controls.

Difference in Susceptibility between Mice and Rats

To further investigate differences in the susceptibility of mice compared to rats, two additional 5 day inhalation studies with the same nanoform of CeO₂ (PROM) were performed; one in mice and one in rats. These additional studies are not presently published in peer-reviewed journals, but were performed within the NanoMILE project (<http://nanomile.eu-vri.eu/>) under GLP and were included in Deliverable D7.2 which is available upon request (NanoMILE 2017). The study design of these additional studies with PROM CeO₂ NPs follow the previously performed 5 day inhalation studies with NM212 (Keller et al. 2014), but used nose-only exposure instead of whole body exposure, to allow better comparison with the 4 week inhalation study with PROM CeO₂ NPs in mice (Dekkers et al. 2017). Animals were exposed to similar concentrations of CeO₂ NPs (0.5, 2 and 5 mg/m³) with similar particle size distributions (MMAD between 1.0 and 1.3 µm for rats and between 0.9 and 1.2 µm for mice). A detailed description of these studies can be found in Annex S2 of the supplementary information.

In male Wistar rats, exposure to PROM CeO₂ NPs led to changes of several BALF parameters, including increased neutrophils, in animals exposed to 2 mg/m³ and 5 mg/m³ CeO₂ NPs (Table 4), the effects of which were still observed 3 weeks post-exposure. At these concentrations, the number of neutrophils was also increased in blood, as were blood monocyte counts. These findings indicate that inflammation in the lungs was persistent, and was accompanied by systemic inflammation. Histopathological findings after the recovery period were only observed at 5 mg/m³. The findings were consistent with a retarded lung clearance after 2 and 5 mg/m³ CeO₂ NP exposure.

In mice, exposure to PROM CeO₂ NPs up to 5 mg/m³ did not lead to any significant change in clinical pathology parameters in blood and in BALF, or treatment-related adverse effects based on histopathology in mice. These findings were consistent with the higher clearance in mice (approximately 30 to 50 % in 3 weeks) compared to rats (approximately 20 to 35 % in 3 weeks).

The measured LB of the two 5 day inhalation studies was much lower than the estimated LB, but showed a high correlation with the estimated LB (R²=0.93 for rats and R²=0.91 for mice; Figure 3). The high LBs estimated by the MPPD model indicate that some of the assumptions made by the MPPD model may not necessarily reflect the reality for the rats and mice in the selected studies and that the assumed clearance rate might have been underestimated by the MPPD model, especially in mice.

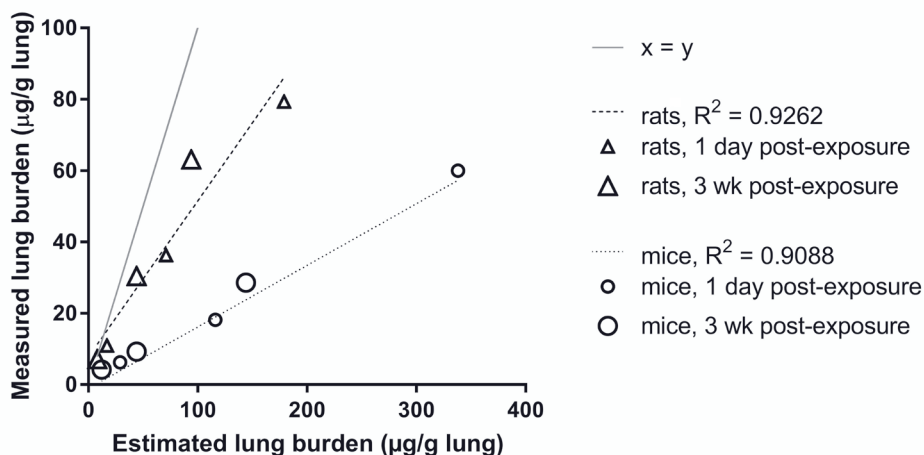


Figure 3: Measured lung burden plotted against the estimated lung burden in rats and mice after 5 days of exposure to PROM CeO₂ NPs. The estimated lung burden was determined using the MPPD model.

The LB and PB was higher in rats compared to mice, especially 3 weeks post-exposure, an effect that is probably due to the higher clearance rates in mice compared to rats. To investigate if the modest toxicity of the PROM CeO₂ NPs can be explained by the species difference in toxicokinetics, a quantitative comparison of pulmonary effect parameters was performed using external as well as internal concentrations (Table 4 and Figure 4). Similar to the curve fitting analyses of the 4 week inhalation studies (Figure 2c and e), the curve fitting analyses of the 5 day inhalation studies with PROM CeO₂ NPs in rats and mice (Figure 4c and e) did not indicate whether LB ($\mu\text{g/g lung}$) or PB (mm^2/cm^2) is a better predictor for the observed toxicity. The differences in internal concentration (LB and PB) cannot fully explain the differences in the severity of the toxicological effects, since changes in BALF and adverse histopathological effects were observed at lower LB and PB levels in rats compared to mice. Furthermore, the dose response curves are steeper in rats compared to mice, indicating PROM CeO₂ NPs are more toxic to rats compared to mice (see Figure 4). This indicates that besides differences in kinetics (resulting in differences in LBs and PBs) between mice and rats, there are other differences in susceptibility between these species. This is in line with outcomes from previous studies in which rats tended to be more susceptible to pulmonary inflammation induced by poorly soluble particles (Bermudez et al. 2004; Borm et al. 2015; Warheit et al. 2016). There are no *in vitro* studies available that compare the toxicity of CeO₂ NPs in mice and rat macrophages. However, the sensitivity of rat alveolar macrophages to various NPs has recently been tested in an *in vitro* assay to predict short-term inhalation of NPs. All four CeO₂ NPs tested in this study (including NM211 and NM212) showed a dose dependent cytotoxicity and were identified as being biologically active in rat alveolar macrophages (Wiemann et al. 2016).

Table 4: Comparison of effects in rats and mice after 5 day exposure to the same CeO₂ NPs (PROM).

Reference	Nanoform of CeO ₂ NP	Species	MMAD (µm)	GSD	Measured exposure concentration (mg/m ³) ^a	Lung burden (µg/g lung)	Pulmonary burden (mm ² /cm ² lung) ^b	BALF analysis (statistically significant difference compared to the controls)	Neutrophils in BAL (% total cells)	Alveolar histiocytosis (% of animals)	Eosinophilic granular material	Macrophage aggregates with particles
0 days after exposure												
NanoMILE, 2017	PROM	mice	1.1	2.5	0.54	6.2	0.23	-	0.1%	0%	-	+
NanoMILE, 2017	PROM	rats	1.3	2.2	0.57	11	0.38	-	5%	0%	-	+
NanoMILE, 2017	PROM	mice	1.1	2.4	2.04	18	0.61	-	0%	0%	-	+
NanoMILE, 2017	PROM	rats	1.2	2.4	2.04	36	1.4	increased TC and NEU	7%	0%	-	+
NanoMILE, 2017	PROM	mice	0.9	3.0	5.04	60 ^c	2.1 ^c	-	0.1%	0%	-	+
NanoMILE, 2017	PROM	rats	1.1	2.3	4.85	79	2.9	increased TC, NEU, MON and EPI	25%	0%	-	+
3 weeks after exposure												
NanoMILE, 2017	PROM	mice	1.1	2.5	0.54	4.2	0.14	-	0.2%	0%	-	+
NanoMILE, 2017	PROM	rats	1.3	2.2	0.57	7.1	0.30	-	2%	0%	-	+
NanoMILE, 2017	PROM	mice	1.1	2.4	2.04	9.2	0.32	-	0.2%	0%	-	+
NanoMILE, 2017	PROM	rats	1.2	2.4	2.04	30	1.3	increased TC and MON	9%	20%	-	+
NanoMILE, 2017	PROM	mice	0.9	3.0	5.04	29	0.94	-	0.7%	0%	-	+
NanoMILE, 2017	PROM	rats	1.1	2.3	4.85	63	3.5	increased TC, NEU, MON, LYM and MAC	50%	100%	+	+

^a These aerosol concentrations are rounded to 0.5, 2 and 5 mg/m³ in the main text. ^b Calculated using the measured lung burden, estimated pulmonary deposition fractions and an estimated surface area of the pulmonary region of the lung, as described in the materials and methods section. ^c Estimated using the measured lung burden 21 days after exposure and the expected clearance based on other dose levels (≈50%). The measured lung burden 0 days after exposure (of 495 µg/g lung) was considered unreliable, and was probably a preparation artefact (e.g. big bronchus included in the sample). TC=total cell count, NEU=neutrophils, LYM=lymphocytes, MON=monocytes, MAC=macrophages, +=increased incidence compared to the controls, -=no increased incidence compared to the controls.

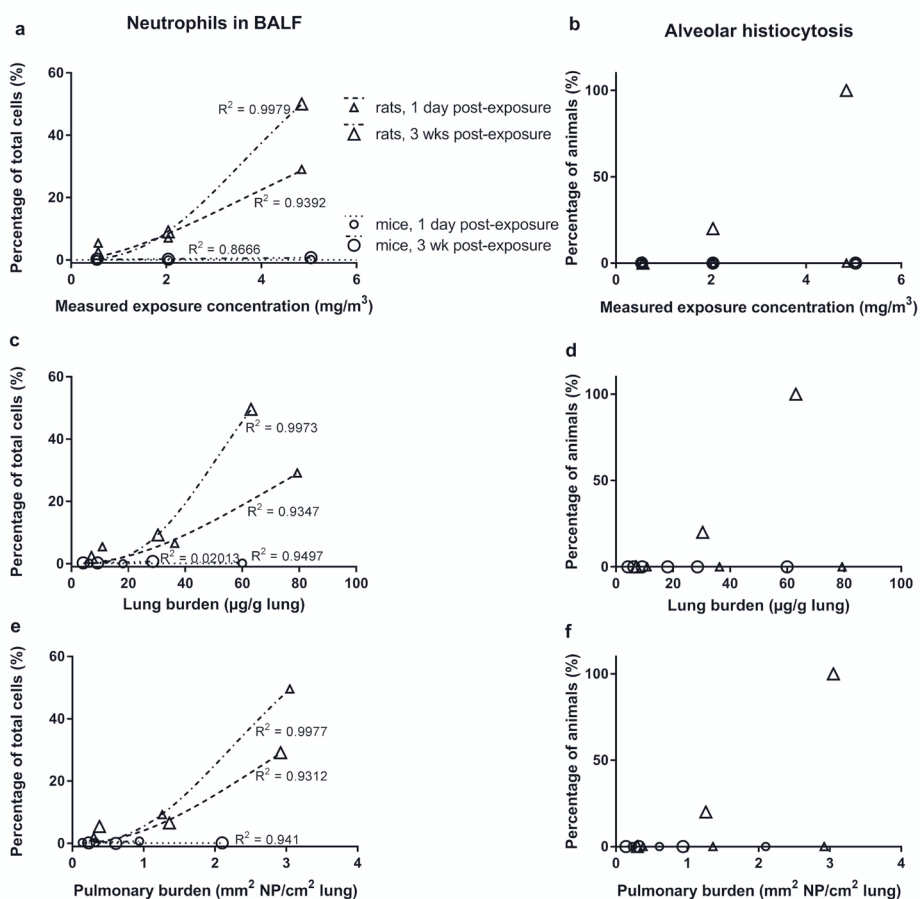


Figure 4: The percentage of neutrophils in the BALF (a, c, and e) and the percentage of animals with alveolar histiocytosis (b, d, and f) after 5 days of exposure of rats and mice to PROM CeO_2 NPs plotted against the measured exposure concentration ($\text{mg NP}/\text{m}^3$ air) (a and b), lung burden ($\mu\text{g NP}/\text{g}$ lung) (c and d) and expected pulmonary burden ($\text{mm}^2 \text{ NP}/\text{cm}^2$ lung) (e and f).

Differences due to Different Nanoforms

To investigate differences in toxicity between the different CeO_2 nanoforms, data from all 5 day inhalation studies in rats with NM211, NM212 and PROM were compared using exposure concentration, LB and PB and dose matrices. The measured LB was lower than the estimated LB but showed a strong correlation ($R^2=0.99$, Figure 5).

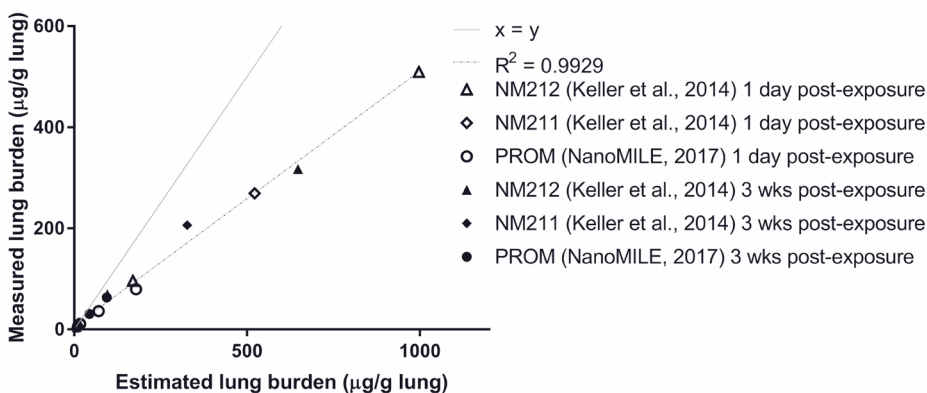


Figure 5: Measured lung burden plotted against the estimated lung burden in rats after 5 days of exposure to various CeO₂ NPs (NM211, NM212 and PROM). The estimated lung burden was determined using the MPPD model.

Exposure to PROM CeO₂ NPs resulted in relatively high PB levels compared to NM211 and NM212 at similar exposure concentrations (Table 5 and Figure 6). This difference in PB in rats is probably caused by differences in clearance, since the measured LB levels and the estimated fractions of the inhaled dose deposited in the lung and pulmonary region of the lung were largely similar across the different CeO₂ nanoforms (see Table S4). Clearance of particles deposited in the lungs is known to depend mainly on the dose, size, shape and dissolution rate of primary particles and their aggregates and agglomerates (Greim and Ziegler-Skylakakis 2007; Keller et al. 2014). Previous studies investigating the influence of particle size on the clearance have either found no influence of particle size on clearance (Semmler et al. 2004; Buckley et al. 2017) or a slower clearance of smaller particles (Geraets et al. 2012; Keller et al. 2014; Han et al. 2015). Indeed, the nanoforms with the smallest primary particle size (PROM: 4.7 nm) seem to have a slower clearance than the larger nanoforms (NM211: 12.5 nm and NM212: 40 nm; see Table S4 and S5 of supplementary information). However, the size of the aerosols has only a modest influence on the clearance rate, with the largest aerosols (NM211) showing a slightly higher clearance rate at all exposure concentrations compared to nanoforms with a smaller MMAD (NM212 and PROM) (see Table S4 and S5 of supplementary information).

To investigate if differences in toxicokinetics across the various nanoforms of CeO₂ might explain the differences in toxicity, a quantitative comparison of parameters measured in BALF as well as histopathological analyses were performed using external as well as internal concentrations of NM211, NM212 and PROM (Table 5 and Figure 7). Similar to the curve fitting analyses of the 4 week inhalation studies (Figure 2c and e) and the 5 day inhalation studies with PROM CeO₂ NPs in rats and mice (Figure 4c and e), curve fitting analyses of the 5 day inhalation studies in rats with the various CeO₂ NPs (Figure 7c and e) did not indicate

whether LB ($\mu\text{g}/\text{g}$ lung) or PB (mm^2/cm^2) is a better predictor for the observed toxicity. More data is needed to investigate the best dose metric.

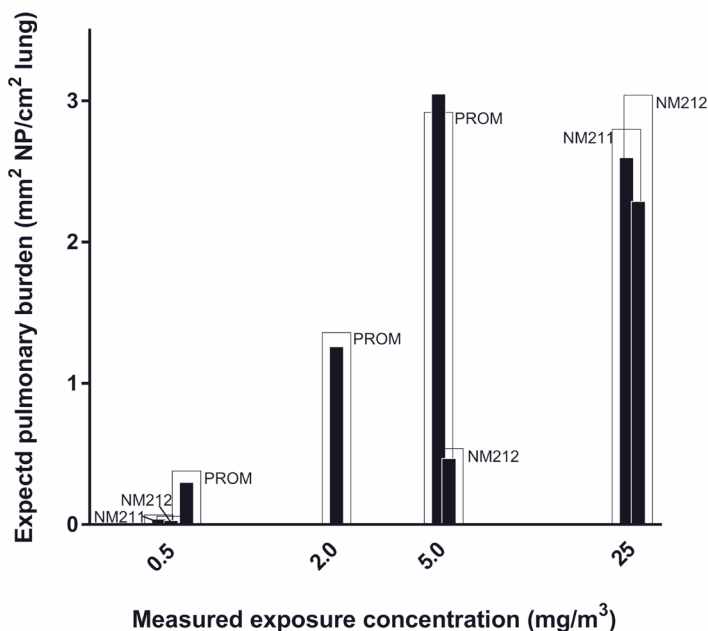


Figure 6: Expected pulmonary burden plotted against the measured exposure concentration in rats after 5 days of exposure to various CeO₂ NPs. Each bar represents the expected pulmonary burden either 1 day (white bars) or 3 weeks (black bars) after exposure to a specific exposure concentration of NM211, NM212 or PROM CeO₂ NPs.

Besides differences in toxicokinetics of CeO₂ NPs (resulting in differences in LB and PB), differences in the toxicodynamics (i.e. toxic potency) of the different nanoforms of CeO₂ may account for the observed differences in toxicity. Immediately after exposure (day 0) more severe changes in BALF parameters and lung histopathology were observed at lower exposure concentrations, LB and PB levels of NM211 and NM212 compared to PROM CeO₂ NPs (Table 5). This indicates that PROM CeO₂ NPs are less toxic than NM211 and NM212 when expressed as external concentration (mg NP/m³ air), internal mass dose (μg NP/g lung), or internal surface area dose (mm^2 NP/cm² lung). Three weeks after exposure, more severe changes in BALF parameters and lung histopathology were observed after exposure to PROM CeO₂ NPs compared to NM212 at certain exposure concentrations (e.g. 5 mg/m³) or LBs (60-70 μg NP/g lung). However, similar effects on BALF parameters and lung histopathology were observed at similar PB levels for all different nanoforms, indicating a similar toxic potency of all nanoforms when the dose is expressed as internal surface area (mm^2 NP/cm² lung).

Table 5: Comparison of effects in rats after 5 day exposure to various CeO₂ NPs (NM211, NM212 and PROM).

Reference	Nanoform of CeO ₂ NP	Measured exposure concentration (mg/m ³) ^a	Lung burden (µg/g lung)	Pulmonary burden (mm ² /cm ² lung) ^b	BALF analysis (statistically significant difference compared to the controls)	Neutrophils in BAL (% total cells)	Alveolar histiocytosis (% of animals)	Eosinophilic granular material	Macrophage aggregates with particles
0 days after exposure									
Keller et al. 2014	NM211	0.45	5.8	0.07	increased NEU	6.2%	0%	-	+
Keller et al. 2014	NM211	25.8	270	2.8	increased TC, NEU, LYM and MON	79%	100%	+	+
Keller et al. 2014	NM212	0.5	11	0.06	increased NEU	5%	0%	-	+
Keller et al. 2014	NM212	5.3	96	0.54	increased TC, NEU, LYM and MON	50%	0%	-	+
Keller et al. 2014	NM212	25.9	510	3.0	increased TC, NEU and LYM and MON	81%	100%	+	+
NanoMILE, 2017	PROM	0.57	11	0.38	-	5.4%	0%	-	+
NanoMILE, 2017	PROM	2.04	36	1.4	increased TC and NEU	6.5%	0%	-	+
NanoMILE, 2017	PROM	4.85	79	2.9	increased TC, NEU, MON and EPI	29%	0%	-	+
3 weeks after exposure									
Keller et al. 2014	NM211	0.45	3.0	0.04	increased NEU	4.8%	0%	-	+
Keller et al. 2014	NM211	25.8	206	2.6	increased NEU and LYM	31%	80%	-	+
Keller et al. 2014	NM212	0.5	4.8	0.03	-	3%	0%	-	+
Keller et al. 2014	NM212	5.3	70	0.47	-	12%	60%	-	+
Keller et al. 2014	NM212	25.9	318	2.3	increased NEU	10%	80%	-	+
NanoMILE, 2017	PROM	0.57	7.1	0.30	-	2%	0%	-	+
NanoMILE, 2017	PROM	2.04	30	1.3	increased TC and MON	9%	20%	-	+
NanoMILE, 2017	PROM	4.85	63	3.5	increased TC, NEU, MON, LYM and MAC	50%	100%	+	+

^a These aerosol concentrations are rounded to 0.5, 2 and 5 mg/m³ in the main text. ^b Calculated using the measured lung burden, estimated pulmonary deposition fractions and an estimated surface area of the pulmonary region of the lung, as described in the materials and methods section. TC=total cell count, NEU=neutrophils, LYM=lymphocytes, MON=monocytes, MAC=macrophages, +=increased incidence compared to the controls, -=no increased incidence compared to the controls.

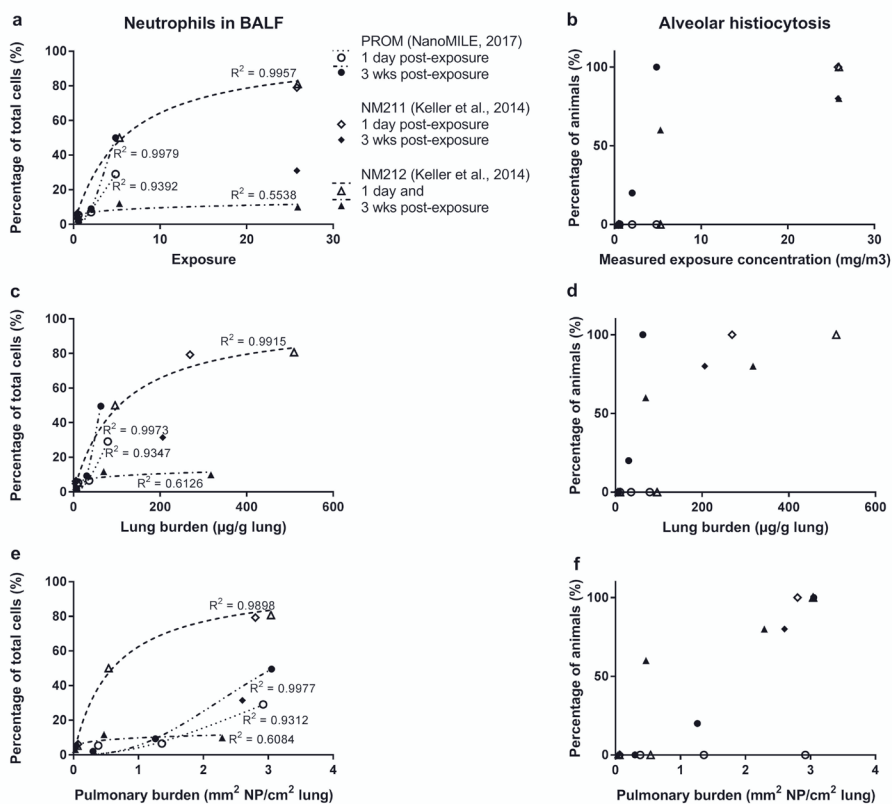


Figure 7: The percentage of neutrophils in the BALF (a, c, and e) and the percentage of animals with alveolar histiocytosis (b, d, and f) after 5 days of exposure of rats to various CeO₂ NPs (NM211, NM212 and PROM) plotted against the measured exposure concentration (mg NP/m³ air) (a and b), lung burden (μg NP/g lung) (c and d) and expected pulmonary burden (mm² NP/cm² lung) (e and f).

When expressed as exposure concentration (mg NP/m³ air) or LB (μg NP/g lung) the dose response curves of the percentage of neutrophils in the BALF are steeper for PROM CeO₂ NPs than for NM212 (see Figure 7a and c), indicating PROM CeO₂ NPs are more toxic than NM212 when the dose is expressed as external concentration or internal mass dose. Conversely, when expressed as PB (mm² NP/cm² lung) the dose response curves are steeper for NM212 compared to PROM CeO₂ NPs 1 day post-exposure (see Figure 7e), indicating NM212 is more acutely toxic than PROM CeO₂ NPs when the dose is expressed as internal surface area. Non-linear curve fitting did not result in a good fit for NM212 at 3 weeks post-exposure ($R^2 = 0.61$), which makes the comparison between the different nanoforms of CeO₂ based on dose response curves of the percentage of neutrophils in the BALF 3 weeks post-exposure difficult.

The observed differences between the different nanoforms of CeO₂ may reflect differences in physicochemical characteristics such as size, shape, surface chemistry (reactivity and charge), dissolution and hydrophobicity of the different nanoforms. Although there are no

studies available in which the cytotoxicity of the NM212, NM211 and PROM are compared in the same *in vitro* assays, previous studies have shown that differences in physicochemical properties such as (primary) particles size, surface reactivity and shape may lead to differences in (cyto)toxicity.

Previous studies indicate that smaller particles, aggregates, agglomerates and aerosols result in higher deposition levels in the deep lung and slower clearance rates than larger particles (Braakhuis et al. 2014; Peng et al. 2014). In addition, smaller particles have a relatively large surface area (for an equivalent mass) available for interaction with the body, and potentially can more easily cross barriers or be taken up by macrophages (Nel et al. 2006; Geiser 2010; Arts et al. 2015; Bakand and Hayes 2016). These differences in toxicokinetics and toxicodynamics generally lead to smaller particles having a more potent pulmonary inflammation (acute and chronic) after inhalation. However, differences in dose response for smaller TiO₂ and Ag NPs were found to disappear when the dose was expressed as surface area instead of mass (Oberdorster et al. 2005; Braakhuis et al. 2014). This is in contrast to the toxicity observed here immediately after exposure to CeO₂ NPs, which suggests that the nanoforms of CeO₂ with the smallest primary particle size (PROM) are less toxic compared to those with larger primary particle sizes and a similar or larger aggregate/agglomerate size (NM211 and NM212). However, the toxicity observed here 3 weeks post-exposure to CeO₂ NPs seems to confirm the findings of Oberdorster and Braakhuis, since the observed differences in toxicity between the nanoforms of CeO₂ NP with different primary particle and aggregate/agglomerate sizes seem to decrease when the dose is expressed as surface area (mm² NP/cm² lung) instead of mass (mg NP/m³ air or µg NP/g lung).

Besides size, surface reactivity may also influence toxicity (Warheit et al. 2007; Braakhuis et al. 2014; Peng et al. 2014; Arts et al. 2015; Bakand and Hayes 2016). NPs with a higher surface reactivity are generally able to generate more reactive oxygen species (ROS) that may lead to oxidative stress and inflammatory responses. CeO₂ NPs have been shown to both induce ROS and oxidative stress (Lin et al. 2006; Park et al. 2008; Eom and Choi 2009) as well as protect against oxidant-induced effects (Xia et al. 2008; Celardo et al. 2011). Gandon et al. (2017) showed that NM212 and NM211 had similar reactivity in the Ferric Reduction Ability of Serum (FRAS) assay when the dose was expressed as NM surface area. This is in line with our findings showing a similar toxicity of NM212 and NM211 at similar external and internal concentrations. The reactivity PROM CeO₂ NPs is slightly higher than that of NM212 and NM211 (see Table S5). Although, this increasing reactivity with decreasing size is consistent with the increase of Ce³⁺ atoms on the surface of smaller particles, this higher reactivity is not in line with our findings showing that PROM CeO₂ NPs are less toxic compared to NM212 and NM211 at similar external and internal concentrations.

Previous studies show contradicting results with respect to the influence of particle shape on the toxicity of CeO₂ NPs. Wang et al. (2015) showed that cube-like and octahedron-like

CeO₂ NPs induced higher cytotoxicity and lower anti-oxidative properties compared to rod-like CeO₂ NPs in HepG2 cells. Forest et al. (2017) on the other hand showed that rod-like CeO₂ NPs produced significantly and dose-dependently enhanced pro-inflammatory and cytotoxicity responses in RAW264.7 cells, that were not observed after exposure to cubic/octahedral NPs. Our findings cannot be compared to the results of these previous studies, as they didn't include cubic, octahedral or rod-like CeO₂ NPs. TEM images of the nanoforms used in the studies discussed here showed that the nanoform with the least toxic potency right after exposure (PROM) was spherical (Dekkers et al. 2017). Near-spherical NM211 and polyhedral shaped NM212 NPs showed similar toxicity. Because these three nanoforms differ in more than one physicochemical characteristic (Table S5), it is difficult to determine the influence of each individual characteristic on the observed toxicity.

Summary and Conclusion

In the present study we have used data from several inhalation studies in which mice or rats were exposed to various nanoforms of CeO₂ to investigate to what extent the observed differences in toxicity between various studies can be explained by differences in lung deposition, species susceptibility and/or physicochemical characteristics of the tested nanoforms. Considerable differences in pulmonary response were observed between mice and rats (Table 4) and between the various CeO₂ nanoforms tested (Table 5). Our evaluations demonstrate that the external exposure concentration, and the NP size and chemical composition (CeO₂) alone cannot fully explain the observed differences in health effects. The level at which an adverse effect starts to develop is also dependent on the internal dose, animal species and the specific nanoform. We have shown that rats are more sensitive than mice based on both external and internal concentrations. These differences do not result purely from differences in the delivered and retained doses (expressed in particle mass as well as surface area). In addition, the different nanoforms showed differences in toxic potency. Particle size is highly important to this response, but also other physicochemical properties of the CeO₂ NPs, such as surface reactivity and surface shape, may influence the toxicity of the nanoform. Based on these findings we conclude that the observed differences in toxicity of the CeO₂ NPs in various inhalation studies can be explained by differences in kinetics and susceptibility of rats compared to mice and differences in size as well as other physicochemical characteristics of the CeO₂ NPs. It remains to be determined to what extent these findings can be generalized to other poorly soluble nanomaterials.

Acknowledgements

The authors would like to thank Dr. Wendel Wohlleben and Kai Werle for the reactivity analysis using the Ferric Reduction Ability of Serum (FRAS) assay. This work was supported by the European Union's Seventh Framework Programme for research, technology development and demonstration under grant agreement n° 310451 (NanoMILE) and the Netherlands Food and Consumer Product Safety Authority (NVWA).

References

- Aalapati S, Ganapathy S, Manapuram S, Anumolu G, Prakya BM. 2014. Toxicity and bio-accumulation of inhaled cerium oxide nanoparticles in CD1 mice. *Nanotoxicology*. 8(7):786-798.
- Arts JH, Hadi M, Irfan MA, Keene AM, Kreiling R, Lyon D, Maier M, Michel K, Petry T, Sauer UG et al. 2015. A decision-making framework for the grouping and testing of nanomaterials (DF4nanoGrouping). *Regul Toxicol Pharmacol*. 71(2 Suppl):S1-27.
- Arts JH, Irfan MA, Keene AM, Kreiling R, Lyon D, Maier M, Michel K, Neubauer N, Petry T, Sauer UG et al. 2016. Case studies putting the decision-making framework for the grouping and testing of nanomaterials (DF4nanoGrouping) into practice. *Regul Toxicol Pharmacol*. 76:234-261.
- Bakand S, Hayes A. 2016. Toxicological Considerations, Toxicity Assessment, and Risk Management of Inhaled Nanoparticles. *Int J Mol Sci*. 17(6).
- Bermudez E, Mangum JB, Wong BA, Asgharian B, Hext PM, Warheit DB, Everitt JI. 2004. Pulmonary responses of mice, rats, and hamsters to subchronic inhalation of ultrafine titanium dioxide particles. *Toxicol Sci*. 77(2):347-357.
- Borm P, Cassee FR, Oberdorster G. 2015. Lung particle overload: old school -new insights? *Part Fibre Toxicol*. 12:10.
- Braakhuis HM, Cassee FR, Fokkens PH, de la Fonteyne LJ, Oomen AG, Krystek P, de Jong WH, van Loveren H, Park MV. 2016. Identification of the appropriate dose metric for pulmonary inflammation of silver nanoparticles in an inhalation toxicity study. *Nanotoxicology*. 10(1):63-73.
- Braakhuis HM, Park MV, Gosens I, De Jong WH, Cassee FR. 2014. Physicochemical characteristics of nanomaterials that affect pulmonary inflammation. *Part Fibre Toxicol*. 11:18.
- Buckley A, Warren J, Hodgson A, Marczylo T, Ignatyev K, Guo C, Smith R. 2017. Slow lung clearance and limited translocation of four sizes of inhaled iridium nanoparticles. *Part Fibre Toxicol*. 14(1):5.
- Celardo I, De Nicola M, Mandoli C, Pedersen JZ, Traversa E, Ghibelli L. 2011. Ce(3)+ ions determine redox-dependent anti-apoptotic effect of cerium oxide nanoparticles. *ACS Nano*. 5(6):4537-4549.
- Dekkers S, Miller MR, Schins RPF, Romer I, Russ M, Vandebriel RJ, Lynch I, Belinga-Desaunay MF, Valsami-Jones E, Connell SP et al. 2017. The effect of zirconium doping of cerium dioxide nanoparticles on pulmonary and cardiovascular toxicity and biodistribution in mice after inhalation. *Nanotoxicology* 11:794-808.
- Dekkers S, Oomen AG, Bleeker EA, Vandebriel RJ, Micheletti C, Cabellos J, Janer G, Fuentes N, Vazquez-Campos S, Borges T et al. 2016. Towards a nanospecific approach for risk assessment. *Regul Toxicol Pharmacol*. 80:46-59.
- EC. 2017. Draft regulation Amendments of the Annexes to REACH for registration of nanomaterials. COMMISSION REGULATION (EU) .../... amending Regulation (EC) No 1907/2006 of the European Parliament and of the Council on the Registration, Evaluation, Authorisation and Restriction of Chemicals (REACH) as regards Annexes I, III, VI, VII, VIII, IX, X, XI, and XII to address nanoforms of substances. In: Environment D-Gf, editor.
- ECHA. 2017. How to prepare registration dossier that cover nanoforms: best practices. Helsinki, Finland: European Chemicals Agency. ECHA-17-G-13-EN.

- Elder A, Gelein R, Finkelstein JN, Driscoll KE, Harkema J, Oberdorster G. 2005. Effects of subchronically inhaled carbon black in three species. I. Retention kinetics, lung inflammation, and histopathology. *Toxicol Sci.* 88(2):614-629.
- Eom HJ, Choi J. 2009. Oxidative stress of CeO₂ nanoparticles via p38-Nrf-2 signaling pathway in human bronchial epithelial cell, Beas-2B. *Toxicol Lett.* 187(2):77-83.
- Forest V, Leclerc L, Hocheplid JF, Trouve A, Sarry G, Pourchez J. 2017. Impact of cerium oxide nanoparticles shape on their in vitro cellular toxicity. *Toxicol In Vitro.* 38:136-141.
- Gandon A, Werle K, Neubauer N, Wohlleben W. 2017. Surface reactivity measurements as required for grouping and read-across: An advanced FRAS protocol. *J Phys. Conf Ser* 838.
- Geiser M. 2010. Update on macrophage clearance of inhaled micro- and nanoparticles. *J Aerosol Med Pulm Drug Deliv.* 23(4):207-217.
- Geraets L, Oomen AG, Schroeter JD, Coleman VA, Cassee FR. 2012. Tissue distribution of inhaled micro- and nano-sized cerium oxide particles in rats: results from a 28-day exposure study. *Toxicol Sci.* 127(2):463-473.
- Gosens I, Mathijssen LE, Bokkers BG, Muijser H, Cassee FR. 2014. Comparative hazard identification of nano- and micro-sized cerium oxide particles based on 28-day inhalation studies in rats. *Nanotoxicology.* 8(6):643-653.
- Greim H, Ziegler-Skylakakis K. 2007. Risk assessment for biopersistent granular particles. *Inhal Toxicol.* 19 Suppl 1:199-204.
- Han SG, Lee JS, Ahn K, Kim YS, Kim JK, Lee JH, Shin JH, Jeon KS, Cho WS, Song NW et al. 2015. Size-dependent clearance of gold nanoparticles from lungs of Sprague-Dawley rats after short-term inhalation exposure. *Arch Toxicol.* 89(7):1083-1094.
- Keller J, Wohlleben W, Ma-Hock L, Strauss V, Groters S, Kuttler K, Wiench K, Herden C, Oberdorster G, van Ravenzwaay B et al. 2014. Time course of lung retention and toxicity of inhaled particles: short-term exposure to nano-Ceria. *Arch Toxicol.* 88(11):2033-2059.
- Kreyling WG, Semmler-Behnke M, Takenaka S, Moller W. 2013. Differences in the biokinetics of inhaled nano- versus micrometer-sized particles. *Acc Chem Res.* 46(3):714-722.
- Kuempel ED, Sweeney LM, Morris JB, Jarabek AM. 2015. Advances in Inhalation Dosimetry Models and Methods for Occupational Risk Assessment and Exposure Limit Derivation. *J Occup Environ Hyg.* 12 Suppl 1:S18-40.
- Landsiedel R, Ma-Hock L, Hofmann T, Wiemann M, Strauss V, Treumann S, Wohlleben W, Groters S, Wiench K, van Ravenzwaay B. 2014. Application of short-term inhalation studies to assess the inhalation toxicity of nanomaterials. *Part Fibre Toxicol.* 11:16.
- Lin W, Huang YW, Zhou XD, Ma Y. 2006. Toxicity of cerium oxide nanoparticles in human lung cancer cells. *Int J Toxicol.* 25(6):451-457.
- NanoMILE. 2017. D 7.2 Molecular mechanisms of toxicity of Manufactured Nanomaterials (MNMs) in vivo: Identification of molecular mechanisms of toxicity in vivo (e.g. inhalation toxicity, myography, blood thrombogenicity) with emphasis on effects of surface coating and charge.: NRCWE, RIVM, UEDIN, BASF SE and IUF.

- Nel A, Xia T, Madler L, Li N. 2006. Toxic potential of materials at the nanolevel. *Science*. 311(5761):622-627.
- Oberdorster G, Oberdorster E, Oberdorster J. 2005. Nanotoxicology: an emerging discipline evolving from studies of ultrafine particles. *Environ Health Perspect*. 113(7):823-839.
- Oomen AG, Bleeker EA, Bos PM, van Broekhuizen F, Gottardo S, Groenewold M, Hristozov D, Hund-Rinke K, Irfan MA, Marcomini A et al. 2015. Grouping and Read-Across Approaches for Risk Assessment of Nanomaterials. *Int J Environ Res Public Health*. 12(10):13415-13434.
- Park EJ, Choi J, Park YK, Park K. 2008. Oxidative stress induced by cerium oxide nanoparticles in cultured BEAS-2B cells. *Toxicology*. 245(1-2):90-100.
- Pauluhn J. 2017. Kinetic modeling of the retention and fate of inhaled cerium oxide nanoparticles in rats: The cumulative displacement volume of agglomerates determines the outcome. *Regul Toxicol Pharmacol*. 86:319-331.
- Peng L, He X, Zhang P, Zhang J, Li Y, Zhang J, Ma Y, Ding Y, Wu Z, Chai Z et al. 2014. Comparative pulmonary toxicity of two ceria nanoparticles with the same primary size. *Int J Mol Sci*. 15(4):6072-6085.
- Semmler M, Seitz J, Erbe F, Mayer P, Heyder J, Oberdorster G, Kreyling WG. 2004. Long-term clearance kinetics of inhaled ultrafine insoluble iridium particles from the rat lung, including transient translocation into secondary organs. *Inhal Toxicol*. 16(6-7):453-459.
- Stone V, Pozzi-Mucelli S, Tran L, Aschberger K, Sabella S, Vogel U, Poland C, Balharry D, Fernandes T, Gottardo S et al. 2014. ITS-NANO--prioritising nanosafety research to develop a stakeholder driven intelligent testing strategy. Part Fibre Toxicol. 11:9.
- Wang L, Ai W, Zhai Y, Li H, Zhou K, Chen H. 2015. Effects of Nano-CeO(2) with Different Nanocrystal Morphologies on Cytotoxicity in HepG2 Cells. *Int J Environ Res Public Health*. 12(9):10806-10819.
- Warheit DB, Kreiling R, Levy LS. 2016. Relevance of the rat lung tumor response to particle overload for human risk assessment-Update and interpretation of new data since ILSI 2000. *Toxicology*. 374:42-59.
- Warheit DB, Webb TR, Colvin VL, Reed KL, Sayes CM. 2007. Pulmonary bioassay studies with nanoscale and fine-quartz particles in rats: toxicity is not dependent upon particle size but on surface characteristics. *Toxicol Sci*. 95(1):270-280.
- Wiemann M, Vennemann A, Sauer UG, Wiench K, Ma-Hock L, Landsiedel R. 2016. An in vitro alveolar macrophage assay for predicting the short-term inhalation toxicity of nanomaterials [journal article]. *Journal of Nanobiotechnology*. 14(1):16.
- Xia T, Kovochich M, Liong M, Madler L, Gilbert B, Shi H, Yeh JI, Zink JI, Nel AE. 2008. Comparison of the mechanism of toxicity of zinc oxide and cerium oxide nanoparticles based on dissolution and oxidative stress properties. *ACS Nano*. 2(10):2121-2134.
- Zhang H, Ji Z, Xia T, Meng H, Low-Kam C, Liu R, Pokhrel S, Lin S, Wang X, Liao YP et al. 2012. Use of metal oxide nanoparticle band gap to develop a predictive paradigm for oxidative stress and acute pulmonary inflammation. *ACS Nano*. 6(5):4349-4368.

Supplementary Information

Table S1: Overview of the pulmonary findings (kinetics and effects) of the selected inhalation studies.

Reference	Nanoform of CeO ₂ NP	Species	Measured exposure concentration (mg/m ³)	Exposure duration (days or weeks)	LB (µg/g lung)	PB (mm ² /nm ² lung)	BALF analysis (statistically significant difference compared to the controls)	NEU in BALF (% total cells)	Alveolar histiocytosis (% of animals)	Eosinophilic granular material	Macrophage aggregates with particles	Granulomatous inflammation
<i>0-1 days after exposure</i>												
Keller et al., 2014	NM211	rat	0.45	5 days	5.8	0.07	increased NEU	6.2	0	-	+	-
			25.8	5 days	270	2.8	increased TC, NEU, LYM and MON	79	100	+	+	-
Keller et al., 2014	NM212	rat	0.5	5 days	11	0.06	increased NEU	5	0	-	+	-
			5.3	5 days	96	0.54	increased TC, NEU, LYM and MON	50	0	-	+	-
NanoMILE, 2017	PROM	rat	25.9	5 days	510	3.0	increased TC, NEU and LYM and MON	81	100	+	+	-
			0.57	5 days	11	0.38	-	5.4	0	-	+	-
NanoMILE, 2017	PROM	rat	2.04	5 days	36	1.4	increased TC and NEU	6.5	0	-	+	-
			4.85	5 days	79	2.9	increased TC, NEU, MON and EPI	29	0	-	+	-
NanoMILE, 2017	PROM	mice	0.54	5 days	6.2	0.23	-	0.1	0	-	+	-
			2.04	5 days	18	0.61	-	0	0	-	+	-
Keller et al., 2014	NM212	rats	5.04	5 days	60a	2.1a	-	0.1	0	-	+	-
			0.48	4 weeks	37	0.22	-	2.3	100	-	+	-
Gosens et al., 2013	NM211	rats	5.2	4 weeks	473	2.8	increased TC, NEU, LYM and MON	49	100	+	+	-
			25.6	4 weeks	2382	15	increased TC, NEU, LYM and MON	75	100	+	+	-
Aalapati et al., 2013	Nano Amor	mice	10.8	4 weeks	639	6.8	increased TC, NEU, LYM and MAC	36	100	-	+	-
			19.9	4 weeks	1260	4.9	increased TC, NEU, LYM and MAC	31	100	-	+	-
			2.0	4 weeks	1353	17	increased TC, NEU, LYM and MAC	74	100	-	+	+

3-5 weeks post-exposure												
Keller et al. 2014	NM211	rat	0.45	5 days	3.0	0.04	increased NEU		4.8	0	-	+
			25.8	5 days	206	2.6	increased NEU and LYM		31	80	-	+
Keller et al. 2014	NM212	rat	0.5	5 days	4.8	0.03	-		3	0	-	+
			5.3	5 days	70	0.47	-		12	60	-	+
NanoMILE, 2017	PROM	rat	25.9	5 days	318	2.3	increased NEU		10	80	-	+
			0.57	5 days	7.1	0.30	-		2	0	-	+
NanoMILE, 2017	PROM	mice	2.04	5 days	30	1.3	increased TC and MON		9	20	-	+
			4.85	5 days	63	3.5	increased TC, NEU, MON, LYM and MAC		50	100	+	+
NanoMILE, 2017	PROM	mice	0.54	5 days	4.2	0.14	-		0.2	0	-	+
			2.04	5 days	9.2	0.32	-		0.2	0	-	+
Keller et al. 2014	NM-212	rat	5.04	5 days	29	0.94	-		0.7	0	-	+
			0.48	4 weeks	18	0.12	-		4	0	-	+
Dekkers et al., 2017	PROM	mice	5.2	4 weeks	444	3.0	increased NEU, LYM and MON		43	100	+	+
			25.6	4 weeks	1960	14	increased TC, NEU, LYM and MON		73	100	+	+
Aalapathi et al., 2013	NanoAmor	mice	4.0	4 weeks	82	3.4	-		1.1	20	-	-
		mice	2.0	4 weeks	615	7.9	increased NEU, LYM and MAC		48	100	-	+

TC=total cell count, NEU=neutrophils, LYM=lymphocytes, MON=monocytes, MAC=macrophages, +=increased incidence compared to the controls, -=no increased incidence compared to the controls. ^a Estimated using the measured lung burden 21 days after exposure and the expected clearance (≈50%). The measured lung burden 0 days after exposure (of 495 µg/g lung) was considered unreliable, and was probably a preparation artefact (e.g. big bronchus included in the sample).

Annex S2: Summary of the short term inhalation studies with PROM CeO₂ NPs

Study design and exposure

The study design for these additional studies with PROM CeO₂ NPs followed that of previously performed 5 day inhalation studies with NM212, but used nose-only exposure instead of whole body exposure, to allow better comparison with the 4 week inhalation study with PROM CeO₂ NPs in mice as reported previously (Dekker et al., 2017). Briefly, male Wistar rats and male C57BL/6 mice were nose-only exposed to target concentrations of 0.5, 2 and 5 mg/m³ CeO₂ NPs in respirable aerosols for 6 hours per day, on 5 consecutive days. The actual exposure concentrations were similar for rats (0.57, 2.04 and 4.85 mg/m³) and mice (0.54, 2.04 and 5.04 mg/m³) with similar particle size distributions (MMAD between 1.0 and 1.3 µm for rats and between 0.9 and 1.2 µm for mice; see Table S3). The concurrent control group was exposed to clean air only. During the study, the animals were monitored for mortality and clinical signs of toxicity. Body weights were determined twice weekly. Autopsy was performed and toxicity parameters were evaluated either 24 hours after the last exposure or after a post-exposure recovery period of 3 weeks (see Table S2). Blood was sampled, selected organs were weighed and a broad set of organs and tissues were preserved. The respiratory tract was examined histologically in 5 animals per group. Clinical chemistry parameters, hematology parameters and acute phase proteins were examined in blood of the same 5 animals per group for rats and 3 or 5 additional animals per group for mice. After blood sampling these animals underwent bronchoalveolar lavage of the left lung. Bronchoalveolar lavage fluid (BALF) was examined for cytological and biochemical parameters including selected antigens. Lung burdens were determined in 3 additional animals per group for both rats and mice.

Table S2: Overview of number of animals per autopsy group.

Species	Post-exposure	Histopathology lung	Blood sampling	BALF	Lung burden
Rat	24 hours		5 animals/group		3 animals/group
	3 weeks		5 animals/group		3 animals/group
Mice	24 hour	5 animals/group	3 animals/group		3 animals/group
		5 animals/group	5 animals/group		3 animals/group

Lung burden

The results of lung burden measured 24 hours after the exposure and after a 3 week recovery period are shown in Figures S2.1 and S2.2, in rats and mice, respectively.

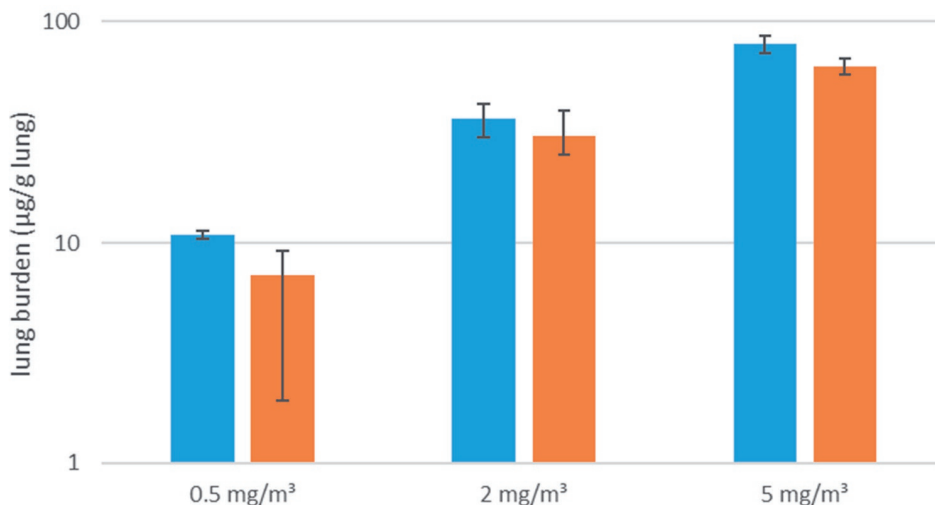


Figure S2.1: Lung burden after 5 days of exposure to CeO₂ NPs 24 hours (blue bars) and 3 weeks (orange bars) post-exposure in rats.

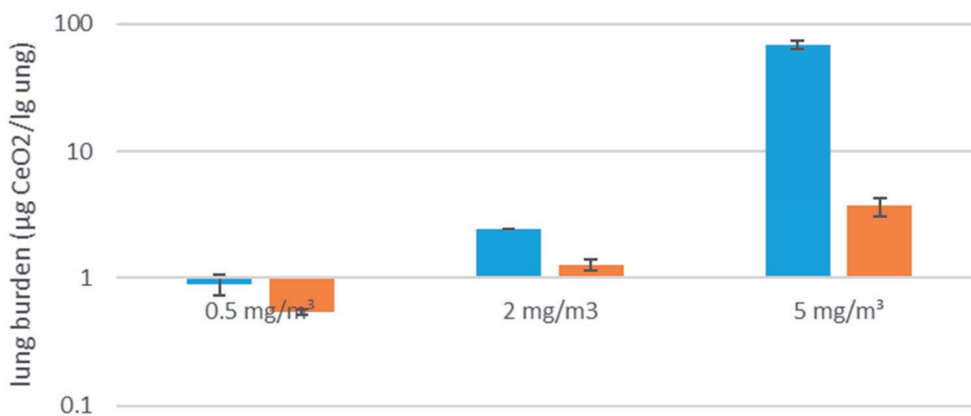


Figure S2.2: Lung burden after 5 days of exposure to CeO₂ NPs 24 hours (blue bars) and 3 weeks (orange bar) post-exposure in mice.

Ce could not be detected in the lung of the control animals (detection limit: 0.3 µg per sample). In rats a modest clearance was observed in animals exposed to 0.5 mg/m³ CeO₂ NPs the after 3 weeks recovery, whereas the clearance of 2 and 5 mg/m³ seemed minimal (Figure S2.1). In mice the lung burden was low (0.9 & 2.4 µg Ce/lung) in animals exposed to 0.5 mg/m³ and 2 mg/m³ CeO₂ NPs after exposure, whereas the mean lung burden in mice exposed to 5 mg/m³ CeO₂ NPs was extraordinary high (~69 µg Ce/lung; Figure S2.2). The high value (of 495 µg/g lung) of mice exposed to 5 mg/m³ CeO₂ NPs on study day 5 (last blue bar) was out of range and probably a preparation artefact (e.g. big bronchus included in the sample). In the mice exposed to 0.5 and 2 mg/m³ CeO₂ NPs a clearance of approximately 50% was observed within the 3 weeks recovery period. A similar clearance rate was assumed for mice exposed to 5 mg/m³ CeO₂ NPs.

Hematology and clinical chemistry

No treatment-related effects were observed for hematology or clinical chemistry parameters, except for a slight, but statistically significant increase in the absolute neutrophil counts in rats exposed to 2 and 5 mg/m³ CeO₂ NPs after the three weeks recovery period (see NanoMILE Deliverable D7.2), indicating a mild systemic inflammation.

Bronchoalveolar lavage fluid (BALF)

A moderate increase in neutrophil counts was found in the BALF of rats exposed to 2 or 5 mg/m³ CeO₂ NPs 24 h after exposure (Figure S2.3). This was associated with higher alkaline phosphatase (ALP) activity and cytokine-induced chemoattractant-1 (CINC-1/IL8) levels. ALP is released by neutrophils and CINC-1 is a cytokine which attracts neutrophils into the lung tissue. Epithelial cell counts in BALF were marginally increased in rats exposed to 5 mg/m³ CeO₂ NPs, indicating an effect on the bronchioles. There was also an increased monocyte number and in the cytokines osteopontin and macrophage colony stimulating factor (M-CSF) in rats exposed to 5 mg/m³ CeO₂ NPs. Increased monocyte chemoattractant protein-1 (MCP-1) in rats exposed to 2 and 5 mg/m³ CeO₂ NPs also indicates that more monocytes and macrophages were attracted into the lung. A higher permeability of the capillaries in the alveoli can be assumed because of slightly higher total protein levels in BALF of rats exposed to 5 mg/m³ CeO₂ NPs. The enzyme activities of lactate dehydrogenase (LDH) and γ-glutamyl transferase (GGT) in BALF of rats exposed to 2 and 5 mg/m³ CeO₂ NPs were only marginally, but statistically significantly, increased.

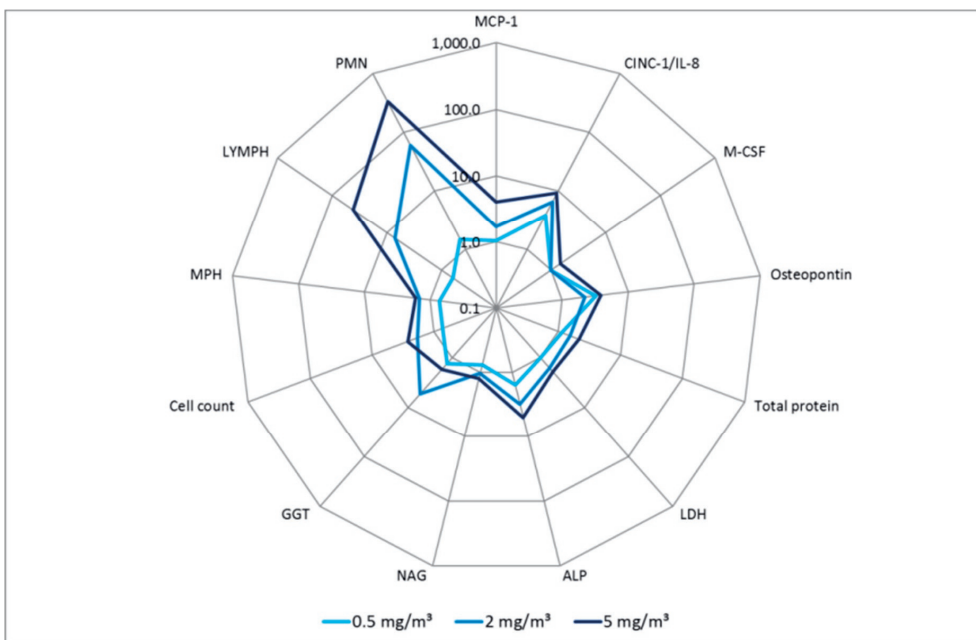


Figure S2.3: Changes in various BALF parameters in rats on study day 5 (24 hours after last exposure). Results are presented as x-fold changes compared to concurrent controls. Cell count = total cell count, MPH = alveolar macrophage, LYMPH = lymphocyte, PMN = polymorphnuclear neutrophilic granulocyte, GGT = γ -Glutamyl-transferase; LDH = Lactate dehydrogenase; ALP = Alkaline phosphatase; NAG = β -N-Acetyl glucosaminidase, GGT = γ -Glutamyl-transferase; LDH = Lactate dehydrogenase; ALP = Alkaline phosphatase; NAG = β -N-Acetyl glucosaminidase, CINC-1/IL-8 = cytokine-induced neutrophil chemoattractant-1; MCP-1 = monocyte chemoattractant protein-1; M-CSF = macrophage colony stimulating factor.

In the BALF, monocyte cell counts were increased in rats exposed to 2 and 5 mg/m³ CeO₂ NPs (Figure S2.4). Absolute neutrophil counts were higher in the BALF of rats exposed to 5 mg/m³ CeO₂ NPs 3 weeks post-exposure compared to 24 hours post-exposure. Lymphocyte counts were also increased in rats exposed to 5 mg/m³ CeO₂ NPs, indicating an ongoing inflammatory process in the lungs. This was also reflected by high levels of MCP-1 in rats exposed to 5 mg/m³ CeO₂ NPs. CINC-1/IL-8 levels in rats exposed to 5 mg/m³ CeO₂ NPs were lower compared to 24 hours post-exposure, but were still raised above control levels. The total protein, LDH and GGT levels in BALF of rats exposed to 5 mg/m³ CeO₂ NPs 3 weeks post-exposure were marginally increased compared to the controls, with levels similar to those 24 hours post-exposure. ALP activity was lower compared to the 24 hours post exposure, but still marginally above control levels.

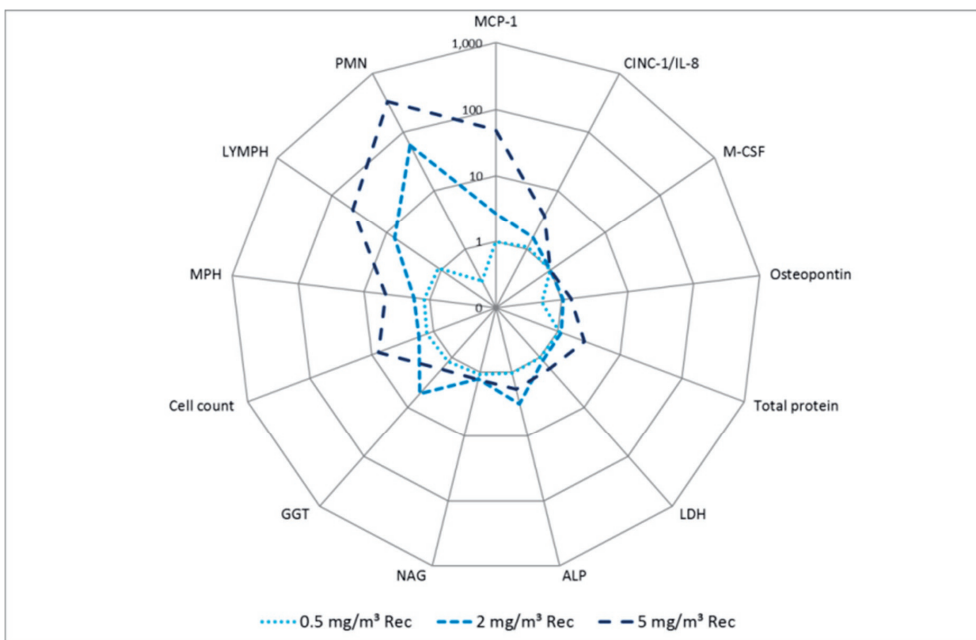


Figure S2.4: Changes in various BALF parameters in rats after a three weeks recovery period on study day 26. Results are presented as x-fold changes compared to concurrent controls. Cell count = total cell count, MPH = alveolar macrophage, LYMPH = lymphocyte, PMN = polymorph nuclear neutrophilic granulocyte, GGT = γ -Glutamyl-transferase; LDH = Lactate dehydrogenase; ALP = Alkaline phosphatase; NAG = β -N-Acetyl glucosaminidase, GGT = γ -Glutamyl-transferase; LDH = Lactate dehydrogenase; ALP = Alkaline phosphatase; NAG = β -N-Acetyl glucosaminidase, CINC-1/IL-8 = cytokine-induced neutrophil chemoattractant-1; MCP-1 = monocyte chemoattractant protein-1; M-CSF = macrophage colony stimulating factor.

No treatment-related changes in cytology parameters, enzyme activities or total protein levels in BALF were observed in mice.

Pathology

Histopathological finding in the lungs

In all exposed groups of both rats and mice, characteristic particles, either single or very few, were observed in the cytoplasm of alveolar macrophages (histiocytes) or free in the alveoli. These particles were considered to represent test substance. They occurred in all animals of all treatment groups, and were still present after the recovery period in all rats exposed to 0.5 mg/m³ CeO₂ NPs, in 4 rats exposed to 2 mg/m³ CeO₂ NPs and all mice of all exposed groups. In rats, the particles were also seen in the bronchus-associated lymphoid tissue (BALT) or in macrophages in the BALT in two rats exposed to 0.5 mg/m³ CeO₂ NPs and in all rats exposed to 2 and 5 mg/m³ CeO₂ NPs. Particles were also present in the BALT after the recovery period in 3 rats exposed to 0.5 mg/m³ CeO₂ NPs and in all rats exposed to 2 and 5 mg/m³ CeO₂ NPs.

After the recovery period, a minimal alveolar histiocytosis with particles occurred in one rat exposed to 2 mg/m³ CeO₂ NPs and in all rats exposed to 5 mg/m³ CeO₂ NPs. In addition, all rats exposed to 5 mg/m³ CeO₂ NPs showed very occasional eosinophilic granular material, most probably debris of degraded macrophages, free in the alveoli.

The occurrence of alveolar histiocytosis with particles in the recovery group in combination with the occurrence of eosinophilic granular material in rats exposed to 5 mg/m³ CeO₂ NPs was regarded to be an indicator of an adverse reaction, whereas the occurrence of particles in single histiocytes or in the BALT in the lungs was considered non-adverse, as there were no signs of any cytotoxicity.

Single or very few particles could be noted within single histiocytes in all exposed mice after the recovery period. The occurrence of these particles in the lungs was considered to be treatment-related, but because there were no signs of an inflammatory response, it was regarded to be non-adverse.

Histopathological findings in the mediastinal and tracheobronchial lymph nodes

In rats exposed to the 5 mg/m³ CeO₂ NPs, single or very few particles were observed in the mediastinal lymph node in one animal and in the tracheobronchial lymph nodes in 3 rats. After the recovery period single or very few particles were seen in the mediastinal lymph node of one rat exposed to 2 mg/m³ CeO₂ NPs and in 4 rats exposed to 5 mg/m³ CeO₂ NPs, as well as in the tracheobronchial lymph nodes of 2 rats exposed to 2 mg/m³ CeO₂ NPs and in all rats exposed to 5 mg/m³ CeO₂ NPs. In mice, particles were seen free in the lymphoid tissue of the tracheobronchial and mediastinal lymph nodes after the recovery period, and in one mouse exposed to 2 mg/m³ CeO₂ NPs and in one mouse exposed to 5 mg/m³ CeO₂ NPs. Because there was no activation or aggregation of macrophages, the occurrence of these particles was regarded to be non-adverse.

Table S3: Models and data used to calculate the lung burden (LB) or retained dose in the lung in the selected inhalation studies.

Reference	MPPD model ^a	body weight (g)	Nanoform of CeO ₂ NP	MMAD (µm)	GSD	aerosol conc. (mg/m ³)	Breathing frequency (#/min)	Tidal volume (mL)	Breathing scenario ^b	exposure duration (h/d)	exposure duration (weeks)	post-exposure period (days)	lung weight (g)	lung weight after recovery (g)
Keller et al., 2014	ASD	270	NM211	1.9	2.9	0.45	119	1.89	WB	6	1	0, 21	1.04	1.26
				2.2	2.4	25.8								
Keller et al., 2014	ASD	270	NM212	1.4	2.3	0.5	119	1.89	WB	6	1	0, 21	1.04	1.26
				1.2	2.1	5.3								
NanoMILE, 2017	ASD	270	PROM	1.0	2.5	25.9	166	1.88	NO	6	1	0, 22	1.03	1.15
				1.3	2.2	0.57								
Keller et al., 2014	ASD	270	NM212	1.2	2.4	2.04	119	1.89	WB	6	4	0, 35	1.10	1.26
				0.9	2.3	4.85								
Geraerts et al., 2012	ASD	224	NM211	1.6	2.1	0.48	166	1.49	NO	6	4	0	0.87	-
				1.3	2.1	5.2								
Geraerts et al., 2012	ASD	212	NM212	0.9	2.5	25.6	166	1.39	NO	6	4	0	0.73	-
				1.1	2.5	0.54								
NanoMILE, 2017	MB6	24	PROM	1.1	2.4	2.04	326	0.19	NO	6	1	0, 21	0.134	0.139
				0.9	3.0	5.04								
Dekkers et al., 2017	MB6	20	PROM	0.29 ^c	1.6	3.98	353	0.20	NO	3	4	28	0.158	0.160
				1.4	2.4	2.00								
Aalipati et al., 2014	MB6	35	Nano Amor	1.4	2.4	2.00	277	0.17	NO	6	4	0, 28	0.160	0.160

^a ASD: Asymmetric Sprague Dawley rat, MB6: Mouse B6C3F1; ^b WB: whole body, NO: nose only; ^c Mass median diameter (MMD) instead of mass median aerodynamic diameter (MMAD), estimated based on the particle size distributions of the scanning mobility particle sizer (SMPS) measurements, assuming spherical aggregation around primary particles of 4.7 nm. -: no data available

Table S4: Data used to calculate the expected pulmonary burden (PB) in the selected inhalation studies.

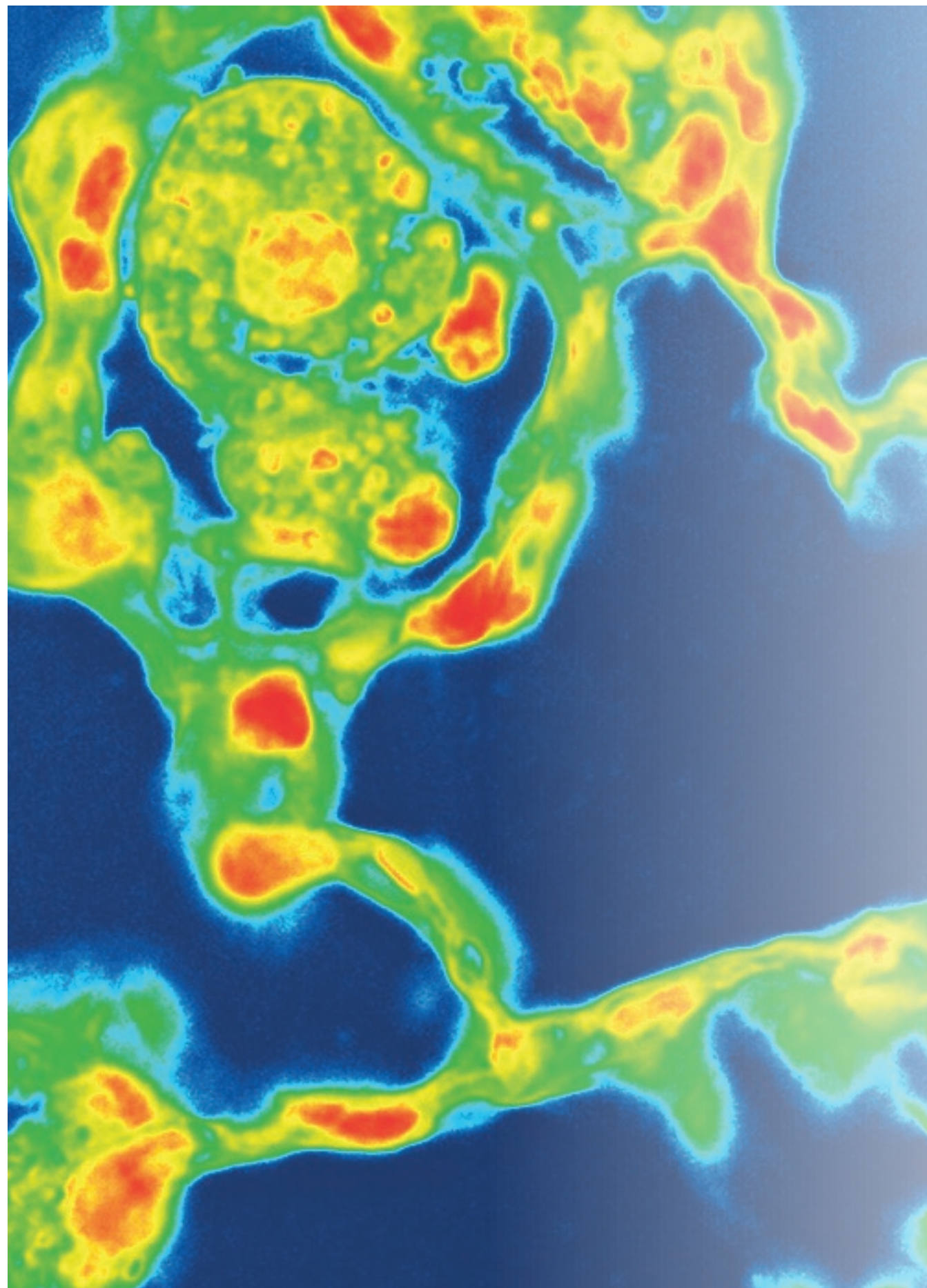
Reference	Species	Nanoform of CeO ₂ NP	Primary particle size (nm)	Aerosol conc. (mg/m ³)	Exposure duration (days or weeks)	Estimated fraction of inhaled dose deposited in lung (%)	Estimated fraction of inhaled dose deposited in pulmonary region (%)	Estimated fraction of lung deposition deposited in pulmonary region (%)	Lung burden 0 days after exposure (µg/lung)	Lung burden 3-5 weeks after exposure (µg/lung)	Surface area per particle (nm ²)	Surface area per g NP (m ² /g)	Surface area of pulmonary region of the lung (nm ²)	Pulmonary burden 0 days after exposure (mm ² /nm ²)	Pulmonary burden 3-5 weeks after exposure (mm ² /nm ²)
Keller et al., 2014	rat	NM211	12.5	0.45	5 days	9.8	6.1	63	6.0	3.8		53	2864	0.07	0.04
				25.8	5 days	9.4	5.1	54	280	260					2.80
Keller et al., 2014	rat	NM212	40	0.5	5 days	11.6	6.9	59	11	6.0				0.06	0.03
				5.3	5 days	14.3	8.1	57	100	88				27	2864
NanoMILE, 2017	rat	PROM	4.7	25.9	5 days	16.2	9.9	61	530	400				3.04	2.29
				0.57	5 days	10.3	5.7	55	11	8.7					
				2.04	5 days	10.8	6.3	58	38	35				1.36	1.26
				4.85	5 days	12.0	6.8	57	83	87					
Keller et al., 2014	rat	NM212	40	0.48	4 weeks	10.7	6.0	56	41	23				0.22	0.12
				5.2	4 weeks	13.1	7.4	57	520	560				27	2864
Geraerts et al., 2012	rat	NM211	12.5	25.6	4 weeks	17.8	10.9	61	2650	2470				15.2	14.3
				10.8	4 weeks	14.8	7.4	50	557	-				64	2612
Geraerts et al., 2012	rat	NM212	40	19.95	4 weeks	13.0	6.4	50	923	-				4.88	-
				0.54	5 days	10.7	7.2	67	0.9	0.5					
NanoMILE, 2017	mice	PROM	4.7	2.04	5 days	10.6	7.2	67	2.4	1.3				0.61	0.32
				5.04	5 days	12.8	8.7	68	8.3	3.7					
Dekkers et al., 2017	mice	PROM	4.7	3.98	4 weeks	11.5	8.0	70	-	13				-	3.37
				2.0	4 weeks	9.3	6.1	65	216	98					
Aalipathi et al., 2014	mice	Nano Amor	45	2.0	4 weeks	9.3	6.1	65	216	98				17.3	7.86

Table S5: Physicochemical characteristics of the CeO₂ nanoparticles used in the 5-day inhalation studies in rats.

Characteristic ↓	Nanoform of CeO ₂ NP →	NM211	NM212	PROM
Shape		near spherical	polyhedral	spherical
Primary particle size (nm)		12.5	40	4.7
Surface area (BET: m ² /g)		64	27	-
Surface reactivity (nmol TEU/m ² NP) ^a		14 ± 0.7	13 ± 0.6	17 ± 03
Charge (mV)		16	42	50
MMAD (μm) ± GSD at an aerosol conc. of 0.5 mg/m ³		1.9 ± 2.9	1.4 ± 2.3	1.3 ± 2.2
MMAD (μm) ± GSD at an aerosol conc. of 2 mg/m ³		-	-	1.2 ± 2.4
MMAD (μm) ± GSD at an aerosol conc. of 5 mg/m ³		-	1.2 ± 2.1	1.1 ± 2.3
MMAD (μm) ± GSD at an aerosol conc. of 25 mg/m ³		2.2 ± 2.4	1.0 ± 2.5	-

^a The surface reactivity was measured with the ferric reduction ability of serum (FRAS) assay (Gandon et al., 2017). The read-out of the FRAS assay is calibrated by a concentration series of Trolox (6-hydroxy-2,5,7,8-tetramethylchroman-2-carboxylic acid, a Vitamin E analogon) and the result expressed as nmol Trolox Equivalent Unites (TEU)/m²NP.

BET= Brunauer, Emmett and Teller method to measure surface area, MMAD=mass median aerodynamic diameter, GSD=geometric standard deviation, -: no data available



Chapter 4

Multi-omics approaches confirm metal ions mediate the main toxicological pathways of metal-bearing nanoparticles in lung epithelial A549 cells

Susan Dekkers*¹, Tim D. Williams*², Jinkang Zhang², Jiarui (Albert) Zhou³, Rob J. Vandebriel¹, Liset J.J. De La Fonteyne¹, Eric R. Gremmer¹, Shan He³, Emily J. Guggenheim⁴, Iseult Lynch⁴, Flemming R. Cassee^{1,5}, Wim H. De Jong¹, Mark R. Viant²

Environmental Science: Nano 5:1506-1517 (2018)

Reproduced by permission of The Royal Society of Chemistry

¹ National Institute for Public Health and the Environment (RIVM), Bilthoven, The Netherlands,

² School of Biosciences, The University of Birmingham, Birmingham, B15 2TT, UK,

³ Centre for Systems Biology, The University of Birmingham, Birmingham, B15 2TT, UK,

⁴ School of Geography Earth and Environmental Sciences, The University of Birmingham, Birmingham, B15 2TT, UK,

⁵ Institute of Risk Assessment Sciences, Utrecht University, Utrecht, The Netherlands,

* These authors contributed equally

Abstract

The toxicity of silver (Ag) and zinc oxide (ZnO) nanoparticles (NPs) has been associated with their dissolution or ability to release metal ions while the toxicity of cerium dioxide (CeO₂) NPs has been related to their ability to induce or reduce oxidative stress dependent on their surface redox state. To examine the underlying biochemical mechanisms, multiple omics technologies were applied to characterise the responses at the molecular level in cells exposed to various metal-based particles and their corresponding metal ions. Human lung epithelial carcinoma cells (A549) were exposed to various Ag, ZnO, and CeO₂ NPs, Ag and ZnO micro-sized particles (MPs), Ag ions (Ag⁺) and zinc ions (Zn²⁺) over a 24h time course. Molecular responses at exposure levels that caused ~20% cytotoxicity were characterised by direct infusion mass spectrometry lipidomics and polar metabolomics and by RNAseq transcriptomics. All Ag, Zn and ZnO exposures resulted in significant metabolic and transcriptional responses and the great majority of these molecular changes were common to both ionic and NP exposures and characteristic of metal ion exposure. The low toxicity CeO₂ NPs elicited few molecular changes, showing slight evidence of oxidative stress for only one of the four CeO₂ NPs tested. The multiple omics analyses highlight the main pathways implicated in metal ions-mediated effects. These results can be used to establish adverse outcome pathways as well as strategies to group nanomaterials for risk assessment.

Introduction

Although nanomaterials are increasingly used in many different applications, detailed knowledge on the underlying biochemical mechanisms by which they may induce harmful effects on humans and the environment is lacking. Several possible mechanisms of action have been proposed¹. One of the proposed mechanisms of action is related to the release of metal ions. For both silver (Ag) and zinc oxide (ZnO) nanoparticles (NPs), toxicity is often related to their dissolution or ability to release metal ions^{2,3}. However, studies comparing the toxicity of these NPs with that of their ionic forms indicate that the toxicity of the NPs cannot always be fully explained by the release of metal ions^{4,5}. Another proposed mechanism of action is via the induction of oxidative stress through the generation of reactive oxygen species (ROS). Cerium dioxide (CeO₂) NPs may have oxidative as well as anti-oxidative properties, depending on their redox surface state. The ability to shift valence states from Ce³⁺ to Ce⁴⁺ or from Ce⁴⁺ to Ce³⁺ at the surface of the NPs is suggested to influence the ability of the CeO₂ NPs to either scavenge or generate reactive oxygen species (ROS), respectively, subsequently increasing or decreasing the ability to induce oxidative stress^{6,7}. However, previous studies comparing CeO₂ NPs with different valence states indicate that the mechanisms by which the redox surface status of NPs influences the toxicity are not yet fully understood⁷.

Transcriptomics (gene transcriptional profiling), metabolomics (profiling of polar metabolites), proteomics (profiling of proteins) and lipidomics (profiling of lipids) are valuable non-hypothesis driven methods to gain insight into the mechanisms of actions or pathways leading to biological effects of NPs on living organisms, especially when these approaches are combined into a multi-omics approach to explore a larger molecular landscape⁸. Computational modelling can be used to search for molecular signatures that can contribute to the discovery of molecular key (initiating) events within adverse outcome pathways (AOPs), i.e. mechanistically based molecular changes that are related to both an (upstream) molecular initiating event and (downstream) key events leading to higher levels of phenotypic change⁹. These signatures can be used in the screening, ranking and risk assessment of nanomaterials. When designing a multi-omic study, it is important to generate time-resolved data to be able to follow the different molecular responses within a pathway leading to a biological response¹⁰. Multi-omics approaches have not yet been widely used within the field of nanotoxicology^{11,12}.

In this study, toxicological, analytical and computational methods are combined to 1) identify the molecular mechanisms by which Ag, ZnO and CeO₂ NPs induce toxicity and 2) investigate the influence of dissolution and redox surface state on the NP toxicity using transcriptomics, metabolomics and lipidomics. A549 lung epithelial cells were exposed to nano, micro and ionic forms of Ag, Zn or ZnO and various CeO₂ NPs over a 24 hour time course. A549 cells

were selected as they are lung epithelial cells and inhalation is considered an important route of exposure in occupational settings and for consumers using spray products^{13, 14}. To investigate the role of dissolution and ionic release on the pathways leading to adverse effects of metal (oxide) NPs, Ag and ZnO NPs and MPs as well as Ag⁺ and Zn²⁺ were studied in parallel. In addition, CeO₂ NPs with different amounts of zirconium (Zr)-doping were studied as a means to investigate the effect of the redox surface state on the biological response. Zr-doping increases the Ce³⁺:Ce⁴⁺-ratio and is therefore expected to increase the antioxidant potential of the CeO₂ NPs^{6, 7}. Concentrations of NPs and their equivalent ions that induced approximately 20% cytotoxicity after 24 h exposure were chosen for this study, aiming to achieve a similar level of cellular damage in all cases. Importantly, temporal responses were investigated by sampling after different exposure times (1, 6 and 24 h) to characterize the development of the toxicological responses over time.

Materials and Methods

Nanomaterials: selection, dispersion and characterisation

Ag, ZnO and CeO₂ NPs were selected because of their expected modes of action that involve either the release of ions or their ability to generate or scavenge ROS. An overview of the physicochemical characteristics of the selected materials is given in **Table 1**. When provided as powder the micro- and nano-sized particles were dispersed using the previously published protocol by Jensen et al.¹⁵. For a final stock concentration of 2.56 mg/mL the powder was pre-wetted with 0.5 vol% ethanol and dispersed in water with 0.05% w/v bovine serum albumin from Sigma-Aldrich Chemie (Zwijndrecht, The Netherlands), and sonicated for 16 minutes on ice using a 400 Watt Branson Sonifier S-450D set at 10% amplitude with a 3 mm probe (Branson Ultrasonics Corp., Danbury, CT, USA). When provided as dispersions, the NPs were vortexed for 15 s and sonicated for 5 mins in an ultrasonic bath (Branson CPX2800, 40 kHz, 110W) to re-disperse any possible agglomerates.

Cell culture and exposures

A549 cells were obtained from ATCC (VA, USA). The cells were cultured in tissue culture flasks in RPMI 1640 medium with Glutamax (Gibco, ThermoFisher Scientific Inc., Landsmeer, the Netherlands) supplemented with 10% Fetal Bovine Serum (FBS, Greiner BioOne BV, Alphen aan de Rijn, the Netherlands) and 1% penicillin/streptomycin (Gibco). Cells were cultured at 37°C in a humidified atmosphere of 5% CO₂ in air. The adherent cells were harvested by a short incubation with 0.5% EDTA trypsin in Ca/Mg free Dulbecco's Phosphate Buffered Saline (Gibco).

To determine the EC₂₀ (effective concentration resulting in 20% cytotoxicity) dose-response studies were performed. A549 cells were harvested and counted 24 h before exposure. Twenty thousand (2x10⁴) cells were seeded in wells of 96-well plates in 100 µL supplemented

RPMI 1640 medium. After 24 h incubation a semi-confluent monolayer of cells was obtained and the cells were exposed to the various materials. Cell survival (i.e. cytotoxicity) was determined after 24 h of exposure by a colorimetric assay using cell proliferation reagent WST-1 (Roche, Sigma-Aldrich Chemie). All exposures were performed in triplicate. Dose-response modelling and derivations of the EC₂₀ were performed using PROAST software¹⁶ version 60.1. For the four CeO₂ NPs and Ag MP no EC₂₀ was obtained, since the highest concentration tested (128 µg/mL) resulted in less than 20% cytotoxicity. An overview of the EC₂₀ values and confidence intervals can be found in **Electronic Supplementary Information (ESI) 1**. Dissolution of nanoparticles and microparticles in cell culture medium was measured using ICP-OES (**ESI 2**).

Table 1.: Physicochemical characteristics of the selected materials^a and cell viability at doses applied in the omics study.

Test material	Batch no	Short Description	Primary size (nm±SD)	Hydrodynamic size (nm±SD) measured with disc centrifuge	Hydrodynamic size (nm±SD) measured with DLS	Dose ^b (µg/mL)	Ion conc. ^c (µg/mL)	Cell viability (%)
Ag NP-NM300K	JRC-Ag-20nm-NM03002a000855b	Ag NPs dispersed in H ₂ O with 4% polyoxy-ethylene glycerol trioleate and 4% Tween 20. mean particle size 15 nm	< 20	n.m. ^d	50 to 70	38.6	0.04	79
Ag MP	SIGMA- AgBulk - 2-3.5microns- 180215a	micro-sized Ag particles powder	>1000?	n.m.	n.m.	128	0.005	95
AgNO ₃	-	ionic silver nitrate (AgNO ₃) soluble powder	n.a. ^e	n.a.	n.a.	8	5.08	83
ZnO NP-NM110	JRC-ZnOun-NM110-0801b	uncoated ZnO NPs powder mean particle size 150 nm, primary particle size 42 nm	151 ± 57	193 ± 3	275 ± 4	15	1.41	94
ZnO NP-NM111	JRC-ZnOTECS-NM111-2995b	ZnO NPs coated with triethoxy-caprylsilane powder mean particle size 140 nm, primary particle size 34 nm	141 ± 66	n.m.	253 ± 1	10	0.989	89
ZnO MP	SIGMA - ZnO- 5 microns- 180215a	micro-sized ZnO particles powder	5000	n.m.	n.m.	30	1.46	82
ZnCl ₂	-	ionic zinc chloride (ZnCl ₂) soluble powder	n.a.	n.a.	n.a.	24.6	11.80	67
CeO ₂ NP-A	PROM-CeO2-20nm-batchCE026A-a	undoped CeO ₂ NPs dispersed in H ₂ O	4.7 ± 1.4	39	172 ± 2	128	<LOD ^f	88
CeO ₂ NP-C	PROM-ZrCeO2-batch-CE026C-a	27% ZrO ₂ -doped CeO ₂ NPs dispersed in H ₂ O	4.6 ± 1.4	40	297 ± 4	128	<LOD	89
CeO ₂ NP-E	PROM-ZrCeO2-batch-CE025E-a	78% ZrO ₂ doped CeO ₂ NPs dispersed in H ₂ O	4.7 ± 1.4	41	358 ± 6	128	<LOD	89
CeO ₂ NP-NM212	Umico-re-CeO2-NM212-RI-VM-batch	uncoated CeO ₂ NPs powder primary particles size 33 nm	28.4 ± 10.4	135 ± 4	213	128	<LOD	87

^a CeO₂ NP-NM212, ZnO NP-NM110, ZnO NP-NM111 and Ag NP-NM300K were characterized within the OECD sponsorship programme^{17,19}. The other NPs were characterized within the NanoMILE project (Lynch et al., in preparation); ^b Exposure doses for the A549 cells, adapted for incubation in the 6-well plates, are shown in bold figures; ^c Ion concentration measured for the NPs and MPs in cell culture medium after 24 h (see ESI 2 for details) and estimated using the molecular weight for AgNO₃ and ZnCl₂; ^d n.m. = not measured; ^e n.a. = not applicable; ^f <LOD = below limit of detection.

For the omics studies, 8×10^5 cells per well were seeded in 6-well plates and cultured for 18 h, after which the cells were exposed to the determined EC_{20} concentrations or to 128 $\mu\text{g}/\text{mL}$ for the particles where EC_{20} was not reached. Because the cytotoxicity of the A549 cells was higher in the 6-well plates compared to the 96-well plates, several concentrations were adapted and applied as presented in **Table 1**. Omics analyses were carried out on independent replicates from 14 exposure and control groups. Biological replication was, for polar metabolomics $n=6$, lipidomics $n=6$ and transcriptomics $n=4$. Different cell plates were exposed for $t=1$, $t=6$ and $t=24$ h to monitor changes in the molecular responses over time. At $t=24$ h, additional control wells were included to measure the actual cytotoxicity and possible interference of the materials with the viability assay. After exposure, the cells (approximately 2×10^6 per well) were quickly washed with PBS (phosphate buffered saline) twice at room temperature after which the 6-well plates were deep frozen by quenching on liquid nitrogen (-196°C) and stored at -80°C until extraction for omics evaluation.

Omics Analyses

Brief descriptions of the methods used for omics analysis are shown. Full methodological details are provided in **ESI 3**.

Extraction of metabolites and lipids

Cells were harvested then vortexed in methanol:chloroform:water (v/v/v at 1:1:0.9) and the phases separated by centrifugation. The polar phase was dried in a speed vac concentrator (Thermo Savant, Holbrook, NY) for 4 h. The non-polar phase was dried under a stream of nitrogen for 5 min. All dried samples were then frozen at -80°C until analysis.

Direct infusion mass spectrometry (DIMS)

The DIMS analysis method used was similar to previous studies^{20, 21}. Dried extracts were re-suspended in 80:20 (v/v) methanol:water with 0.25% formic acid (for positive ion mode analysis of polar extracts) or 80 μL 2:1 methanol:chloroform with 5 mM ammonium acetate (for negative ion mode analysis of lipids). Samples were analysed (in quadruplicate) using direct infusion mass spectrometry (Q Exactive, Thermo Fisher Scientific, Germany) in positive ion mode (for polar metabolomics) or negative ion mode (for lipidomics), utilising a Triversa nanoelectrospray ion source (Advion Biosciences, Ithaca, NY, USA).

Metabolomics Data Processing

Mass spectra were recorded using the selected ion monitoring (SIM) stitching approach from m/z 50-620 (for polar metabolomics) or from m/z 50-1020 (for lipidomics) and then processed using custom-written Matlab scripts as previously reported^{22, 23}. The resulting matrices of peak intensities (termed "DIMS dataset") were probabilistic-quotient normalised (PQN) and intensity-drift corrected using a Quality Control-Robust Spline Correction (QC-

RSC) algorithm. Finally, the missing values were imputed using the k-nearest neighbours (KNN) algorithm. For multivariate analysis, generalized log (Glog) transformation of the DIMS dataset was performed.

RNA seq gene expression profiling

Sequencing

Total RNA was extracted from A549 cells using a micro RNeasy Kit (Qiagen, Crawley, UK). All RNA libraries were produced using the Biomek FxP (Beckman Coulter A31842) with Ultra Directional RNA Library Prep Kit (New England Biolabs E7420L) and NEBnext Multiplex Oligos for Illumina Dual Index Primers (New England Biolabs E7600S), using provided protocols and 500ng of total RNA. Multiplex library clustering and sequencing was performed upon the HiSeq2500 (Illumina) with HiSeq Rapid Cluster Kit v2 (Illumina GD-402-4002) at 12pM library concentration with 10% PhiX Control v3 spiked in (Illumina FC-110-3001). The sequencing run was carried out using HiSeq Rapid SBS Kit v2 (Illumina FC-402-4021).

RNA seq Data Processing

The binary base call (BCL) files were converted to FASTQ format (containing a biological sequence and its corresponding quality scores) using Illumina bcl2fastq conversion software (v1.8.4). Sequences were then trimmed using Trimmomatic (v0.36). Five low quality samples were identified and removed accordingly. The FASTQ files were aligned to the GENCODE human transcript sequences (release 25, GRCh38.p7) using Bowtie2 (v2.3.0). The resulting Sequence Alignment Map (SAM) data were converted into Browser Extensible Data (BED) format using SAMtools (v1.3.1) and bamToBed (v2.19.1). Finally, the RNA read counts were extracted from the BED files with a Python script. To provide gene-level analysis, the RNA reads were collapsed to the counts of their coding genes. The gene annotation information was retrieved from the Ensembl database (release 87).

Omics Data Analysis

Putative metabolite annotations were added using MI-Pack²⁴. ANOVA, t-tests and principal components analyses (PCA) were performed in Genespring (v7.3.1, Agilent) using multiple testing corrections²⁵. DESeq²⁶ was used for differential gene expression analysis with a $q < 0.05$ cut-off. Combined gene and metabolite pathway over-representation analyses were performed with IMPaLA²⁷, using gene identifiers and Human Metabolite Database (HMDB) identifiers²⁸ for each peak identified as significantly altered as input lists. Comparative pathway analyses were performed with Ingenuity Pathway Analysis (IPA; Qiagen) on combined sets of genes, lipids and polar metabolite identifiers. Raw transcriptomic data and experimental details are archived at ArrayExpress (accession number: E-MTAB-5734).

Results

In total, 259 polar metabolomic, 250 lipidomic and 156 transcriptomic samples passed the quality control metrics. Four RNAseq samples were removed prior to further analysis due to anomalously low counts. The full results of univariate analyses comparing each exposure group with its time-matched control group are shown in **ESI 4**. Comparisons were made with time-matched controls since gene expression and metabolite profiles varied significantly with time between the control groups sampled at 1h, 6h and 24h. **Figure 1** illustrates the overall numbers of significantly changing ($q < 0.05$) genes and metabolites in comparison with time-matched controls. The numbers of molecular (transcript and metabolic) changes at 24h correlated significantly with cytotoxicity (Table 1) for all silver (Ag MP, Ag NP and Ag⁺) exposures ($r^2 = 0.98$; $p < 0.01$) and all zinc (ZnO MP, ZnO NP and Zn²⁺) exposures ($r^2 = 0.85$; $p < 0.03$) but not for the CeO₂ NP exposures. All silver exposures resulted in significantly more changes than CeO₂ exposures, and all zinc exposures led to the most numerous alterations. Silver exposures ranked from the largest to the smallest effect in the order Ag⁺, Ag NP and then Ag MP, whereas zinc exposures ranked highest for Zn²⁺, followed by ZnO MP, ZnO NP-NM110 and ZnO NP-NM111. These rank orders matched the orders of ionic concentrations determined by dissolution analysis (Table 1). CeO₂ NP exposures resulted in few gene expression or metabolic changes, and ionic dissolution was below the limit of detection. Of these few changes, CeO₂ NP-A (undoped CeO₂ NPs) was the only CeO₂ NP that increased metabolites putatively identified as cysteine at 1 h (3.5 fold; $q < 0.032$) and γ -glutamylcysteine at 6h (1.5 fold; $q < 0.02$).

PCA scores plots of transcriptomic and polar metabolomic data after 6h of exposure are shown in **Figure 2**, with PCAs for all other timepoints, as well as for the lipidomics data, shown in **ESI 5**. For silver there was grouping of replicate samples and separation from the controls was apparent for all exposure groups. For zinc, replicate samples grouped tightly and clearly diverged from the control group along PC1, with the degree of divergence corresponding with the number of molecular changes outlined above (see also Figure 1). There was little or no apparent grouping of the CeO₂ NP samples or divergence from the control group.

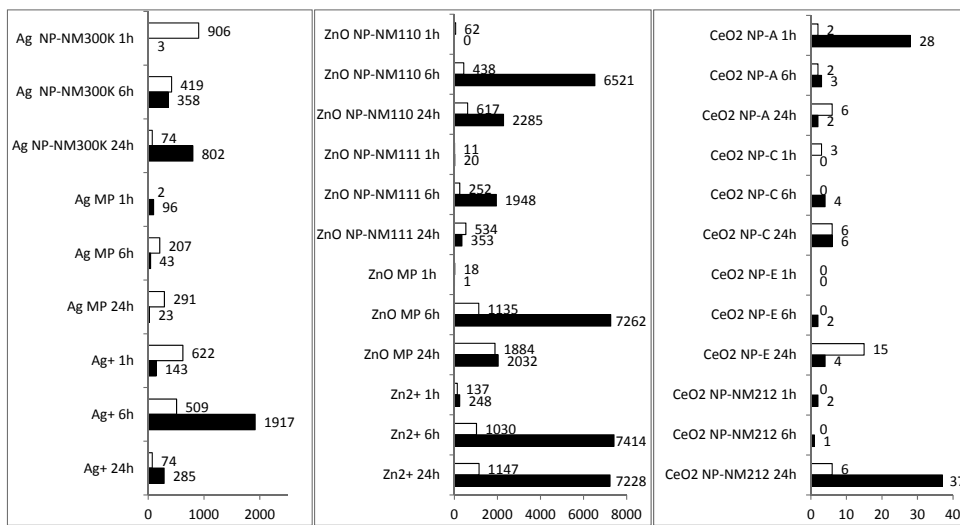


Figure 1: Number of genes significantly differentially expressed (black bars) and metabolite peaks significantly altered in concentration (clear bars) ($q < 0.05$) in A549 cells after silver, zinc, or CeO₂ NPs, MPs and/or ionic exposures for 1, 6 or 24 h.

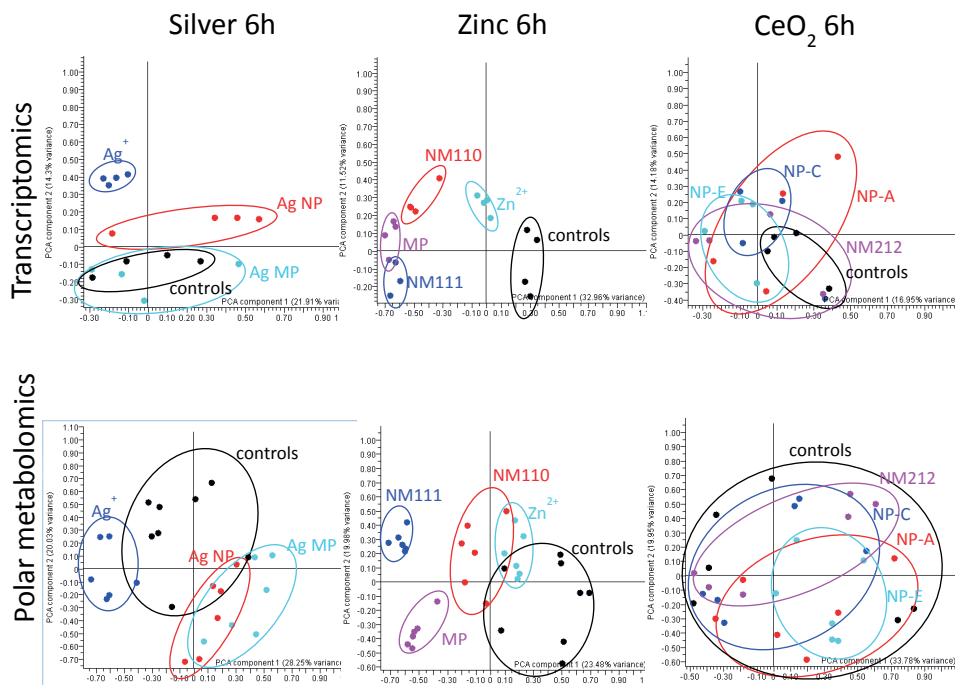


Figure 2: Principal components analysis scores plots of transcriptomics and metabolomics data from A549 cells exposed to silver, zinc, or CeO₂ for 6 h. For silver, control samples are shown in black, Ag NP treated in red, Ag MP in cyan, Ag⁺ in blue. For zinc, control samples are shown in black, ZnO NP-NM110 in red, ZnO NP-NM111 in blue, Zn²⁺ in cyan and ZnO MP in pink. For CeO₂, control samples are shown in black, CeO₂ NP-A treated in red, CeO₂ NP-C in blue, CeO₂ NP-E in cyan and CeO₂ NP-NM212 in pink. PCAs for all timepoints are shown in ESI 5.

IMPALA pathway over-representation analysis results are shown in full in **ESI 6**, while over-representation of selected pathways is illustrated in **Figure 3**. All silver and zinc exposures at 6h and 24h resulted in significant enrichment of the terms 'Response to metal ions' and 'Metallothioneins bind metals'. Terms relating to the heat shock response were enriched in the same groups at 6h but not at 24h, except for the Ag⁺ and Zn²⁺ exposures where they persisted. Other enriched terms, including 'Translation', 'Nonsense-Mediated Decay', 'Apoptosis' and 'Immune System' were highlighted with all zinc exposures and either Ag⁺ or Ag NP exposure at 6h and sometimes also at 24 h. Zn²⁺, ZnO MP and ZnO NP-NM110 repressed molecules related to DNA repair. CeO₂ exposures elicited few molecular changes and showed no enriched pathway annotations, apart from 'HIF-1 alpha transcription network' induced at 24h with CeO₂ NM212 and 'ID signalling pathway' repressed at 6 and 24h with CeO₂ NP-A,- C and E.

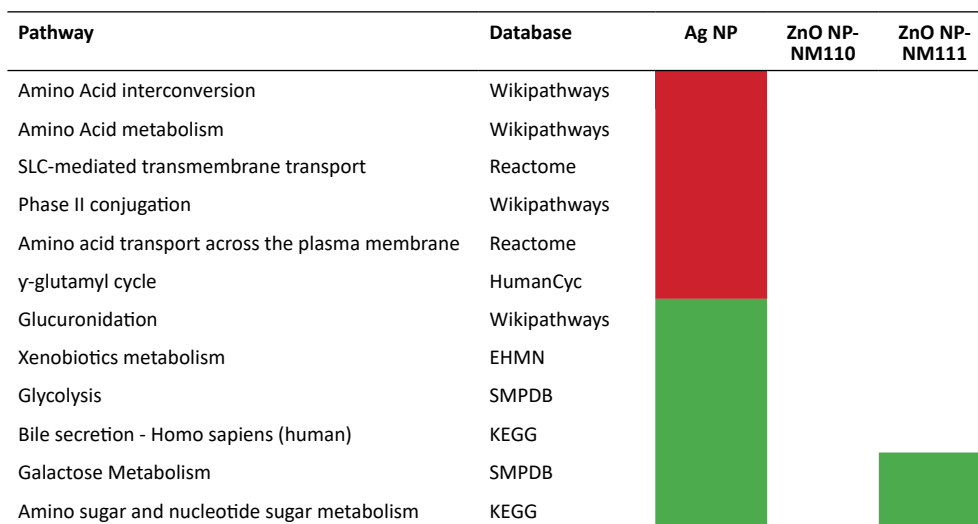
Ingenuity Pathway Analysis (IPA) Comparison Analyses were used to compare molecular pathway responses to the various silver and zinc exposures. **Figure 4** shows the top 20 canonical pathways and the top 20 'diseases and bio-functions' associated with the silver and zinc exposures, ordered by function or process from IPA's Pathway Activity Analysis function, representing predicted pathway activation or inhibition. Particularly prominent for silver was the Nrf2-mediated oxidative stress response pathway, predicted to be activated by Ag NP at 6h and by Ag⁺ at all timepoints. The Nrf2 pathway was also predicted to be activated by all Zn exposures at 6h, but repressed at 24h. The canonical pathway comparison of silver exposures was otherwise dominated by modulation of several molecular signalling pathways, particularly with Ag⁺ at 6h. All Zn exposures resulted in very similar profiles of predicted pathway activation, highlighting co-ordinated induction of signalling pathways at 6h, followed by repression at 24h, except for Zn²⁺ for which these pathways were predicted to still be activated at 24h. Data from CeO₂ NP exposures were not used due to the low numbers of responsive molecules.

To identify candidate nano-specific responses, t-tests were performed comparing, for silver, the Ag NP group versus respectively the control, Ag⁺ and Ag MP groups. Molecules were only selected if statistically significantly (FDR<0.05) changed in all comparisons. A similar procedure was followed for ZnO NP-NM110 and ZnO NP-NM111. The results of these comparisons and IMPALA pathway analyses using these data are shown in **Figure 5 and ESI 7**. For Ag NPs, 17.6% of transcriptional and 22% of metabolic changes were assessed as candidate nano-specific. The induced molecules associated with several pathways, particularly those concerned with amino acid metabolism, while the decreasing molecules associated with glycolysis and galactose metabolism and reduced transcription relating to phase II xenobiotic metabolism. ZnO NP-NM110 elicited only 12 (0.15%) candidate nano-specific changes and ZnO NP-NM111 elicited 22 (0.77%), mostly reduction in metabolites associated with galactose metabolism.

Figure 3: Heatmap illustrating selected pathway annotation terms significantly differentially represented ($q < 0.05$) by IMPaLA among genes and metabolites induced (red) or repressed (green) in comparison with time matched control groups after exposure of A549 cells to silver, zinc, or CeO₂ (NPs, MPs or ions) for 1, 6 or 24h. Full data are shown in ESI 6.

Pathway	Database			Silver						Zinc						CeO ₂					
	Ag NP- NM300K	Ag MP	Ag ⁺	Ag NP- NM300K	Ag MP	Ag ⁺	ZnO NP-NM110	ZnO NP-NM111	ZnO MP	Zn ²⁺	CeO ₂ NP-A	CeO ₂ NP-C	CeO ₂ NP-C	CeO ₂ NP-NM212	CeO ₂ NP-NM212						
Exposure duration (h)	1	6	24	1	6	24	1	6	24	1	6	24	1	6	24	1	6	24			
Response to metal ions																					
Metallothioneins bind metals																					
Zinc homeostasis																					
Cellular response heat stress																					
HSF1 activation																					
AP-1 transcription factor																					
HIF-1- α transcription factor																					
γ -glutamyl cycle																					
Translation																					
Nonsense-mediated decay																					
Selenocysteine synthesis																					
Apoptosis																					
Immune system																					
ID signalling pathway																					
Cell cycle																					
TCA cycle																					
DNA repair																					

Figure 5: Heatmap illustrating selected pathway annotation terms significantly differentially represented ($q < 0.05$) by IMPaLA among candidate nano-specific transcripts and metabolites induced (red) or repressed (green) in comparison with control, microparticle and ionic exposures over all timepoints. Full data are shown in ESI 7.



Discussion

In our study molecular changes were sought that were unique to the nanomaterial exposures, not appearing in response to the ionic or micro-sized particle exposures at any timepoint. These were termed ‘candidate nano-specific responses’ as only three timepoints were examined for each exposure, raising the possibility of these responses having occurred at an unexamined timepoint in the non-NP exposures. For silver there was evidence for candidate nano-specific changes supported by both the transcriptomics and metabolomics data (**Figure 5 and ESI 7**). These were related to increases in amino-acid transport, reduced glycolysis and galactose metabolism and reduced glucuronidation and xenobiotic metabolism. Potentially these changes could result in lower capacity to detoxify organic xenobiotics and it could be instructive to compare modulation of organic xenobiotic toxicity in co-exposures with Ag NP or Ag⁺. However, since no dispersant control (for Ag NP-NM300K) was included in the omics study, some of these nano-specific changes may be caused by the dispersant (water with 4% polyoxyethylene glycerol trioleate and 4% Tween 20), instead of the Ag NPs. Although previous studies with the same Ag NPs and its dispersant indicated that the dispersant was not cytotoxic to A549 cells up to 256 µg/mL,^{29,30} DNA damage was observed in the absence of cytotoxicity³¹ in A549 cells. For zinc there was very little evidence of candidate nano-specific responses, limited to metabolomics changes related in pathway analyses to a reduction in galactose metabolism. Although candidate nano-specific responses were found for Ag NPs, by far the majority (>78%) of responses to the Ag NPs were also seen with Ag⁺ and Ag MP, as was found by NMR metabolomics in HaCaT cells³², implying that nano-specific toxicity is likely a minor component compared with that elicited by silver ions.

All silver and zinc exposures induced transcription of genes responsive to metal ions at 6h and 24h. Metallothionein induction was particularly notable, with *MT1A*, *MT1B*, *MT1F*, *MT1G*, *MT1X*, and *MT2A* highly and significantly induced with all Ag and Zn exposures but *MT1H* and *MT1E* induced only with Zn. Several of these *MT* transcript inductions exceeded 1000-fold, including *MT1B* with Ag NPs and Ag⁺ at 6h and *MT1H* with ZnO NM-110, Zn²⁺ and Zn MP at 6h and 24h. Additionally the zinc transporter *SLC30A1* (ZnT-1), responsible for export of zinc ions, was induced by both Zn and Ag exposures. Ag ions have been shown to release Zn ions in fibroblasts³³.

Metallothioneins have long been considered biomarkers for metal ion exposure and oxidative stress³⁴ and metal-based NP studies frequently report their induction^{35,36}. Metallothionein induction may be viewed as an adaptive response enabling cells to bind and sequester metal ions and for Ag MP exposure this response appeared effective, resulting in only 5% cytotoxicity (**Table 1**) and few significant alterations in other biological pathways (**Figure 3; ESI 6**). However with the other Ag and Zn exposures resulting in higher cytotoxicity, it was apparent that this capacity was exceeded, leading to stress responses and cellular damage.

The heat shock response was activated in all 6h and 24h Zn exposures and with Ag²⁺ and Ag NPs; transcripts encoding the molecular chaperones HSPA1A, HSPA1L, HSPA6, HSPA7, HSPB1, HSPH1, HSP90AA1, HSP90AB1, DNAJB1 and DNAJB6 were induced, implying a response to protein damage.

Oxidative stress is a well-established outcome following NP exposure, including Ag, ZnO and CeO₂, NPs^{37,38}. IPA highlighted the Nrf2 mediated oxidative stress response as activated by Ag⁺ and all 6h Zn exposures. Nrf-2 (*NFE2L2*) transcript was significantly but not highly induced (<1.6-fold) with Zn²⁺ and Zn MP and several key antioxidant enzyme transcripts were either mildly but significantly induced (*SOD1*, *TXN*, *GLRX*, *GCLM*, *GSS*) at 6h or mildly repressed (*CAT*, *GCLC*, *GSR*, *PRDX1*). Aldehyde oxidase *AOX1* was induced over 2-fold, as were heme oxygenase (*HMOX1*), several chaperones mentioned above and transcription factors *FOS*, *JUN* and *ATF4*. Transcription of *KEAP1*, a repressor of Nrf-2 signalling, was significantly repressed with ZnO NM-110, Zn²⁺ and Zn MP at 6h. Nrf2 pathway induction has previously been found for Ag NPs³⁹ and for ionic Ag and Zn⁴⁰. Several polar metabolite peaks that were putatively annotated as glutathione (GSH) followed a similar profile of a significant increase with Ag⁺ at 1h but a significant decrease with all zinc exposures at 6h and 24h. GSH is the major intracellular antioxidant and its depletion implies vulnerability to further oxidative damage. GSH has previously been found to decrease with ZnO NP treatment in mouse livers and kidneys^{41, 42}.

A metabolite peak putatively annotated as cysteine was particularly highly increased with all Ag exposures, and amino acid concentrations were significantly altered with most exposures. This may represent an adaptive reorganisation of amino acid synthesis and transport. Expression of transcripts involved in translation, including those encoding ribosomal subunits, was increased with Ag NP, ZnO MP and Zn²⁺ exposure. Interestingly nonsense mediated decay pathway transcripts were induced in the same exposures, implying an increase in mRNAs with premature stop codons. Potentially this could be due to an increased rate of DNA damage, as transcription of DNA repair genes was reduced, including those of the base excision repair, mismatch repair, nucleotide excision repair and double-strand break repair pathways, particularly with Zn²⁺, Zn MP and ZnO NP-NM110. DNA damage has previously been described for Ag⁺, Ag NPs^{43,44}, Zn²⁺ and Zn NPs⁴⁵. Transcription of the stress-inducible AP-1 transcription factor genes was increased by Zn²⁺ and ZnO NP exposure, and by Ag⁺, including induction of *FOS*, *FOSB*, *FOSL1*, *JUN* and *JUNB*. Cell cycle gene transcription was significantly repressed with both Ag and Zn exposures. These effects have previously been seen with Ag NPs^{43, 46, 47}. There was an induction of transcription associated with apoptosis and with immune signalling with Ag⁺ and all Zn exposures at 6h, persisting to 24h with Zn²⁺. Both ionic and NP Ag and Zn can increase apoptosis in A549 cells^{48, 49}. By 24h Zn²⁺ exposure, both transcripts and metabolites of the TCA cycle were significantly

reduced, indicating major disruption of cellular respiration pathways, consistent with the bioenergetic disruption reported for ZnO NP exposure of A549 cells⁵⁰.

These molecular alterations illustrate a progression from adaptive changes, such as metallothionein induction, to depletion of antioxidants, such as glutathione, repressed DNA repair and induction of apoptosis. Several of these molecular changes have been proposed as key events (KE) in the Adverse Outcome Pathway (AOP) paradigm⁵¹. Examples include increase in oxidative stress, activation of Nrf-2, depletion of glutathione, repression of DNA repair and increased apoptosis. It is however apparent that many additional pathways, genes and metabolites were altered during the exposures to Ag and Zn (**ESI 5 and 6**) and that using a cell line model one can only examine those events leading up to cell death.

For ZnO NPs and MPs, responses indicative of damage tended to peak at 6h, with a reduction by 24h, for example acute phase signalling (**Figure 5**), while with Zn²⁺ these changes persisted to 24h, consistent with the greater cytotoxicity caused by this treatment. The responses to Ag and Zn clearly demonstrated the importance of measuring molecular responses over time in order to robustly assess molecular toxicity. At 1h there were relatively few molecular pathway changes (**Figure 3**), at 6h molecular responses indicative of toxicity had developed, but at 24h for several exposures (Ag⁺, Ag MP, ZnO NP-NM110, ZnO NP-NM111 and Zn MP) the responses had declined, or even reversed (**Figure 4**) whereas these persisted with the more cytotoxic ZnCl₂ exposure. This time-dependence of molecular response can be explained by adaptive changes, such as induction of metallothioneins that ameliorate cellular damage by sequestering the metal ions, as illustrated by the Ag MP exposure. There may also be a time dependency in exposure to the metal ions, due to different uptake rates and dissolution kinetics of the different micro- and nano-sized particles resulting in different intracellular concentrations, or different intracellular compartmentalisation of the metal ions. In A549 cells and phagocytic murine macrophages, Ag NPs were associated with lysosomes⁵², whereas ionic Ag⁺ was bound to metallothioneins⁵³. ZnO NPs showed intracellular dissolution in lysosomes of macrophages⁵⁴ and extracellular dissolution with only ions entering hepatocytes⁵⁵. Additionally NP dissolution can also occur within the NP preparations⁵⁶ and in cell culture medium (ESI 2). The dynamic molecular responses detected could therefore reflect changing intracellular doses of metal ions. For future studies it is therefore recommended to obtain additional supporting data to estimate the intracellular doses, including time-resolved data on the bioavailable ion concentrations after exposure to the salts and cellular uptake rates of MPs, NPs and ions.

CeO₂ NPs led to relatively few significant alterations of transcription or metabolism compared with silver and zinc, reflecting both a decrease in molecular alterations with increasing EC₂₀ concentrations (effective concentrations resulting in 20% cytotoxicity) and their low solubility (Table 1). A similar mild metabolomic and transcriptomic response to CeO₂ NPs was found

by Taylor et al.¹² in algae. Among the few significant alterations induced by the CeO₂ NPs, only CeO₂ NP-A (undoped CeO₂ NP) exposure significantly increased metabolites putatively identified as cysteine and γ-glutamylcysteine, potentially representing an adaptive response to oxidative stress by increased uptake and synthesis of these glutathione precursors. Because these changes were not observed after exposure to CeO₂ NP-C (27% Zr-doped CeO₂ NPs) or CeO₂ NP-E (78% Zr-doped CeO₂ NPs), this finding might indicate that modification of the surface redox state by Zr-doping increases the ability to scavenge ROS, resulting in a decreased induction of oxidative stress of the CeO₂ NPs. Since all CeO₂ NPs showed very low cytotoxicity and exposure to only one of the four CeO₂ NPs showed any slight evidence of molecular responses to oxidative stress, the actual occurrence of oxidative stress, ROS or damage related to ROS was not further investigated.

CeO₂ NP-A, -C and -E exposures all resulted in repression of ID family gene expression (**Figure 4**). Verstraelen et al.⁵⁷ similarly found repression of *ID2* transcription in A549 cells treated with CeO₂ NPs. The ID, or Inhibitor of DNA binding, genes are binding partners of bHLH transcription factors and are involved in regulation of a wide variety of biological processes, including metastasis and vascularisation⁵⁸. CeO₂ NP-NM212 elicited a different molecular response from the other CeO₂ NPs, activating genes of the HIF1-α transcription factor network (**Figure 4**) by 24h. This response was also shared by the 6h Ag and Zn exposures, with additional induction of heme oxygenase (*HMOX1*). HIF1-α responsive genes are also commonly induced by several metal ions and particles⁵⁹ and in cancer cells by ROS⁶⁰, leading to angiogenesis via VEGF. This finding is consistent with CeO₂ and Ag NPs inducing angiogenesis^{61, 62}.

Conclusions

A time series experiment was used to determine the similarity of A549 cellular responses following exposure to NPs and ions, as focussing on a single timepoint would have led to erroneous conclusions in the absence of internal dose measurements. The majority of molecular responses of A549 cells to the Ag and Zn NPs, such as metallothionein induction, depletion of antioxidants, repressed DNA repair and induction of apoptosis, are similar to their responses to Ag and Zn ions, respectively, confirming that the modes of action of these NPs are largely mediated by dissolved metal ions rather than by the physical aspects of the NPs. Low toxicity CeO₂ NPs elicited only minor molecular responses. Of the four CeO₂ NPs tested, only CeO₂ NP-A elicited any molecular changes indicative of oxidative stress.

Acknowledgements

The authors would like to thank Stephen Kissane and Fay Hughes for their assistance with RNA sequencing and Dr. Ralf Weber for bioinformatics assistance. The study has received funding from the European Union's Seventh Framework Programme under grant agreement n° 310451 (NanoMILE) and the Netherlands Food and Consumer Product Safety Authority (NVWA).

References

1. A. Nel, T. Xia, H. Meng, X. Wang, S. Lin, Z. Ji and H. Zhang. Nanomaterial toxicity testing in the 21st century: use of a predictive toxicological approach and high-throughput screening. *Acc Chem Res*, 2013, **46**, 607-621.
2. V. De Matteis, M. A. Malvindi, A. Galeone, V. Brunetti, E. De Luca, S. Kote, P. Kshirsagar, S. Sabella, G. Bardi and P. P. Pompa. Negligible particle-specific toxicity mechanism of silver nanoparticles: the role of Ag⁺ ion release in the cytosol. *Nanomedicine*, 2015, **11**, 731-739.
3. J. Liu, X. Feng, L. Wei, L. Chen, B. Song and L. Shao. The toxicology of ion-shedding zinc oxide nanoparticles. *Crit Rev Toxicol*, 2016, **46**, 348-384.
4. A. R. Gliga, S. Skoglund, I. O. Wallinder, B. Fadeel and H. L. Karlsson. Size-dependent cytotoxicity of silver nanoparticles in human lung cells: the role of cellular uptake, agglomeration and Ag release. *Part Fibre Toxicol*, 2014, **11**, 11.
5. A. Ivask, K. Juganson, O. Bondarenko, M. Mortimer, V. Aruoja, K. Kasemets, I. Blinova, M. Heinlaan, V. Slaveykova and A. Kahru. Mechanisms of toxic action of Ag, ZnO and CuO nanoparticles to selected ecotoxicological test organisms and mammalian cells in vitro: a comparative review. *Nanotoxicology*, 2014, **8 Suppl 1**, 57-71.
6. I. Celardo, M. De Nicola, C. Mandoli, J. Z. Pedersen, E. Traversa and L. Ghibelli. Ce(3)⁺ ions determine redox-dependent anti-apoptotic effect of cerium oxide nanoparticles. *ACS Nano*, 2011, **5**, 4537-4549.
7. K. M. Dunnick, R. Pillai, K. L. Pisane, A. B. Stefaniak, E. M. Sabolsky and S. S. Leonard. The Effect of Cerium Oxide Nanoparticle Valence State on Reactive Oxygen Species and Toxicity. *Biol Trace Elem Res*, 2015, **166**, 96-107.
8. P. M. Costa and B. Fadeel. Emerging systems biology approaches in nanotoxicology: Towards a mechanism-based understanding of nanomaterial hazard and risk. *Toxicol Appl Pharmacol*, 2016, **299**, 101-111.
9. S. Labib, A. Williams, C. L. Yauk, J. K. Nikota, H. Wallin, U. Vogel and S. Halappanavar. Nano-risk Science: application of toxicogenomics in an adverse outcome pathway framework for risk assessment of multi-walled carbon nanotubes. *Part Fibre Toxicol*, 2016, **13**, 15.
10. J. M. Buescher and E. M. Driggers. Integration of omics: more than the sum of its parts. *Cancer Metab*, 2016, **4**, 4.
11. S. Halappanavar, U. Vogel, H. Wallin and C. L. Yauk. Promise and peril in nanomedicine: the challenges and needs for integrated systems biology approaches to define health risk. *Wiley Interdiscip Rev Nanomed Nanobiotechnol*, 2018, **10**, DOI: 10.1002/wnan.1465.
12. N. S. Taylor, R. Merrifield, T. D. Williams, J. K. Chipman, J. R. Lead and M. R. Viant. Molecular toxicity of cerium oxide nanoparticles to the freshwater alga *Chlamydomonas reinhardtii* is associated with supra-environmental exposure concentrations. *Nanotoxicology*, 2016, **10**, 32-41.
13. S. Losert, N. von Goetz, C. Bekker, W. Fransman, S. W. Wijnhoven, C. Delmaar, K. Hungerbuehler and A. Ulrich. Human exposure to conventional and nanoparticle-containing sprays-a critical review. *Environ Sci Technol*, 2014, **48**, 5366-5378.

14. A. D. Maynard and E. D. Kuempel. Airborne Nanostructured Particles and Occupational Health. *Journal of Nanoparticle Research*, 2005, **7**, 587-614.
15. K. Jensen, Kembouche, Y, Christiansen, E, Jacobsen, NR, Wallin, H *Final protocol for producing suitable manufactured nanomaterial exposure media. The generic NANOGENOTOX dispersion protocol*, 2011.
16. W. Slob. Dose-response modeling of continuous endpoints. *Toxicol Sci*, 2002, **66**, 298-312.
17. C. L. Klein, Comero, S., Stahlmecke, B., Romazanov, J., Kuhlbusch, T. A. J., Van Doren, E., De Temmerman, P-J., Mast, J., Wick, P., Krug, H., Locoro, G., Hund-Rinke, K., Kördel, W., Friedrichs, S., Maier, G., Werner, J., Linsinger Th., Gawlik, B. M. , *NM-Series of Representative Manufactured Nanomaterials NM-300 Silver Characterisation, Stability, Homogeneity*, European Commission Joint Research Centre, Luxembourg, 2011.
18. C. Singh, Friedrichs, S., Levin, M., Birkedal, R., Jensen, K. A., Pojana, G., Wohlleben, W., Schulte, S., Wiench, K., Turney, T., Koulaeva, O., Marshall, D., Hund-Rinke, K., Kördel, W., Van Doren, E., De Temmerman, P-J., Abi Daoud Francisco, M., Mast, J., Gibson, N., Koeber, R., Linsinger, T., Klein C. L., *NM-Series of Representative Manufactured Nanomaterials Zinc Oxide NM-110, NM-111, NM-112, NM-113 Characterisation and Test Item Preparation*, European Commission Joint Research Centre, Luxembourg, 2011.
19. C. Singh, S. Friedrichs, G. Ceccone, N. Gibson, K. Alstrup Jensen, M. Levin, H. Goenaga Infante, D. Carlander, K. Rasmussen., *Cerium Dioxide, NM-211, NM-212, NM-213. Characterisation and test item preparation*, Luxembourg, 2014.
20. A. D. Southam, T. G. Payne, H. J. Cooper, T. N. Arvanitis and M. R. Viant. Dynamic range and mass accuracy of wide-scan direct infusion nano-electrospray fourier transform ion cyclotron resonance mass spectrometry-based metabolomics increased by the spectral stitching method. *Anal Chem*, 2007, **79**, 4595-4602.
21. J. Zhang, M. A. Abdallah, T. D. Williams, S. Harrad, J. K. Chipman and M. R. Viant. Gene expression and metabolic responses of HepG2/C3A cells exposed to flame retardants and dust extracts at concentrations relevant to indoor environmental exposures. *Chemosphere*, 2016, **144**, 1996-2003.
22. J. A. Kirwan, R. J. Weber, D. I. Broadhurst and M. R. Viant. Direct infusion mass spectrometry metabolomics dataset: a benchmark for data processing and quality control. *Sci Data*, 2014, **1**, 140012.
23. A. D. Southam, R. J. Weber, J. Engel, M. R. Jones and M. R. Viant. A complete workflow for high-resolution spectral-stitching nano-electrospray direct-infusion mass-spectrometry-based metabolomics and lipidomics. *Nat Protoc*, 2016, **12**, 310-328.
24. R. J. Weber, A. D. Southam, U. Sommer and M. R. Viant. Characterization of isotopic abundance measurements in high resolution FT-ICR and Orbitrap mass spectra for improved confidence of metabolite identification. *Anal Chem*, 2011, **83**, 3737-3743.
25. Y. Benjamini and Y. Hochberg. Controlling the False Discovery Rate: a Practical and Powerful Approach to Multiple Testing. *J.R.Statist.Soc.B*, 1995, **57**, 289-300.

26. M. I. Love, W. Huber and S. Anders. Moderated estimation of fold change and dispersion for RNA-seq data with DESeq2. *Genome Biol*, 2014, **15**, 550.
27. A. Kamburov, R. Cavill, T. M. Ebbels, R. Herwig and H. C. Keun. Integrated pathway-level analysis of transcriptomics and metabolomics data with IMPaLA. *Bioinformatics*, 2011, **27**, 2917-2918.
28. D. S. Wishart, T. Jewison, A. C. Guo, M. Wilson, C. Knox, Y. Liu, Y. Djoumbou, R. Mandal, F. Aziat, E. Dong, S. Bouatra, I. Sinelnikov, D. Arndt, J. Xia, P. Liu, F. Yallou, T. Bjorn Dahl, R. Perez-Pineiro, R. Eisner, F. Allen, V. Neveu, R. Greiner and A. Scalbert. HMDB 3.0--The Human Metabolome Database in 2013. *Nucleic Acids Res*, 2013, **41**, D801-807.
29. B. K. Gaiser, S. Hirn, A. Kermanzadeh, N. Kanase, K. Fytianos, A. Wenk, N. Haberl, A. Brunelli, W. G. Kreyling and V. Stone. Effects of silver nanoparticles on the liver and hepatocytes in vitro. *Toxicol Sci*, 2013, **131**, 537-547.
30. M. M. Sthijns, W. Thongkam, C. Albrecht, B. Hellack, A. Bast, G. R. Haenen and R. P. Schins. Silver nanoparticles induce hormesis in A549 human epithelial cells. *Toxicol In Vitro*, 2017, **40**, 223-233.
31. W. Thongkam, K. Gerloff, D. van Berlo, C. Albrecht and R. P. Schins. Oxidant generation, DNA damage and cytotoxicity by a panel of engineered nanomaterials in three different human epithelial cell lines. *Mutagenesis*, 2017, **32**, 105-115.
32. J. Carrola, V. Bastos, I. Jarak, R. Oliveira-Silva, E. Malheiro, A. L. Daniel-da-Silva, H. Oliveira, C. Santos, A. M. Gil and I. F. Duarte. Metabolomics of silver nanoparticles toxicity in HaCaT cells: structure-activity relationships and role of ionic silver and oxidative stress. *Nanotoxicology*, 2016, **10**, 1105-1117.
33. M. M. Cortese-Krott, M. Munchow, E. Pirev, F. Hessner, A. Bozkurt, P. Uciechowski, N. Pallua, K. D. Kroncke and C. V. Suschek. Silver ions induce oxidative stress and intracellular zinc release in human skin fibroblasts. *Free Radic Biol Med*, 2009, **47**, 1570-1577.
34. M. Murata, P. Gong, K. Suzuki and S. Koizumi. Differential metal response and regulation of human heavy metal-inducible genes. *J Cell Physiol*, 1999, **180**, 105-113.
35. Y. Li, T. Qin, T. Ingle, J. Yan, W. He, J. J. Yin and T. Chen. Differential genotoxicity mechanisms of silver nanoparticles and silver ions. *Arch Toxicol*, 2017, **91**, 509-519.
36. S. F. Lin, H. Wei, D. Maeder, R. B. Franklin and P. Feng. Profiling of zinc-altered gene expression in human prostate normal vs. cancer cells: a time course study. *J Nutr Biochem*, 2009, **20**, 1000-1012.
37. M. Simko, S. Tischler and M. O. Mattsson. Pooling and Analysis of Published in Vitro Data: A Proof of Concept Study for the Grouping of Nanoparticles. *Int J Mol Sci*, 2015, **16**, 26211-26236.
38. P. Chairuangkitti, S. Lawanprasert, S. Roytrakul, S. Aueviriyavit, D. Phummiratch, K. Kulthong, P. Chanvorachote and R. Maniratanachote. Silver nanoparticles induce toxicity in A549 cells via ROS-dependent and ROS-independent pathways. *Toxicol In Vitro*, 2013, **27**, 330-338.
39. S. Aueviriyavit, D. Phummiratch and R. Maniratanachote. Mechanistic study on the biological effects of silver and gold nanoparticles in Caco-2 cells--induction of the Nrf2/HO-1 pathway by high concentrations of silver nanoparticles. *Toxicol Lett*, 2014, **224**, 73-83.
40. S. O. Simmons, C. Y. Fan, K. Yeoman, J. Wakefield and R. Ramabhadran. NRF2 Oxidative Stress Induced by Heavy Metals is Cell Type Dependent. *Curr Chem Genomics*, 2011, **5**, 1-12.

41. L. M. Faddah, N. A. Abdel Baky, N. M. Al-Rasheed, N. M. Al-Rasheed, A. J. Fatani and M. Atteya. Role of quercetin and arginine in ameliorating nano zinc oxide-induced nephrotoxicity in rats. *BMC Complement Altern Med*, 2012, **12**, 60.
42. X. Yang, H. Shao, W. Liu, W. Gu, X. Shu, Y. Mo, X. Chen, Q. Zhang and M. Jiang. Endoplasmic reticulum stress and oxidative stress are involved in ZnO nanoparticle-induced hepatotoxicity. *Toxicol Lett*, 2015, **234**, 40-49.
43. P. Dubey, I. Matai, S. U. Kumar, A. Sachdev, B. Bhushan and P. Gopinath. Perturbation of cellular mechanistic system by silver nanoparticle toxicity: Cytotoxic, genotoxic and epigenetic potentials. *Adv Colloid Interface Sci*, 2015, **221**, 4-21.
44. R. Foldbjerg, D. A. Dang and H. Autrup. Cytotoxicity and genotoxicity of silver nanoparticles in the human lung cancer cell line, A549. *Arch Toxicol*, 2011, **85**, 743-750.
45. J. Heim, E. Felder, M. N. Tahir, A. Kaltbeitzel, U. R. Heinrich, C. Brochhausen, V. Mailander, W. Tremel and J. Brieger. Genotoxic effects of zinc oxide nanoparticles. *Nanoscale*, 2015, **7**, 8931-8938.
46. Y. S. Lee, D. W. Kim, Y. H. Lee, J. H. Oh, S. Yoon, M. S. Choi, S. K. Lee, J. W. Kim, K. Lee and C. W. Song. Silver nanoparticles induce apoptosis and G2/M arrest via PKCzeta-dependent signaling in A549 lung cells. *Arch Toxicol*, 2011, **85**, 1529-1540.
47. R. Y. Prasad, J. K. McGee, M. G. Killius, D. A. Suarez, C. F. Blackman, D. M. DeMarini and S. O. Simmons. Investigating oxidative stress and inflammatory responses elicited by silver nanoparticles using high-throughput reporter genes in HepG2 cells: effect of size, surface coating, and intracellular uptake. *Toxicol In Vitro*, 2013, **27**, 2013-2021.
48. H. Kocdor, H. Ates, S. Aydin, R. Cehreli, F. Soyarat, P. Kemanli, D. Harmanci, H. Cengiz and M. A. Kocdor. Zinc supplementation induces apoptosis and enhances antitumor efficacy of docetaxel in non-small-cell lung cancer. *Drug Des Devel Ther*, 2015, **9**, 3899-3909.
49. P. J. Shiny, Mukherjee, A., Chandrasekaran, N. DNA damage and mitochondria-mediated apoptosis of A549 lung carcinoma cells induced by biosynthesised silver and platinum nanoparticles. *RSC Advances*, 2016, **6**, 27775-27787.
50. X. Lai, Y. Wei, H. Zhao, S. Chen, X. Bu, F. Lu, D. Qu, L. Yao, J. Zheng and J. Zhang. The effect of Fe₂O₃ and ZnO nanoparticles on cytotoxicity and glucose metabolism in lung epithelial cells. *J Appl Toxicol*, 2015, **35**, 651-664.
51. G. T. Ankley, R. S. Bennett, R. J. Erickson, D. J. Hoff, M. W. Hornung, R. D. Johnson, D. R. Mount, J. W. Nichols, C. L. Russom, P. K. Schmieder, J. A. Serrano, J. E. Tietge and D. L. Villeneuve. Adverse outcome pathways: a conceptual framework to support ecotoxicology research and risk assessment. *Environ Toxicol Chem*, 2010, **29**, 730-741.
52. T. Miyayama and M. Matsuoka. Involvement of lysosomal dysfunction in silver nanoparticle-induced cellular damage in A549 human lung alveolar epithelial cells. *J Occup Med Toxicol*, 2016, **11**, 1.
53. Y. Arai, T. Miyayama and S. Hirano. Difference in the toxicity mechanism between ion and nanoparticle forms of silver in the mouse lung and in macrophages. *Toxicology*, 2015, **328**, 84-92.

54. T. Xia, M. Kovochich, M. Liong, L. Madler, B. Gilbert, H. Shi, J. I. Yeh, J. I. Zink and A. E. Nel. Comparison of the mechanism of toxicity of zinc oxide and cerium oxide nanoparticles based on dissolution and oxidative stress properties. *ACS Nano*, 2008, **2**, 2121-2134.
55. M. Chevallet, B. Gallet, A. Fuchs, P. H. Jouneau, K. Um, E. Mintz and I. Michaud-Soret. Metal homeostasis disruption and mitochondrial dysfunction in hepatocytes exposed to sub-toxic doses of zinc oxide nanoparticles. *Nanoscale*, 2016, **8**, 18495-18506.
56. C. Beer, R. Foldbjerg, Y. Hayashi, D. S. Sutherland and H. Autrup. Toxicity of silver nanoparticles - nanoparticle or silver ion? *Toxicol Lett*, 2012, **208**, 286-292.
57. S. Verstraelen, S. Remy, E. Casals, P. De Boever, H. Witters, A. Gatti, V. Puentes and I. Nelissen. Gene expression profiles reveal distinct immunological responses of cobalt and cerium dioxide nanoparticles in two in vitro lung epithelial cell models. *Toxicol Lett*, 2014, **228**, 157-169.
58. F. Ling, B. Kang and X. H. Sun. Id proteins: small molecules, mighty regulators. *Curr Top Dev Biol*, 2014, **110**, 189-216.
59. R. M. Harris, T. D. Williams, R. H. Waring and N. J. Hodges. Molecular basis of carcinogenicity of tungsten alloy particles. *Toxicol Appl Pharmacol*, 2015, **283**, 223-233.
60. L. Z. Liu, X. W. Hu, C. Xia, J. He, Q. Zhou, X. Shi, J. Fang and B. H. Jiang. Reactive oxygen species regulate epidermal growth factor-induced vascular endothelial growth factor and hypoxia-inducible factor-1alpha expression through activation of AKT and P70S6K1 in human ovarian cancer cells. *Free Radic Biol Med*, 2006, **41**, 1521-1533.
61. S. Das, S. Singh, J. M. Dowding, S. Oommen, A. Kumar, T. X. Sayle, S. Saraf, C. R. Patra, N. E. Vlahakis, D. C. Sayle, W. T. Self and S. Seal. The induction of angiogenesis by cerium oxide nanoparticles through the modulation of oxygen in intracellular environments. *Biomaterials*, 2012, **33**, 7746-7755.
62. K. Kang, D. H. Lim, I. H. Choi, T. Kang, K. Lee, E. Y. Moon, Y. Yang, M. S. Lee and J. S. Lim. Vascular tube formation and angiogenesis induced by polyvinylpyrrolidone-coated silver nanoparticles. *Toxicol Lett*, 2011, **205**, 227-234.

Supporting Information

ESI 1: Cytotoxicity of tested particles to A549 cells

Table S1: Overview of EC₂₀ and confidence interval for dose calculation.

Test material	EC ₂₀ Exponential model µg/mL	Confidence interval µg/mL	EC ₂₀ Hill model µg/mL	Confidence interval µg/mL	Selected Dose ² µg/mL
CeO ₂ NP-A	n.d. ¹		n.d.		128
CeO ₂ NP-C	n.d.		n.d.		128
CeO ₂ NP-E	n.d.		n.d.		128
CeO ₂ NP-NM212	n.d.		n.d.		128
ZnO NP-NM110	29.4	22.4-37.3	33.9	29.2-38.9	31.6
ZnO NP-NM111	23.3	16.9-30.6	42.6	37.9-51.4	32.9
ZnO MP	57.6	54.9-61.6	57	54.3-61.1	57.3
ZnCl ₂	19.7	14.2– 26.1	29.4	27.7-31.4	24.5
Ag NP-NM300K	37.9	33.5 – 50.1	39.3	34.0-49.7	38.6
Ag MP	n.d.		n.d.		128
AgNO ₃	9.6	2.6 – 12.8	10.1	5.2 – 11.3	9.8

¹ n.d. = dose could not be determined, highest dose (i.e. 128 µg/mL) was used for the omics experiments.

² Selected Dose = the highest concentration tested or the average of the EC₂₀s of the Exponential and Hill model.

ESI 2: Dissolution of NPs and MPs in cell culture medium using ICP-OES

The NP and MP dispersions in cell culture medium (pH 7.1) were prepared according to the same procedure as used for the preparation of the dispersions for the omics study. Dissolution of the NPs and MPs in cell culture medium was measured at various time intervals (0, 6, and 24 h). At each time interval, 10 mL of the dispersion was transferred to 3 kDa Millipore centrifuge tubes (Satorius, UK) and subjected to centrifugal ultrafiltration at 5000 g for 50 minutes to separate the dissolved fraction. Nitric acid (ICP grade) was added to the filtrate samples to a final concentration of 2% and samples were subsequently analysed using a Perkin Elmer ICP-OES Optima 8000 platform in order to assess how much, if any, dissolution of the NMs or MPs had occurred. Each sample was prepared and analysed in triplicate. Prior to acquisition the torch was aligned (radially and axially) using the Mn wavelengths and calibration curves were constructed using standard solutions of each element prepared by serial dilutions of 1000 ppm in 2% nitric acid. A calibration curve with R² value of >0.999 was deemed sufficient for analysis.

The concentrations of ions detected at each time point are presented in Table S2 below. Interestingly, the dissolved concentration from ZnO NPs determined at 24 hours in complete cell culture medium were higher than the dissolved concentrations determined at pH 7 in DI water (Papadiamantis *et al.*, manuscript in preparation), consistent with the known

affinity of Zn²⁺ for biological components (protein, lysosomes etc.)¹ and its known tendency to form complexes with organic components in the long term^{2,4}. Clearly, this would also be the case for the Zn²⁺ ions released from the ionic control, which would be similarly bound to biomolecules.

Table S2: Ion concentrations in cell culture medium after 0, 6 and 24 hours.

Incubation (hours) → Test material ↓	Initial MP or NM concentration (mg/L)	Ion concentration (µg/mL)		
	0	0	6	24
Ag NP-NM300K	38.6	0.075 +/- 0.01	0.093 +/- 0.03	0.040 +/- 0.003
Ag MP	128	0.005 +/- 0.0002	0.004 +/- 0.0001	0.005 +/- 0.0004
ZnO NP-NM110	15	1.401 +/- 0.06	1.378 +/- 0.07	1.411 +/- 0.01
ZnO NP- NM 111	10	0.439 +/- 0.02	0.899 +/- 0.07	0.989 +/- 0.03
ZnO MP	30	1.323 +/- 0.22	1.338 +/- 0.10	1.461 +/- 0.03
CeO ₂ NP-A	128	<LOD	<LOD	<LOD
CeO ₂ NP-C	128	<LOD	<LOD	<LOD
CeO ₂ NP-E	128	<LOD	<LOD	<LOD
CeO ₂ NP-NM212	128	<LOD	<LOD	<LOD

References:

- ¹ V. Frazzini, E. Rockabrand, E. Mocchegiani and S. L. Sensi. Oxidative stress and brain aging: is zinc the link? *Biogerontology*, 2006, 7, 307-314.
- ² M. Li, L. Zhu and D. Lin. Toxicity of ZnO nanoparticles to *Escherichia coli*: mechanism and the influence of medium components. *Environ Sci Technol*, 2011, 45, 1977-1983.
- ³ R. B. Reed, D. A. Ladner, C. P. Higgins, P. Westerhoff and J. F. Ranville. Solubility of nano-zinc oxide in environmentally and biologically important matrices. *Environ Toxicol Chem*, 2012, 31, 93-99.
- ⁴ T. Xia, M. Kovoichich, M. Liang, L. Madler, B. Gilbert, H. Shi, J. I. Yeh, J. I. Zink and A. E. Nel. Comparison of the mechanism of toxicity of zinc oxide and cerium oxide nanoparticles based on dissolution and oxidative stress properties. *ACS Nano*, 2008, 2, 2121-2134.

ESI 3: Methods

Omics Analyses

S1.1 Extraction of metabolites and lipids

Deep frozen cells were harvested by adding 400 µL 80% methanol (pre-cooled on dry ice) into each well. Cells were scraped from each well on dry ice and were transferred into a 1.8 mL glass vial which was pre-filled with 640 µL pre-cooled chloroform and 416 µL H₂O. 400 µL 80% methanol (pre-cooled on dry ice) was used to wash each well and the wash solution was transferred into the same glass vial. After adjusting the ratio of methanol:chloroform:water (v/v/v) to 1:1:0.9, each glass vial was vortexed for 30 s twice, at 30 s intervals. The glass vials were then cooled on dry ice for 10 mins before centrifugation for 10 mins at 3000-g at -9 °C, which separated the mixture into two phases (upper polar phase and lower non-polar phase). 300 µL aliquots of the polar phase were transferred into clean 1.5mL Eppendorf

tubes and then dried in a speed vac concentrator (Thermo Savant, Holbrook, NY) for 4 h. 300 μ L aliquots of the non-polar phase were transferred into clean 1.8 mL glass vials and dried under a stream of nitrogen for 5 mins. All dried samples were then frozen at -80°C until analysis.

S1.2 Direct infusion mass spectrometry (DIMS)

The DIMS analysis method used was similar to the one reported previously (Southam et al. 2007; Zhang et al. 2016). The dried polar or non-polar extracts were re-suspended in 80 μ L 80:20 (v/v) methanol:water (HPLC grade) with 0.25% formic acid (for positive ion mode analysis of polar extracts) or 80 μ L 2:1 methanol:chloroform with 5 mM ammonium acetate (for negative ion mode analysis of lipids). After centrifugation at 22000g, 4°C for 10 min, 10 μ L supernatant of each sample was loaded into each of four well of a 384-well plate and then analysed (in quadruplicate) using direct infusion mass spectrometry (Q Exactive, Thermo Fisher Scientific, Germany) in positive ion mode (for polar metabolomics) or negative ion mode (for lipidomics), utilising a Triversa nanoelectrospray ion source (Advion Biosciences, Ithaca, NY, USA).

S1.3 Metabolomics Data Processing

Mass spectra were recorded using the selected ion monitoring (SIM) stitching approach from m/z 50-620 (for polar metabolomics) or from m/z 50-1020 (for lipidomics) and then processed using custom-written Matlab scripts as previously reported (Kirwan et al. 2014; Southam et al. 2016). In brief, only mass spectral peaks with a signal-to-noise ratio exceeding 3.5 were retained. For each sample the combination of three of the four technical replicates that has the smallest relative standard deviation (RSD) was selected, which were aligned with a 2ppm mass range and filtered into a single peak list (with only those peaks present in ≥ 2 of the 3 spectra retained). Each filtered peak list (one per sample) was then further aligned with a 2ppm mass range, and filtered to retain only those peaks that were present in 80% of all biological samples in the entire dataset (this filtering step was reduced to 50% for the Zn and Ag lipidomics data). Peaks in the blank samples were removed from the sample spectra. The resulting matrices of peak intensities (termed "DIMS dataset") were probabilistic-quotient normalised (PQN) and intensity-drift corrected using a Quality Control-Robust Spline Correction (QC-RSC) algorithm. Finally, the missing values were imputed using the k-nearest neighbours (KNN) algorithm. For multivariate analysis, generalized log (Glog) transformation of the DIMS dataset was also performed.

S1.4 RNA seq gene expression profiling

Total RNA was extracted from A549 cells using a micro RNeasy Kit (Qiagen, Crawley, UK) according to the manufacturer's protocol. RNA was quantified with a NanoDrop 8000 spectrophotometer (Thermo Scientific, Waltham, MA), and the integrity of RNA was evaluated with a Agilent 2200 Tapestation (Agilent Technologies, Santa Clara, CA). Only RNA with

integrity numbers (RINs) greater than 7.0 were used for subsequent RNA-seq experiments. All RNA libraries were produced using the Biomek FxP (Beckman Coulter A31842) with Ultra Directional RNA Library Prep Kit (New England Biolab E7420L) and NEBnext Multiplex Oligos for Illumina Dual Index Primers (New England Biolabs E7600S), using provided protocols and 500ng of total RNA. Constructed libraries were assessed for quality using the TapeStation 2200 (Agilent G2964AA) with High Sensitivity D1000 DNA screentape (5067-5584), and quantified using Kapa Library Quantification Kit (Kapa Biosystems KK4824) on an AriaMx Realtime PCR System (Agilent G8830A). Multiplex library clustering and sequencing was performed upon the HiSeq2500 with HiSeq Rapid Cluster Kit v2 (Illumina GD-402-4002) at 12pM library concentration with 10% PhiX Control v3 spiked in (Illumina FC-110-3001). The sequencing run was carried out using HiSeq Rapid SBS Kit v2 (Illumina FC-402-4021).

51.5 RNA seq Data Processing

The BCL files were converted to FASTQ format using Illumina bcl2fastq conversion software (v1.8.4). Sequences were then trimmed using Trimmomatic (v0.36). FastQC (v0.11.2) was utilised to assess the data quality, and the QC results were summarised with MultiQC (v0.8). Five low quality samples were identified and removed accordingly. The remaining FASTQ files were aligned to the GENCODE human transcript sequences (release 25, GRCh38.p7) using Bowtie2 (v2.3.0). The resulting SAM data were converted into BED format using SAMtools (v1.3.1) and bamToBed (v2.19.1). Finally, the RNA read counts were extracted from the BED files with a Python script. To provide gene-level analysis, the RNA reads were collapsed to the counts of their coding genes. The gene annotation information was retrieved from the Ensembl database (release 87).

51.6 Omics Data Analysis

Lipidomics and polar metabolomics peak intensity data were visualised in Genespring (v7.3.1; Agilent) and putative annotations were added using MI-Pack (Weber et al. 2011). ANOVAs and t-tests were performed in Genespring using multiple testing corrections (Benjamini and Hochberg 1995) for false discovery rate corrected p-values (FDR) of <0.05. Transcriptional data was mapped by gene. DESeq2 (Love et al. 2014) and used for differential expression analysis with a $q < 0.05$ cut-off. Genespring was used to generate principal components analysis (PCA) scores plots from all omics datasets. Combined gene and metabolite pathway over-representation analyses were performed with IMPaLA (Kamburov et al. 2011), using gene identifiers and all Human Metabolite Database (HMDB) identifiers (Wishart et al. 2013) for each peak identified as significantly altered as input lists. The background sets were all detected transcripts and all identifiers annotated to detected lipid and polar metabolite peaks, respectively. Comparative pathway analyses were performed with Ingenuity Pathway Analysis (IPA; Qiagen) on combined sets of genes, lipids and polar metabolite identifiers using the mean fold change and FDR for each exposure group versus time-matched controls; analyses used only those identifiers with $FDR < 0.05$. Raw data and experimental details are archived at ArrayExpress for transcriptomics (accession number E-MTAB-5734).

References

- Benjamini Y, Hochberg Y (1995) Controlling the False Discovery Rate: a Practical and Powerful Approach to Multiple Testing. *JRStatistSocB* 57(1):289-300
- Kamburov A, Cavill R, Ebbels TM, Herwig R, Keun HC (2011) Integrated pathway-level analysis of transcriptomics and metabolomics data with IMPaLA. *Bioinformatics* 27(20):2917-8 doi:10.1093/bioinformatics/btr499
- Kirwan JA, Weber RJ, Broadhurst DI, Viant MR (2014) Direct infusion mass spectrometry metabolomics dataset: a benchmark for data processing and quality control. *Sci Data* 1:140012 doi:10.1038/sdata.2014.12
- Love MI, Huber W, Anders S (2014) Moderated estimation of fold change and dispersion for RNA-seq data with DESeq2. *Genome Biol* 15(12):550 doi:10.1186/s13059-014-0550-8
- Southam AD, Weber RJ, Engel J, Jones MR, Viant MR (2016) A complete workflow for high-resolution spectral-stitching nano-electrospray direct-infusion mass-spectrometry-based metabolomics and lipidomics. *Nat Protoc* 12(2):310-328 doi:10.1038/nprot.2016.156
- Weber RJ, Southam AD, Sommer U, Viant MR (2011) Characterization of isotopic abundance measurements in high resolution FT-ICR and Orbitrap mass spectra for improved confidence of metabolite identification. *Anal Chem* 83(10):3737-43 doi:10.1021/ac2001803
- Wishart DS, Jewison T, Guo AC, et al. (2013) HMDB 3.0--The Human Metabolome Database in 2013. *Nucleic Acids Res* 41(Database issue):D801-7 doi:10.1093/nar/gks1065

ESI 4: Univariate analyses of omics data

See:



ESI 5: PCA scores plots of omics data

Principal components analysis (PCA) scores plots of transcriptomic, lipidomic and metabolomic data derived from exposure of A549 cells to silver, zinc and CeO₂ nanoparticles, microparticles and/or ions.

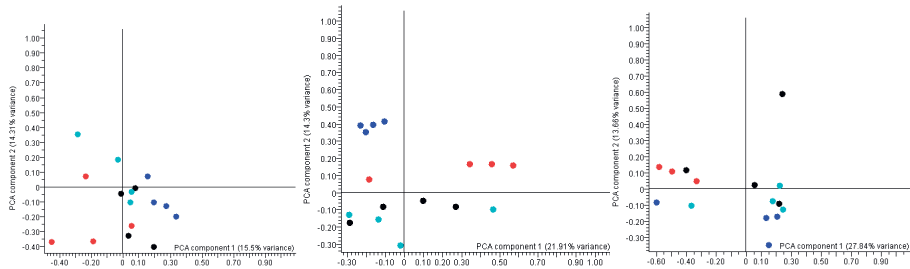
Silver

1 hour

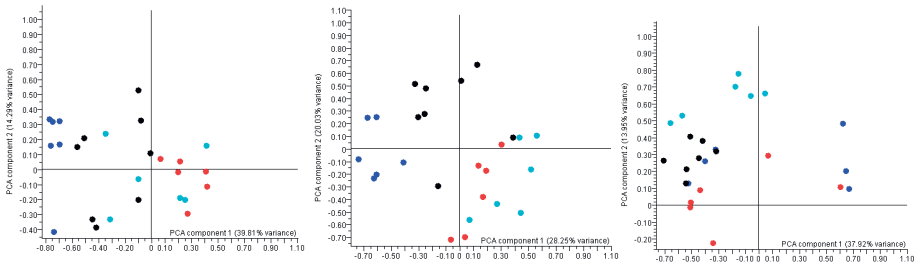
6 hours

24 hours

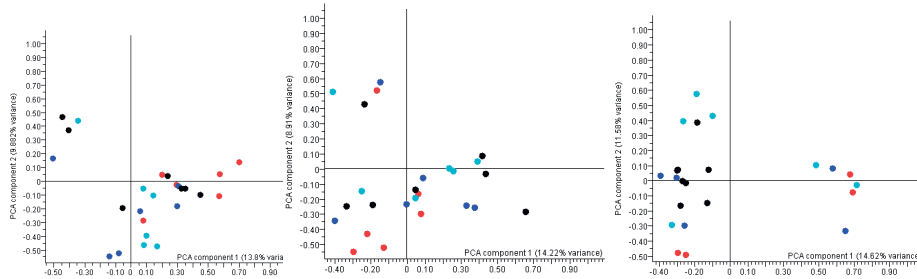
Transcriptomics



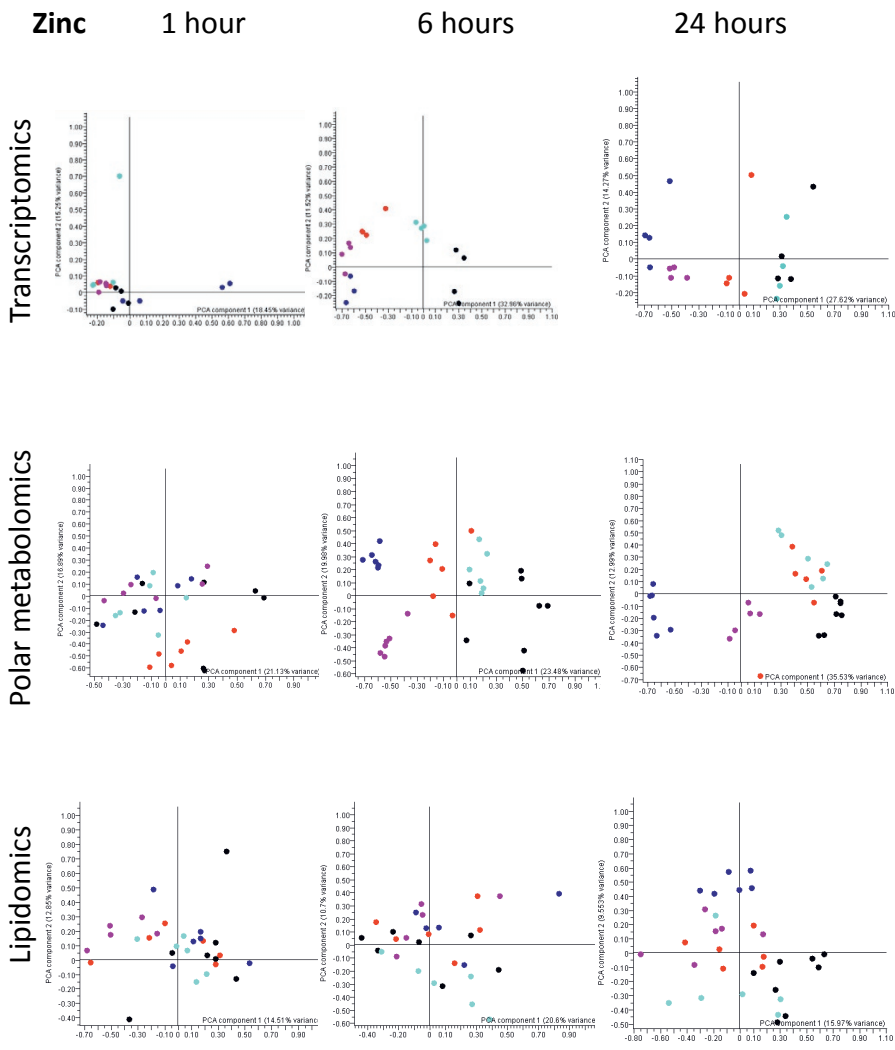
Polar metabolomics



Lipidomics



control samples are shown in black,
Ag NP-NM300K treated in red,
Ag MP in cyan,
Ag⁺ in blue.



control samples are shown in black,
 ZnO NP-NM110 treated in red,
 ZnO NP-NM111 in cyan,
 Zn₂₊ in blue
 ZnO MP in pink.

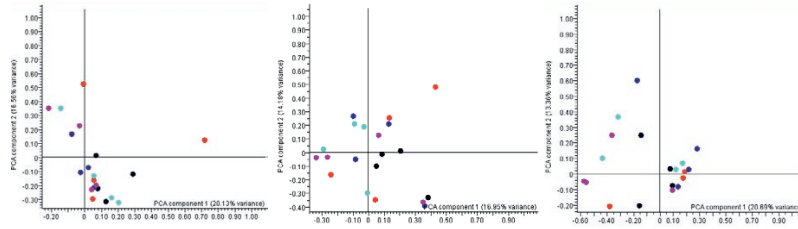
CeO₂

1 hour

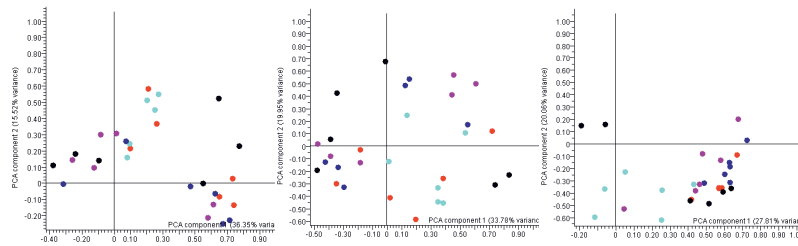
6 hours

24 hours

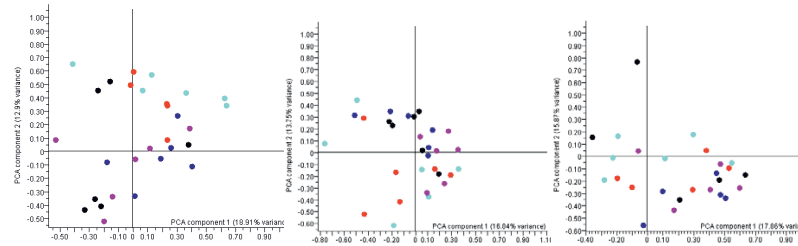
Transcriptomics



Polar metabolomics



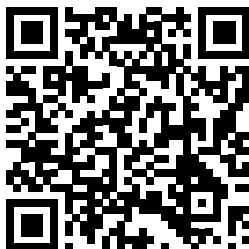
Lipidomics



control samples are shown in black,
CeO₂ NP-A treated in red,
CeO₂ NP-C in cyan,
CeO₂ NP-E in blue
CeO₂ NP-NM212 in pink.

ESI 6: IMPaLA pathway analysis of omics data

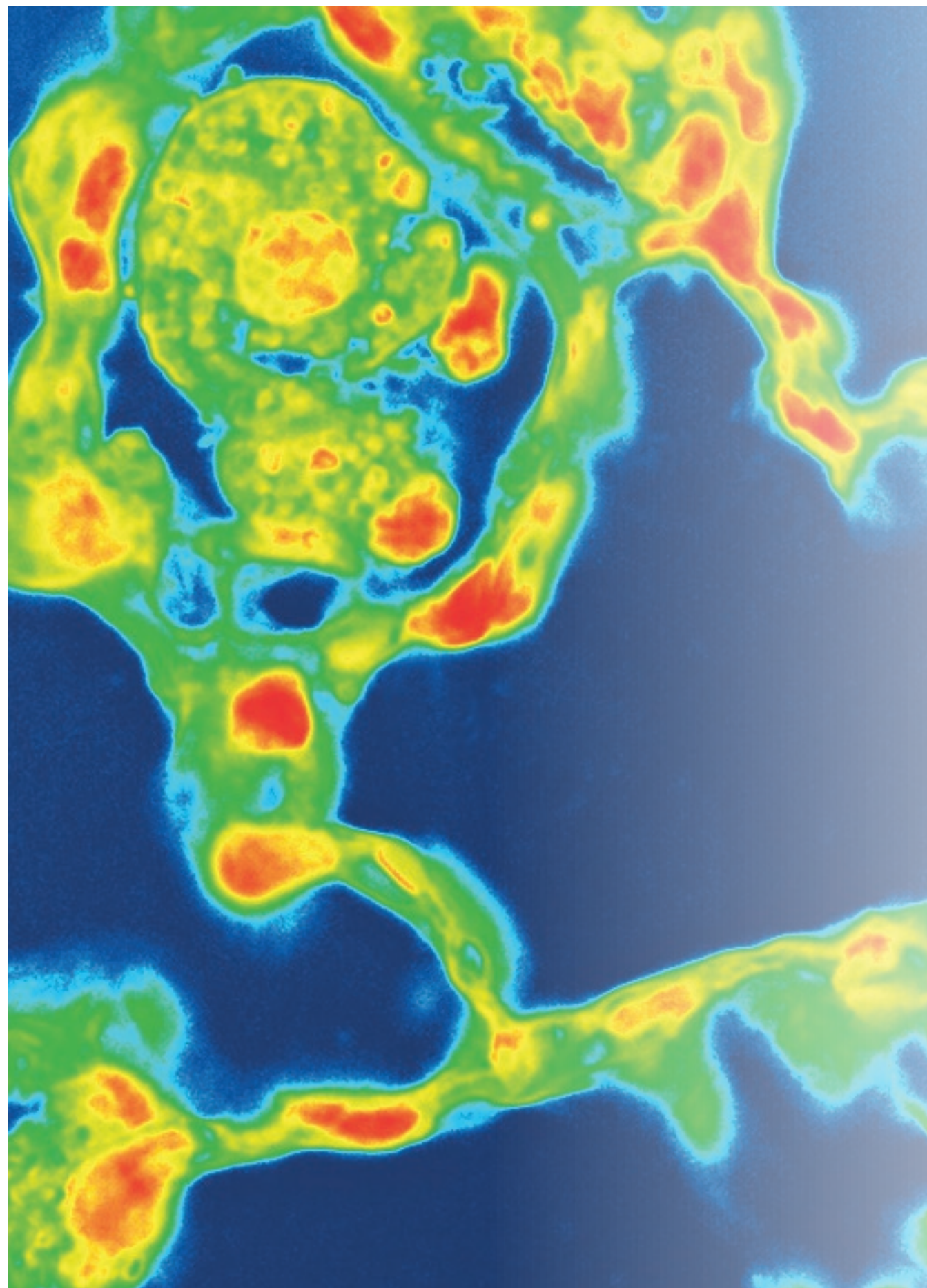
See:



ESI 7: Methods

See:





Chapter 5

Role of chemical composition and redox modification of poorly soluble nanomaterials on their ability to enhance allergic airway sensitisation in mice

Susan Dekkers¹, James G. Wagner², Rob J. Vandebriel¹, Elyse A. Eldridge², Selina V.Y. Tang³, Mark R. Miller⁴, Isabella Römer⁵, Wim H. de Jong¹, Jack R. Harkema² and Flemming R. Cassee^{1,6}

Particle and Fibre Toxicology 16: 39 (2019)

¹ National Institute for Public Health and the Environment, Bilthoven, the Netherlands,

² Department of Pathobiology and Diagnostic Investigation, Michigan State University, East Lansing, MI, United States of America,

³ Promethean Particles Ltd, Nottingham, United Kingdom,

⁴ Centre for Cardiovascular Science, University of Edinburgh, Edinburgh, United Kingdom,

⁵ School of Geography, Earth and Environmental Sciences, University of Birmingham, Birmingham, United Kingdom.

⁶ Institute for Risk Assessment Sciences, Utrecht University, Utrecht, the Netherlands

Abstract

Background: Engineered nanoparticles (NPs) have been shown to enhance allergic airways disease in mice. However, the influence of the different physicochemical properties of these particles on their adjuvant properties is largely unknown. Here we investigate the effects of chemical composition and redox activity of poorly soluble NPs on their adjuvant potency in a mouse model of airway hypersensitivity.

Results: NPs of roughly similar sizes with different chemical composition and redox activity, including CeO₂, Zr-doped CeO₂, Co₃O₄, Fe-doped Co₃O₄ (using Fe₂O₃ or Fe₃O₄) and TiO₂ NPs, all showed adjuvant activity. OVA induced immune responses following intranasal exposure of BALB/c mice to 0.02% OVA in combination with 200 µg NPs during sensitization (on day 1, 3, 6 and 8) and 0.5% OVA only during challenge (day 22, 23 and 24) were more pronounced compared to the same OVA treatment regime without NPs. Changes in OVA-specific IgE and IgG1 plasma levels, differential cell count and cytokines in bronchoalveolar lavage fluid (BALF), and histopathological detection of mucosa cell metaplasia and eosinophil density in the conducting airways were observed. Adjuvant activity of the CeO₂ NPs was primarily mediated via the Th2 response, while that of the Co₃O₄ NPs was characterised by no or less marked increases in IgE plasma levels, BALF IL-4 and IL-5 concentrations and percentages of eosinophils in BALF and more pronounced increases in BALF IL-6 concentrations and percentages of lymphocytes in BALF. Co-exposure to Co₃O₄ NPs with OVA and subsequent OVA challenge also induced perivascular and peribronchiolar lymphoid cell accumulation and formation of ectopic lymphoid tissue in lungs. Responses to OVA combined with various NPs were not affected by the amount of doping or redox activity of the NPs.

Conclusions: The findings indicate that chemical composition of NPs influences both the relative potency of NPs to exacerbate allergic airway sensitization and the type of immune response. However, no relation between the acellular redox activity and the observed adjuvant activity of the different NPs was found. Further research is needed to pinpoint the precise physiological properties of NPs and biological mechanisms determining adjuvant activity in order to facilitate a safe-by-design approach to NP development.

Background

Engineered nanoparticles (NPs) are under increasing development for a wide-range of applications, however, their potential for toxicity still remains poorly understood. Identifying which physicochemical properties of NPs affect the potential toxicological effects will therefore facilitate predictive risk assessment, grouping and safe-by-design of NPs [1-4].

The relative large surface-to-volume ratio and surface reactivity of NPs are, for example, known to increase reactive oxygen species (ROS) generation [5,6]. As a consequence, inhalation of NPs may lead to greater levels of cellular oxidative stress and, subsequently inflammation in the respiratory system, than their larger counterparts. In addition, existing inflammation (e.g. from asthma) can also be exacerbated by NP exposure [7, 8]. Nano-sized silica and titanium dioxide particles have been shown to enhance allergic airways sensitisation in mice [9, 10], however, there is limited understanding of the different physicochemical properties of NPs which influence their adjuvant properties. Previous studies on the influence of NPs on allergic airway sensitisation initially focused on the role of the dendritic cell and T-cell interaction. Increases in the proliferation, maturation and/or differentiation of dendritic cells and T-cells have been observed after *in vitro* exposure to NPs and after *in vivo* exposure to NPs during the sensitisation phase [7]. Molecular interactions that drive these cellular responses have been suggested to involve increases in reactive oxygen species (ROS) caused by NPs with an oxidative surface chemistry, inflammasome activation, cellular injury and the induction of dendritic cell stimulating cytokines or chemokines by epithelial cells (either direct or via oxidative stress) [7].

Nano-sized metal oxides are known to facilitate the formation of ROS by depleting electrons from cellular redox species (cellular components able to release electrons) or by serving as catalysts in ROS production through Fenton reactions or Haber-Weiss cycle reactions [11]. Additionally, NPs can stimulate free radical generation from cellular enzymes. Furthermore, biological fluids (e.g. epithelial lining fluid) and cells also contain antioxidants and numerous compensatory mechanisms, thus the relationship between ROS induction and toxicity is complex.

While there are clear associations between ROS generation and the toxicity of nanomaterials [11-13], the specific role of the redox activity of nanomaterials in the generation of ROS is difficult to investigate, since changing the redox activity of nanomaterials usually also changes other properties (such as the chemical composition or size). In a recent study, we applied chemical doping (intentional substitution of one element by another while maintaining the lattice structure and arrangement) of cerium dioxide to specifically investigate the influence of NP redox activity on ROS formation, and associated induction of oxidative stress responses in mice *in vivo* [14]. Different quantities of zirconium (Zr) were incorporated into the crystalline

structure of the cerium dioxide nanoparticles (CeO_2 NPs) to increase the antioxidant potential. However, Zr-doping of CeO_2 NPs had limited effect on the inflammatory responses after inhalation in otherwise healthy mice.

Metal oxides with a conduction band energy (E_c) level that overlaps with the cellular redox potential (-4.12 to -4.84 eV) have been shown to have the ability to induce oxygen radicals, oxidative stress, and acute pulmonary inflammation [15]. Therefore, Co_3O_4 , a metal oxide that (unlike CeO_2) has an E_c level overlapping with the cellular redox potential was doped using Fe_2O_3 or Fe_3O_4 (Fe oxides themselves do not overlap with the cellular redox potential). Here we present an airway exposure study in a mouse model for airway allergy using the following poorly soluble NPs differing in redox potential but with similar sizes: a) Co_3O_4 NPs doped with different amounts of Fe, b) CeO_2 NPs doped with different amounts of Zr, c) CeO_2 NM212 NPs (for comparison to other *in vivo* studies) and d) TiO_2 NPs (as a positive control [10]). We hypothesise that Co_3O_4 NPs will have a greater ability to enhance allergic airway sensitisation compared to (Zr-doped) CeO_2 NPs, but that these effects of Co_3O_4 NPs can be reduced by Fe-doping. The outcome of this work will facilitate the assessment of the potential hazard of NPs to enhance allergic airway sensitisation and inform efforts to group NPs or to apply a safe-by-design approach in their development.

Methods

Experimental protocol

Studies were designed to test the enhancement of allergic sensitization by airway co-exposure (intranasal instillation) of an experimental allergen (OVA) with a range of NPs that differ in chemical composition (Figure 1). Animals were divided into 10 test groups and 3 control groups, each with 6 mice except OVA-control (n=8) (see Table 1). On days 1, 3, 6 and 8 the mice were sensitized with 0.02% OVA in combination with 200 μg TiO_2 NPs (positive controls), 0.02% OVA in combination with 200 μg of one of the other NPs (test groups), 0.02% OVA in PBS (OVA control) or PBS alone (PBS control). On days 22 and 23 all mice were challenged with 30 μl of 0.5% OVA in PBS. The animals were sacrificed 24 hours after the last intranasal challenge (day 24).

A dose of 200 μg of NPs was chosen based on our results in previous studies (with dose-ranges between 100 and 400 μg) using silica [9] and titanium dioxide [10]. The mouse model was developed with low concentrations of OVA during sensitization (0.02%) that produce minimal allergic responses with challenge, but can be dramatically enhanced with co-sensitization with an adjuvant such as particulate matter [9].

No experimental groups were included to measure the effects of exposure to NPs without OVA during the sensitisation phase, since previous studies showed that the allergic

sensitisation response can only be enhanced via co-exposure of the allergen and SiO₂ or TiO₂ NPs, and not by exposure to SiO₂ and TiO₂ NP NPs alone [9, 10]. Although other studies have shown that separate administration of the allergen and NPs may also lead to adjuvant effects [16], in this study we have chosen to administer OVA and NPs in one suspension, in alignment with our previous studies.

Table 1: Overview of the study groups.

group	n	Day 1, 3, 6 and 8	Day 22 and 23	Day 24
1	6	PBS controls	OVA	necropsy
2	8	OVA controls	OVA	necropsy
3	6	TiO ₂ + OVA (NP positive controls)	OVA	necropsy
4	6	CeO ₂ NM212 + OVA	OVA	necropsy
5	6	Co ₃ O ₄ (0% Fe ₂ O ₃) + OVA	OVA	necropsy
6	6	Co ₃ O ₄ (25% Fe ₂ O ₃) + OVA	OVA	necropsy
7	6	Co ₃ O ₄ (75% Fe ₂ O ₃) + OVA	OVA	necropsy
8	6	Co ₃ O ₄ (0% Fe ₃ O ₄) + OVA	OVA	necropsy
9	6	Co ₃ O ₄ (25% Fe ₃ O ₄) + OVA	OVA	necropsy
10	6	Co ₃ O ₄ (75 % Fe ₃ O ₄) + OVA	OVA	necropsy
11	6	CeO ₂ (0% Zr) + OVA	OVA	necropsy
12	6	CeO ₂ (27% Zr) + OVA	OVA	necropsy
13	6	CeO ₂ (78% Zr) + OVA	OVA	necropsy

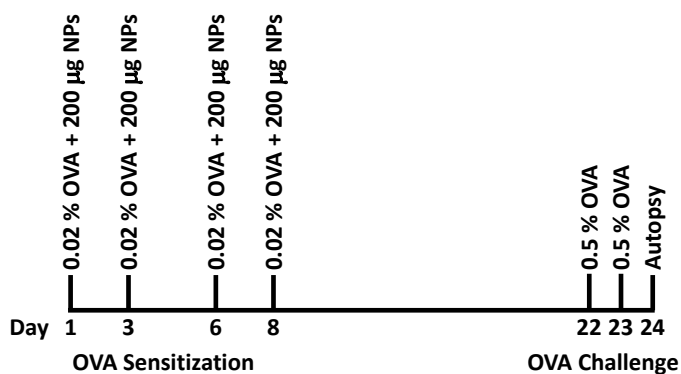


Figure 1: Schematic overview of the study design.

Nanomaterial production and characterization

TiO₂ NPs (NO-0058-HP) were obtained from Ionic Liquids Technologies GmbH, Germany. These uncoated anatase TiO₂ NPs were the same NPs as used on our previous *in vivo* study^[10]. The OECD representative manufactured nanomaterial CeO₂ (NM212) was obtained from Umicore, Belgium. The other CeO₂ NPs, Zr-doped CeO₂ NPs, Co₃O₄ NPs and Fe-doped Co₃O₄ NPs were produced using supercritical water hydrothermal synthesis^[17,18]. Briefly, H₂O was pumped through a pre-heating coil (~ 400°C), brought into contact with a concurrently flowing solution of metal salts at room temperature (RT), while maintaining the flow rates, temperature and the pressure constant at 240 bar. The mixture was cooled immediately after the mixing point and passed through a back pressure regulator to decrease the pressure back down to ambient conditions. Solids in the aqueous suspensions were washed by centrifuging and re-dispersing in clean MilliQ water 3 times. The particles were characterised in suspension or, where solid particles were required, the suspensions were oven dried (~100°C). For the synthesis of the Fe-doped Co₃O₄ NPs, different ratios of cobalt and iron salts were used as precursors. Two different iron salts (iron(III) nitrate nonahydrate and ammonium iron(III) citrate) were used, resulting in two different series of NPs, with Fe₂O₃ or Fe₃O₄ as a precursor, respectively. These different series (Co₃O₄(x% Fe₂O₃) NPs and Co₃O₄(x% Fe₃O₄) NPs) have different degrees of crystallinity, aggregation, Co/Fe ratio and spatial distributions of the metals in the NPs^[18].

The particle size in ultra-pure water was measured with disc centrifuge. The particle size in cell culture medium (RPMI 1640, Gibco) with 25mM HEPES and 2mM L-Glutamine, 1% Penicilline-Streptomycine (Pen/Strep 10000 U/mL, Gibco) and 10% heat inactivated Fetal Calf Serum (FCS, Gibco), was measured with dynamic light scattering (DLS). The redox activity was tested with electron paramagnetic resonance (EPR) using a cell free system with a superoxide-selective spin-trap (tempone-H) to detect the generation of superoxide production and the spin trap DMPO^[19] in combination with H₂O₂ and CuSO₄ to analyse the capacity to scavenge hydroxyl free radicals. For the superoxide-selective spin-trap nanoparticle suspensions (0.56 mg/mL) were prepared and incubated with the spin-trap, Tempone-H (1 mM) immediately before the initial measurement. Samples were kept at 37°C throughout and measurements were taken with an X-band EPR spectrometer (Magnetech MS-200, Berlin, Germany) at 60 min by drawing 50 µL of sample into a capillary tube (Scientific Laboratory Ltd, Coatbridge, UK) and sealing with a plug of soft sealant (Cristaseal, VWR International, UK). For the DMPO spin trap a sample was made of 12.5 µL nanoparticle suspension (1.28 mg/mL), 12.5 µL CuSO₄ (20 µM), 25 µL H₂O₂ (0.5 M) and 50 µL DMPO (0.05 M). This sample was incubated in a shaker water bath at 37 °C for 15 minutes at 100 rpm, vortexed and taken up in a capillary tube, which was then sealed at the bottom with haematocrit and measured with the ESR Spectroscope (Miniscope MS 400; MT MagnetTech GmbH). All NPs were tested for endotoxin contamination using either a Limulus Amoebocyte Lysate Assay (chromogenic kinetic LAL assay) or LC-MS/MS determination^[20].

Animals

Female BALB/c mice (~20 grams body weight; 6–8 weeks old) were obtained from Charles River (Portage, MI). Mice were maintained at the Michigan State University (MSU) animal housing facilities at room temperature (21°C–24°C) and relative humidity of 45–70%, with a 12 h light/dark cycle. MSU is AAALAC accredited and all animal procedures & experimental protocols were approved by the MSU Institutional Animal Care and Use Committee.

Intranasal Instillation

Mice were lightly anesthetized for 1-2 min with 4% isoflurane in oxygen using an isoflurane vaporizer. Cradling the mouse in an upright position, the thumb was used to support the lower jaw and position the nose of the mouse so it was easily accessible. A volume of 30 μ L was delivered to the tip of the nares. Once the instillate was fully inhaled, the mouse was placed back in its cage and monitored until conscious with normal respirations.

Necropsy, lavage collection and tissue preparation

Mice were anesthetized with an intraperitoneal injection of sodium pentobarbital (60 mg/kg body weight). A midline laparotomy was performed and approximately 0.5 mL of blood was drawn from the vena cava and collected in heparinized tubes (BD Microtainer, Franklin Lakes, NJ) for separation of plasma. The plasma was stored at -80°C for later biochemical analysis (OVA-specific IgE and IgG1). Animals were exsanguinated and the trachea was exposed and cannulated, and the heart and lungs were excised en bloc. A volume of 0.8 mL sterile saline was instilled through the tracheal cannula and withdrawn to recover bronchoalveolar lavage fluid (BALF). A second intratracheal saline lavage was performed and the collected BALF was combined with the first sample for analysis.

After the BALF was collected, the left lung lobe was intratracheally fixed with neutral-buffered formalin at a constant pressure (30 cm H_2O) for 2 h and then submersed in the same fixative for >24 h until further tissue processing for light microscopy. Two sections were excised at the level of the 5th and 11th airway along the main axial airway (G5 and G11), to sample proximal and distal bronchiolar airways, respectively^[21]. Tissue was embedded in paraffin and 5- to 6- μm -thick sections were cut from the anterior surface. Lung sections were stained with hematoxylin and eosin (H&E) for routine light microscopic examination and with Alcian Blue (pH 2.5)/Periodic Acid–Schiff (AB/PAS) for identification of intraepithelial neutral and acidic mucosubstances in pulmonary bronchiolar epithelium. To detect eosinophils, slides were immunostained using a polyclonal rabbit antibody directed against murine eosinophil-specific major basic protein (MBP; 1:500; Mayo Clinic, AZ). Accumulations of B-lymphocytes in lung tissues were detected by immunohistochemical staining with rat anti-CD45R monoclonal (1:600; Becton Dickinson, Franklin Lakes, NJ, catalog # 550286).

OVA-specific IgE and IgG1 in plasma

Plasma was separated from blood and analysed for OVA-specific IgE and IgG1 using an ELISA kit (Cayman, Ann Arbor, MI) according to the manufacturer's instructions. The plasma samples were diluted 8 times for the IgE and 1000 times for the IgG1 analysis.

BALF analyses

The total number of cells in the BALF was determined using a hemocytometer. Cytological slides were prepared by centrifugation at 40 x g for 10 min at 20°C using a Shandon cytopsin 3 (Shandon Scientific, PA) and stained with Diff-Quick (Dade Behring, DE). Differential cell counts for neutrophils, eosinophils, macrophages/monocytes, and lymphocytes were assessed from a total of at least 200 cells. The remaining BALF was centrifuged at 240 x g for 15 min at 4°C and the supernatant was collected and stored at -80°C for subsequent measurement of inflammatory cytokines (IFN γ , IL-4, IL-5, IL-1 β , IL-6, IL-13, IL-17 and TNF α) using a Luminex-kit (Millipore, MA).

Lung morphometry

Histologic slides with lung tissue sections were scanned and digitized with a slide scanner (VS110, Olympus America, Center Valley, PA), and evaluated using stereological methods with newCAST software (VisioPharm, Hoersholm, Denmark). For quantification of major basic protein (MBP)-positive eosinophils, digitized images of the lung were selected as regions of interest and 40% of the lung tissue was captured at 400x magnification by systematic random sampling. Percentage of MBP-positive cells in the total lung tissue and in three discrete regions of 1) the parenchyma (alveoli and alveolar ducts), 2) perivascular and peribronchial interstitial spaces, and 3) other regions (inside blood vessels, bronchiole airspaces and pleura), were estimated using Stepanizer stereology software with a point grid by dividing the number of points hitting areas positive for MPB ($a_{(p)positive}$) by the total number of points falling on all lung tissue (MBP-positive and -negative; $a_{(p)reference\ tissue}$). For each region, percent density of eosinophils was calculated with the equation:

$$Eosinophil\ Density\ (\%) = \frac{(No.\ positive\ cells) \times a_{(p)positive\ cell}}{(No.\ reference\ tissue) \times a_{(p)reference\ tissue}} \times 100$$

For quantification of CD45R-positive staining cells (the B-lymphocyte density), digitized images of G5 and G11 lung sections were selected as regions of interest and 40% of the lung tissue was captured at 400x magnification by systematic random sampling. Percentage of CD45R-positive cells in the perivascular and peribronchial interstitial spaces were estimated using Stepanizer stereology software using a point grid by dividing the number of points hitting areas positive for CD45R ($a_{(p)positive}$) by the total number of points falling on all lung tissue (CD45R-positive and -negative; $a_{(p)reference\ tissue}$). For each region, percent density of B-lymphocytes was calculated with the equation:

$$B - \text{lymphocyte Density (\%)} = \frac{(\text{No. positive cells}) \times a_{(p)\text{positive cell}}}{(\text{No. reference tissue}) \times a_{(p)\text{reference tissue}}} \times 100$$

For quantification of AB/PAS-positive mucosubstances in the bronchiolar epithelium, all bronchiolar epithelium lining the main axial airway was selected and captured at 400x magnification. A point intercept grid was placed over the sampled images to estimate the density of mucosubstances per basal lamina. The number of points hitting AB/PAS-positive mucosubstances (P_m) was counted. The density of AB/PAS-positive mucosubstances (\hat{V}_m) was estimated by multiplying the total number of P_m by the area/point (a/p) and dividing them by the number of points hitting the reference space (n) as shown in the equation.

$$\hat{V}_m = \frac{\sum P_m \times a/p}{n}$$

The surface density of the basal lamina (\hat{S}_{BL}) in the selected images was estimated by counting the number of intercepts (I) of the line probe with the basal lamina of the lateral wall divided by the length per point (l/p) and the number of points falling on the reference space (n) as described:

$$\hat{S}_{BL} = \frac{2 \times \sum I}{l/p \times n}$$

The positive density per basal lamina of the bronchiolar epithelium was then estimated by dividing \hat{V}_m by \hat{S}_{BL} .

Statistical analyses

GraphPad Prism v7.00 (GraphPad Software, San Diego, California, USA) was used to analyse the data. All data are depicted as group means \pm standard deviation (SD). First, outliers were identified with Grubbs' test ($\alpha = 0.05$) and removed. The Shapiro-Wilk test and the Brown-Forsythe test were used to test for normality and equal variances, respectively. Differences between the OVA control group and a) the other control groups (PBS or TiO₂ NP exposed), b) the CeO₂ NP exposed groups, c) the Co₃O₄(x% Fe₂O₃) NP exposed groups and d) the Co₃O₄(x% Fe₃O₄) NPs exposed groups were analysed using a one-way analysis of variance (ANOVA), followed by a Dunnett's post-hoc multiple comparisons test comparing groups exposed to OVA with NPs to groups exposed to OVA alone. For all statistical analyses, a p-value of ≤ 0.05 was considered statistically significant.

If the p-value of the Shapiro-Wilk or Brown-Forsythe test was ≤ 0.05 , the data were log-normally transformed and again tested for normality and equal variances. If the p-values of the Shapiro-Wilk and Brown-Forsythe tests of the log-normally transformed data were > 0.05 , a one-way ANOVA followed by a Dunnett's post-hoc multiple comparisons test was performed on the log-normally transformed data. If the p-values of the Shapiro-Wilk test

were still ≤ 0.05 , a non-parametric (Kruskal Wallis) ANOVA was performed on the non-transformed data followed by a Dunn's post-hoc multiple comparisons test.

Results

Nanomaterial characterization

Fe-doping had small, but not statistically significant, effects on NP size in suspension (Table 2). Other characteristics, such as shape and crystalline structure, did not significantly change with increasing amounts of doping. In Figure 2, the redox activity of the NPs as measured in a cell free system by EPR using two different spin-traps are shown. EPR analysis using tempone-H demonstrated an increased capacity of Co_3O_4 (25% Fe_3O_4) NPs to generate reactive superoxide free radicals compared to Co_3O_4 (0 and 75% Fe_3O_4) NPs. Increasing amounts of Fe-doping using Fe_3O_4 led a significant decrease in scavenging capacity of Co_3O_4 NPs. Co_3O_4 (0, 25 and 75% Fe_2O_3) NPs had a similar ROS generation and scavenging capacity (Figure 2). Endotoxin levels were below the recommended endotoxin limits for preclinical research in animal models (5 EU/kg bw/day or 36 EU/mL for mice with a body weight of 30 g and a daily dose of 100 μL) [22].

Table 2: Physicochemical characteristics of the nanoparticles.

	Primary particle size (Mean \pm SD) (nm)	Particle diameter in water (Median) (nm)	Particle diameter in cell culture medium + 10% foetal calf serum (Mean \pm SD) (arbitrary units)
Measured with \rightarrow	STEM	Disc Centrifuge (128 $\mu\text{g}/\text{mL}$)	DLS (128 $\mu\text{g}/\text{mL}$)
Anatase TiO_2	10-15 ^a	121 ^b	-
CeO_2 NM212	17.1 \pm 10.9	-	428 \pm 11.7
CeO_2 (0% Zr)	4.7 \pm 1.4	39	288 \pm 4.8
CeO_2 (27% Zr)	4.6 \pm 1.4	40	176 \pm 4.0
CeO_2 (78% Zr)	4.7 \pm 1.4	41	415 \pm 27.6
Co_3O_4 (0% Fe_2O_3)	17.5 \pm 15.0	42	176 \pm 2.9
Co_3O_4 (25% Fe_2O_3)	10.6 \pm 3.6	62	303 \pm 6.7
Co_3O_4 (75% Fe_2O_3)	8.6 \pm 1.7	39	373 \pm 9.9
Co_3O_4 (0% Fe_3O_4)	18.7 \pm 11.2	44	160 \pm 1.3
Co_3O_4 (25% Fe_3O_4)	13.0 \pm 5.2	61	828 \pm 3.8
Co_3O_4 (75 % Fe_3O_4)	10.2 \pm 6.2	69	1165 \pm 66.5

^a Information provided by the manufacturer instead of measured with STEM;

^b Particles size as measured in our previous study with Nanoparticle Tracking Analysis instead of Disc Centrifuge; SD = Standard Deviation, STEM = Scanning Transmission Electron Microscopy; DLS = Dynamic Light Scattering, - = no data available.

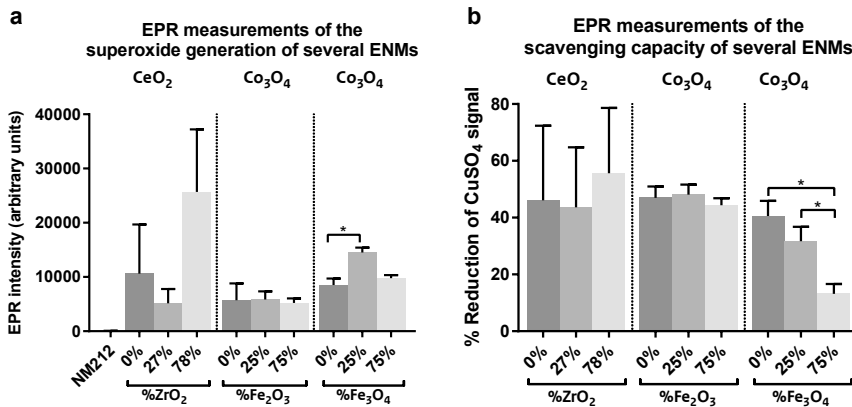


Figure 2: Reactive oxygen species (ROS) generation and scavenging capacity of NPs.

Superoxide generation of NPs measured in a cell free system by electron paramagnetic resonance (EPR) using Tempone-H (a). The EPR signal of the Co₃O₄(25% Fe₃O₄) NPs was statistically significantly higher than the Co₃O₄(0% Fe₃O₄) NPs (n=4) indicating a larger capacity to generate ROS. Scavenging capacity of several NPs expressed as the percentage reduction of the EPR signal of CuSO₄ and NPs compared to CuSO₄ alone, using a cell free system with a 5,5-dimethyl-1-pyrroline N-oxide (DMPO) spin trap in combination with H₂O₂ (b). The percentage reduction of the CuSO₄ signal by the Co₃O₄(75% Fe₃O₄) NPs was significantly lower than that of the Co₃O₄(0 and 25% Fe₃O₄) NPs (n=3), indicating a lower scavenging capacity of ROS.

OVA-specific IgE and IgG1 in plasma

OVA-specific IgE and IgG1 antibodies in plasma, indicating an OVA-specific immune response, were measured using an ELISA kit. OVA sensitization (0.02% OVA) and challenge (0.5% OVA) caused minimal, non-significant increases in plasma OVA-specific IgE and IgG1 compared to non-sensitized mice (phosphate-buffered saline (PBS) treated controls). Co-sensitization with NPs further increased the plasma OVA-specific IgE or IgG1 concentrations for all NPs. For all NPs, except for Co₃O₄(0 and 75% Fe₃O₄) NPs, the OVA-specific IgE and/or the IgG1 concentration was statistically significantly increased compared to OVA alone (Figure 3).

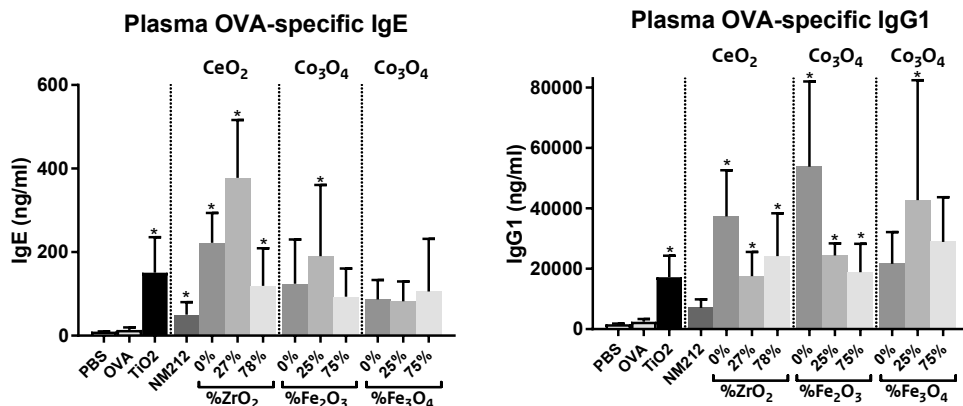


Figure 3: Concentration of OVA-specific IgE and IgG1 in plasma.

Mean \pm SD, n=6 except OVA controls where n=8, *=statistically significant different from OVA controls (p<0.05).

BALF analyses

BALF total cell count

The total and differential cell counts were determined using a hemocytometer and analysis of cytospin prepared slides. All mice sensitized with NP plus OVA showed a significant increase in total BALF cells compared to the OVA controls, indicating an increased inflammatory response, except for animals exposed to Co_3O_4 (0% Fe_2O_3) NPs ($p = 0.18$; see Figure 4a). For CeO_2 NPs the total cell count increased with increasing amounts of Zr doping.

Neutrophils

An increase in neutrophils in the BALF is indicative for a non-allergic, acute inflammatory response. No statistically significant differences between the percentage of neutrophils of the OVA controls and that of OVA plus NP exposed animals were observed, except for a decreased percentage of neutrophils in mice exposed to OVA plus CeO_2 (78% Zr) NPs, Co_3O_4 (25 and 75% Fe_2O_3) NPs and Co_3O_4 (75% Fe_3O_4) NPs. No major differences were observed between the different types of NPs (see Figure 4b). The percentage of neutrophils decreased with the amount of doping for Zr-doped CeO_2 NPs and Fe-doped Co_3O_4 NPs (using both Fe_2O_3 and Fe_3O_4).

Eosinophils and lymphocytes

The animals exposed to OVA plus CeO_2 NPs showed a statistically significant increase in the percentage of eosinophils compared to the OVA controls (Figure 4c), which is a typical feature of allergic asthma. For CeO_2 (27 and 78% Zr) NPs there was also a statistically significant increase in the percentage of lymphocytes (Figure 4d), indicative for a chronic inflammatory response. Fe-doped Co_3O_4 NPs (using both Fe_2O_3 and Fe_3O_4) caused a statistically significant increase in the percentage of lymphocytes only, and not of eosinophils.

Monocytes

No major differences in the percentage of monocytes were observed between mice sensitized with NP plus OVA compared to the OVA controls (data not shown). More detailed data, including the absolute differential cell counts, can be found in Additional file 1.

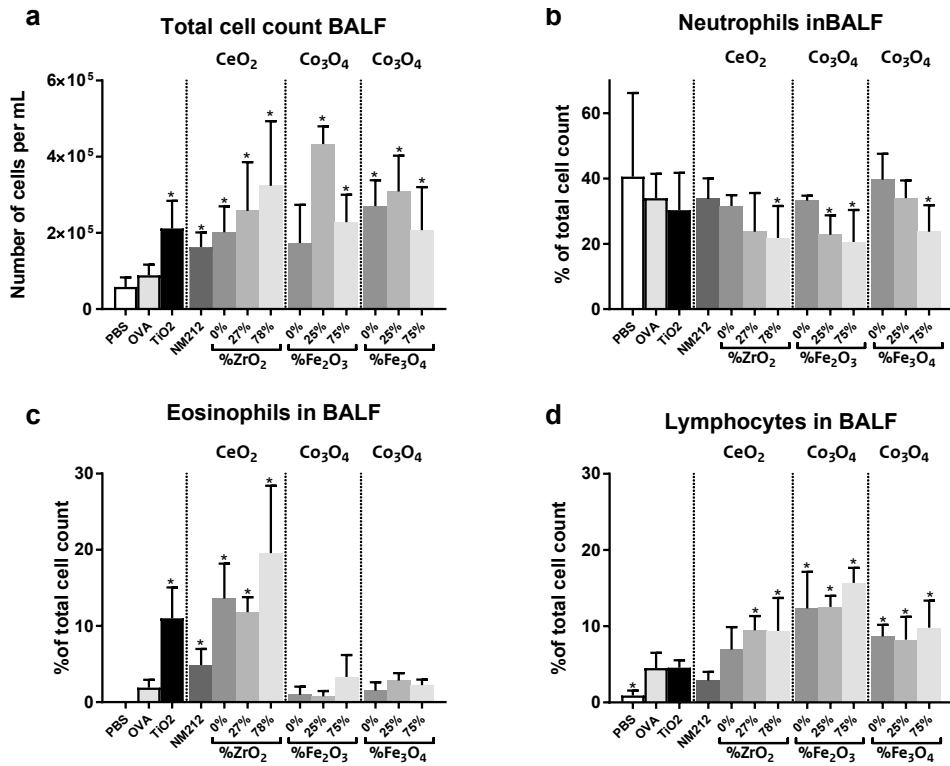


Figure 4: Differential cell counts in bronchoalveolar lavage fluid (BALF).

Total cell count (a) and percentage of neutrophils (b), eosinophils (c) and lymphocytes (d) in the BALF. Mean \pm SD, n=6 except OVA where n=8, *=statistically significant different from OVA controls ($p < 0.05$).

BALF cytokines

The concentrations of several inflammatory cytokines in the BALF were determined in using a Luminex-kit specific for the various cytokines evaluated. Animals exposed to OVA plus CeO₂ NPs showed increased concentrations of the Th2 cytokines IL-4 and IL-5 (but not IL-6 or IL-13) in the BALF compared to the OVA controls. Animals exposed to OVA plus most undoped and Fe-doped Co₃O₄ NPs showed increased concentrations of IL-6 compared to the OVA controls. All animals, including the controls (exposed to PBS, OVA and OVA plus TiO₂ NPs during sensitization) had detectable concentrations of IL-13 (20-50 ng/mL) but these were not significantly different from one another (see Figure 5d).

The concentrations of the other cytokines (IFN γ , IL-1 β , IL-17 and TNF α) measured in BALF were either below the limits of detection or showed no significant changes in the OVA plus NP exposed groups compared to the OVA controls. More detailed data can be found in Additional file 2.

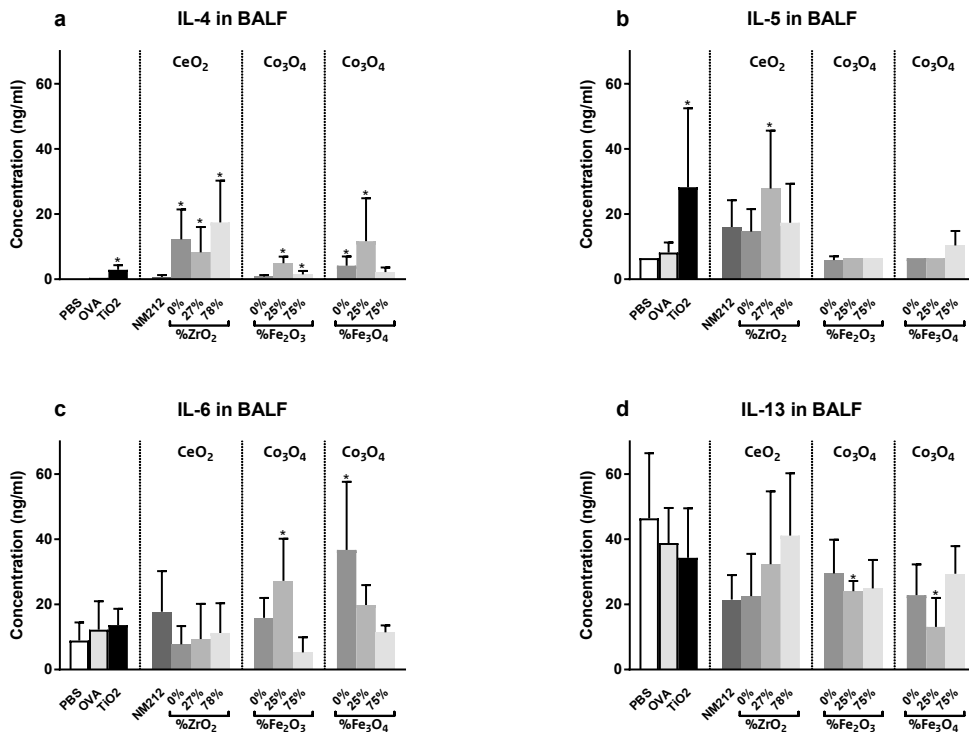


Figure 5: Cytokines in bronchoalveolar lavage fluid (BALF).

Concentration of IL-4 (a), IL-5 (b), IL-6 (c) and IL-13 (d), in the BALF. Mean \pm SD, n=6 except OVA where n=8, *=statistically significant different from OVA controls ($p < 0.05$).

Lung morphology

Mucous cell metaplasia.

For quantification of epithelial mucous, lung tissue sections were stained with Alcian Blue/Periodic Acid Schiff (AB/PAS), a marker for neutral and acidic mucosubstances. Increased epithelial mucous production is a characteristic feature of allergic airway disease.

Sensitization and challenge with OVA caused a significant accumulation of intraepithelial mucosubstances (mucous cell metaplasia) in the epithelium lining the main proximal axial airways (G5), which was further enhanced by co-administration of OVA with TiO₂ NPs (positive control). All CeO₂ NPs enhanced mucosubstance accumulation; this was statistically significant for CeO₂ NM212 and CeO₂ with 27%, but not 78%, Zr doping (see Figure 6).

By comparison, in the distal axial airways (G11), OVA sensitization and challenge did not affect epithelial accumulated mucosubstances. Co-sensitization with OVA plus TiO₂ (positive control), CeO₂ NM212, CeO₂ (0, 27 and 78% Zr), Co₃O₄ (25% Fe₂O₃) and Co₃O₄ (25% Fe₃O₄) NPs led to a statistically significant increase in mucosubstances compared to the OVA controls.

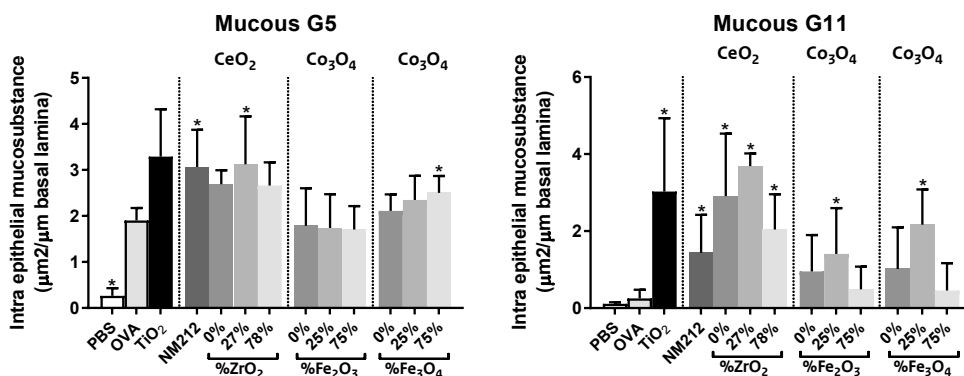


Figure 6: Mucous cell metaplasia.

Quantification of the increase in intraepithelial mucosubstance in the epithelium lining the main proximal axial airway (G5;left) and distal axial airway (G11;right) of the left lung lobe. Mean \pm SD, n=6 except OVA where n=8, *=statistically significant different from OVA controls (p<0.05).

Eosinophil density

For quantification of the eosinophil density, a biomarker for an allergic airway response, lung tissue sections were stained for murine major basic protein (MBP), a specific marker for eosinophils.

Parenchymal lung tissue - OVA sensitization and challenge did not increase the overall eosinophil density in the pulmonary parenchyma compared to non-sensitized mice (PBS controls). Co-sensitization of OVA with TiO₂ (positive control) and CeO₂ NPs significantly increased eosinophil density compared to OVA alone. This increase was statistically significant in all these groups, except for the OVA plus CeO₂ NM212 NPs group. Co-sensitization of OVA with undoped and doped Co₃O₄ NPs had no effect on eosinophil density (Figure 7a).

Perivascular and peribronchial lung tissue - OVA sensitization and challenge did not significantly affect the eosinophil density in the peribronchial and perivascular region of the lung compared to non-sensitized mice (PBS controls). Co-sensitization of OVA with TiO₂ (positive control), CeO₂(0, 27 and 78% Zr) and Co₃O₄(25 and 75% Fe₃O₄) NPs caused significant increases in eosinophil density compared to OVA alone (Figure 7b).

Total lung - OVA sensitization and challenge did not significantly alter the overall pulmonary eosinophil density compared to non-sensitized mice (PBS controls). Co-sensitization of OVA with TiO₂ NPs (positive control), CeO₂(0 and 78% Zr) and Co₃O₄(25 and 75% Fe₃O₄) NPs caused significant increases in eosinophil density compared to OVA alone (Figure 7c).

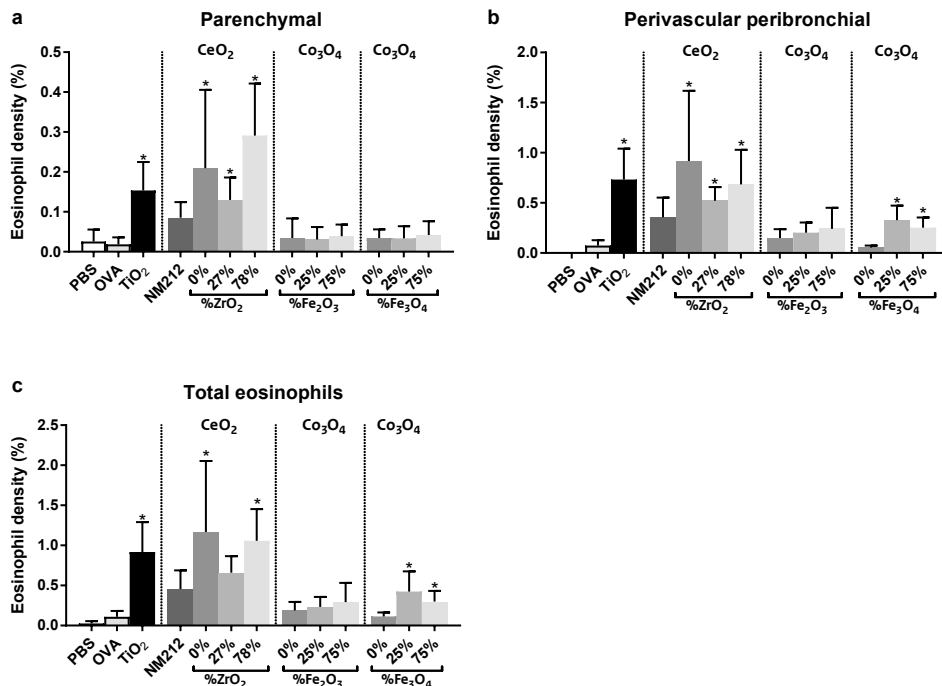


Figure 7: Eosinophil density.

Quantification of the eosinophil density in the parenchymal (a), perivascular and peribronchial (b), and total (c) lung tissue. Mean \pm SD, n=8 except OVA where n=8, *=statistically significant different from OVA controls ($p < 0.05$).

B-lymphocytes density

For quantification of the B-lymphocytes density lung tissue sections were stained for CD45R, a marker for B-lymphocytes.

Co-sensitization with OVA and Co₃O₄ NPs induced a severe accumulation of B-lymphocytes (CD45+ cells) in the perivascular/peribronchiolar interstitium, indicative for a chronic inflammatory response. By comparison, accumulation of B-lymphocytes in lungs from OVA plus CeO₂ NP-sensitised mice was not as evident (Figure 8).

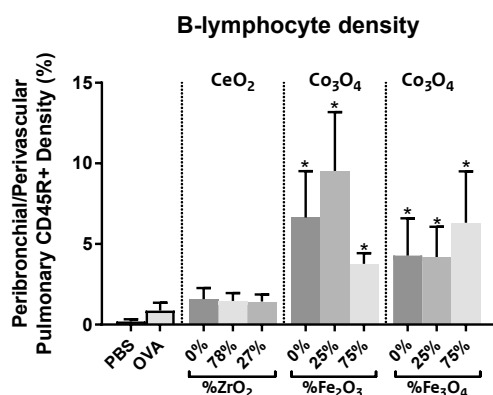


Figure 8: B-lymphocyte density.

Quantification of the B-lymphocyte density in the perivascular and peribronchial lung tissue. Mean \pm SD, n=6 except OVA where n=8, *=statistically significant different from OVA controls (p<0.05).

Lung histopathology

Examples of histopathological findings in the scanned and digitized histologic slides of the lung tissue sections are shown in Figure 9 and 10. No exposure related microscopically observable lung lesions were found in the PBS control group (Figure 9a and b). All mice that were intranasally sensitized and challenged with OVA (OVA controls) had some degree of histopathology in the lung that was characteristic of allergic airway disease. This histopathology consisted of a mixed inflammatory cell influx containing eosinophils, lymphoid cells (lymphocytes and plasma cells) and, to a lesser extent, neutrophils in the interstitial tissue surrounding blood vessels and conducting airways (perivascular and peribronchiolar inflammation) (most conspicuous in G5, see Figure 9c, but also in G11). Associated with these inflammatory lesions, there was mucous cell metaplasia of the airway epithelium (appearance of mucous cells with AB/PAS-stained mucosubstances) (see Figure 9d).

Mice co-exposed to OVA and NPs had a mild to moderate multifocal accumulation of particle-laden, hypertrophic macrophages in alveolar air spaces (most conspicuous in centriacinar regions of the lung) and more severe inflammatory or epithelial lung lesions compared to mice exposed to OVA alone. Mice co-exposed to OVA and TiO₂, CeO₂ NM212, or Zr-doped CeO₂ NPs had more severe lymphocytic and eosinophilic inflammation as (see Figure 9e) as well as more severe mucous cell metaplasia (most conspicuous in G11, see Figure 9f) compared to the OVA-alone treated mice (see Figure 9c and d).

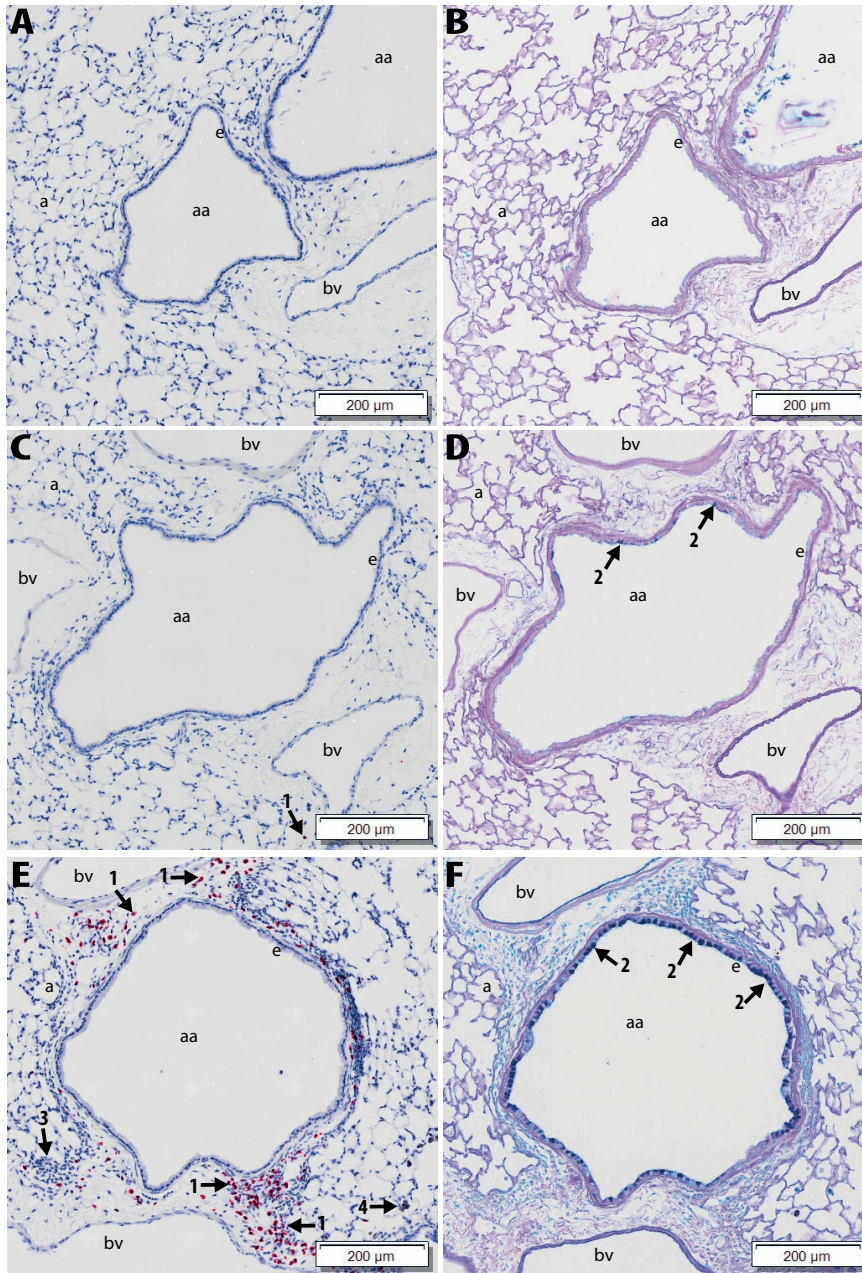


Figure 9: Examples of observed histopathological findings in lungs.

Light photomicrographs of G11, small-diameter, distal axial airway from the lungs of PBS-treated mice (A, B), OVA-treated mice (C,D) and OVA+TiO₂ NP treated mice (E,F). Lung tissue sections for A, C and E were stained for murine major basic protein, a specific marker for eosinophils (red chromogen-stained cells; arrow 1). Tissue sections B, D and F were stained with Alcian Blue/Periodic Acid Schiff (AB/PAS) for neutral and acidic mucosubstances (dark magenta stain; arrow 2) in mucous cells of the airway epithelium (e). aa: axial airway lumen; bv: blood vessel; a: alveolus; arrow 3: mononuclear cell infiltrate (mainly lymphoid) ; arrow 4: TiO₂ NP-laden alveolar macrophages

In contrast, OVA and Co_3O_4 (with or without Fe-doping) co-exposed mice did not have more severe eosinophilic inflammation or mucous cell metaplasia as compared to OVA-alone treated mice. Interestingly, these OVA and Co_3O_4 co-exposed mice exhibited more severe perivascular or peribronchiolar lymphoid cell accumulation compared to mice co-exposed to the other NPs, organized in ectopic lymphoid-like structures (ELS, see Figure 10a, b and c). ELS are tertiary lymphoid organs, associated for example with infections and autoimmune diseases, that develop in areas of chronic inflammation and are characterized by the formation of organized B- and T-cell aggregates and germinal centres with follicular dendritic cell networks^[23, 24]. These lung lesions were also observed in mice co-exposed to OVA and Co_3O_4 with Fe-doping (using both Fe_2O_3 and Fe_3O_4 , see Figure 10d, e and f).

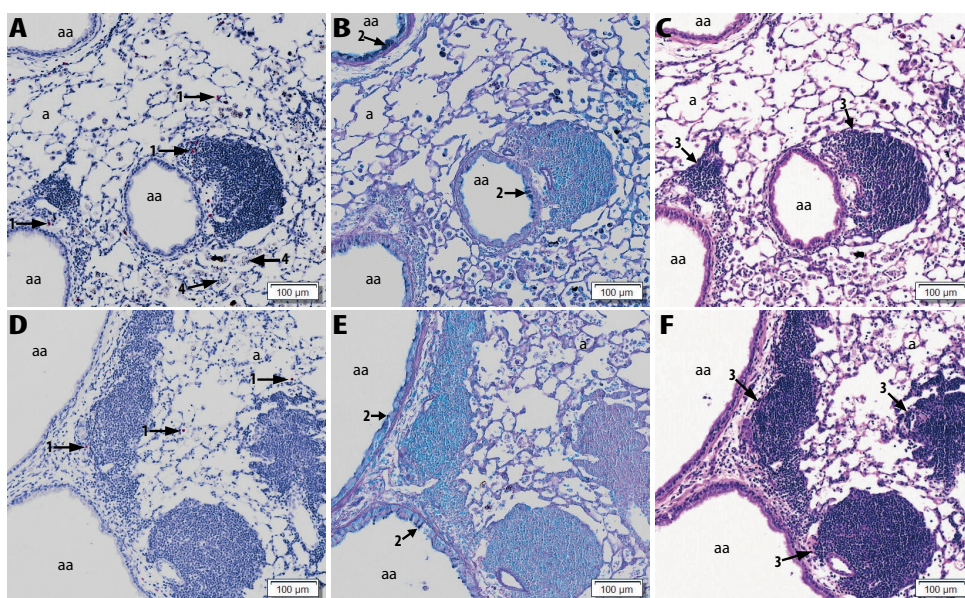


Figure 10: Examples of observed ectopic lymphoid structures in lungs.

Light photomicrographs of G5, principally large-diameter, proximal axial airway from the lungs of OVA+ Co_3O_4 (0% Fe_2O_3) NP treated mice (A, B,C), and OVA+ Co_3O_4 (25% Fe_2O_3) NP-treated mice (D,E,F). Lung tissue sections for A and D were stained for murine major basic protein, a specific marker for eosinophils (red chromogen-stained cells; arrow 1). Tissue sections B and E were stained with Alcian Blue/Periodic Acid Schiff (AB/PAS) for neutral and acidic mucosubstances (dark magenta stain; arrow 2) in mucous cells of the airway epithelium. Tissue sections C and F were stained with hematoxylin and eosin (H&E). arrow 3: ectopic lymphoid structures (ELS), arrow 4: Co_3O_4 NP-laden alveolar macrophages; aa: axial airway lumen; a: alveolus.

Discussion

All NPs investigated possessed adjuvant activity, leading to changes in OVA-specific IgE and IgG1 plasma levels, differential cell count and cytokines in BALF, and histopathological detection of mucosa cell metaplasia and eosinophil density in the conducting airways. Co-exposure of OVA and Co_3O_4 NPs also induced perivascular and peribronchiolar lymphoid cell accumulation and the formation of ELS in lungs.

Adjuvant activity

Although the increased OVA-specific IgE and IgG1 plasma levels of all OVA + NP exposed groups compared to OVA controls were not statistically significant for all NPs, they do indicate that NPs have the capacity to enhance allergic sensitisation in mice. This is supported by the increases in eosinophils, lymphocytes, IL-4, IL-5 and IL-6 in BALF after co-exposure of OVA and many NPs compared to the OVA controls. In our previous study, we found that SiO₂ and TiO₂ NP exposure alone (without OVA) during the induction phase did not lead to an increase in OVA-specific IgE and IgG1 plasma levels or eosinophils in BALF after OVA challenge [9, 10]. These findings suggest that the allergic response can only be enhanced via co-exposure of the allergen and NPs, and not by exposure to NPs alone. In the current study, all NPs were only tested in combination with OVA, and the results show that all NPs were able to act as adjuvant, albeit to varying degrees.

The influence of the chemical composition

The differences in OVA-specific IgE and IgG1 plasma levels of the animals co-sensitized to OVA and the different NPs indicate that the chemical composition of the NPs influences their potency to exacerbate allergic airway sensitization. The relative adjuvant potencies of the different NPs varied with the different biomarkers of effects (Figure 11), indicating that the chemical composition also influences the type of the allergic response.

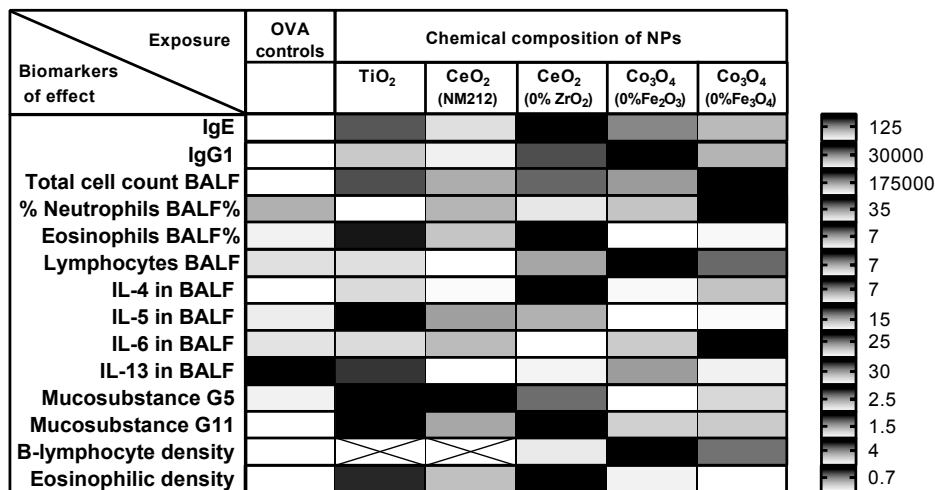


Figure 11: The influence of the chemical composition on the different biomarkers of effect.

The shading indicates the lowest (light grey), intermediate (medium grey) or highest (dark grey) response of an NP (relative to the OVA controls) for each of the biomarkers. The bar on the right side shows for each row the value corresponding with the indicated (medium) grey shading.

Type of the immune responses

Animals co-exposed to OVA and undoped CeO₂ NPs showed higher OVA-specific IgE plasma levels compared to animals co-exposed to OVA and the other undoped NPs (TiO₂ NPs, CeO₂ NM212 NPs, and Co₃O₄ NPs), indicative for a type 1 (immediate or IgE mediated) allergic response. Additionally, indications for a Th2 type immune response were observed, characterised by an increase in the percentage of eosinophils and increased concentrations of the Th2 cytokines IL-4 and IL-5 (but not IL-13) in the BALF. Animals co-exposed to OVA and the OECD representative manufactured nanomaterial CeO₂ (NM212), also showed some indications of a Th2 type response, albeit less marked than those observed in animals co-exposed to OVA and CeO₂(0% Zr) NPs: plasma OVA-specific IgE levels, percentage of eosinophils in BALF and BALF IL-4 concentrations were much lower in animals co-exposed to OVA and CeO₂ NM212 than in animals co-exposed to OVA and CeO₂(0% Zr) NPs. In contrast, concentrations of IL-5 in BALF were similarly affected by both forms of CeO₂. These findings are in line with a previous *in vivo* study in which CeO₂ NPs induced increased antigen specific IgE levels, eosinophils, Th2 cytokines and Th2 chemokines when co-exposed with house dust mite ^[25] and an *in vitro* study in which CeO₂ NPs exposure of human dendritic cells induced a Th2-dominated cell profile ^[26].

Co-exposure to OVA and undoped Co₃O₄ NPs also showed responses indicative of a type 1 allergic response, albeit, the OVA-specific IgE plasma levels were lower compared to co-exposure to OVA and the CeO₂(0% Zr) NPs. Furthermore, the response after co-exposure to OVA and Co₃O₄ NPs was characterised by no or less marked increases in BALF IL-4 and IL-5 concentrations and the percentage of eosinophils in BALF, but a more pronounced increase in the BALF IL-6 concentration and the percentage of lymphocytes in BALF compared to co-exposure to OVA and the CeO₂(0% Zr) NPs. This pattern of response is in line with a previous *in vivo* study in C57Bl/6 mice in which subcutaneous administration of Co₃O₄ NPs with OVA induced both Th1 and Th2 type responses ^[27]. Several biomarkers, including the OVA-specific IgG1 plasma levels and IL-6 concentrations in the BALF, were remarkably different in animals co-exposed to OVA and the two different types of undoped Co₃O₄ NPs, indicating that not only chemical composition, but also other physicochemical characteristics of the NPs are of influence to the allergic response. Although, the production process of the two undoped Co₃O₄ NPs was the same, they differed in the degree of crystallinity, aggregation, Co/Fe ratio and spatial distributions of the metals in the NPs ^[18].

The immune response after co-exposure to OVA and TiO₂ NPs was indicative for a Th2 immune response, characterised by an increase in eosinophils, IL-4 and IL-5 in BALF. Previous studies with TiO₂ NPs have found contradictory results regarding effects on immune responses. Schanen *et al.* ^[26] found that exposure of dendritic cells to TiO₂ NPs led towards Th1-based responses, while Vandebriel *et al.* ^[10] and de Haar *et al.* ^[28] observed Th2 type immune responses in mice after co-exposure to OVA plus TiO₂ NPs. However, the contradictory result

may have been caused by differences in the physicochemical characteristics (e.g. sizes and/or crystallinity) of the TiO₂ NPs used in the studies by Schanen *et al.* [26] and de Haar *et al.* [28], compared to the TiO₂ NPs used in our study, which were the same TiO₂ NPs as Vandebriel *et al.* [10]. Although this study adds weight to the steering of the immune response towards a Th2 response by TiO₂ NP co-exposure with antigens, more studies which measure a wide range of Th2 and Th1/Th17 associated biomarkers are needed to gain more insight in the type of adjuvant activity associated with by TiO₂ NPs exposure.

Lung morphology and ectopic lymphoid-like structures

Animals co-exposed to OVA and TiO₂, CeO₂ NM212, or CeO₂(0% Zr) NPs had more severe mucous cell metaplasia (most conspicuous in G11, but also in G5), as well as more severe eosinophilic inflammation, compared to the OVA-alone treated mice. OVA and Co₃O₄ co-exposed mice showed more severe perivascular and peribronchiolar lymphoid cell accumulation, organized into ELS. These findings were accompanied by an increase in lymphocytes in BALF. In mice broncho-associated lymphoid tissue (BALT) is usually absent, however, it can be induced (inducible BALT or iBALT) by inflammatory processes and infections [29]. In humans, iBALT formation can be observed in the lung in response to various types of infectious and inflammatory states, caused by infectious organisms, diesel exhaust, cigarette smoke silica, and various autoimmune diseases [30, 31]. In previous studies lymphocyte foci or aggregates have been observed in lungs of rats after intratracheal instillation of Co₃O₄ NPs [32], as well as in lungs of mice after intranasal exposure to OVA [33], crystalline silica particles (1.5-2.0 μm) [34] and after inhalation of CdO NPs [35]. However, the role of iBALT in the pathophysiology of chronic allergic diseases, such as asthma, is poorly understood [30, 31]. Studies investigating whether or not iBALT is involved in the development or progression of allergy or asthma showed conflicting results and the pathways that control the development and function of iBALT are poorly understood.

The influence of redox modification by doping

The differences in immune responses observed between the groups exposed to the same type of NPs, but different amounts of doping (Zr-doping for CeO₂ NPs and Fe-doping for Co₃O₄ NPs), indicate that redox modification can influence the adjuvant activity of NPs. However, the amount of doping did not always show a clear trend in the response of the different biomarkers of effects. Some biomarkers indicated that the undoped NPs exhibit most adjuvant activity, while other biomarkers indicated that either the NP with the lowest amount of doping or the NPs with the highest amount of doping exhibited most adjuvant activity. Additionally, most biomarkers of effects neither decreased nor increased with greater degrees of doping (see Additional file 3).

This lack of trend between increasing amounts of doping and the biomarkers of effects is also observed in the EPR data, in which only the Co₃O₄(0, 25 and 75% Fe₃O₄) NPs showed

a decreasing scavenging capacity with increasing amounts of doping (see Figure 2). This decrease in free hydroxyl radical scavenging capacity was unexpected based on the E_c levels of Co_3O_4 and Fe_3O_4 . We expected that doping using Fe_3O_4 would increase, rather than decrease the ability of Co_3O_4 to scavenge free hydroxyl radicals, because the E_c level of Co_3O_4 overlaps with the cellular redox potential, whereas that of Fe_3O_4 does not. On the other hand, the superoxide generation did increase with Fe-doping of Co_3O_4 NPs using 25% Fe_3O_4 , but this ROS generation was not further increased with increasing amounts of Fe-doping. It is possible that differences in particle size and aggregation counterbalanced any doping-related differences in free radical generation or scavenging ^[11, 36], as the particle size in water as measured with disc centrifuge was larger for the Co_3O_4 (75% Fe_3O_4) NPs compared to Co_3O_4 (25% Fe_3O_4) NPs, although the difference in particle size between these two NPs was relatively small. Nonetheless, we would still have expected more notable differences in free radical generation from the surfaces of the differently doped materials. Physicochemical characterisation of the materials indicates successful incorporation of the doping into the crystal structure of the NP ^[18], thus at present we can only speculate as to the reason for the limited effect of doping on free radical generation.

Since, the amount of doping or band gap energy of the NPs were not predictive for adjuvant activity or the ability to generate or scavenge specific radical, we also investigated if the ability of the NPs to generate or scavenge specific radicals was predictive for the adjuvant activity.

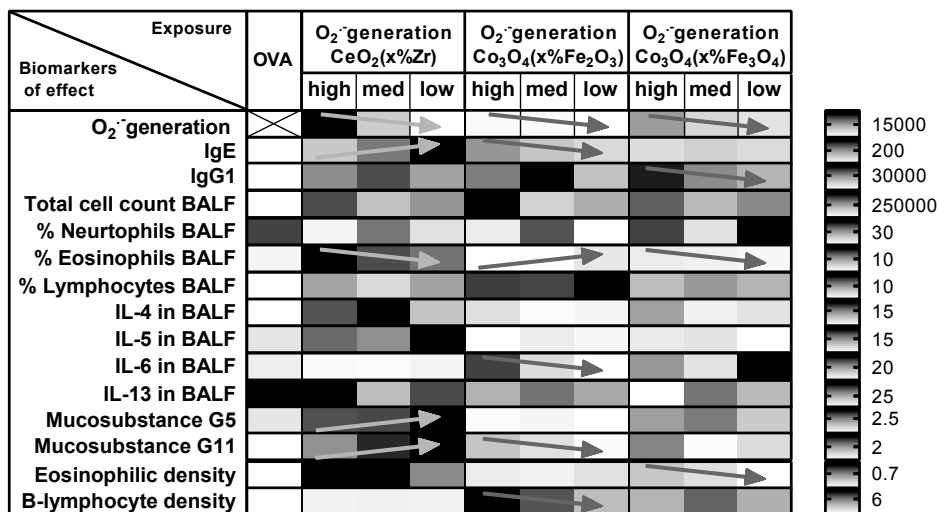


Figure 12: The influence of the ability of NPs to induce superoxide generation as measured in an acellular EPR assay on the different biomarkers of effects.

The shading indicates the lowest (light grey) to highest (dark grey) response of an NP (relative to each other) for each of the biomarkers. The arrows indicate an increase (\nearrow) or decrease (\searrow) with decreasing amount of superoxide generation. The bar on the right side shows for each row the value corresponding with the indicated (medium) grey shading.

The superoxide generation as measured with the EPR was not predictive for the adjuvant activity. Only a few biomarkers of effects decreased with decreasing amounts of superoxide generation and these biomarkers of effects were different for each of the NP series (see arrows in Figure 12).

The scavenging capacity as measured with the EPR was also not predictive for the adjuvant activity. Only a few biomarkers of effects decreased with increasing amounts of scavenging capacity and these biomarkers of effects were different for each of the NP series (see arrows in Figure 13).

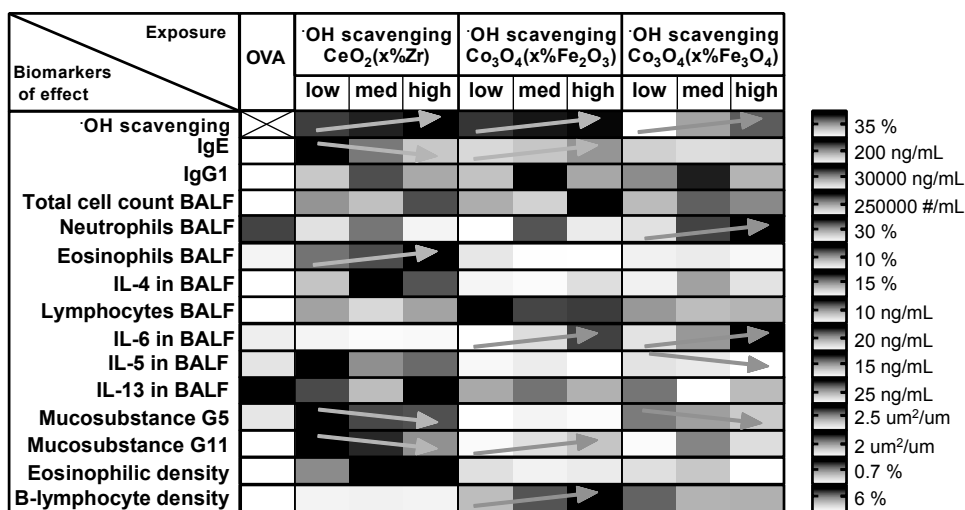


Figure 13: The influence of the scavenging capacity of the NPs as measured in an acellular EPR assay on the different biomarkers of effects.

The shading indicates the lowest (light grey) to highest (dark grey) response of an NP (relative to each other) for each of the biomarkers. The arrows indicate an increase (↗) or decrease (↘) with increasing scavenging capacity. The bar on the right side shows for each row the value corresponding with the indicated (medium) grey shading.

While EPR is a useful technique to predict the ability of NPs to generate cellular oxidative stress, this acellular approach provides only a facet of the redox reactivity of NPs within cellular compartments. However, due to the number of NPs under investigation, a comprehensive comparison of redox activity in cellular assays was not possible within the current study. Therefore, a possible explanation for the lack of trend between the EPR results and the adjuvant activity is that redox activity of the NPs may change due to interaction with the physiological environment, e.g. by corona formation, aggregation, elimination, redox reactions, etc. Interactions with the physiological environment are known to influence the reactivity, cellular uptake and toxicity of the NPs [37-40]. Han et al. [41] found that co-exposure of OVA and polyethylene glycol-conjugated (PEGylated) SiO₂ NPs induced less severe airway inflammation compared to non-coated SiO₂ NPs. It was suggested that

this was due to an increased aggregation of the PEGylated SiO₂ NPs in saline compared to the non-coated SiO₂. However, the small differences in the (aggregated) particle diameter of the NPs in water observed in our study (see Table 2) would be very unlikely to significantly influence adjuvant potency. Larger differences in the (aggregated) particle diameter of the NPs were observed in a more physiologically relevant environment (i.e. buffered cell culture medium with proteins from fetal calf serum) (see Table 2). However, no relation between these differences in aggregated size and the adjuvant potencies of the different NPs found. Horie et al. [42] found differences in OVA-specific IgE and IgG1 concentrations in the blood of mice exposed to ZnO compared to SiO₂-coated ZnO NPs after subsequent exposure to OVA. The investigators suggested that these differences might be due to differences in solubility and continuous Zn²⁺ release from the NPs. Although the NPs in our study are expected to be relatively insoluble, further evaluation of the possible degradation and ion release under various physiological conditions (e.g. in lysosomal fluid) are needed to rule out this possibility. Further research is needed to better understand the mechanisms of the adjuvant activity of NPs, including the influence of the NP properties and NP interactions with their physiological environment, including allergens (such as OVA), on the adjuvant activity.

Conclusions

The chemical composition of NPs in this study influenced both their relative potency to exacerbate allergic airway sensitization to ovalbumin (OVA), and the type of the immune response. The adjuvant activity of CeO₂ NPs seems to be primarily mediated via a Th2-type immune response, whereas the adjuvant activity of Co₃O₄ NPs was characterised by no or less marked increases in OVA-specific IgE plasma levels, BALF IL-4 and IL-5 concentrations and percentages of eosinophils in BALF and more pronounced increases in the BALF IL-6 concentrations and percentages of lymphocytes in BALF. Co-exposure to OVA and Co₃O₄ NPs also induced lymphoid cell accumulation and the formation of ectopic lymphoid tissues in the lungs. No relation between the acellular redox potential and the observed adjuvant activity of the different of NPs was found, suggesting that acellular ROS assays may not be suitable to predict adjuvant capacity. These findings highlight the complexity of biological interplay between different NP species and the need for additional data and methods to formulate scenarios that better predict the adjuvant activity of nanomaterial families.

Abbreviations

NP: Nanoparticle; OVA: ovalbumin; EPR: Electron Paramagnetic Resonance; STEM: Scanning Transmission Electron Microscopy; ROS: Reactive Oxygen Species; Ec: Conduction band energy level; BALF: Bronchoalveolar Lavage Fluid; PBS: Phosphate-Buffered Saline; MBP: Major Basic Protein; ANOVA: analysis of variance; SD: Standard Deviation; RT: Room Temperature; LAL: Limulus Amoebocyte Lysate; DMPO: 5,5-dimethyl-1-pyrroline N-oxide.

Funding

The work leading to these results has received funding from the European Union's Seventh Framework Programme for research, technology development and demonstration under grant agreement n° 310451 (NanoMILE) and the Netherlands Food and Consumer Product Safety Authority (V090016) (NVWA). MRM is supported by a British Heart Foundation (BHF) Special Project Grant (SP/15/8/31575).

Acknowledgements

The authors would like to thank Ryan Lewandowski and Amy Freeland of MSU for their help during the conduction of the animal experiment and valuable technical assistance, Amy Porter, Kathleen Joseph and William Lienhart of MSU Investigative Histopathology Laboratory for their histotechnology support, Daan Leseman and Eric Gremmer of RIVM for their support in the characterizing the particles and for the IgG and IgE ELISA and cytokine analyses of the BALF, respectively, Ed Lester of Promethean Particles for his contribution to the design and production of the particles, Christina Giannakou of RIVM for the LCMS-MS analysis of the endotoxin levels, and Eva Valsami-Jones of UoB coordinator of the NanoMILE project.

References

1. Cho WS, Duffin R, Thielbeer F, Bradley M, Megson IL, Macnee W, Poland CA, Tran CL, Donaldson K: **Zeta potential and solubility to toxic ions as mechanisms of lung inflammation caused by metal/metal oxide nanoparticles.** *Toxicol Sci* 2012, **126**:469-477.
2. Dekkers S, Oomen AG, Bleeker EA, Vandebriel RJ, Micheletti C, Cabellos J, Janer G, Fuentes N, Vazquez-Campos S, Borges T, et al: **Towards a nanospecific approach for risk assessment.** *Regul Toxicol Pharmacol* 2016, **80**:46-59.
3. Teunenbroek TV, Baker J, Dijkzeul A: **Towards a more effective and efficient governance and regulation of nanomaterials.** *Part Fibre Toxicol* 2017, **14**:54.
4. Zhang H, Ji Z, Xia T, Meng H, Low-Kam C, Liu R, Pokhrel S, Lin S, Wang X, Liao YP, et al: **Use of metal oxide nanoparticle band gap to develop a predictive paradigm for oxidative stress and acute pulmonary inflammation.** *ACS Nano* 2012, **6**:4349-4368.
5. Miller MR, Shaw CA, Langrish JP: **From particles to patients: oxidative stress and the cardiovascular effects of air pollution.** *Future Cardiol* 2012, **8**:577-602.
6. Unfried KA, Catrin; Klotz, Lars-Oliver; Von Mikecz, Anna; Grether-Beck, Susanne; Schins, Roel P.F.: **Cellular responses to nanoparticles: Target structures and mechanisms.** *Nanotoxicology* 2007, **1**:52-71.
7. Meldrum K, Guo C, Marczylo EL, Gant TW, Smith R, Leonard MO: **Mechanistic insight into the impact of nanomaterials on asthma and allergic airway disease.** *Part Fibre Toxicol* 2017, **14**:45.
8. Pisoschi AM, Pop A: **The role of antioxidants in the chemistry of oxidative stress: A review.** *Eur J Med Chem* 2015, **97**:55-74.
9. Brandenberger C, Rowley NL, Jackson-Humbles DN, Zhang Q, Bramble LA, Lewandowski RP, Wagner JG, Chen W, Kaplan BL, Kaminski NE, et al: **Engineered silica nanoparticles act as adjuvants to enhance allergic airway disease in mice.** *Part Fibre Toxicol* 2013, **10**:26.
10. Vandebriel RJ, Vermeulen JP, van Engelen LB, de Jong B, Verhagen LM, de la Fonteyne-Blankestijn LJ, Hoonakker ME, de Jong WH: **The crystal structure of titanium dioxide nanoparticles influences immune activity in vitro and in vivo.** *Part Fibre Toxicol* 2018, **15**:9.
11. Fu PP, Xia Q, Hwang HM, Ray PC, Yu H: **Mechanisms of nanotoxicity: generation of reactive oxygen species.** *J Food Drug Anal* 2014, **22**:64-75.
12. Khanna P, Ong C, Bay BH, Baeg GH: **Nanotoxicity: An Interplay of Oxidative Stress, Inflammation and Cell Death.** *Nanomaterials (Basel)* 2015, **5**:1163-1180.
13. Nel A, Xia T, Madler L, Li N: **Toxic potential of materials at the nanolevel.** *Science* 2006, **311**:622-627.
14. Dekkers S, Miller MR, Schins RPF, Romer I, Russ M, Vandebriel RJ, Lynch I, Belinga-Desaunay MF, Valsami-Jones E, Connell SP, et al: **The effect of zirconium doping of cerium dioxide nanoparticles on pulmonary and cardiovascular toxicity and biodistribution in mice after inhalation.** *Nanotoxicology* 2017, **11**:794-808.

15. Zhang H, Pokhrel S, Ji Z, Meng H, Wang X, Lin S, Chang CH, Li L, Li R, Sun B, et al: **PdO doping tunes band-gap energy levels as well as oxidative stress responses to a Co(3)O(4) p-type semiconductor in cells and the lung.** *J Am Chem Soc* 2014, **136**:6406-6420.
16. Kroker M, Sydlik U, Autengruber A, Cavelius C, Weighardt H, Kraegeloh A, Unfried K: **Preventing carbon nanoparticle-induced lung inflammation reduces antigen-specific sensitization and subsequent allergic reactions in a mouse model.** *Part Fibre Toxicol* 2015, **12**:20.
17. Cabanas A, Darr JA, E. L, Poliakoff M: **A continuous and clean one-step synthesis of nanoparticulate Ce_{1-x}Zr_xO₂ solid solutions in near-critical water.** *Chem Comm* 2000, **2000**:901-902.
18. Liu J, Römer I, Tang SVY, Valsami-Jones E, Palmer RE: **Crystallinity depends on choice of iron salt precursor in the continuous hydrothermal synthesis of Fe-Co oxide nanoparticles.** *RSC Adv* 2017, **7**:37436-37440.
19. He W, Liu Y, Wamer WG, Yin JJ: **Electron spin resonance spectroscopy for the study of nanomaterial-mediated generation of reactive oxygen species.** *J Food Drug Anal* 2014, **22**:49-63.
20. Giannakou C, Aimonen K, Bloois LV, Catalan J, Geertsma RE, Gremmer ER, de Jong WH, Keizers PH, Schwillens PL, Vandebriel RJ, Park MV: **Sensitive method for endotoxin determination in nanomedicinal product samples.** *Nanomedicine (Lond)* 2019, **14**:1231-1246.
21. Harkema JR, Hotchkiss JA: **In vivo effects of endotoxin on intraepithelial mucosubstances in rat pulmonary airways. Quantitative histochemistry.** *Am J Pathol* 1992, **141**:307-317.
22. Malyala P, Singh M: **Endotoxin limits in formulations for preclinical research.** *J Pharm Sci* 2008, **97**:2041-2044.
23. Carragher DM, Rangel-Moreno J, Randall TD: **Ectopic lymphoid tissues and local immunity.** *Semin Immunol* 2008, **20**:26-42.
24. Pitzalis C, Jones GW, Bombardieri M, Jones SA: **Ectopic lymphoid-like structures in infection, cancer and autoimmunity.** *Nat Rev Immunol* 2014, **14**:447-462.
25. Meldrum K, Robertson SB, Romer I, Marczylo T, Dean LSN, Rogers A, Gant TW, Smith R, Tetley TD, Leonard MO: **Cerium dioxide nanoparticles exacerbate house dust mite induced type II airway inflammation.** *Part Fibre Toxicol* 2018, **15**:24.
26. Schanen BC, Das S, Reilly CM, Warren WL, Self WT, Seal S, Drake DR, 3rd: **Immunomodulation and T helper TH(1)/TH(2) response polarization by CeO(2) and TiO(2) nanoparticles.** *PLoS One* 2013, **8**:e62816.
27. Cho WS, Dart K, Nowakowska DJ, Zheng X, Donaldson K, Howie SE: **Adjuvanticity and toxicity of cobalt oxide nanoparticles as an alternative vaccine adjuvant.** *Nanomedicine (Lond)* 2012, **7**:1495-1505.
28. de Haar C, Hassing I, Bol M, Bleumink R, Pieters R: **Ultrafine but not fine particulate matter causes airway inflammation and allergic airway sensitization to co-administered antigen in mice.** *Clin Exp Allergy* 2006, **36**:1469-1479.
29. Randall TD: **Bronchus-associated lymphoid tissue (BALT) structure and function.** *Adv Immunol* 2010, **107**:187-241.
30. Hirahara K, Shinoda K, Endo Y, Ichikawa T, Nakayama T: **Maintenance of memory-type pathogenic Th2 cells in the pathophysiology of chronic airway inflammation.** *Inflamm Regen* 2018, **38**:10.

31. Hwang JY, Randall TD, Silva-Sanchez A: **Inducible Bronchus-Associated Lymphoid Tissue: Taming Inflammation in the Lung.** *Front Immunol* 2016, **7**:258.
32. Cho WS, Duffin R, Bradley M, Megson IL, Macnee W, Howie SE, Donaldson K: **NiO and Co3O4 nanoparticles induce lung DTH-like responses and alveolar lipoproteinosis.** *Eur Respir J* 2012, **39**:546-557.
33. Guest IC, Sell S: **Bronchial lesions of mouse model of asthma are preceded by immune complex vasculitis and induced bronchial associated lymphoid tissue (iBALT).** *Lab Invest* 2015, **95**:886-902.
34. Bates MA, Brandenberger C, Langohr I, Kumagai K, Harkema JR, Holian A, Pestka JJ: **Silica Triggers Inflammation and Ectopic Lymphoid Neogenesis in the Lungs in Parallel with Accelerated Onset of Systemic Autoimmunity and Glomerulonephritis in the Lupus-Prone NZBWF1 Mouse.** *PLoS One* 2015, **10**:e0125481.
35. Blum JL, Rosenblum LK, Grunig G, Beasley MB, Xiong JQ, Zelikoff JT: **Short-term inhalation of cadmium oxide nanoparticles alters pulmonary dynamics associated with lung injury, inflammation, and repair in a mouse model.** *Inhal Toxicol* 2014, **26**:48-58.
36. Hsieh SF, Bello D, Schmidt DF, Pal AK, Stella A, Isaacs JA, Rogers EJ: **Mapping the biological oxidative damage of engineered nanomaterials.** *Small* 2013, **9**:1853-1865.
37. Ahsan SM, Rao CM, Ahmad MF: **Nanoparticle-Protein Interaction: The Significance and Role of Protein Corona.** *Adv Exp Med Biol* 2018, **1048**:175-198.
38. Barbero F, Russo L, Vitali M, Piella J, Salvo I, Borrajo ML, Busquets-Fite M, Grandori R, Bastus NG, Casals E, Puentes V: **Formation of the Protein Corona: The Interface between Nanoparticles and the Immune System.** *Semin Immunol* 2017, **34**:52-60.
39. Saptarshi SR, Duschl A, Lopata AL: **Interaction of nanoparticles with proteins: relation to bio-reactivity of the nanoparticle.** *J Nanobiotechnology* 2013, **11**:26.
40. Shannahan JH, Brown JM: **Engineered nanomaterial exposure and the risk of allergic disease.** *Curr Opin Allergy Clin Immunol* 2014, **14**:95-99.
41. Han H, Park YH, Park HJ, Lee K, Um K, Park JW, Lee JH: **Toxic and adjuvant effects of silica nanoparticles on ovalbumin-induced allergic airway inflammation in mice.** *Respir Res* 2016, **17**:60.
42. Horie M, Stowe M, Tabei M, Kuroda E: **Pharyngeal aspiration of metal oxide nanoparticles showed potential of allergy aggravation effect to inhaled ovalbumin.** *Inhal Toxicol* 2015, **27**:181-190.

Supplementary information

Additional file 1: Total and differential cell counts in bronchoalveolar lavage fluid.

Mice #	Group	Total cells/ml	%mono	%eos	%PMN	%lymph	mono/ml	eos/ml	PMN/ml	lymph/ml	counts	volume
1	PBS	97.500	74,0	0,0	21,0	5,0	72.150,00	0,00	20.475,00	4.875,00	39	1,1
2	PBS	32.500	98,0	0,0	0,5	2,0	31.850,00	0,00	162,50	0,00	13	0,9
3	PBS	62.500	42,0	0,0	57,5	0,5	26.250,00	0,00	35.937,50	0,00	25	1
4	PBS	30.000	52,0	0,0	47,5	0,5	15.600,00	0,00	14.250,00	0,00	12	1,25
5	PBS	60.000	53,0	0,0	46,0	1,0	31.800,00	0,00	27.600,00	0,00	24	0,8
6	PBS	67.500	28,5	0,0	71,0	0,5	19.237,50	0,00	47.925,00	0,00	27	1,25
Mean		58.333,33	57,92	0,00	40,58	1,58	32.814,58	0,00	24.391,67	812,50		
SEM		10.178,95	10,07	0,00	10,45	0,72	8.312,66	0,00	6.837,80	812,50		
7	OVA	130.000	58,6	0,0	37,8	3,6	76.180,00	0,00	49.140,00	4.680,00	52	1
8	OVA	75.000	70,4	1,6	26,8	1,2	52.800,00	1.200,00	20.100,00	900,00	30	1,25
9	OVA	67.500	50,7	2,1	41,1	6,1	34.222,50	1.417,50	27.742,50	4.117,50	27	0,9
10	OVA	92.500	55,1	2,2	37,2	5,5	50.967,50	2.035,00	34.410,00	5.087,50	37	0,9
11	OVA	42.500	63,6	1,8	32,0	2,6	27.030,00	765,00	13.600,00	1.105,00	17	1,1
12	OVA	100.000	72,4	3,8	19,9	3,8	72.400,00	3.800,00	19.900,00	3.800,00	40	1,25
79	OVA	117.500	50,0	1,9	41,7	6,3	58.750,00	2.232,50	48.997,50	7.402,50	47	1
80	OVA	85.000	56,0	1,8	35,3	6,9	47.600,00	1.530,00	30.005,00	5.865,00	34	1
Mean		88.750,00	59,60	1,90	33,98	4,50	52.493,75	1.622,50	30.486,88	4.119,69		
SEM		9.876,47	2,99	0,36	2,64	0,71	5.983,68	398,23	4.665,36	786,39		
13	TiO2	345.000	77,7	8,1	9,5	4,6	268.065,00	27.945,00	32.775,00	15.870,00	138	1,2
14	TiO2	147.500	48,6	9,7	37,4	4,4	71.685,00	14.307,50	55.165,00	6.490,00	59	1,1
15	TiO2	225.000	47,3	11,8	37,3	3,6	106.425,00	26.550,00	83.925,00	8.100,00	90	1,1

16	TiO2	150,000	49,0	6,2	40,8	3,7	73,500,00	9,300,00	61,200,00	5,550,00	60	1,1
17	TiO2	195,000	53,9	12,5	27,3	6,3	105,105,00	24,375,00	53,235,00	12,285,00	78	1,2
18	TiO2	207,500	47,9	17,8	29,5	4,8	99,392,50	36,935,00	61,212,50	9,960,00	83	1,1
	Mean	211,666,67	54,07	11,02	30,30	4,57	120,695,42	20,495,50	58,855,50	9,659,00		
	SEM	29,535,76	4,82	1,66	4,66	0,40	30,137,32	4,066,31	6,732,18	1,580,14		
19	CeO2NM212	107,500	64,9	2,4	30,9	1,8	69,767,50	2,580,00	33,217,50	1,935,00	43	1
20	CeO2NM212	185,000	58,6	3,6	33,9	3,9	108,410,00	6,660,00	62,715,00	7,215,00	74	1,1
21	CeO2NM212	172,500	57,0	5,5	34,5	3,0	98,325,00	9,487,50	59,512,50	5,175,00	69	1
22	CeO2NM212	122,500	69,1	3,2	23,3	4,4	84,647,50	3,920,00	28,542,50	5,390,00	49	1,25
23	CeO2NM212	207,500	53,1	6,5	38,8	1,6	110,182,50	13,487,50	80,510,00	3,320,00	83	1
24	CeO2NM212	180,000	48,3	7,9	41,2	2,6	86,940,00	14,220,00	74,160,00	4,680,00	72	1,1
	Mean	162,500,00	58,50	4,85	33,77	2,88	93,045,42	7,227,00	51,629,50	4,607,00		
	SEM	15,877,13	3,10	0,87	2,57	0,46	6,343,73	1,982,49	8,678,97	742,47		
25	Co3O4 (0%Fe2O3)	272,500	47,0	2,8	32,8	17,4	128,075,00	7,630,00	89,380,00	47,415,00	109	0,8
26	Co3O4 (0%Fe2O3)	92,500	55,0	0,3	33,7	11,0	50,875,00	2,77,50	31,172,50	10,175,00	37	0,8
27	Co3O4 (0%Fe2O3)	285,000	64,5	0,8	22,6	12,1	183,825,00	2,280,00	64,410,00	34,485,00	114	1
28	Co3O4 (0%Fe2O3)	202,500	59,8	0,0	31,1	9,1	121,095,00	0,00	62,977,50	18,427,50	81	1,3
29	Co3O4 (0%Fe2O3)	30,000	46,7	1,6	33,2	18,4	14,010,00	480,00	9,960,00	5,520,00	12	1,2
30	Co3O4 (0%Fe2O3)	157,500	58,1	0,3	35,3	6,0	91,507,50	472,50	55,597,50	9,450,00	63	1
	Mean	173,333,33	55,18	0,97	31,45	12,33	98,231,25	2,133,50	60,707,50	23,204,50		
	SEM	41,021,67	2,92	0,43	1,85	1,96	24,576,91	1,200,87	11,380,53	6,773,43		
31	Co3O4 (25%Fe2O3)	475,000	60,6	1,5	23,9	14,0	287,850,00	7,125,00	113,525,00	66,500,00	190	1,25
32	Co3O4 (25%Fe2O3)	367,500	63,6	1,6	24,4	11,4	233,730,00	5,880,00	89,670,00	41,895,00	147	1,25
33	Co3O4 (25%Fe2O3)	390,000	48,6	1,0	22,1	28,3	189,540,00	3,900,00	86,190,00	110,370,00	156	1,25
34	Co3O4 (25%Fe2O3)	457,500	54,6	0,0	32,0	13,4	249,795,00	0,00	146,217,00	61,305,00	183	1,25

Mice #	Group	Total cells/ml	%mono	%eos	%PMN	%lymph	mono/ml	eos/ml	PMN/ml	lymph/ml	counts	volume
35	Co3O4 (25%Fe2O3)	480.000	69,0	0,0	20,4	10,6	331.200,00	0,00	97.920,00	50.880,00	192	1
36	Co3O4 (25%Fe2O3)	430.000	72,5	0,4	13,7	13,3	311.750,00	1.720,00	58.910,00	57.190,00	172	1
	Mean	433.333,33	61,48	0,75	22,74	15,17	267.310,83	3.381,00	98.902,40	66.190,00		
	SEM	18.904,00	3,64	0,29	2,43	2,68	21.572,59	1.234,14	11.971,54	9.777,48		
37	Co3O4 (75%Fe2O3)	210.000	55,8	1,8	24,9	17,5	117.180,00	3.780,00	52.290,00	36.750,00	84	1,1
38	Co3O4 (75%Fe2O3)	192.500	57,8	0,2	28,3	13,7	111.265,00	385,00	54.477,50	26.372,50	77	1,2
39	Co3O4 (75%Fe2O3)	327.500	64,4	1,0	17,3	17,3	210.910,00	3.275,00	56.657,50	56.657,50	131	1
40	Co3O4 (75%Fe2O3)	120.000	54,7	7,0	33,2	5,0	65.640,00	8.400,00	39.840,00	6.000,00	48	0,75
41	Co3O4 (75%Fe2O3)	277.500	69,4	3,4	10,7	16,5	192.585,00	9.435,00	29.692,50	45.787,50	111	1,25
42	Co3O4 (75%Fe2O3)	242.500	71,0	6,5	9,1	13,4	172.175,00	15.762,50	22.067,50	32.495,00	97	1
	Mean	228.333,33	62,18	3,32	20,58	13,90	144.959,17	5.055,00	45.066,50	34.313,50		
	SEM	29.330,49	2,89	1,17	3,99	1,92	22.772,02	2.254,76	5.854,72	7.081,23		
43	Co3O4 (0%Fe3O4)	312.500	45,1	1,4	45,4	8,1	140.937,50	4.375,00	141.875,00	25.312,50	125	1
44	Co3O4 (0%Fe3O4)	312.500	52,3	3,0	37,0	7,8	163.437,50	9.312,50	115.625,00	24.375,00	125	1,1
45	Co3O4 (0%Fe3O4)	292.500	51,8	1,0	40,7	6,6	151.515,00	2.925,00	119.047,50	19.305,00	117	1,3
46	Co3O4 (0%Fe3O4)	335.000	57,0	1,0	31,1	10,8	190.950,00	3.350,00	104.185,00	36.180,00	134	1
47	Co3O4 (0%Fe3O4)	175.000	35,8	2,6	51,6	10,0	62.650,00	4.550,00	90.300,00	17.500,00	70	1,25
48	Co3O4 (0%Fe3O4)	192.500	59,3	0,0	32,0	8,7	114.152,50	0,00	61.600,00	16.747,50	77	1,2
	Mean	270.000,00	50,22	1,50	39,63	8,67	137.273,75	4.902,50	108.466,50	24.534,50		
	SEM	27.913,56	3,51	0,45	3,24	0,62	18.152,33	1.240,97	11.208,85	2.964,30		
49	Co3O4 (25%Fe3O4)	447.500	60,8	3,9	24,1	11,0	272.080,00	17.452,50	107.847,50	49.359,25	179	1
50	Co3O4 (25%Fe3O4)	325.000	46,4	3,4	39,2	11,0	150.800,00	11.050,00	127.400,00	35.750,00	130	1
51	Co3O4 (25%Fe3O4)	215.000	60,5	1,6	32,9	5,0	130.075,00	3.440,00	70.735,00	10.750,00	86	1
52	Co3O4 (25%Fe3O4)	260.000	55,7	2,8	34,8	6,8	144.820,00	7.280,00	90.480,00	17.680,00	104	0,75
53	Co3O4 (25%Fe3O4)	385.000	53,3	3,6	38,2	4,9	205.205,00	13.860,00	147.070,00	18.865,00	154	1,3

54	Co3O4 (25%Fe3O4)	220.000	52,8	1,7	34,8	10,7	116.160,00	3.740,00	76.560,00	23.540,00	88	1
	Mean	308.750,00	54,92	2,83	34,00	8,24	169.856,67	10.616,50	94.604,50	26.480,85		
	SEM	38.458,58	2,21	0,40	2,20	1,23	23.913,05	2.305,64	12.188,99	5.771,95		
55	Co3O4 (75%Fe3O4)	165.000	67,1	2,7	17,4	12,8	110.715,00	4.455,00	28.710,00	21.120,00	66	0,9
56	Co3O4 (75%Fe3O4)	70.000	57,6	1,3	36,1	5,0	40.320,00	910,00	25.270,00	3.500,00	28	0,9
57	Co3O4 (75%Fe3O4)	310.000	64,2	3,2	24,5	8,2	199.020,00	9.920,00	75.950,00	25.420,00	124	0,8
58	Co3O4 (75%Fe3O4)	315.000	66,7	1,9	24,1	7,3	210.105,00	5.985,00	75.915,00	22.995,00	126	1
59	Co3O4 (75%Fe3O4)	90.000	56,3	2,1	27,4	14,2	50.670,00	1.890,00	24.660,00	12.780,00	36	1,2
60	Co3O4 (75%Fe3O4)	292.500	69,3	6,5	12,8	11,4	202.702,50	19.012,50	37.440,00	33.345,00	117	1,25
	Mean	207.083,33	63,53	2,95	23,72	9,82	135.588,75	4.632,00	48.657,00	17.163,00		
	SEM	46.117,68	2,19	0,76	3,30	1,45	32.138,49	2.729,65	10.063,87	4.250,30		
61	CeO2 (0%ZrO2)	132.500	48,0	14,7	30,1	7,1	63.600,00	19.477,50	39.882,50	9.407,50	53	1,25
62	CeO2 (0%ZrO2)	140.000	53,0	7,3	33,3	6,3	74.200,00	10.220,00	46.620,00	8.820,00	56	1,2
63	CeO2 (0%ZrO2)	162.500	37,5	15,6	36,4	10,5	60.937,50	25.350,00	59.150,00	17.062,50	65	1
64	CeO2 (0%ZrO2)	305.000	46,8	20,8	29,1	3,3	142.740,00	63.440,00	88.755,00	10.065,00	122	1,25
65	CeO2 (0%ZrO2)	245.000	51,2	11,2	33,2	4,3	125.440,00	27.440,00	81.340,00	10.535,00	98	1,25
66	CeO2 (0%ZrO2)	225.000	50,6	12,0	27,3	10,1	113.850,00	27.000,00	61.425,00	22.725,00	90	1
	Mean	201.666,67	47,85	13,60	31,57	6,93	96.794,58	29.185,50	59.166,50	11.178,00		
	SEM	27.821,35	2,26	1,87	1,36	1,20	14.283,50	7.414,05	7.788,00	2.280,97		
67	CeO2 (25%ZrO2)	422.500	55,8	13,4	22,7	8,1	235.755,00	56.615,00	95.907,50	34.222,50	169	1,3
68	CeO2 (25%ZrO2)	82.500	49,6	13,8	29,7	6,9	40.920,00	11.385,00	24.502,50	5.692,50	33	1,25
69	CeO2 (25%ZrO2)	262.500	41,4	13,4	36,4	8,7	108.675,00	35.175,00	95.550,00	22.837,50	105	1,1
70	CeO2 (25%ZrO2)	160.000	46,9	9,1	34,0	10,0	75.040,00	14.560,00	54.400,00	16.000,00	64	1
71	CeO2 (25%ZrO2)	377.500	66,3	10,6	12,0	11,2	250.282,50	40.015,00	45.224,50	42.280,00	151	1,25
72	CeO2 (25%ZrO2)	240.000	70,1	10,5	7,6	11,8	168.240,00	25.200,00	18.240,00	28.320,00	96	1,25

Mice #	Group	Total cells/ml	%mono	%eos	%PMN	%lymph	mono/ml	eos/ml	PMN/ml	lymph/ml	counts	volume
	Mean	257,500,00	55,02	11,80	23,73	9,45	146.485,42	31.550,00	57.720,00	24.206,50		
	SEM	52.309,18	4,60	0,81	4,83	0,77	35.068,64	6.932,87	13.775,10	5.332,48		
73	CeO2 (75%ZrO2)	500.000	48,8	33,0	8,4	9,8	244.000,00	#####	42.000,00	49.000,00	200	1,25
74	CeO2 (75%ZrO2)	170.000	47,8	6,3	33,9	12,0	81.260,00	10.710,00	57.630,00	20.400,00	68	1,25
75	CeO2 (75%ZrO2)	552.500	55,5	24,3	12,1	8,1	306.637,50	#####	66.852,50	44.752,50	221	0,8
76	CeO2 (75%ZrO2)	337.500	56,6	16,7	21,7	5,0	191.025,00	56.362,50	73.237,50	16.875,00	135	0,8
77	CeO2 (75%ZrO2)	217.500	47,7	19,5	27,8	5,1	103.747,50	42.412,50	60.465,00	11.092,50	87	1,1
78	CeO2 (75%ZrO2)	165.000	39,4	17,6	26,7	16,3	65.010,00	29.040,00	44.055,00	26.895,00	66	1,25
	Mean	323.750,00	49,30	19,57	21,77	9,38	165.280,00	81.748,50	56.755,00	28.424,00		
	SEM	69.212,08	2,55	3,61	4,00	1,77	39.892,05	25.325,48	5.049,32	6.298,37		

Additional file 2: Cytokines in bronchoalveolar lavage fluid.

Mice #	Group	IFNy	IL-4	IL-5	IL-1b	IL-6	IL-13	IL-17	TNFa
1	PBS	9,47					43,26		10,03
2	PBS	17,73			4,27	12,04	79,64	0,61	8,4
3	PBS	18,35		6,46	4,27	0,92	40,15		10,83
4	PBS	13,66		6,46	7,82	13,22	47,03		13,52
5	PBS	15,41		6,46	7,82	9,43	50,69		11,07
6	PBS	3,76					17,76	2,04	11,37
	Mean	13,06	#DIV/0!	6,46	6,05	8,90	46,42	1,33	10,87
	SEM	2,27	#DIV/0!	0,00	1,02	2,78	8,15	0,72	0,69
7	OVA	23,5		6,46	7,82	12,04	40,15		9,79
8	OVA	11,85		6,46	4,27		49,23		8,93
9	OVA	9,96			4,27		35,31		12,26

10	OVA	21,56		8,13	4,27	26,6	50,69		11,37
11	OVA	4,08	0,45	13,56	13,12	6,24	20,87		11,37
12	OVA	14,97			7,82	4,19	49,23		13,25
79	OVA	20,37	0,45	6,46	4,27	12,04	28,44		9,95
80	OVA	8,98					36,95		8,49
	Mean	14,41	0,45	8,21	6,55	12,22	38,86	#DIV/0!	10,68
	SEM	2,44	0,00	1,38	1,26	3,92	3,79	#DIV/0!	0,59
13	TiO2	9,96	4,61	11,72	4,27	9,43	35,31		10,36
14	TiO2	5,83	2,07	20,29		9,43	17,76	1,3	10,6
15	TiO2	4,08	2,2	30,68		19,28	26,63	2,85	12,76
16	TiO2	4,08	3,58	13,56	4,27		21,87	4,3	14,2
17	TiO2	11,85	0,92	17,28	1,69	16,43	47,77	2,46	10,12
18	TiO2	17,31	4,07	75,81	1,69	54,15	56,34	4,3	12,83
	Mean	8,85	2,91	28,22	2,98	21,74	34,28	3,04	11,81
	SEM	2,13	0,57	9,90	0,74	8,33	6,21	0,57	0,69
19	CeO2NM212	17,1	1,72	9,49		9,43	23,81		8,03
20	CeO2NM212	38,69	0,62	20,29	4,27	21,89	74,71	1,69	10,12
21	CeO2NM212	10,44	0,62	14,39		6,24	13,26		9,95
22	CeO2NM212	10,68	0,45	9,49			24,77		9,79
23	CeO2NM212	23,89	8,01	30,68	15,37	33,47	31,09	1,81	12,69
24	CeO2NM212	6,92	0,35	11,72	1,69		14,43	1,81	11,07
	Mean	17,95	1,96	16,01	7,11	21,60	30,35	1,77	10,28
	SEM	4,82	1,23	3,36	4,20	6,01	9,29	0,04	0,63
25	Co3O4 (0%Fe2O3)	9,47	1,46	6,46	4,27	12,04	26,63	2,26	14,91
26	Co3O4 (0%Fe2O3)	8,22	1,05		4,27	20,17	29,33	0,99	16,23

Mice #	Group	IFNy	IL-4	IL-5	IL-1b	IL-6	IL-13	IL-17	TNFA
27	Co3O4 (0%Fe2O3)	13,43	1,11	6,46	9,29	9,43	41,72		17,07
28	Co3O4 (0%Fe2O3)	15,41	0,45	6,46	1,69	21,89	41,72	1,93	11,29
29	Co3O4 (0%Fe2O3)	11,15	0,62				18,82		13,04
30	Co3O4 (0%Fe2O3)	9,47	0,24	4,09			18,82		11,22
	Mean	11,19	0,82	5,87	4,88	15,88	29,51	1,73	13,96
	SEM	1,12	0,19	0,59	1,59	3,04	4,22	0,38	1,02
31	Co3O4 (25%Fe2O3)	9,96	6,41		6,18	46,68	20,87	4,3	21,32
32	Co3O4 (25%Fe2O3)	14,1	3,28		7,82	21,04	28,44	0,99	14,98
33	Co3O4 (25%Fe2O3)	9,22	5,48	6,46	7,82	18,36	24,77	3,12	17,07
34	Co3O4 (25%Fe2O3)	9,96	6,3		7,82	18,36	20,87	4,73	21,68
35	Co3O4 (25%Fe2O3)	9,22	6,41		1,69	40,7	22,85	12,28	24,97
36	Co3O4 (25%Fe2O3)	14,97	1,62		9,29	18,36	26,63	0,61	15,49
	Mean	11,24	4,92	6,46	6,77	27,25	24,07	4,34	19,25
	SEM	1,06	0,82	#DIV/0!	1,09	5,27	1,27	1,73	1,63
37	Co3O4 (75%Fe2O3)	8,98	1,82		7,82	0,92	27,54	0,99	12,04
38	Co3O4 (75%Fe2O3)	7,71	0,78			6,24	18,82	1,57	9,79
39	Co3O4 (75%Fe2O3)	3,76	0,62				12,04		9,45
40	Co3O4 (75%Fe2O3)	11,38	1,92	6,46		0,92	33,65		9,11
41	Co3O4 (75%Fe2O3)	14,32	0,45		7,82	6,24	22,85		9,95
42	Co3O4 (75%Fe2O3)	12,3	3,24			12,04	34,48		12,55
	Mean	9,74	1,47	6,46	7,82	5,27	24,90	1,28	10,48
	SEM	1,53	0,44	0,00	0,00	2,07	3,57	0,29	0,59
43	Co3O4 (0%Fe3O4)	6,38	4		4,27	40,7	28,44	2,04	15,23
44	Co3O4 (0%Fe3O4)	0,35	4,8			28,05	8,07		7,55
45	Co3O4 (0%Fe3O4)	6,38	8,21		10,64	54,15	20,87		12,19

46	Co3O4 (0%Fe3O4)	7,71	2,02	7,82	37,19	30,21	14,46
47	Co3O4 (0%Fe3O4)	9,71	5,72	4,27	59,24	16,68	13,52
48	Co3O4 (0%Fe3O4)	10,91	0,24	6,46	0,92	32,8	12,26
	Mean	6,91	4,17	6,75	36,71	22,85	1,52
	SEM	1,51	1,14	#DIV/0!	8,53	3,85	0,53
49	Co3O4 (25%Fe3O4)	12,76	0,92	4,27	9,43	6,58	2,26
50	Co3O4 (25%Fe3O4)	11,38	33,3	6,46	18,36	6,58	9,77
51	Co3O4 (25%Fe3O4)	12,76	2,38	1,69	21,89	22,85	0,61
52	Co3O4 (25%Fe3O4)	8,98	8,85	1,69	23,52	6,58	0,99
53	Co3O4 (25%Fe3O4)	14,1	22,1	10,64	18,36	77,19	2,46
54	Co3O4 (25%Fe3O4)	10,44	2,43	7,82	27,33	22,85	0,99
	Mean	11,74	11,66	5,22	19,82	23,77	2,85
	SEM	0,75	5,39	1,76	2,49	11,17	1,42
55	Co3O4 (75%Fe3O4)	9,96	4,48	4,27	14,34	38,57	2,56
56	Co3O4 (75%Fe3O4)	17,52	0,24	6,46	12,04	33,65	10,44
57	Co3O4 (75%Fe3O4)	16,89	1,51	4,27	9,43	33,65	11,82
58	Co3O4 (75%Fe3O4)	11,85	2,11	4,27	12,04	31,95	2,26
59	Co3O4 (75%Fe3O4)	5,55	1,82	4,27	12,04	22,85	12,19
60	Co3O4 (75%Fe3O4)	11,15	2,97	15,17	9,43	15,57	11,22
	Mean	12,15	2,19	4,27	11,46	29,37	2,41
	SEM	1,83	0,58	0,00	0,93	3,47	0,15
61	CeO2 (0%ZrO2)	14,76	16,97	13,56	9,43	36,95	10,28
62	CeO2 (0%ZrO2)	6,92	7,34	9,49	9,46	9,46	7,65
63	CeO2 (0%ZrO2)	14,97	10,96	16,61	0,92	12,04	0,61
64	CeO2 (0%ZrO2)	8,73	95,6	26,47	6,24	16,68	0,99

Mice #	Group	IFN γ	IL-4	IL-5	IL-1b	IL-6	IL-13	IL-17	TNFA
65	CeO2 (0%ZrO2)	14,76	0,92	6,46			19,86		8,58
66	CeO2 (0%ZrO2)	18,55	24,94	15,17		14,34	40,15		11,82
	Mean	13,12	26,12	14,63	#DIV/0!	7,73	22,52	0,80	10,55
	SEM	1,79	14,29	2,82	#DIV/0!	2,82	5,29	0,19	0,95
67	CeO2 (25%ZrO2)	13,66	2,97	15,91	7,82	0,92	19,86		11,07
68	CeO2 (25%ZrO2)	7,18	3,93	24,29					11,22
69	CeO2 (25%ZrO2)	9,47	19,65	38,21	4,27	23,52	68,37	3,7	15,86
70	CeO2 (25%ZrO2)	10,68	2,29	58,82	4,27	0,92	12,04		14,33
71	CeO2 (25%ZrO2)	11,38	16,75	11,72			38,57		9,62
72	CeO2 (25%ZrO2)	12,76	3,86	17,93		12,04	22,85		10,12
	Mean	10,86	8,24	27,81	5,45	9,35	32,34	3,70	12,04
	SEM	0,95	3,18	7,26	1,18	5,40	9,99	#DIV/0!	1,02
73	CeO2 (75%ZrO2)	5,26	24,08	11,72					10,6
74	CeO2 (75%ZrO2)	10,91	3,05	11,72			13,26		8,76
75	CeO2 (75%ZrO2)	19,37	34,22	41,68	4,27	18,36	56,34	2,04	12,19
76	CeO2 (75%ZrO2)	6,38	4,54	13,56		14,34	49,96		7,84
77	CeO2 (75%ZrO2)	16,68	26,87	13,56		0,92	44,78		9,28
78	CeO2 (75%ZrO2)	2,08	11,93	11,72					9,87
	Mean	10,11	17,45	17,33	4,27	11,21	41,09	2,04	9,76
	SEM	2,78	5,22	4,88	#DIV/0!	5,27	9,57	#DIV/0!	0,62

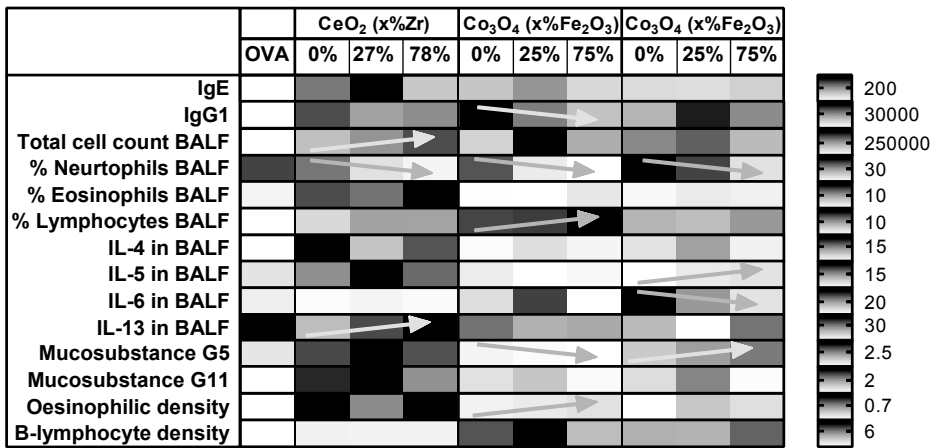
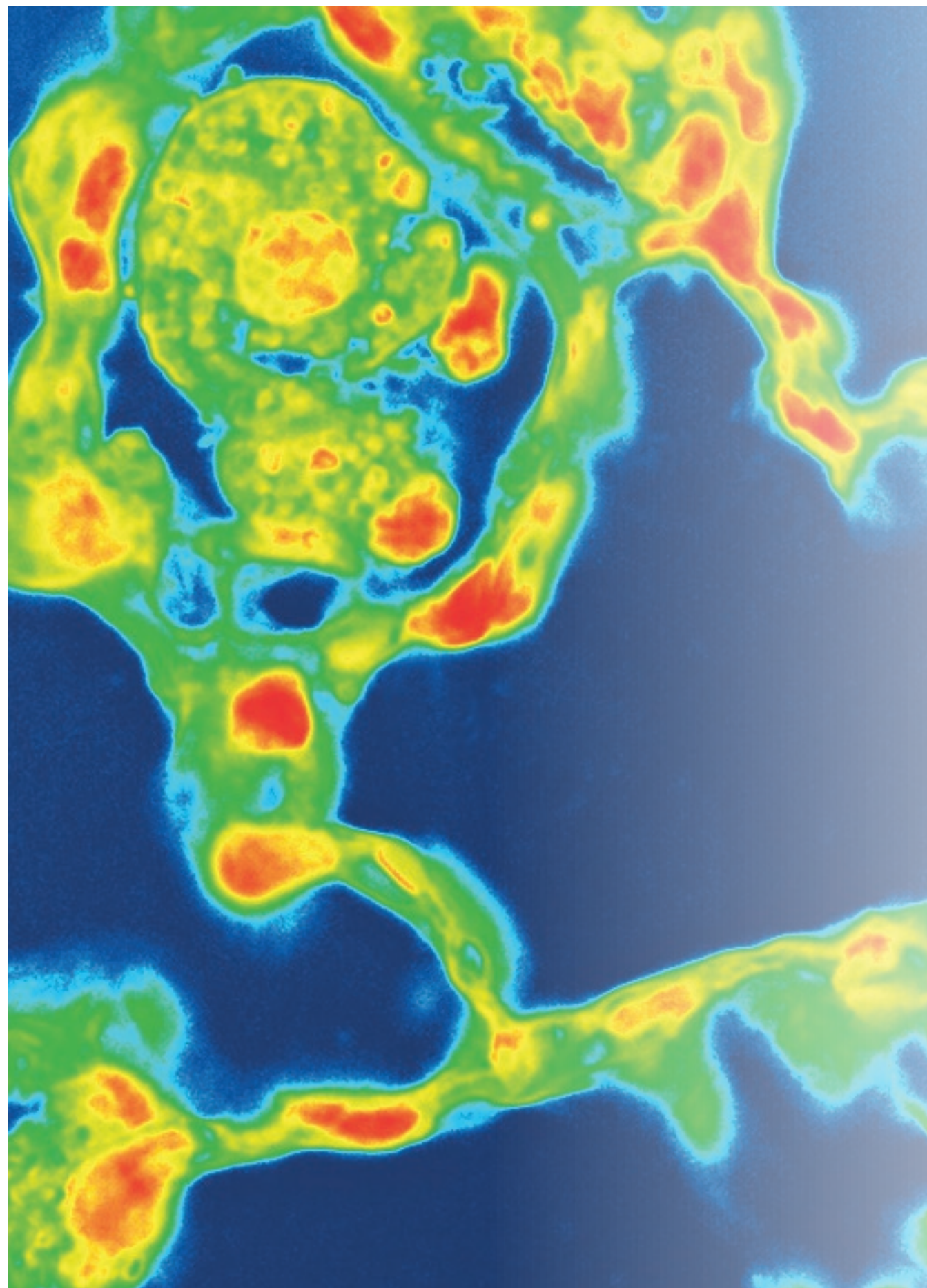


Figure S1: The influence of the ability of NPs to induce superoxide generation as measured in an acellular EPR assay on the different biomarkers of effects.

The shading indicates the lowest (light grey) to highest (dark grey) response of an NP (relative to each other) for each of the biomarkers. The arrows indicate an increase (↗) or decrease (↘) with decreasing amount of superoxide generation.



Chapter 6

The influence of chemical composition and redox activity of nanomaterials on in vitro inflammasome activation and dendritic cell maturation

Susan Dekkers¹, Jolanda P. Vermeulen¹, Jasper G.D. Wigger¹,
Geert van der Horst¹, Rory Verhagen¹, Jia Ning¹, Isabella Römer²,
Wim H. de Jong¹, Flemming R. Cassee^{1,3}, Rob J. Vandebrriel¹

¹ National Institute for Public Health and the Environment (RIVM), Bilthoven, The Netherlands,

² School of Geography, Earth and Environmental Sciences, University of Birmingham, Birmingham, United Kingdom,

³ Institute for Risk Assessment Sciences, Utrecht University, The Netherlands

Abstract

There is limited understanding on how physicochemical properties of nanoparticles (NPs) may influence their ability to enhance the induction of allergic responses. One of the proposed mechanisms of toxicity is the redox activity of the NPs. However, in our recent *in vivo* study on adjuvant properties of various NPs no relation was observed between the acellular redox activity of the NPs and the ability to enhance allergic airway sensitisation. Here we study the same Zr-doped CeO_2 and Fe-doped Co_3O_4 NPs in two different *in vitro* assays, inflammasome activation in macrophages and maturation of dendritic cells (DCs), to investigate whether the differences between the type of immune responses observed *in vivo* can be predicted using these *in vitro* assays. CeO_2 NPs (doped and undoped) but not Co_3O_4 NPs (doped and undoped) induced inflammasome activation. Undoped Co_3O_4 NPs increased interleukine-12p40 (IL-12p40) production by DCs, while CeO_2 NPs (doped and undoped) did not. Doping effects of Co_3O_4 NPs were mixed. The results of these *in vitro* assays indicate that the type of immune response of the NPs is primarily related to chemical composition and not to size or acellular redox activity, similar to our previous results in the *in vivo* study. Furthermore, a pronounced increase in IL-12p40 in DCs *in vitro* seemed to be indicative for lymphoid accumulation in lung tissue *in vivo*. However, additional studies with NPs with different chemical compositions and *in vitro* assays covering other mechanisms are needed to more accurately predict the adjuvant activity of NPs *in vivo*.

Introduction

Metal oxide nanoparticles (NPs) have been shown to be able to act as adjuvants ^[1-3]. In vaccines, this property is further investigated and can be beneficial ^[1]. However, the adjuvant properties of NPs may also have negative health effects, for example in the development of allergic airway diseases like asthma.

There is limited understanding on the physicochemical properties of NPs that influence their adjuvant properties ^[2]. From the use of NPs in vaccines, we know that NPs can induce adjuvant activities by enhancing antigen processing or by inducing and amplifying protective immunity, for example by inflammasome activation ^[4]. Increases in the maturation of dendritic cells (DCs) and proliferation and differentiation of T-cells have been observed after *in vitro* exposure to NPs and after *in vivo* co-exposure of an allergen and NPs during the sensitisation phase in mouse models for airway allergy ^[2]. Molecular interactions that drive these cellular responses have been suggested to involve increases in reactive oxygen species (ROS) caused by NPs with an oxidative surface chemistry, inflammasome activation, cellular injury and the induction of DC stimulating cytokines and chemokines by epithelial cells (either direct or via oxidative stress) ^[2].

Physicochemical properties of metal and metal oxide NPs that have been postulated to drive these molecular interactions are amongst others a large surface area ^[5,6], reactive surface chemistry (e.g. through Haber-Weiss and Fenton reaction mechanisms) ^[7], a conduction band energy (Ec) level that overlaps with the cellular redox potential ^[8] and a fibre- or urchin-like shape ^[9,10].

Results of a recent study on adjuvant properties of various NPs in a mouse model of airway hypersensitivity indicated that chemical composition of NPs influences the type of immune response, but no relation was found between the acellular redox activity of the NPs and their adjuvant properties ^[11]. To investigate the influence of chemical composition and redox activity, Zr-doped CeO₂ NPs and Fe-doped Co₃O₄ NPs were selected, as the ability to induce oxygen radicals was expected to be larger for Co₃O₄ compared to CeO₂ NPs based on their Ec levels, while Zr- and Fe- doping was expected to reduce the redox activity of CeO₂ and Co₃O₄ NPs, respectively ^[11]. Here we investigate the same NPs in two different *in vitro* assays, to study whether the differences between the type of immune responses observed after exposure to CeO₂ and Co₃O₄ NPs *in vivo* can be predicted using these *in vitro* assays. These two *in vitro* assays are inflammasome activation in macrophages and maturation of dendritic cells, as these mechanisms are known to play an important role in NP-enhanced induction of allergic airway responses ^[2,12]. Inflammasome activation has been associated with interleukine-1 β (IL-1 β) induced Th17 responses, IL-18 induced Th1 immune responses, and neutrophilic inflammation *in vivo* ^[13]. Inflammasome activation, IL-1 β and IL-

18 have also been associated with Th2 immune responses, but these pathways are less well established [14-18]. DC maturation *in vitro* has been associated with T- and B-cell proliferation *in vivo*. Depending on the chemical composition, surface chemistry, shape and dose, NPs may promote DCs' capability to induce an IL-12 induced Th1 response, an IL-4 induced Th2 response and/or an IL-6 induced Th17 response [12,19]. For inflammasome activation, phorbol 12-myristate 13-acetate (PMA) differentiated THP-1 macrophages were used as this well-studied, easy to handle cell type is a robust and reproducible model to investigate inflammasome activation [20]. Furthermore, NLRP3- and ASC-deficient THP-1 macrophages are commercially available, enabling a reliable way to control for the involvement of the NLRP3 inflammasome in the responses obtained [21,22]. For dendritic cell maturation, differentiated monocytes isolated from human peripheral blood mononuclear cells (PBMCs) were used as this *in vitro* model is generally accepted to measure effects on DC maturation and has been suggested as a promising *in vitro* screen predictive for adjuvant activity of NPs *in vivo* [3].

Our hypothesis is that the influence of chemical composition and doping of NPs on the type of immune response underlying the adjuvant activity of NPs *in vivo* can be predicted using *in vitro* inflammasome activation and DC maturation assays.

Materials and Methods

2.1 NP production and characterization

All NPs were produced using supercritical water hydrothermal synthesis [23,24]. The production and characterization of the NPs has been described in our previous publication [11]. The main characteristics are summarised in Table 1. Zr-doping of the CeO₂ NPs did not increase the primary or gravimetric particle size, but did increase the hydrodynamic size in water as measured with Dynamic Light Scattering (DLS). Fe-doping of the Co₃O₄ NPs reduced the primary particle size and increased the gravimetric size for the Co₃O₄ NPs, except for the Co₃O₄ (75% Fe₂O₃) NPs. Fe-doping with Fe₃O₄ as a precursor increased the hydrodynamic particle size of the Co₃O₄ (25% and 75% Fe₃O₄) NPs, however, this increase was larger with 25%, than with 75% Fe-doping (see Table 1). Electron Paramagnetic Resonance (EPR) analysis using tempone-H demonstrated an increased capacity of Co₃O₄ (25% Fe₃O₄) NPs to generate reactive superoxide free radicals compared to Co₃O₄ (0% and 75% Fe₃O₄) NPs. Increasing amounts of Fe-doping using Fe₃O₄ led to a significant decrease in scavenging capacity of Co₃O₄ NPs. Co₃O₄ (0%, 25% and 75% Fe₂O₃) NPs had a similar ROS generation and scavenging capacity (Table 1).

Table 1: Primary, gravimetric and hydrodynamic particle size of the NPs in water and cell culture medium and the ROS generation and scavenging capacity of the NPs in a cell free system (modified from Dekkers *et al.*, 2019^(1,11)).

Measured with	STEM		Disc Centrifuge		DLS		DLS		Hydrodynamic particle size in water (nm)		Hydrodynamic particle size in cell culture medium (nm)		Superoxide generation (arbitrary units)*		ROS scavenging (% reduction of the signal of CuSO ₄ and NPs compared to CuSO ₄ alone)**	
	Average ± SD	Peak	Z-average ± SD	PDI average ± SD	Z-average ± SD	PDI average ± SD	Z-average ± SD	PDI average ± SD	Z-average ± SD	PDI average ± SD	Z-average ± SD	PDI average ± SD	Average ± SD	EPR	Average ± SD (%)	EPR
CeO ₂ (0% Zr)	4.7 ± 1.4	39	172 ± 1.7	0.27 ± 0.01	288 ± 4.8	0.26 ± 0.09	288 ± 4.8	0.26 ± 0.09	10622 ± 9058	46.1 ± 26.2						
CeO ₂ (27% Zr)	4.6 ± 1.4	40	298 ± 4.0	0.47 ± 0.01	176 ± 4.0	0.32 ± 0.02	176 ± 4.0	0.32 ± 0.02	5138 ± 2656	43.6 ± 21.1						
CeO ₂ (78% Zr)	4.7 ± 1.4	41	358 ± 6.4	0.49 ± 0.03	415 ± 27.6	0.70 ± 0.10	415 ± 27.6	0.70 ± 0.10	25672 ± 11553	55.6 ± 23.0						
Co ₃ O ₄ (0% Fe ₂ O ₃)	17.5 ± 15	42	nd	nd	176 ± 2.9	0.26 ± 0.01	176 ± 2.9	0.26 ± 0.01	5723 ± 3094	47.0 ± 4.0						
Co ₃ O ₄ (25% Fe ₂ O ₃)	10.6 ± 3.6	62	nd	nd	303 ± 6.7	0.32 ± 0.03	303 ± 6.7	0.32 ± 0.03	5848 ± 1518	48.1 ± 3.5						
Co ₃ O ₄ (75% Fe ₂ O ₃)	8.6 ± 1.7	39	nd	nd	375 ± 6.5	0.57 ± 0.05	375 ± 6.5	0.57 ± 0.05	5204 ± 838	44.4 ± 2.5						
Co ₃ O ₄ (0% Fe ₃ O ₄)	18.7 ± 11	44	117 ± 1.6	0.24 ± 0.00	160 ± 1.3	0.22 ± 0.00	160 ± 1.3	0.22 ± 0.00	8507 ± 1215	40.5 ± 5.3						
Co ₃ O ₄ (25% Fe ₃ O ₄)	13.0 ± 5.2	61	1120 ± 89	0.24 ± 0.11	828 ± 3.8	0.29 ± 0.03	828 ± 3.8	0.29 ± 0.03	14520 ± 907	31.7 ± 5.1						
Co ₃ O ₄ (75% Fe ₃ O ₄)	10.2 ± 6.2	69	547 ± 17	0.23 ± 0.02	1165 ± 66	0.37 ± 0.08	1165 ± 66	0.37 ± 0.08	9773 ± 583	13.2 ± 3.5						

* Superoxide generation in a cell-free system using Tempone-H spin trap, ** ROS scavenging in a cell-free system using a 5,5-dimethyl-pyrroline N-oxide (DMPO) spin trap in combination with H₂O₂; nd: not determined.

The Scanning Transmission Electron Microscope (STEM) images show differences in the morphology of undoped CeO_2 NPs in water (a) and cell culture medium (b) and between the two different batches of undoped Co_3O_4 NPs in water (c and d) (see Figure 1).

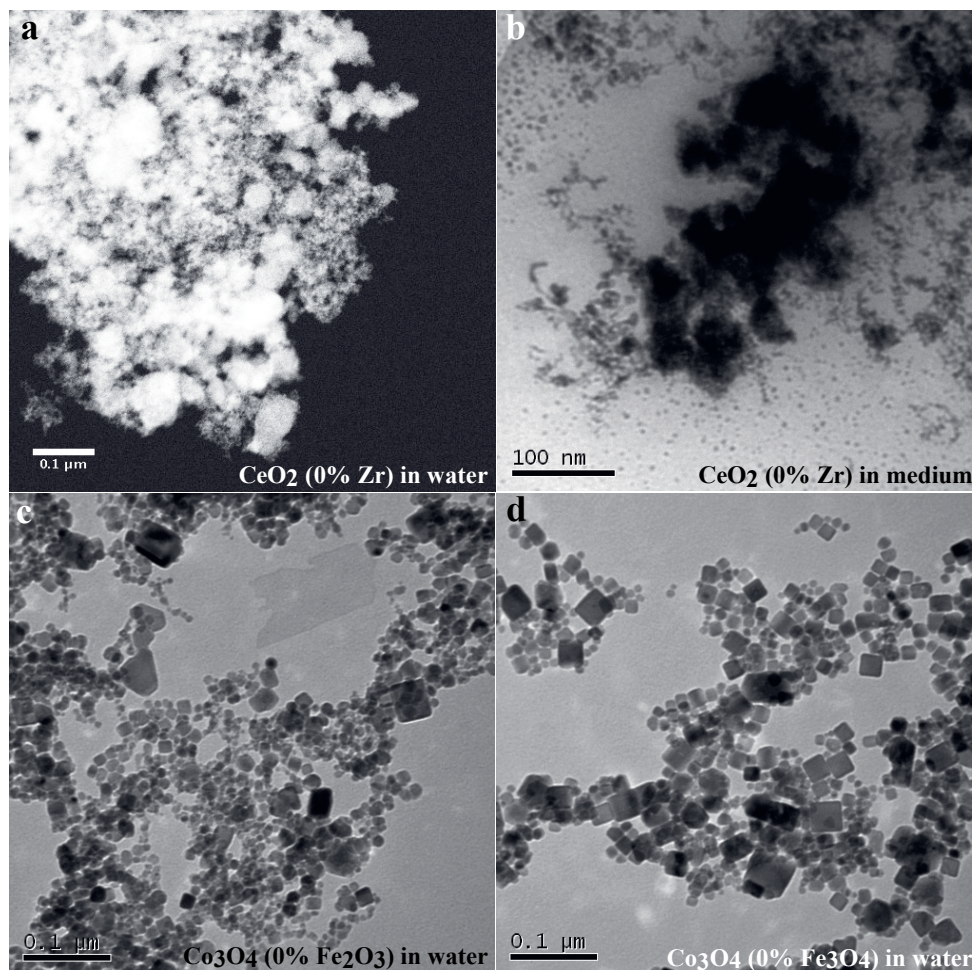


Figure 1: TEM images of undoped CeO_2 NPs in water (a) and undoped CeO_2 NPs in cell culture medium (b) and the two different batches of undoped Co_3O_4 NPs in water (c and d).

All NPs were tested for endotoxin contamination using either a Limulus Amoebocyte Lysate Assay (chromogenic kinetic LAL assay) or Ultra High Performance Liquid Chromatography coupled with Mass Spectrometry (UHPLC-MS/MS) determination [25]. Endotoxin levels were below the detection limit of 0.3 Endotoxin Units/mL of the UHPLC-MS/MS method for most NPs, except for the Co_3O_4 (75% Fe_3O_4) and Co_3O_4 (25% Fe_3O_4) NPs for which the endotoxin levels were 0.4 EU/mL sample (of dispersions with a concentration of 128 μg NPs/mL). This was below the recommended endotoxin limits for preclinical research in animal models (5

IU/kg bw/day or 36 IU/mL for mice with a body weight of 30 g and a daily dose of 100 µL and exposure limits for intravenous administration of medicinal products (5 IU/kg bw/h) [26].

2.2 *In vitro* deposition

In vitro deposition on cells was determined using part 2 and 3 of the protocol described in DeLoid *et al.*, 2017 [27]. The first part of the protocol, the preparation of the NP dispersions was not needed, since all NPs were already produced in dispersion. To re-disperse any potential agglomerates, the NP dispersions were vortexed for 10 seconds and sonicated for 5 minutes in an ultrasonic bath (Branson CPX2800, 40 KHz, 100W) before dilution in cell culture media to a concentration of 128 µg/mL. The determination of the volume weighted size distribution and effective density of the NPs in cell culture medium was determined according to part 2 of the protocol, using DLS and the volumetric centrifugation method. According to part 3 of the protocol, the volume weighted size distribution in cell culture medium, the raw density and the effective density were used to estimate the percentage of the NPs deposited on the bottom of the cell culture well with the distorted grid (DG) model of Harvard University [28]. Other experimental conditions entered as input parameters in the DG model were: the use of a 96 wells plate, 200 µl cell culture medium per well, a temperature of 37°C, a viscosity of 0.00074 Pa s [29], a density of 1.008 g/cm³ of the cell culture medium, a concentration 128 µg NPs/mL cell culture medium and a duration of 48 h for the experiment.

2.3 Cell culture and treatment

Wild type as well as NLRP3- or ASC-deficient THP-1 macrophages were cultured at 37°C and 5% CO₂ in RPMI 1640 (Gibco) with 25mM HEPES and 2mM L-Glutamine, 100 U/mL Penicillin, 100 µg/mL Streptomycin (Pen/Strep; Gibco) and 10% heat inactivated Foetal Calf Serum (FCS; Gibco), in a T75 flask in 15 mL. The THP-1 cell line was a kind gift from Samantha Kloet at Wageningen University. The NLRP3- and ASC-deficient THP-1 macrophages were obtained from InvivoGen. The THP-1 macrophages were cultured twice a week during which the cell concentration was adjusted to approximately 2×10⁵ cells/mL. Hygromycin B (HygroGold, InvivoGen) was added to the cell culture medium of the NLRP3- or ASC-deficient THP-1 macrophages as a selective antibiotic at a concentration 200 µg/mL.

The THP-1 macrophages (5.0 × 10⁵ cells/mL) were differentiated with 100 ng/mL phorbol 12-myristate 13-acetate (PMA; Sigma) in 200 µl cell suspension in a 96-wells cell culture plate (sterile, F-bottom, with lid, CellStar) (Greiner bio-one) in an incubator at 37°C with 5 % CO₂ in air. After 3 h, the medium of the cells was changed with 100 µl fresh medium without PMA and the cells were incubated for 20-24 h before exposure to NPs. After this resting period, 100 µl fresh medium with different NP concentrations was added to each of the wells to obtain a range of concentrations from 0 to 128 µg/mL of NPs. Following this, the

cells were incubated for another 48 h before measuring the cell viability (with WST-1) and collecting the supernatant for measuring IL-1 β levels.

Dendritic cells (DC) were obtained and cultured as previously described [3]. Briefly, they were derived from buffy coats obtained from Sanquin (Amsterdam, the Netherlands). Peripheral blood mononuclear cells were isolated from buffy coats by density centrifugation (Lymphoprep; Axis Shield, Oslo, Norway). The cells were washed, harvested, and re-suspended in RPMI-1640 (Gibco, Grand Island, NY, USA) supplemented with 2% heat-inactivated human serum (Harlan, Boxmeer, the Netherlands), 100 μ g/mL streptomycin, 100 IU/mL penicillin, and 0.3 mg/mL L-glutamine. They were seeded in tissue culture flasks (Corning, Amsterdam, the Netherlands) and were incubated for 1 h. After this incubation non-attached cells were removed by rinsing with warm (37°C) PBS and medium was added (RPMI-1640 supplemented with 10% heat-inactivated Foetal Calf Serum (“FCS”; Hyclone; GE Healthcare, Logan, UT, USA), streptomycin, penicillin, L-glutamine, 500 U/mL GM-CSF and 250 U/mL IL-4). At day 3, half the volume of the medium was replaced with fresh medium with fresh cytokines. At day 6, the immature DC were harvested by rinsing with cold PBS and adding cold PBS to the flask, placing the flask in the refrigerator for one hour and tapping the flask to detach the cells. Hundred μ L of the freshly prepared cell suspension (6×10^5 cells/mL) was then added to each well of a 96-wells plate and placed in an incubator at 37°C in a humidified atmosphere containing 5% CO₂ in air awaiting NP exposure. The DC were exposed by adding 100 μ L medium with different NP concentrations to each of the wells to obtain a range of concentrations from 0 to 128 μ g/mL of NPs. Following this, the cells were incubated for 48 h before measuring the cell viability (using the CFDA assay) and collecting the supernatant for measuring IL-12p40 levels.

2.4 Measuring cell viability

The cell viability of wild type and NLRP3- or ASC-deficient THP-1 macrophages was measured using the WST-1 conversion assay. After 48 hours exposure to NPs, 20 μ L of WST-1 reagent (Roche Diagnostics GmbH) was added to each well and incubated at 37°C for 1, 2 and 3 h before measurement. The absorbance (440 nm) was measured with a Spectramax M2 spectrophotometer.

The cell viability of DCs was measured using the CFDA assay. After 48 h 5-Carboxyfluorescein Diacetate, Acetoxymethyl Ester (5AM-CFDA) (Fisher Scientific) was added to each well (final concentration 4 μ M). The DCs were incubated at 37°C and fluorescence (excitation 491 nm, emission 530 nm) was measured after 1, 2 and 3 h with a Spectramax M2 spectrophotometer.

Interference of the NPs with the read out systems of the WST-1 and 5AM-CFDA assays was evaluated by including additional wells with only NPs in cell culture medium (without cells) in these assays. Samples were measured in triplicate, and in duplicate for NP interference

in wells without cells. To correct for any interference, the signal of the wells measuring the NP interference was subtracted from the signal of the wells with NPs and cells. If the interference was larger than 20% of the signal, the interference was considered too large for a reliable measurement and the data was not used for further analyses. After subtraction of the interference, the signal of the different dose levels was normalised to the signal of the control wells (without NP, but with cells).

2.5 Detection of cytokines

Supernatants of exposed cells were collected after centrifuging at 4°C for 5 min at a speed of 1200 RPM, and stored at -80°C until analysis. THP-1 cell supernatant, harvested after 48 h exposure to NPs, was tested for human IL-1 β using the Human IL-1 β (2nd Gen) Ready-SET-Go! ELISA kit (eBioscience) according to the manufacturer's instructions. The samples were diluted 2 to 25 times before loading on the IL-1 β ELISA plate.

DC supernatant, harvested after 48 h exposure to NPs, was tested for human IL-12p40 using the Human IL-12p40 ELISA set (BD OptEIA), according to the manufacturer's instructions. The samples were not diluted.

2.6 Statistical analysis and dose response modelling

The cell viability and IL-1 β production data of at least three THP-1 experiments were combined, plotted and used for non-linear regression analyses (curve-fitting) for each NP in Graph Pad Prism (version 7.04). For the DC experiments, the cell viability and IL-12p40 production data of each experiment (each individual donor) was plotted and used for non-linear regression analyses (curve-fitting) for each NP.

For further statistical analysis and dose response modelling with PROAST software ^[30] (www.rivm.nl/proast) (version 63.5), the same data was used as for the analysis in Graph Pad Prism. Statistical testing was performed by fitting the best dose response curve and determining the critical effect dose (CED) and the 90% confidence interval. To determine the CED, a critical effect size (CES) of 20% for cell viability and 5% for cytokine levels (IL-1 β and IL-12p40 concentrations) was used. PROAST uses the Hill and Exponential models to predict the "best fit" dose response curve by comparing the log likelihood value of each selected model with the full model. The log likelihood value relates to the goodness of fit for the dose response curve: the higher the value, the better the model. A conservative 90% confidence interval was determined as the range of the lowest 5% level and highest 95% level of the 90% confidence intervals of the best fitted Hill and the best fitted Exponential model. Differences between the CEDs of the different NPs are statistically significantly different if the 95% upper and lower confidence limits of the CEDs from the NPs do not overlap.

Results

3.1 *In vitro* deposition

Zr-doping of the CeO₂ NPs decreased the volume weighted hydrodynamic size in cell culture medium, resulting in a slight decrease in the deposited dose of CeO₂ (27% Zr) NPs after 48 h. A more pronounced influence was observed for both types of Fe-doping. Both types of Fe-doping doubled or tripled the volume weighted hydrodynamic size of the Co₃O₄ NPs in cell culture medium, resulting in a two- to three-fold increase in the estimated deposited dose after 48 h (see Table 2).

Table 2: Hydrodynamic particle size and estimated deposition after 48 h as calculated with the distorted grid model.

	Hydrodynamic particle size in cell culture medium (nm) by DLS			Raw density (g/cm ³)	Effective density (g/cm ³)	Deposited dose after 48 h*	
	Z-average ± SD (nm)	PDI ± SD	Volume-weighted average ± SD (nm)			(%)	(µg/cm ²)
CeO ₂ (0% Zr)	288 ± 4.8	0.26 ± 0.09	731 ± 185	7.215	1.601	69	54
CeO ₂ (27% Zr)	176 ± 4.0	0.31 ± 0.02	484 ± 82	6.801	1.754	51	39
CeO ₂ (78% Zr)	415 ± 27.6	0.70 ± 0.10	558 ± 47	6.018	2.129	68	53
Co ₃ O ₄ (0% Fe ₂ O ₃)	176 ± 2.9	0.26 ± 0.01	522 ± 114	6.110	1.634	51	39
Co ₃ O ₄ (25% Fe ₂ O ₃)	303 ± 6.7	0.32 ± 0.03	1020 ± 267	5.893	1.739	86	67
Co ₃ O ₄ (75% Fe ₂ O ₃)	375 ± 6.5	0.57 ± 0.05	1316 ± 106	5.458	1.327	90	70
Co ₃ O ₄ (0% Fe ₃ O ₄)	160 ± 1.3	0.22 ± 0.00	381 ± 44	6.110	1.564	29	22
Co ₃ O ₄ (25% Fe ₃ O ₄)	828 ± 3.8	0.29 ± 0.03	1372 ± 45	5.833	1.353	94	73
Co ₃ O ₄ (75% Fe ₃ O ₄)	1165 ± 66	0.37 ± 0.08	1465 ± 57	5.278	1.626	99	76

* Deposited dose is estimated for the situation in which 200 µl of the highest concentration (128 µg/mL or 80 µg/cm²) per well is administered.

3.2 *In vitro* cell viability and cytokine production by THP-1 macrophages

After exposure of THP-1 macrophages to the various CeO₂ NPs (Zr-doped and undoped) a dose-related increase in IL-1β production was already observed at non-cytotoxic dose levels. No increase in IL-1β induction was observed and no dose-response curve could be fitted to the data of any of the Co₃O₄ NPs (Fe-doped or undoped) (Figure 2). Only very limited to no IL-1β production was observed in the NLRP3- or ASC-deficient THP-1 macrophages after exposure to any of the NPs. In addition, no or only very low IL-1β production was seen in NLRP3- and ASC-deficient THP-1 macrophages without NP exposure or with exposure to the positive control SiO₂ NPs (Figure 3).

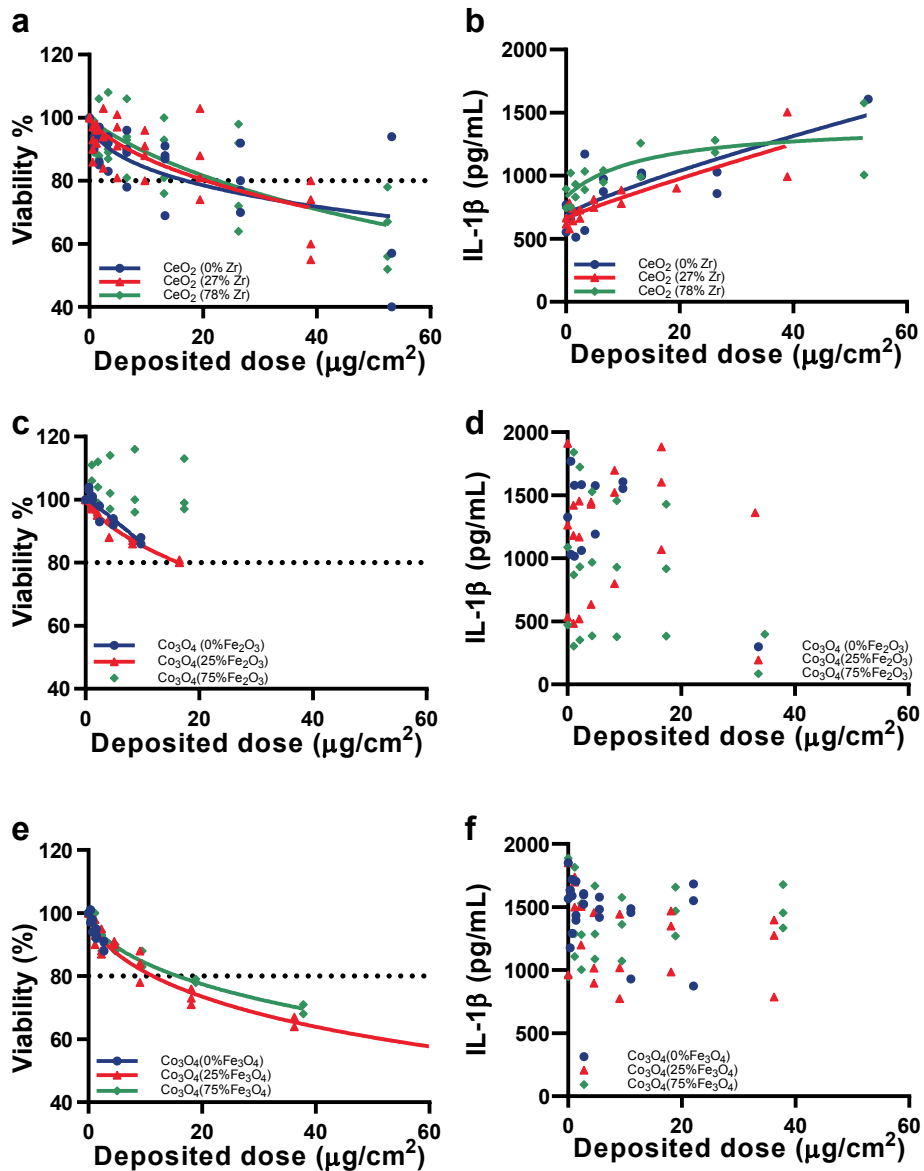


Figure 2: Cell viability and IL-1 β production in THP-1 macrophages exposed to Zr-doped CeO₂ NPs (a and b), Fe-doped Co₃O₄ NPs (using Fe₂O₃) (c and d) and Fe-doped Co₃O₄ NPs (using Fe₃O₄) (e and f) for 48 h (n=3). The dose-response curves show a clear increase in IL-1 β production for all CeO₂ NPs already at non-cytotoxic dose levels. No increase in IL-1 β production was observed after exposure to any of the Fe-doped Co₃O₄ NPs and no dose-response curves could be fitted to these data.

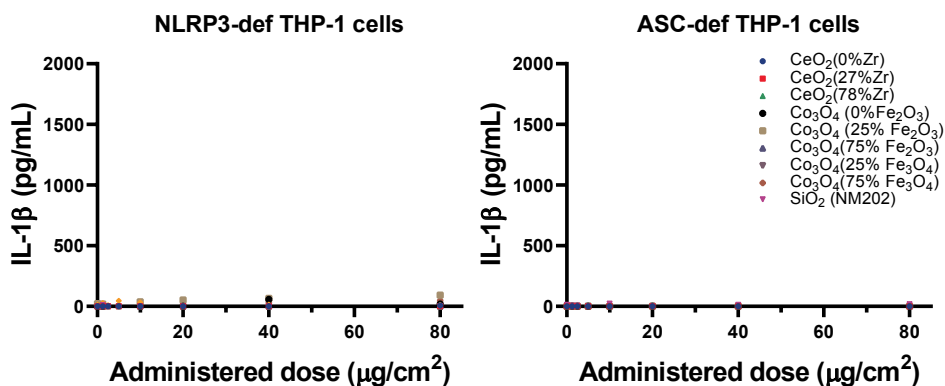


Figure 3: IL-1 β production in NLRP3- and ASC-deficient THP-1 macrophages exposed to Zr-doped CeO₂ NPs, Fe-doped Co₃O₄ NPs (using Fe₂O₃ or Fe₃O₄) and SiO₂ NPs (NM202) for 48 h (n=1). No or only very low IL-1 β concentrations were measured.

Dose response modelling with PROAST confirmed that IL-1 β production was already observed at non-cytotoxic dose levels, as the CED_{5%} of IL-1 β production after exposure to CeO₂ NPs (\approx 0.01-3.2 $\mu\text{g}/\text{cm}^2$) was lower than the CED_{20%} of cell viability (\approx 14-28 $\mu\text{g}/\text{cm}^2$). PROAST analysis could not reliably fit a dose response curve to the IL-1 β production data of THP-1 macrophages exposed to Co₃O₄ NPs, confirming that there was no increase in IL-1 β production for Co₃O₄ (0%, 25% and 75% Fe₂O₃) or Co₃O₄ (0%, 25% and 75% Fe₃O₄).

3.3 In vitro cell viability and cytokine production by DCs

A clear increase in IL-12p40 production was observed after exposure of DCs from all blood donors to Co₃O₄ (0% Fe₂O₃) (n=3) and Co₃O₄ (25% Fe₂O₃) (n=4) already at non-cytotoxic dose levels. DCs from all donors showed a clear to moderate increase in IL-12p40 production after exposure to Co₃O₄ (0% Fe₃O₄) (n=4) and Co₃O₄ (75% Fe₃O₄) (n=4). There was no increase in IL-12p40 production after exposure of DCs of any of the donors to undoped and Zr-doped CeO₂ NPs (n=3), Co₃O₄ (75% Fe₂O₃) (n=4) and Co₃O₄ (25% Fe₃O₄) (n=3). A dose response curve for both cell viability and IL-12p40 production after exposure of DCs from one of the donors to each of the NPs is shown in Figure 4.

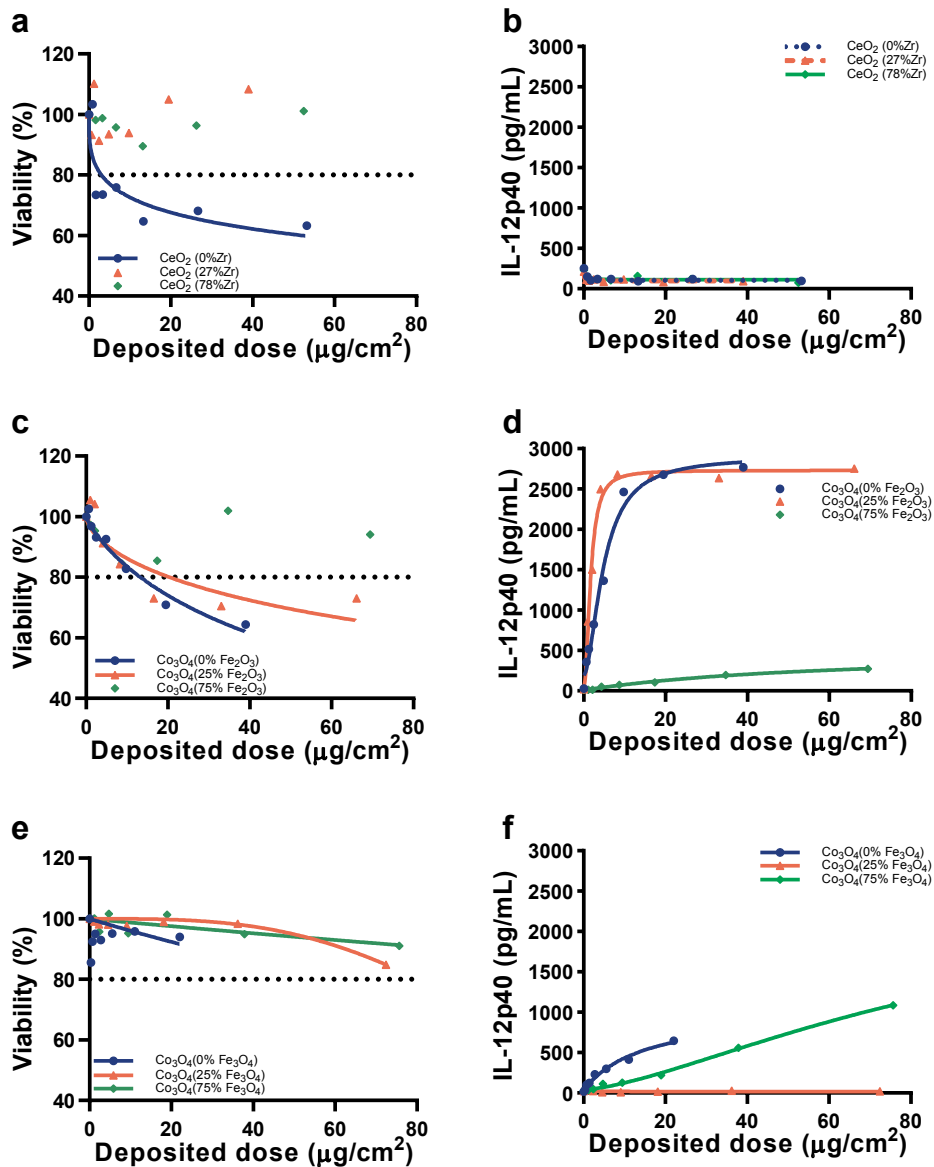


Figure 4: Representative dose-response curves of cell viability and IL-12p40 production in DC from one of the donors exposed to a) Zr-doped CeO_2 NPs, b) Fe-doped Co_3O_4 NPs (using Fe_2O_3) and c) Fe-doped Co_3O_4 NPs (using Fe_3O_4) for 48 h ($n=1$). There was no increase in IL-12p40 production after exposure to undoped and Zr-doped CeO_2 NPs, Co_3O_4 (75% Fe_2O_3) and Co_3O_4 (25% Co_3O_4), a clear increase in IL-12p40 production for Co_3O_4 (0% Fe_2O_3) and Co_3O_4 (25% Fe_2O_3) and a moderate increase in IL-12p40 production for Co_3O_4 (0% Fe_3O_4) and Co_3O_4 (75% Fe_3O_4) at non-cytotoxic dose levels.

PROAST analysis confirmed that the increases in IL-12p40 production were already observed at non-cytotoxic dose levels. For Co_3O_4 (0% Fe_2O_3) and Co_3O_4 (25% Fe_2O_3) the $\text{CED}_{5\%}$ of IL-12p40 production was lower ($\approx 0.001\text{-}0.03 \mu\text{g}/\text{cm}^2$) than the $\text{CED}_{20\%}$ of cell viability ($\approx 5\text{-}15 \mu\text{g}/\text{cm}^2$). For Co_3O_4 (0% Fe_3O_4) and Co_3O_4 (75% Fe_3O_4) the $\text{CED}_{5\%}$ of IL-12p40 production was lower ($\approx 0\text{-}0.5 \mu\text{g}/\text{cm}^2$) than the $\text{CED}_{20\%}$ of cell viability ($\approx 16\text{-}\infty \mu\text{g}/\text{cm}^2$). No increase in IL-12p40 production was observed for Co_3O_4 (75% Fe_2O_3), Co_3O_4 (25% Fe_3O_4) and the undoped and Zr-doped CeO_2 NPs.

Discussion

4.1 NP characterization

No consistent increase or decrease in primary or gravimetric particle size was observed due to the Zr-doping of the CeO_2 or Fe-doping of the Co_3O_4 NPs. However, with a few exceptions, doping of the CeO_2 and Co_3O_4 NPs did increase the hydrodynamic particle size in water and in cell culture medium (Table 1). Both the DLS and STEM analyses indicate that the agglomerated particle size of the same NPs is generally larger in cell culture medium compared to water (Table 1 and Figure 1). However, the polydispersity index of some of the DLS measurements in cell culture medium was larger than 0.5, indicating a large variability in the diameter of the particles within the dispersion (Table 2). In addition, the two different batches of the non-doped Co_3O_4 NPs showed differences in the primary and hydrodynamic particle size and shape (Table 1, Figure 1 and [24]). These observed variations and differences in the primary, gravimetric and hydrodynamic particle size and shape of the NPs may affect their ability to generate ROS, their deposition in the *in vitro* assays and subsequent results in the *in vitro* assays (cytotoxicity and cytokine induction).

Based on our data (Table 1), the influence of doping or particle size on the ability of the NPs to either generate or scavenge ROS is limited. Most NPs showed neither a decrease nor an increase in their ability to either generate or scavenge ROS with increasing amounts of doping or with increasing hydrodynamic particle diameter in water. Only Fe-doping using Fe_3O_4 led to a significant decrease in the scavenging capacity of Co_3O_4 NPs with increasing amounts of doping and increasing hydrodynamic size in cell culture medium. This is in accordance with the ROS generating capacity of Fe_3O_4 NPs in bacterial cells observed by Al-Shabib *et al.* [31]. In our previous paper studying the same NPs *in vivo*, we proposed that differences in particle size and aggregation may counterbalance any doping-related differences in free radical generation or scavenging [11]. However, to demonstrate this, more data on the ability to generate or scavenge ROS of the same NPs with varying particle and aggregated sizes are needed.

4.2 *In vitro* deposition

The amount of doping influenced the estimated deposition of the NPs in the *in vitro* assays for the Fe-doped Co_3O_4 , but not the Zr-doped CeO_2 NPs (Table 2). Since the estimated deposition in the *in vitro* assays is mainly determined by the hydrodynamic particle size in cell culture medium, an increase in the hydrodynamic particle size resulted in an increase in the estimated deposition in the *in vitro* assays for all NPs, especially when expressed as volume weighted averages (Table 2). To take the differences in deposition into account, the dose response curves were plotted using the deposited (i.e. biological effective) dose instead of the administered dose. The use of the deposited dose led to slightly different dose-response curves compared to the use of the administered concentration of the NPs in the cell culture medium (data not shown). In our study we preferred the use of the deposited dose, since the dose that reaches the cells and not the concentration of NPs in the cell culture medium drives the biological effect [28].

4.3 Inflammasome activation

The dose response curves of IL-1 β production of THP-1 macrophages exposed to 0%, 27% and 78% Zr doped CeO_2 NPs, indicated that inflammasome activation occurred at lower dose levels after exposure to CeO_2 (78% Zr) as compared to CeO_2 (0% Zr) or CeO_2 (27% Zr). A possible explanation for this difference might be the different capacity of the NPs to generate ROS, which is larger for CeO_2 (78% Zr) compared to CeO_2 (0% Zr) or CeO_2 (27% Zr) (Table 1). This concurs with the study by Zhou *et al.* which showed that ROS is an important mediator of inflammasome activation [32]. This is however not supported by their difference in scavenging capacity which also seemed higher for CeO_2 (78% Zr) compared to CeO_2 (0% Zr) or CeO_2 (27% Zr) (Table 1). This may suggest that ROS generation is more important for inflammasome activation than scavenging capacity. No increase in IL-1 β production was observed after exposure to any doped or undoped Co_3O_4 NPs, indicating that exposure of THP-1 macrophages to any of the Co_3O_4 NPs does not result in inflammasome activation. No increase in IL-1 β production was observed in the ASC- and NLRP3-deficient cell lines after exposure to CeO_2 (0%, 27% and 78% Zr) (Figure 3) indicating that the NLRP3 inflammasome is responsible for a large part of the IL-1 β production. The relatively high IL-1 β production observed in non-exposed wild type THP-1 macrophages in the absence of NPs exposure was unexpected, however comparable IL-1 β background levels were observed in a study by a different group, also using THP-1 macrophages [33]. Differences in background levels of IL-1 β between different studies can be due to differences in cell stimulation, cell numbers, incubation times, passage number of the cells, etc. The observed variability in background levels of IL-1 β within this study are probably due to differences in passage number of the cells. No major differences in the cell viability of THP-1 macrophages exposed to doped and undoped CeO_2 and Co_3O_4 NPs were observed (Figure 2).

In contrast to our *in vitro* experiments in THP-1 macrophages, most other *in vitro* studies showed no inflammasome activation after exposure of macrophages to CeO₂ NPs^[9,34-36]. Only one other *in vitro* study with THP-1 macrophages found increased IL-1 β production after CeO₂ NP exposure^[37]. Several other studies have demonstrated CeO₂ NP to be the only rare earth oxide which does not induce IL-1 β *in vitro*^[9,10]. The authors of these studies suggest that this might be due to the reduced dissolution of CeO₂ NPs under acidifying conditions such as in lysosomes, which prevents the release of rare earth ions that bind to phosphates leading to the formation of urchin-shaped structures, causing lysosomal membrane damage and subsequent NLRP3 inflammasome activation^[9,10]. Although no urchin-shaped structures were observed after exposure to CeO₂ NP *in vitro*, *in vivo* intravenous CeO₂ NP exposure has been shown to produce Ce-phosphate nanoneedles in the spleen, while intratracheal CeCl₃ exposure led to the formation of Ce-phosphate rod-shaped nanoneedles and spider-like structures in the lung^[38,39]. Differences in the experimental conditions between the different *in vitro* assays may have led to different dissolution rates of the CeO₂ NPs and subsequent IL-1 β production.

In vivo experiments investigating inflammasome activation after CeO₂ NPs exposure also show contradicting results. Sager *et al.*^[40] found increased IL-1 β levels in BALF of mice after pharyngeal aspiration of CeO₂ NPs, while Lin *et al.*^[9] did not. These differences might be explained by differences in particle characteristics, dissolution rate, dispersion state and dispersion medium. Sager *et al.*^[40] showed that the pre-exposure dispersion status of CeO₂ NPs is a factor that contributes to the post-exposure pulmonary response (cytotoxicity and IL-1 β induction in BALF) after pharyngeal aspiration in mice. Another possible explanation is a difference in the (anti-)oxidant properties of the different CeO₂ NPs. CeO₂ NPs can act as both a scavenger and an inducer of ROS, depending on its immediate environment. Generation of intracellular ROS is one of the most studied pathways by which NPs can induce NLRP3 inflammasome activation^[3,6,10]. Intracellular ROS may trigger inflammasome activation via lysosomal damage, cytochrome C production or thioredoxin oxidation^[6]. Since scavenging or oxidative properties of CeO₂ NPs are dependent on the pH of the immediate environment, differences in the experimental set up (e.g. use of different exposure medium, pH, etc.) could explain the differences in the ability of CeO₂ to induce inflammasome activation. However, also in this respect results from different studies are not consistent. Asati *et al.*^[41] found that while an acidic environment promoted the oxidative properties, a physiological environment promoted the anti-oxidant properties, whereas Sager *et al.*^[40] found the opposite relationship. In the ESR studies by Sager *et al.*, CeO₂ NPs were shown to scavenge radicals in an acidic environment (pH~ 4.5) but not in a physiological environment (pH 7.4). This was in line with their findings that CeO₂ NPs activated the NLRP3 inflammasome via lysosomal damage and cathepsin B release to a similar extent as NiO NPs did, but induced less IL-1 β and IL-18 compared to NiO NPs. In contrast to CeO₂ NPs, NiO NPs showed scavenging properties in a physiological, but not in an acidic environment^[40].

Our results are in line with those of Cho *et al.* [37] and Sager *et al.* [40] and suggest that the CeO₂ NPs that induced most ROS species in water, also induced a higher amount of IL-1β via inflammasome activation in THP-1 macrophages

For Co₃O₄ NPs, the results of our *in vitro* experiments in THP-1 macrophages are in agreement with other *in vitro* studies that also showed no inflammasome activation *in vitro* [9,42]. To our knowledge, no *in vivo* studies investigating inflammasome activation with Co₃O₄ NPs have been reported.

4.4 DC maturation

The dose response curves of cell viability of DC indicated that undoped CeO₂ NPs were more toxic compared to Zr-doped CeO₂ NPs. Undoped Co₃O₄ NPs were more toxic compared to Fe-doped Co₃O₄, irrespective of the type of doping (Fe₂O₃ or Fe₃O₄), or the percentage of doping. The dose response curves of IL-12p40 production indicated that DC maturation occurred after exposure to Co₃O₄ (0% Fe₂O₃), Co₃O₄ (25% Fe₂O₃), Co₃O₄ (0% Fe₃O₄) and Co₃O₄ (75% Fe₃O₄), but not after exposure to Co₃O₄ (75% Fe₂O₃), Co₃O₄ (25% Fe₃O₄) or any of the doped or undoped CeO₂ NPs.

An increased capacity to generate ROS or a decreased capacity to scavenge ROS is expected to enhance the ability of the NPs to induce cytotoxicity and to generate IL-12p40 in DCs. However, the observed differences in the dose response curves cannot be explained by the different capacity of the NPs to generate or scavenge ROS in water, except maybe for the dose response curves of cell viability after exposure to Co₃O₄ (0%, 25%, and 75% Fe₃O₄), which show a decrease in their capacity to scavenge ROS with increasing amounts of doping. A possible explanation why the results of this *in vitro* assay cannot be explained by the ability of the NPs to generate or scavenge ROS, might be that this ability to generate or scavenge ROS was measured in water and may be different under the conditions of the *in vitro* assay (in cell culture medium and in cells).

For CeO₂ NPs, the results of our *in vitro* experiments on DC maturation are in agreement with other *in vitro* studies that also showed an absence of DC maturation *in vitro* [43,44]. For Co₃O₄, one other *in vitro* study investigated DC maturation and in that study no DC maturation was observed [43]. To our knowledge, no *in vivo* studies investigating DC maturation by CeO₂ or Co₃O₄ NPs were reported.

4.5 Comparison of *in vitro* and *in vivo* results

To relate the dose levels from our *in vitro* studies to the dose levels from our *in vivo* study, we estimated the deposited dose in the pulmonary region of the lung in our *in vivo* study to be approximately 0.44 μg/cm². For this estimate, we assumed that the entire intranasally administered dose (of 200 μg/animal) deposited in the pulmonary region of the lung, which

was assumed approximately 450 cm² for mice weighing approximately 20 g. This dose is far below the estimated deposited doses of the highest dose levels in our *in vitro* studies (between 22 and 76 µg/cm², Table 2), but in the same range of the lowest dose levels (between 0.34 and 1.18 µg/cm²).

From both the *in vitro* and *in vivo* activities of the tested NPs (Table 3), it is apparent that the influence of doping on the immune responses is very limited, whereas the main chemical components (CeO₂ with Zr or Co₃O₄ with Fe) does influence the type of immune responses *in vitro* and *in vivo*. To determine whether the observed immune responses *in vivo* can be predicted using the results of the *in vitro* assays is, however, not straightforward for both CeO₂ or Co₃O₄ NPs based on the data from the current *in vitro* study.

Table 3: Comparison of *in vitro* and *in vivo* data.

	<i>In vitro</i> data		<i>In vivo</i> data ¹						
	IL-1β	IL-12p40	IgE	Eosinophils BALF	Eosinophils Lung	IL-4 and/or IL-5	Lymphocytes BALF	Lymphocytes Lung	ELS in Lung
CeO ₂ (0% Zr)	+	-	+	+	+	+	+/-	-	-
CeO ₂ (27% Zr)	+	-	+	+	+	+	+	-	-
CeO ₂ (78% Zr)	+	-	+/-	+	+	+	+	-	-
Co ₃ O ₄ (0% Fe ₂ O ₃)	-	+	+/-	-	+/-	-	+	+	+
Co ₃ O ₄ (25% Fe ₂ O ₃)	-	+	+	-	+/-	+/-	+	+	+
Co ₃ O ₄ (75% Fe ₂ O ₃)	-	-	+/-	-	+/-	+/-	+	+	+
Co ₃ O ₄ (0% Fe ₃ O ₄)	-	+/-	+/-	-	-	+/-	+	+	+
Co ₃ O ₄ (25% Fe ₃ O ₄)	-	-	+/-	-	+/-	+/-	+	+	+
Co ₃ O ₄ (75% Fe ₃ O ₄)	-	+/-	+/-	-	+/-	+/-	+	+	+

¹ Source: Dekkers et al., 2019 [13]. +: clear increase, +/-: moderate increase, -: no increase in the biomarker of effect.

Our *in vivo* study indicates that the adjuvant properties of CeO₂ NPs are primarily associated with a Th2 type immune response (IL-4, IL-5, IgE and eosinophils in BALF and lung) (Table 3, [11]). Linking this *in vivo* response to inflammasome activation by these NPs is not straightforward (Table 3). Inflammasome activation is directly involved in a Th17 type immune response via IL-1β induction and also has a function in Th1 cell development via IL-18 induction. Th17 responses induce the recruitment of neutrophils and macrophages to tissues, while Th1 responses enhance the killing efficacy of macrophages and the proliferation of cytotoxic T cells [13]. These Th17 and Th1 responses, do not match with the observed Th2 type responses observed in our *in vivo* study. However, data from aluminium adjuvants indicate that NLRP3

inflammasome activation may also enhance Th2 cell responses ^[15]. IL-1 β can enhance humoral immunity, while IL-18 has been shown to increase IgE antibody production ^[15]. Although inflammasome induced Th2 cell responses are not as well established as the Th17 and Th1 responses, they would better match with the immune responses observed *in vivo* (Table 3). The fact that CeO₂ NPs exposure of DC did not increase IL-12p40 production (Table 3) may be indicative for a lack of Th1 response, since IL-12p40 is associated with a Th1 type immune response that is related to cellular inflammation ^[12,19]. Taken together, the Th2 type immune responses observed *in vivo* cannot be readily predicted using the inflammasome activation and DC maturation assays.

The adjuvant activity of the Co₃O₄ NPs in our *in vivo* study was characterised by a less pronounced Th2 type immune response and an increase in lymphocytes in BALF and the development of ectopic lymphoid-like structures (ELS) in the lung tissue. ELS are tertiary lymphoid organs, characterized by well-organized T- and B-cell areas enmeshed with dendritic and stromal cells, usually localized within the perivascular or interstitial areas of the lung ^[45]. ELS formation is associated with lymphoid tissue inducer cells, and the induction of lymphotoxin- α , CXCL13, CCL19, and CCL21. However, these mediators are not mandatory for its formation ^[46]. Dendritic cells, however, have been identified as pivotal players required to form and sustain the presence of inducible bronchus-associated lymphoid tissue ^[46]. The observed increase in IL-12p40 production in DC exposed to Co₃O₄ NPs are therefore in line with these observed immune responses *in vivo*. IL-12 induction triggers the cellular immune system via the differentiation of naïve T cells into Th1 and cytotoxic T lymphocytes. In response to IL-12 signalling, Th1 cells induce IFN- γ , IL-2, lymphotoxin α , and TNF- β resulting in the recruitment of macrophages, neutrophils, NK cells, cytotoxic T cells and B cells ^[47]. Although no increase in IFN- γ concentrations was found in the BALF, the increase in IL-12p40 production by DC is consistent with the increased numbers of lymphocytes in BALF and lung tissue and the formation of ELS observed in our *in vivo* study. In our *in vitro* assay with DCs only IL-12p40 was measured as an indicator of DC maturation. Measuring other biomarkers in the DC assay, including surface markers and other cytokines, may provide further information to link the *in vitro* to the *in vivo* results. In a study using the same DC assay, IL-12p40 production was found to have a rather similar potential as CD83 and CD86 expression to discriminate between two crystal structures of TiO₂ NPs ^[3]. The lack of inflammasome activation by Co₃O₄ NPs exposure are not in line with the induction of ELS. IL-1 β is a known inducer of a Th17 immune response, including IL-17 production, which is known to induce ELS ^[48]. Taken together, although the increase in IL-12p40 may be indicative for the ELS observed *in vivo*, the observed immune responses *in vivo* cannot be readily predicted using the inflammasome activation and DC maturation assays.

Conclusions

The results from our *in vitro* studies and previously performed *in vivo* study indicate that the type of immune response of NPs in *in vitro* or *in vivo* models is not related to the percentage of doping, the size, or the acellular redox activity. The chemical composition seems to be more important in determining the type of response. CeO₂ NPs (doped and undoped) but not Co₃O₄ NPs (doped and undoped) induced inflammasome activation. The results from our *in vitro* studies may indicated some specific immune responses *in vivo*, such as the potential lymphoid accumulation, which is associated with a pronounced increase in IL-12p40 in DC *in vitro*. However, more studies with NPs with different chemical compositions are needed to investigate the predictivity of the *in vitro* DC maturation assay for lymphoid accumulation *in vivo*. Next to the inflammasome activation and DC maturation assay, additional *in vitro* assays covering other immune mechanisms that can be influenced by NP exposure are needed to more accurately predict the different types of immune responses underlying the adjuvant activity of NPs *in vivo*.

Acknowledgement

The authors would like to thank Daan Leseman of RIVM for his technical support.

Funding

This work was supported by the Seventh Framework Programme for research, technology development and demonstration of the European Union under Grant Agreement Number 310451 (NanoMILE) and the Netherlands Food and Consumer Product Safety Authority (NVWA, project number V090016).

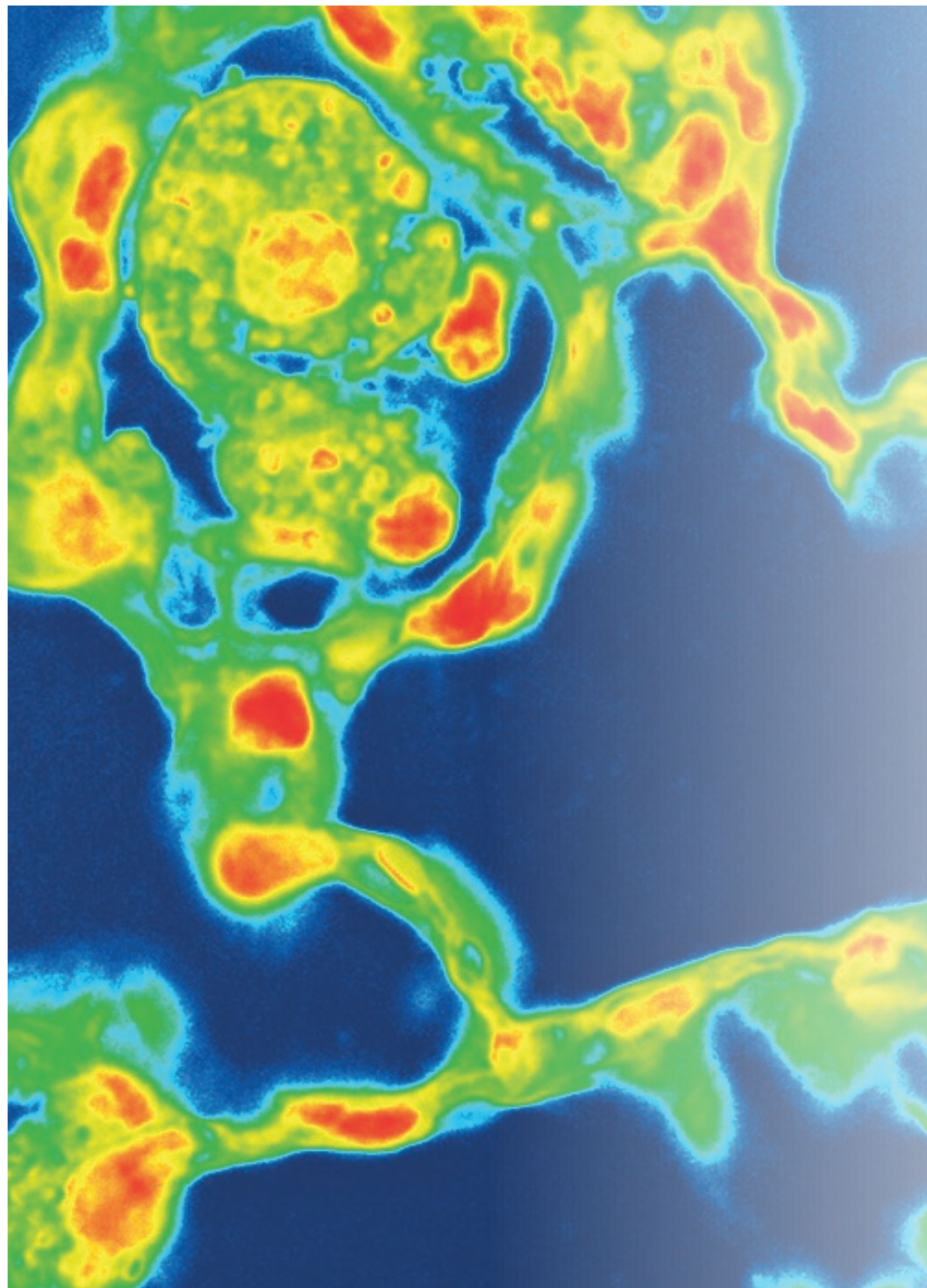
References

1. Boraschi, D.; Swartzwelter, B.J.; Italiani, P. Interaction of engineered nanomaterials with the immune system: Health-related safety and possible benefits. *Current Opinion in Toxicology* **2018**, *10*, 74-83, doi:<https://doi.org/10.1016/j.cotox.2018.02.002>.
2. Meldrum, K.; Guo, C.; Marczylo, E.L.; Gant, T.W.; Smith, R.; Leonard, M.O. Mechanistic insight into the impact of nanomaterials on asthma and allergic airway disease. *Part Fibre Toxicol* **2017**, *14*, 45, doi:[10.1186/s12989-017-0228-y](https://doi.org/10.1186/s12989-017-0228-y).
3. Vandebriel, R.J.; Vermeulen, J.P.; van Engelen, L.B.; de Jong, B.; Verhagen, L.M.; de la Fonteyne-Blankestijn, L.J.; Hoonakker, M.E.; de Jong, W.H. The crystal structure of titanium dioxide nanoparticles influences immune activity in vitro and in vivo. *Part Fibre Toxicol* **2018**, *15*, 9, doi:[10.1186/s12989-018-0245-5](https://doi.org/10.1186/s12989-018-0245-5).
4. Boraschi, D.; Italiani, P. From Antigen Delivery System to Adjuvanticy: The Board Application of Nanoparticles in Vaccinology. *Vaccines (Basel)* **2015**, *3*, 930-939, doi:[10.3390/vaccines3040930](https://doi.org/10.3390/vaccines3040930).
5. Bakand, S.; Hayes, A. Toxicological Considerations, Toxicity Assessment, and Risk Management of Inhaled Nanoparticles. *Int J Mol Sci* **2016**, *17*, doi:[10.3390/ijms17060929](https://doi.org/10.3390/ijms17060929).
6. Sun, B.; Wang, X.; Ji, Z.; Li, R.; Xia, T. NLRP3 inflammasome activation induced by engineered nanomaterials. *Small* **2013**, *9*, 1595-1607, doi:[10.1002/sml.201201962](https://doi.org/10.1002/sml.201201962).
7. Dayem, A.A.; Kim, B.; Gurunathan, S.; Choi, H.Y.; Yang, G.; Saha, S.K.; Han, D.; Han, J.; Kim, K.; Kim, J.H., et al. Biologically synthesized silver nanoparticles induce neuronal differentiation of SH-SY5Y cells via modulation of reactive oxygen species, phosphatases, and kinase signaling pathways. *Biotechnol J* **2014**, *9*, 934-943, doi:[10.1002/biot.201300555](https://doi.org/10.1002/biot.201300555).
8. Zhang, H.; Ji, Z.; Xia, T.; Meng, H.; Low-Kam, C.; Liu, R.; Pokhrel, S.; Lin, S.; Wang, X.; Liao, Y.P., et al. Use of metal oxide nanoparticle band gap to develop a predictive paradigm for oxidative stress and acute pulmonary inflammation. *ACS Nano* **2012**, *6*, 4349-4368, doi:[10.1021/nn3010087](https://doi.org/10.1021/nn3010087).
9. Li, R.; Ji, Z.; Chang, C.H.; Dunphy, D.R.; Cai, X.; Meng, H.; Zhang, H.; Sun, B.; Wang, X.; Dong, J., et al. Surface interactions with compartmentalized cellular phosphates explain rare earth oxide nanoparticle hazard and provide opportunities for safer design. *ACS Nano* **2014**, *8*, 1771-1783, doi:[10.1021/nn406166n](https://doi.org/10.1021/nn406166n).
10. Wang, X.; Sun, B.; Liu, S.; Xia, T. Structure Activity Relationships of Engineered Nanomaterials in inducing NLRP3 Inflammasome Activation and Chronic Lung Fibrosis. *NanoImpact* **2017**, *6*, 99-108, doi:[10.1016/j.impact.2016.08.002](https://doi.org/10.1016/j.impact.2016.08.002).
11. Dekkers, S.; Wagner, J.G.; Vandebriel, R.J.; Eldridge, E.A.; Tang, S.V.Y.; Miller, M.R.; Römer, I.; de Jong, W.H.; Harkema, J.R.; Cassee, F.R. Role of chemical composition and redox modification of poorly soluble nanomaterials on their ability to enhance allergic airway sensitisation in mice. *Particle and Fibre Toxicology* **2019**, *16*, 39, doi:[10.1186/s12989-019-0320-6](https://doi.org/10.1186/s12989-019-0320-6).
12. Ihrie, M.D.; Bonner, J.C. The Toxicology of Engineered Nanomaterials in Asthma. *Curr Environ Health Rep* **2018**, *5*, 100-109, doi:[10.1007/s40572-018-0181-4](https://doi.org/10.1007/s40572-018-0181-4).
13. Lee, T.H.; Song, H.J.; Park, C.S. Role of inflammasome activation in development and exacerbation of asthma. *Asia Pac Allergy* **2014**, *4*, 187-196, doi:[10.5415/apallergy.2014.4.4.187](https://doi.org/10.5415/apallergy.2014.4.4.187).

14. Besnard, A.G.; Guillou, N.; Tschopp, J.; Erard, F.; Couillin, I.; Iwakura, Y.; Quesniaux, V.; Ryffel, B.; Togbe, D. NLRP3 inflammasome is required in murine asthma in the absence of aluminum adjuvant. *Allergy* **2011**, *66*, 1047-1057, doi:10.1111/j.1398-9995.2011.02586.x.
15. Chen, M.; Wang, H.; Chen, W.; Meng, G. Regulation of adaptive immunity by the NLRP3 inflammasome. *Int Immunopharmacol* **2011**, *11*, 549-554, doi:10.1016/j.intimp.2010.11.025.
16. Evavold, C.L.; Kagan, J.C. How Inflammasomes Inform Adaptive Immunity. *J Mol Biol* **2018**, *430*, 217-237, doi:10.1016/j.jmb.2017.09.019.
17. Nakanishi, K. Unique Action of Interleukin-18 on T Cells and Other Immune Cells. *Front Immunol* **2018**, *9*, 763, doi:10.3389/fimmu.2018.00763.
18. Xu, D.; Trajkovic, V.; Hunter, D.; Leung, B.P.; Schulz, K.; Gracie, J.A.; McInnes, I.B.; Liew, F.Y. IL-18 induces the differentiation of Th1 or Th2 cells depending upon cytokine milieu and genetic background. *Eur J Immunol* **2000**, *30*, 3147-3156, doi:10.1002/1521-4141(200011)30:11<3147::AID-IMMU3147>3.0.CO;2-J.
19. Jia, J.; Zhang, Y.; Xin, Y.; Jiang, C.; Yan, B.; Zhai, S. Interactions Between Nanoparticles and Dendritic Cells: From the Perspective of Cancer Immunotherapy. *Front Oncol* **2018**, *8*, 404, doi:10.3389/fonc.2018.00404.
20. Xia, T.; Hamilton, R.F.; Bonner, J.C.; Crandall, E.D.; Elder, A.; Fazlollahi, F.; Girtsman, T.A.; Kim, K.; Mitra, S.; Ntim, S.A., et al. Interlaboratory evaluation of in vitro cytotoxicity and inflammatory responses to engineered nanomaterials: the NIEHS Nano GO Consortium. *Environ Health Perspect* **2013**, *121*, 683-690, doi:10.1289/ehp.1306561.
21. Chanput, W.; Mes, J.J.; Wichers, H.J. THP-1 cell line: an in vitro cell model for immune modulation approach. *Int Immunopharmacol* **2014**, *23*, 37-45, doi:10.1016/j.intimp.2014.08.002.
22. Hamilton, R.F., Jr.; Xiang, C.; Li, M.; Ka, I.; Yang, F.; Ma, D.; Porter, D.W.; Wu, N.; Holian, A. Purification and sidewall functionalization of multiwalled carbon nanotubes and resulting bioactivity in two macrophage models. *Inhal Toxicol* **2013**, *25*, 199-210, doi:10.3109/08958378.2013.775197.
23. Cabanas, A.; Darr, J.A.; E., L.; Poliakoff, M. A continuous and clean one-step synthesis of nanoparticulate Ce_{1-x}Zr_xO₂ solid solutions in near-critical water. *Chem Comm* **2000**, *2000*, 901-902.
24. Liu, J.; Römer, I.; Tang, S.V.Y.; Valsami-Jones, E.; Palmer, R.E. Crystallinity depends on choice of iron salt precursor in the continuous hydrothermal synthesis of Fe-Co oxide nanoparticles. *RSC Adv* **2017**, *7*, 37436-37440, doi:DOI: 10.1039/c7ra06647c.
25. Giannakou, C.; Aimonen, K.; Bloois, L.V.; Catalan, J.; Geertsma, R.E.; Gremmer, E.R.; de Jong, W.H.; Keizers, P.H.; Schwillens, P.L.; Vandebriel, R.J., et al. Sensitive method for endotoxin determination in nanomedicinal product samples. *Nanomedicine (Lond)* **2019**, *14*, 1231-1246, doi:10.2217/nnm-2018-0339.
26. Malyala, P.; Singh, M. Endotoxin limits in formulations for preclinical research. *J Pharm Sci* **2008**, *97*, 2041-2044, doi:10.1002/jps.21152.
27. DeLoid, G.M.; Cohen, J.M.; Pyrgiotakis, G.; Demokritou, P. Preparation, characterization, and in vitro dosimetry of dispersed, engineered nanomaterials. *Nat Protoc* **2017**, *12*, 355-371, doi:10.1038/nprot.2016.172.

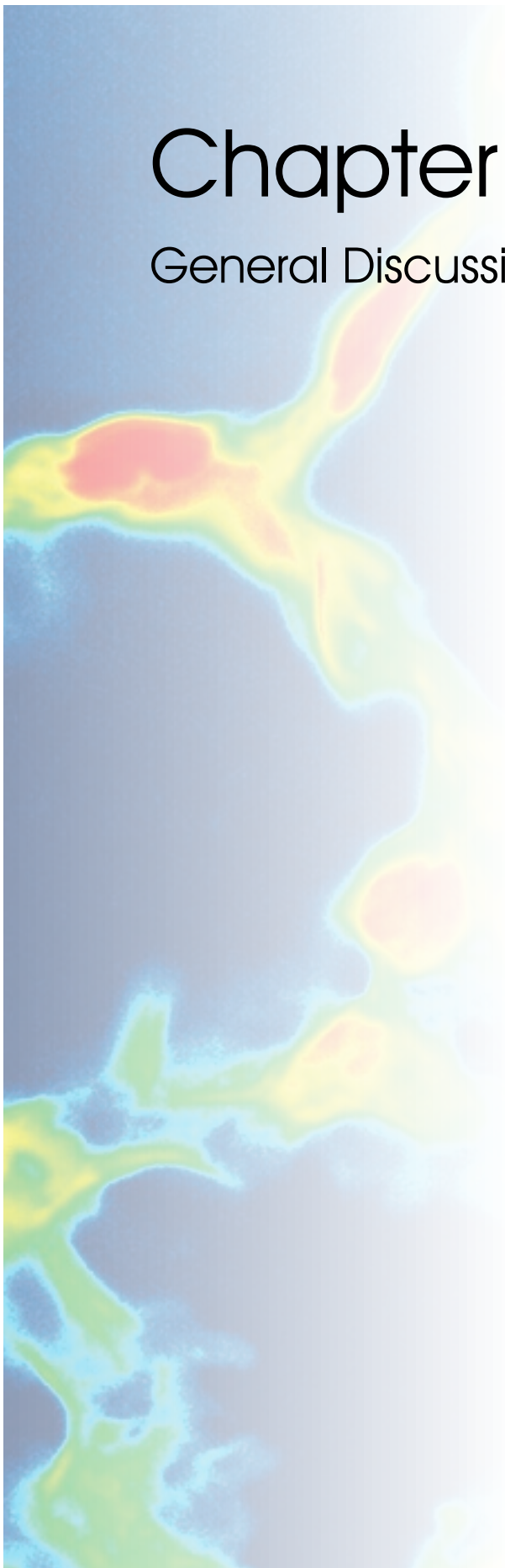
28. DeLoid, G.M.; Cohen, J.M.; Pyrgiotakis, G.; Pirela, S.V.; Pal, A.; Liu, J.; Srebric, J.; Demokritou, P. Advanced computational modeling for in vitro nanomaterial dosimetry. *Part Fibre Toxicol* **2015**, *12*, 32, doi:10.1186/s12989-015-0109-1.
29. Cohen, J.M.; Teeguarden, J.G.; Demokritou, P. An integrated approach for the in vitro dosimetry of engineered nanomaterials. *Part Fibre Toxicol* **2014**, *11*, 20, doi:10.1186/1743-8977-11-20.
30. Slob, W. Dose-response modeling of continuous endpoints. *Toxicol Sci* **2002**, *66*, 298-312, doi:10.1093/toxsci/66.2.298.
31. Al-Shabib, N.A.; Husain, F.M.; Ahmed, F.; Khan, R.A.; Khan, M.S.; Ansari, F.A.; Alam, M.Z.; Ahmed, M.A.; Khan, M.S.; Baig, M.H., et al. Low Temperature Synthesis of Superparamagnetic Iron Oxide (Fe₃O₄) Nanoparticles and Their ROS Mediated Inhibition of Biofilm Formed by Food-Associated Bacteria. *Front Microbiol* **2018**, *9*, 2567, doi:10.3389/fmicb.2018.02567.
32. Zhou, R.; Tardivel, A.; Thorens, B.; Choi, I.; Tschopp, J. Thioredoxin-interacting protein links oxidative stress to inflammasome activation. *Nat Immunol* **2010**, *11*, 136-140, doi:10.1038/ni.1831.
33. Hamilton, R.F., Jr.; Wu, Z.; Mitra, S.; Shaw, P.K.; Holian, A. Effect of MWCNT size, carboxylation, and purification on in vitro and in vivo toxicity, inflammation and lung pathology. *Part Fibre Toxicol* **2013**, *10*, 57, doi:10.1186/1743-8977-10-57.
34. Ji, Z.; Wang, X.; Zhang, H.; Lin, S.; Meng, H.; Sun, B.; George, S.; Xia, T.; Nel, A.E.; Zink, J.I. Designed synthesis of CeO₂ nanorods and nanowires for studying toxicological effects of high aspect ratio nanomaterials. *ACS Nano* **2012**, *6*, 5366-5380, doi:10.1021/nn3012114.
35. Mizutani, N.; Nabe, T.; Yoshino, S. Exposure to multiwalled carbon nanotubes and allergen promotes early- and late-phase increases in airway resistance in mice. *Biol Pharm Bull* **2012**, *35*, 2133-2140.
36. Vandebriel, R.J.; Dekkers, S.; de Jong, W.H.; Cassee, F.R. An Update on NLRP3 Inflammasome Activation by Engineered Nanomaterials. *Current Bionanotechnology* **2016**, *2*, 40-46.
37. Cho, W.S.; Duffin, R.; Bradley, M.; Megson, I.L.; Macnee, W.; Lee, J.K.; Jeong, J.; Donaldson, K. Predictive value of in vitro assays depends on the mechanism of toxicity of metal oxide nanoparticles. *Part Fibre Toxicol* **2013**, *10*, doi:10.1186/1743-8977-10-55.
38. Graham, U.M.; Wang, C.; Fernback, J.; Dozier, A.K.; Drummy, L.; Mahalingam, K.; Molina, R.M.; Konduru, N.V.; Birch, E.; Brain, J.D. In vivo formation of Ce-phosphate Nanoparticles following Intratracheal Instillation of CeCl₃: Subcellular sites, Nanostructures, Precipitation Mechanisms and Nanoparticle 3D-Alignment. *Microsc. Microanal.* **2017**, *23*, 1342-1343, doi:doi:10.1017/S1431927617007371.
39. Graham, U.M.; Yokel, R.A.; Dozier, A.K.; Drummy, L.; Mahalingam, K.; Tseng, M.T.; Birch, E.; Fernback, J. Analytical High-resolution Electron Microscopy Reveals Organ-specific Nanoceria Bioprocessing. *Toxicol Pathol* **2018**, *46*, 47-61, doi:10.1177/0192623317737254.
40. Sager, T.M.; Wolfarth, M.; Leonard, S.S.; Morris, A.M.; Porter, D.W.; Castranova, V.; Holian, A. Role of engineered metal oxide nanoparticle agglomeration in reactive oxygen species generation and cathepsin B release in NLRP3 inflammasome activation and pulmonary toxicity. *Inhal Toxicol* **2016**, *28*, 686-697, doi:10.1080/08958378.2016.1257664.

41. Asati, A.; Santra, S.; Kaittanis, C.; Nath, S.; Perez, J.M. Oxidase-like activity of polymer-coated cerium oxide nanoparticles. *Angew Chem Int Ed Engl* **2009**, *48*, 2308-2312, doi:10.1002/anie.200805279.
42. Mirshafiee, V.; Sun, B.; Chang, C.H.; Liao, Y.P.; Jiang, W.; Jiang, J.; Liu, X.; Wang, X.; Xia, T.; Nel, A.E. Toxicological Profiling of Metal Oxide Nanoparticles in Liver Context Reveals Pyroptosis in Kupffer Cells and Macrophages versus Apoptosis in Hepatocytes. *ACS Nano* **2018**, *12*, 3836-3852, doi:10.1021/acsnano.8b01086.
43. Dankers, A.C.A.; Kuper, C.F.; Boumeester, A.J.; Fabriek, B.O.; Kooter, I.M.; Grollers-Mulderij, M.; Tromp, P.; Nelissen, I.; Zondervan-Van Den Beuken, E.K.; Vandebriel, R.J. A practical approach to assess inhalation toxicity of metal oxide nanoparticles in vitro. *J Appl Toxicol* **2018**, *38*, 160-171, doi:10.1002/jat.3518.
44. Schanen, B.C.; Das, S.; Reilly, C.M.; Warren, W.L.; Self, W.T.; Seal, S.; Drake, D.R., 3rd. Immunomodulation and T helper TH(1)/TH(2) response polarization by CeO(2) and TiO(2) nanoparticles. *PLoS One* **2013**, *8*, e62816, doi:10.1371/journal.pone.0062816.
45. Marin, N.D.; Dunlap, M.D.; Kaushal, D.; Khader, S.A. Friend or Foe: The Protective and Pathological Roles of Inducible Bronchus-Associated Lymphoid Tissue in Pulmonary Diseases. *J Immunol* **2019**, *202*, 2519-2526, doi:10.4049/jimmunol.1801135.
46. Foo, S.Y.; Phipps, S. Regulation of inducible BALT formation and contribution to immunity and pathology. *Mucosal Immunol* **2010**, *3*, 537-544, doi:10.1038/mi.2010.52.
47. Kumar, S.; Jeong, Y.; Ashraf, M.U.; Bae, Y.S. Dendritic Cell-Mediated Th2 Immunity and Immune Disorders. *Int J Mol Sci* **2019**, *20*, doi:10.3390/ijms20092159.
48. Jones, G.W.; Hill, D.G.; Jones, S.A. Understanding Immune Cells in Tertiary Lymphoid Organ Development: It Is All Starting to Come Together. *Front Immunol* **2016**, *7*, 401, doi:10.3389/fimmu.2016.00401.



Chapter 7

General Discussion



Introduction

The research described in this thesis investigated the influence of several physicochemical properties of nanoparticles (NPs) on their biodistribution, molecular pathways and toxicity after inhalation. Investigating the influence of physicochemical properties of NPs on their potential to cause toxicological effects is more complicated than it seems, because the physicochemical properties of NPs may change due to interactions of the NPs with their surrounding environment within a toxicity assay. In this chapter, the key findings, overall conclusions, future perspectives and implications of this research are discussed.

Inhalation toxicity *in vivo*

After four weeks of exposure to undoped and Zr-doped CeO₂ NPs via inhalation, no major toxicological effects were observed in mice, apart from minimal inflammatory histopathology in the lung (chapter 2). This was unexpected, since previous inhalation studies in rats and mice showed more pronounced effects after exposure to CeO₂ NPs (Aalapati et al., 2014; Arts et al., 2016; Gosens et al., 2014; Keller et al., 2014). From a toxicological point of view, this was a bit disappointing, since it is more difficult to determine the influence of redox activity on the toxicity if only minimal effects are observed. From the perspective of risk assessment, this was an interesting observation that was important to publish, knowing that studies with clear toxicological effects are generally more represented in literature than studies with negative results (Mlinaric et al., 2017). A detailed comparison of data on the undoped CeO₂ NP from our study with data from other inhalation studies with various CeO₂ NPs showed that the difference in the pulmonary responses to CeO₂ NPs can be explained by differences in the tested species and size, but also on other physicochemical characteristics of the particles (chapter 3). No relation between the redox activity of the CeO₂ NPs, as measured using the acellular Ferric Reduction Ability of Serum (FRAS) assay and the observed toxicological responses was found. However, since the various CeO₂ NPs in the analyzed studies differed in more than one physicochemical characteristic, it was difficult to determine the influence of each individual characteristic on the observed toxicity.

Within our inhalation study, we used a structural series of CeO₂ NPs that only differed with respect to the amount of Zr-doping. Besides redox activity, the Zr-doping also changed the chemical composition, but most of the other physicochemical characteristics, such as primary particles size, aggregation and agglomeration were similar. The redox modification via Zr-doping had limited effects on the observed pulmonary toxicity after subchronic inhalation of CeO₂ NPs. However, because only minimal toxicological pulmonary effects were observed after exposure of to the undoped CeO₂ NPs, most of the hypothesized ameliorative effects resulting from the ZrO₂-doping may not have been visible in this study. Another factor that makes investigating the influence of redox activity difficult, is that the redox activity of NPs is not only dependent on physicochemical properties such as chemical composition, size,

surface area and surface chemistry, but also on the environmental conditions which the NPs encounter in the *in vivo* study, including changes in pH and the presence of proteins and salts. There are many different assays to measure the redox activity or the subsequent chemical and biological responses. A combination of different assays and environmental conditions is needed to investigate the influence of the redox activity of a NP on the outcome of a toxicological assay. In preparation of our four week inhalation study, the redox activity was measured with Electron Paramagnetic Resonance (EPR) under several acellular conditions. Additional information on the redox activity of the NPs under the environmental conditions relevant for the *in vivo* inhalation study, e.g. in lung lining, lysosomal fluid, or cellular conditions, may have provided more insight why Zr-doping of CeO₂ NPs did not influence the toxicological responses observed in the inhalation study. Maybe Zr-doping of CeO₂ NPs does not lead to differences in the ability of these NPs to generate or reduce reactive oxygen species (ROS) under the environmental conditions of the *in vivo* inhalation study, because of modification or transformation of the NPs. Maybe other mechanisms of toxicity are more important in the inhalation toxicity than the hypothesized redox activity, ROS generation, oxidative stress and subsequent inflammation.

Molecular mechanisms of *in vitro* toxicity

Further investigation into the molecular pathways of the undoped and Zr-doped CeO₂ NPs was performed within our *in vitro* multi-omics study (chapter 4). Surprisingly, exposure to the same Zr-doped CeO₂ NPs showed remarkably less cytotoxicity compared to the previous *in vitro* study in the same cell type (A549) (chapter 2). Furthermore, only minor molecular responses were observed, which indicated that the influence of redox activity on the assumed oxidative stress mechanistic pathway of CeO₂ NP toxicity was very limited. Similar to the *in vivo* inhalation study, additional information on the redox activity of the NPs under the environmental conditions relevant for the *in vitro* assay, e.g. in cell culture medium, lysosomal fluid, or cellular conditions, may have provided more insight why Zr-doping of CeO₂ NPs did not influence the toxicological responses observed in this *in vitro* study.

In contrast to these somewhat discouraging results for the undoped and Zr-doped CeO₂ NPs within our *in vitro* multi-omics study, the results for the Ag and ZnO NPs confirmed our hypothesis that dissolution and the release of Ag and Zn ions are the main drivers of the *in vitro* toxicity Ag and ZnO NPs. The majority of molecular responses of A549 cells to the Ag and ZnO NPs, were similar to their responses to Ag and Zn ions, respectively, confirming previous findings that the main toxicological pathways of Ag and ZnO NPs were mediated by dissolved metal ions rather than by the physical aspects of the NPs (De Matteis et al., 2015; Liu et al., 2016). This study shows the advantage of designing a toxicity assay in such a way that the influence of time dependent effects and environmental conditions can be taken into account. Including ionic controls in the study design, made it possible to compare the molecular responses of the NPs plus their released ions to those of the ions alone.

Measuring the molecular responses over time, made it possible to follow the development and reversibility or persistence of the observed molecular responses. Dissolution testing in cell culture medium provided additional information on the influence of relevant environmental conditions on the dissolution of the Ag and ZnO NPs.

Adjuvant activity *in vivo*

The ability of NPs to generate ROS has not only been related to inflammatory pulmonary responses, but also to cellular responses associated with the ability of NPs to influence allergic airways sensitization (Meldrum et al., 2017). As Zr-doping of CeO₂ NPs had limited effect on the inflammatory responses after inhalation, additional NPs were included in our *in vivo* study investigating the influence of redox activity and chemical composition on the adjuvant activity on NPs. Fe-doped Co₃O₄ NPs were included as they were expected to have a greater ability to induce oxygen radicals, oxidative stress, pulmonary inflammation and adjuvant activity. Similar to the results from the four week inhalation study and the *in vitro* assays in A549 cells, again no relation between the acellular redox activity of the undoped and Zr-doped CeO₂ NPs, and the observed toxicological responses were found. Also for the undoped and Fe-doped Co₃O₄ NPs the influence of the redox activity on the toxicological responses was very limited.

However, the adjuvant potency of the different NPs varied with the different immune responses and indicated that different immunological pathways are involved in the adjuvant activity of undoped and Zr-doped CeO₂ NPs compared to undoped and Fe-doped Co₃O₄ NPs. These differences in immune responses suggest that chemical composition has more influence on the type of allergic immune responses than the redox activity of NPs. The most interesting observations were the lymphoid cell accumulation and formation of ectopic lymphoid tissues in the lungs after co-exposure to OVA and undoped or Fe-doped Co₃O₄ NPs. Although, broncho-associated lymphoid tissue has been associated with chronic allergic diseases, such as asthma, the pathways that control the development and function of ectopic or broncho-associated lymphoid tissues are poorly understood (Hirahara et al., 2018; Hwang et al., 2016). More knowledge on the underlying mechanistic pathways, their interrelationships and control mechanisms are needed to better understand the influence of various physicochemical properties on the adjuvant activity of NPs.

Inflammasome activation and dendritic cell maturation *in vitro*

To gain more insight into the different immunological responses involved in the adjuvant activity of undoped and Zr-doped CeO₂ NPs compared to undoped and Fe-doped Co₃O₄ NPs, the same NPs were tested in two *in vitro* assays as model for interaction of NPs and cells of the immune system. These *in vitro* assays investigate two mechanisms known to play an important role in NP-enhanced induction of allergic airway responses (Ihrie and Bonner, 2018; Meldrum et al., 2017), inflammasome activation and dendritic cell maturation. Similar

to the *in vivo* study on adjuvant activity, the outcomes of the *in vitro* studies indicated that inflammasome activation and dendritic cell maturation is primarily related to the chemical composition and not to the size or acellular redox activity of undoped and Zr-doped CeO₂ NPs or undoped and Fe-doped Co₃O₄ NPs. Undoped and Zr-doped CeO₂ NPs induced inflammasome activation, while several undoped and Fe-doped Co₃O₄ NPs induced dendritic cell maturation. The ranking of the various NPs with respect to their *in vitro* IL-12p40 response was similar to the ranking of their *in vivo* B-cell density in the lungs, indicating that the results of the DC maturation assay may be indicative for the potential of NPs to induce *in vivo* lymphoid accumulation in lungs. However, more studies measuring not only IL-12p40, but also other cytokines, chemokines and surface makers after exposure to a larger variety of NPs are needed to further investigate the mechanisms of action and to verify the predictive value of this assay for lymphoid accumulation in the lungs. Moreover, the type of immune responses observed *in vivo* cannot be readily predicted using *in vitro* assays on DC maturation and inflammasome activation alone, since these assays only cover two of the key events in the AOP network on respiratory allergic responses.

Overall conclusions

Redox modification through Zr-doping of CeO₂ NPs and Fe-doping of Co₃O₄ NPs did not decrease the *in vitro* and *in vivo* toxicity and adjuvant activity of these NPs. The influence of the redox activity of these NPs on the investigated biological responses was very limited and did not follow a consequent trend of either an increase or a decrease with increasing redox activity. Comparison of the results of our inhalation study with other inhalation studies suggested that species, size and other physicochemical properties of the NPs are more important determinants of the inflammatory responses observed after inhalation of CeO₂ NPs than the redox activity of the NPs. The results of our *in vitro* multi-omics study indicated that chemical composition and dissolution were more important drivers of the molecular responses observed in A549 cells than redox activity. After exposure to CeO₂ NPs, only minor molecular responses were observed, while exposure to Ag and ZnO NPs resulted in more pronounced molecular responses that were mediated by dissolved metal ions rather than by the physical aspects of the NPs. The results of the *in vivo* study on the adjuvant activity and the *in vitro* studies on inflammasome activation and DC maturation indicated that chemical composition has more influence on the type of immune responses than the redox activity of NPs. Although the role of redox activity in the toxicity of NPs cannot be ruled out, its influence on the various biological responses investigated in this thesis was limited and not very clear, as this property strongly depends on the environmental conditions of the toxicological assays, which is difficult to measure, simulate or predict. When investigating the influence of the physicochemical properties of NPs on the biological response, it is important to assess how these properties may change over time depending on their surrounding environment. Although full characterization of the NPs throughout

the whole assay may not always be possible, it is always important to take the potential influence of the experimental conditions on the NP properties and subsequent outcomes of the assay into account.

Future perspectives and implications

Working with nanomaterials within toxicological assays is more complicated than it seems. To investigate the influence of physicochemical properties of NPs on their potential to cause toxicological effects structural series of NPs that only differed with respect to one physicochemical property are needed. This is challenging because changing one property usually influences at least one, but often several other properties. This makes it difficult to separate the effect of one property from that of the other properties. Therefore it is very important to measure how changes in the physicochemical property of interest may also change other physicochemical properties. In addition, physicochemical properties of NPs may change over time due to interaction of the NPs with their surrounding environment. Consequently, knowledge on changes within physicochemical properties of the NPs under the environmental conditions relevant for the toxicological assay is needed to evaluate the influence of the different physicochemical properties on the outcome of the toxicological assay. Furthermore, variabilities in the toxicity assays used to investigate the potential toxicological effects of NPs often hampers comparisons between adverse effects of NPs with different characteristics across different studies. Therefore, more systematic research and harmonization or standardization of the various *in vitro* and *in vivo* assays to evaluate the potential toxicity of NPs is needed.

The research described in this thesis highlights the importance of not only the intrinsic physicochemical properties of NPs, but also the changes in these properties due to changes in their surrounding environment, the (extrinsic) physicochemical properties. Although, many researchers have stressed the importance of good physicochemical characterization of NMs within nanotoxicological research, a lot of scientific papers only include the physicochemical characteristics of the NMs as manufactured, but lack detailed analysis of the physicochemical properties under the changing environmental conditions of the toxicological assay (Gao and Lowry, 2018). Transformations, such as dissolution, changes in surface chemistry (including protein coating of NPs in the biological environment i.e. corona formation), aggregation and agglomeration are of great influence on the deposition, uptake, distribution and potential toxicity of the NPs. Although it is not always possible to measure these transformations and changes in physicochemical properties throughout the whole toxicity assay, it is important to know which physicochemical properties may change throughout each assay and how this may influence the outcome of the assay. Within many nanotoxicological research projects access to the right expertise and technical equipment for NM characterization is obtained via collaboration with material and analytical scientists.

It is recommended to fully utilize this collaboration to enable the characterization of the NMs under the environmental conditions relevant for the toxicological assays of interest.

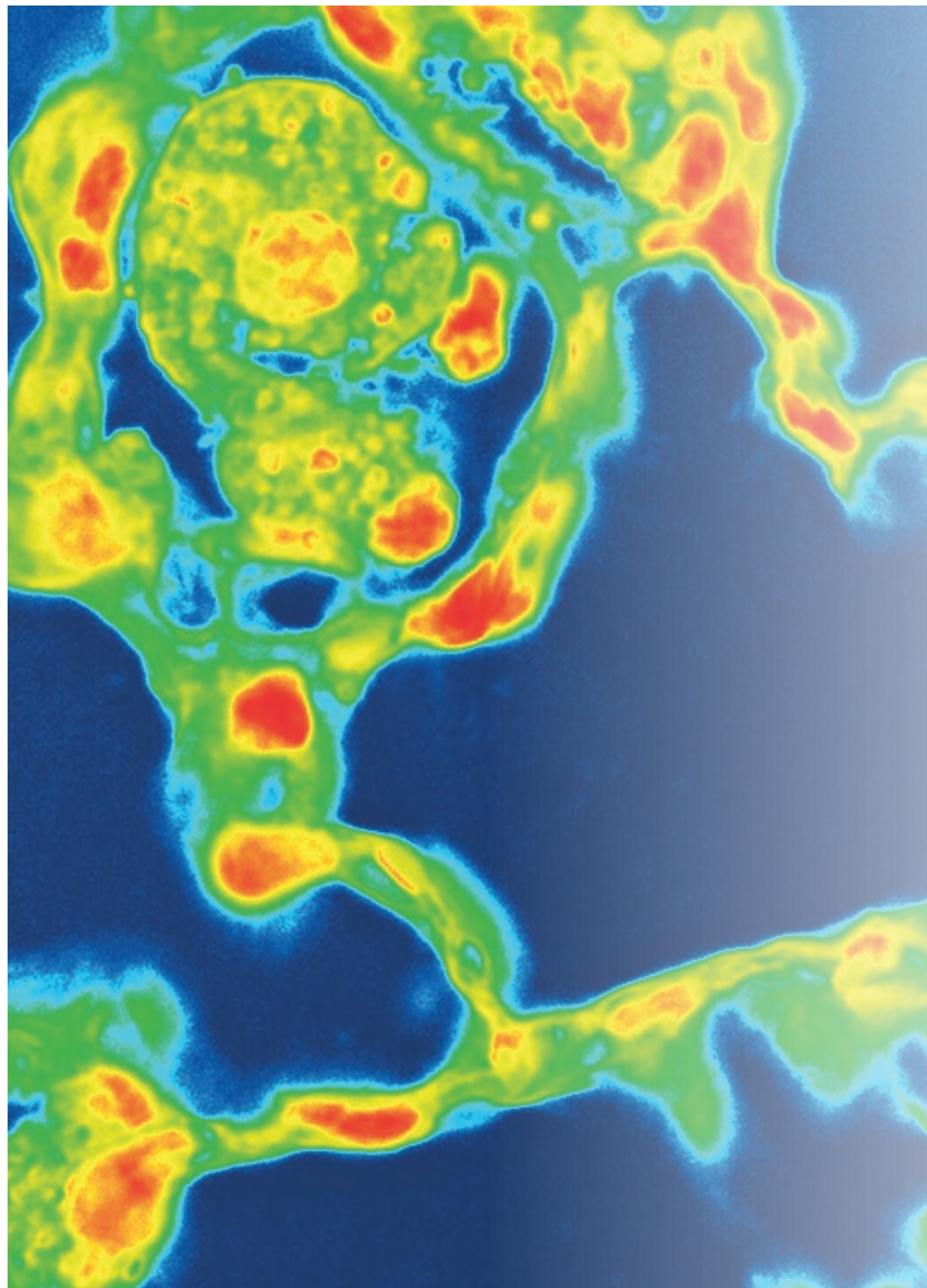
Insight into which conditions change which physicochemical properties of NPs and how this influences their biodistribution, mechanistic pathways and toxicity will support further development of the various approaches to assess and predict the toxicity of NPs. This will facilitate the selection or verification of the physicochemical properties, functional assays and toxicity assays included in the various risk assessment approaches, Integrated Approaches to Testing and Assessment (IATAs), risk assessment tools, grouping, read across approaches and predictive models. Furthermore it will help to determine the experimental conditions and the experimental design of the analytical, functional and toxicity assays.

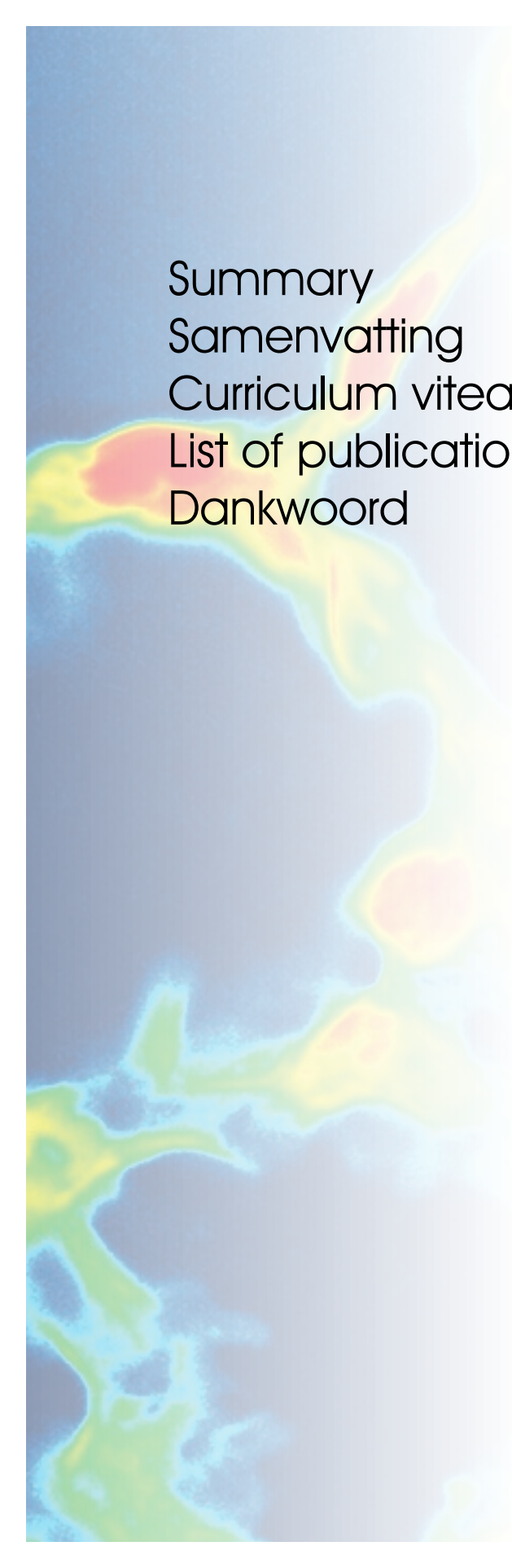
Another challenge when investigating the influence of physicochemical properties on the biological responses of NPs is that there is usually more than one mechanistic pathway by which NPs can cause a specific biological response. Moreover, the body generally also has ways to maintain or repair the homeostasis, leading to a complex situation of connected AOP network. Therefore, it is important to know how the various mechanisms of toxicity by which NPs may cause a specific biological response are connected to each other. Immunological responses are, for example, regulated via various mechanistic pathways, which are often connected to each other. It is therefore difficult if not impossible to predict all potential adverse effects *in vivo* based on *in vitro* assays. Currently, there are several Adverse Outcome Pathways (AOPs) developed and under development. Omics studies can help to identify the various mechanisms of toxicity of different NMs under different circumstances within these AOPs. Depending on the chemical composition, other NP properties, route of exposure, expected changes or transformations of the NPs and knowledge on the mechanisms by which this NPs may cause adverse effects, a different set of acellular (functional) assays and cellular *in vitro* assays is needed to predict the toxicity *in vivo*. However, it cannot be expected that such a set of functional assays and *in vitro* assays will result in a perfect prediction of the *in vivo* toxicity, since this is currently not even possible for non-nanomaterials.

The research in this thesis provides more insight into some of the environmental conditions that influence some of the physicochemical properties and how this may influence various biological responses after exposure to NPs in the lung. The challenge for future research is to fill the remaining knowledge gaps on how the various intrinsic properties, extrinsic properties and mechanistic pathways are connected to each other.

References

- Aalapati S, Ganapathy S, Manapuram S, Anumolu G and Prakya BM (2014) Toxicity and bio-accumulation of inhaled cerium oxide nanoparticles in CD1 mice. *Nanotoxicology* **8**:786-798.
- Arts JH, Irfan MA, Keene AM, Kreiling R, Lyon D, Maier M, Michel K, Neubauer N, Petry T, Sauer UG, Warheit D, Wiench K, Wohlleben W and Landsiedel R (2016) Case studies putting the decision-making framework for the grouping and testing of nanomaterials (DF4nanoGrouping) into practice. *Regul Toxicol Pharmacol* **76**:234-261.
- De Matteis V, Malvindi MA, Galeone A, Brunetti V, De Luca E, Kote S, Kshirsagar P, Sabella S, Bardi G and Pompa PP (2015) Negligible particle-specific toxicity mechanism of silver nanoparticles: the role of Ag⁺ ion release in the cytosol. *Nanomedicine* **11**:731-739.
- Gao X and Lowry GV (2018) Progress towards standardized and validated characterizations for measuring physicochemical properties of manufactured nanomaterials relevant to nano health and safety risks. *NanoImpact* **9**:14-30.
- Gosens I, Mathijssen LE, Bokkers BG, Muijser H and Cassee FR (2014) Comparative hazard identification of nano- and micro-sized cerium oxide particles based on 28-day inhalation studies in rats. *Nanotoxicology* **8**:643-653.
- Hirahara K, Shinoda K, Endo Y, Ichikawa T and Nakayama T (2018) Maintenance of memory-type pathogenic Th2 cells in the pathophysiology of chronic airway inflammation. *Inflamm Regen* **38**:10.
- Hwang JY, Randall TD and Silva-Sanchez A (2016) Inducible Bronchus-Associated Lymphoid Tissue: Taming Inflammation in the Lung. *Front Immunol* **7**:258.
- Ihrie MD and Bonner JC (2018) The Toxicology of Engineered Nanomaterials in Asthma. *Curr Environ Health Rep* **5**:100-109.
- Keller J, Wohlleben W, Ma-Hock L, Strauss V, Gröters S, Küttler K, Wiench K, Herden C, Oberdörster G, Ravenzwaay B and Landsiedel R (2014) Time course of lung retention and toxicity of inhaled particles: short-term exposure to nano-Ceria. *Arch Toxicol* **88**.
- Liu J, Feng X, Wei L, Chen L, Song B and Shao L (2016) The toxicology of ion-shedding zinc oxide nanoparticles. *Crit Rev Toxicol* **46**:348-384.
- Meldrum K, Guo C, Marcylo EL, Gant TW, Smith R and Leonard MO (2017) Mechanistic insight into the impact of nanomaterials on asthma and allergic airway disease. *Part Fibre Toxicol* **14**:45.
- Mlinaric A, Horvat M and Supak Smolicic V (2017) Dealing with the positive publication bias: Why you should really publish your negative results. *Biochem Med (Zagreb)* **27**:030201.





Summary
Samenvatting
Curriculum vitae
List of publications
Dankwoord

Summary

Nanotechnology makes it possible to develop products with amazing features. By changing the various properties of nanomaterials it is possible to develop materials with remarkable functionalities. However, it is often not known how changing the properties may affect the ability of nanomaterials to cause adverse human health effects. More knowledge in the influence of the various physicochemical properties on the potential human health effects will allow the development of nanomaterials with amazing features without introducing increased human health risks.

The main aim of the research described in this thesis is to investigate how the physicochemical properties of nanomaterials influence assumed pathways of toxicity after inhalation. This was done using a carefully selected range of *in vivo* and *in vitro* toxicity assays in combination with a carefully selected set nanoparticles (NPs) with specific properties that were synthesized within the European NanoMILE project. This research aim and approach can be translated into the following research objectives:

1. Assess the influence of size and redox activity of undoped and zirconium(Zr)-doped cerium dioxide (CeO_2) NPs on their deposition, biodistribution and pulmonary (and cardiovascular) effects in mice and rats following inhalation (chapter 2 and 3) .
2. Investigate the influence of dissolution and redox activity of silver (Ag), zinc oxide (ZnO) and undoped and Zr-doped CeO_2 NPs on the molecular mechanisms by which these NPs induce toxicity in A549 cells *in vitro* (chapter 4).
3. Evaluate the influence of chemical composition and redox activity of undoped and Zr-doped CeO_2 and undoped and iron(Fe)-doped cobalt oxide (Co_3O_4) NPs on their adjuvant properties *in vivo* (chapter 5).
4. Study the influence of chemical composition and redox activity of undoped and Zr-doped CeO_2 and undoped and Fe-doped Co_3O_4 NPs on *in vitro* inflammasome activation and dendritic cell maturation (chapter 6).

The central hypothesis was that redox modification (changing the tendency to acquire or lose electrons) through Zr-doping of CeO_2 and Fe-doping of Co_3O_4 NPs would lead to a decrease in the ability of the NPs to generate Reactive Oxygen Species (ROS), oxidative stress and subsequent *in vitro* and *in vivo* toxicity and *in vivo* adjuvant activity. Furthermore, it is expected that the pathways of toxicity of Ag and ZnO NPs are related to their dissolution and ability to release metal ions.

***In vivo* biodistribution and toxicity after inhalation**

The influence of redox activity of CeO_2 NPs on the biodistribution, pulmonary and cardiovascular effects after inhalation was investigated by exposure of mice to CeO_2 NPs

with varying amounts of Zr-doping (0%, 27% or 78% Zr) (chapter 2). Healthy mice (C57BL/6J), mice prone to cardiovascular disease (ApoE^{-/-}, western-diet fed) and a mouse model of neurological disease (5xFAD) were exposed via nose-only inhalation over a four-week period (4 mg/m³ for 3 h/day, 5 days/week). Effects were assessed four weeks post-exposure.

In all three mouse models exposure to 4 mg CeO₂ NP/m³ had no major toxicological effects apart from some modest inflammatory responses in the lung, which were not related to the amount of Zr-doping. In ApoE^{-/-} mice CeO₂ NP exposure did not change the size of atherosclerotic plaques in the brachiocephalic artery compared to non-exposed animals, but there was a trend towards increased inflammatory cell content in the plaques in relation to the Zr content of the CeO₂ NPs. These findings indicate that redox modification of CeO₂ NPs via Zr-doping has limited effects on the pulmonary and cardiovascular toxicity after subchronic exposure. However, because only minimal effects were observed after exposure to the CeO₂ NPs without Zr-doping, the hypothesized ameliorative effects resulting from the Zr-doping may not have been visible in this study.

Indeed in comparison to other inhalation studies with CeO₂ NPs, the observed toxicological effects in our study were relatively mild. A detailed analysis of the data from several inhalation studies with different exposure durations, species and CeO₂ nanoforms, indicated that the differences in the observed toxicity between these studies can be explained by rats being generally more susceptible to the effects of exposure to particles compared to mice and by differences in kinetics of the NPs (chapter 3). However, differences in species and kinetics could not fully explain the differences in observed toxicity in the analysed studies, indicating that pulmonary responses do not only depend on the species and NP properties that influence the kinetics, such as particle size, but also on other physicochemical characteristics of the NPs.

Molecular mechanisms of *in vitro* toxicity

The influence of redox modification of CeO₂ NPs via Zr-doping was further explored by investigating the molecular pathways by which undoped and Zr-doped CeO₂ NPs induce *in vitro* toxicity in a multi-omics study (chapter 4). Next to the influence of redox activity of Zr-doped CeO₂ NPs, also the influence of the dissolution or ability to release metal ions on the molecular pathways of *in vitro* toxicity of Ag and ZnO NPs was investigated in this study. Human lung epithelial cells (A549) were exposed to various Ag, ZnO, and CeO₂ NPs, Ag and ZnO micro-sized particles (MPs), Ag ions (Ag⁺) and zinc ions (Zn²⁺) over a 24 h time course. Molecular responses at exposure levels that caused ~20% cytotoxicity were characterised by direct infusion mass spectrometry lipidomics and polar metabolomics and by RNAseq transcriptomics.

Exposure to undoped and Zr-doped CeO₂ NPs showed remarkably less cytotoxicity compared to the previous *in vitro* study using the same NPs in the same cell type (A549) (chapter 2). Furthermore, CeO₂ NPs elicited few molecular changes, showing slight evidence of oxidative stress for only one of the four CeO₂ NPs tested, indicating that the influence of redox activity on the assumed oxidative stress mechanistic pathway of CeO₂ NP toxicity was very limited.

All Ag, Zn and ZnO exposures resulted in significant metabolic and transcriptional responses. The majority of these molecular changes were common to both ionic and NP exposures and characteristic of metal ion exposure, confirming that the modes of action of these NPs are largely mediated by dissolved metal ions rather than by the physical aspects of the NPs. The molecular changes were time dependent, which can be explained by differences in uptake rates and dissolution kinetics resulting in different intracellular concentrations or different intracellular compartmentalization of the metal ions. The time dependency of the molecular changes may also be explained by adaptive changes, such as induction of metallothioneins that ameliorate cellular damage by sequestering the metal ions.

Adjuvant activity *in vivo*

The influence of redox activity on the adjuvant activity of NPs was investigated in a mouse model of airway sensitization (chapter 5). As Zr-doping of CeO₂ NPs had limited effect on the inflammatory responses after inhalation, additional NPs were included in this *in vivo* study. Fe-doped Co₃O₄ NPs were included as they were expected to have a greater ability to induce oxygen radicals, oxidative stress, pulmonary inflammation and adjuvant activity. Co-exposure of BALB/c mice to ovalbumin (OVA) and all tested NPs resulted in enhanced immune responses to OVA. The responses to co-exposure of OVA and the various NPs were not affected by the amount of doping or the level of acellular redox activity of the NPs, but the type of immune response was affected chemical composition of the NPs. The cytokine profiles showed that co-exposure to OVA and undoped or Zr-doped CeO₂ NPs primarily induced Th2 type responses, while co-exposure to OVA and undoped or Fe-doped Co₃O₄ NPs induced no or less marked increases in IgE plasma levels, BALF IL-4 and IL-5 concentrations and percentages of eosinophils in BALF, but more pronounced increases in BALF IL-6 concentrations and percentages of lymphocytes in BALF. In addition, co-exposure to OVA and Co₃O₄ NPs, but not CeO₂ NPs, induced lymphoid cell accumulation and ectopic lymphoid structures (ELS) in the lungs, which are normally absent in mice, but can be induced by inflammatory processes and infections.

***In vitro* inflammasome activation and dendritic cell maturation**

In vitro exposure of THP-1 macrophages to various NPs indicated that undoped and Zr-doped CeO₂ NPs induced inflammasome activation, while undoped and Fe-doped Co₃O₄ NPs did not (chapter 6). Inflammasomes are protein complexes that can be formed and activated in macrophages in reaction to various stimuli, such as bacteria, viruses, asbestos or NPs.

Inflammasome activation leads to the production of pro-inflammatory cytokines, including as IL-1 β .

Undoped Co₃O₄ NPs increased interleukine-12p40 (IL-12p40) production by dendritic cells, indicative for dendritic cell maturation, while undoped and Zr-doped CeO₂ NPs did not. Dendritic cell maturation is the process by which dendritic cells are further evolved or developed to enable antigen presentation and activation of T-cells. Doping effects of Co₃O₄ NPs on the IL-12p40 production were mixed.

Similar to the results of our *in vivo* study (chapter 5), the results of these *in vitro* assays indicate that the type of immune response of the NPs is primarily related to the chemical composition and not to the particle size or acellular redox activity of the NPs. Furthermore, a pronounced increase in IL-12p40 in dendritic cells *in vitro* seemed to be indicative for lymphoid accumulation in lung tissue *in vivo*. However, additional studies with NPs with different chemical compositions and *in vitro* assays covering other mechanisms are needed to more accurately predict the adjuvant activity of NPs *in vivo*.

Conclusions and future perspectives

Redox modification through Zr-doping of CeO₂ NPs and Fe-doping of Co₃O₄ NPs did not decrease the *in vitro* and *in vivo* toxicity and adjuvant activity of these NPs. The influence of the redox activity of these NPs on the investigated biological responses was very limited and did not follow a consequent trend of either an increase or a decrease with increasing redox activity. However, investigating the influence of redox activity on biological responses is complicated, as changing the redox activity of NPs usually also changes other properties, such as chemical composition. This makes it difficult to separate the effect of redox activity from that of the other NP properties. Furthermore, the redox activity of NPs may change over time due to interaction of the NPs with their surrounding environment. The environmental conditions, including pH and the presence of proteins and salt, are different in the various *in vitro* and *in vivo* toxicity assays and may change over time throughout the assay. Therefore, a combination of different assays and environmental conditions is needed to investigate the influence of the redox activity of a NP on the outcome of a toxicological assay. The choice of these assays and environmental conditions should be based on the chemical composition of the NP under investigation and the specific environmental conditions the NP is expected to encounter in the toxicity assay.

Although the role of redox activity in the toxicity of NPs cannot be ruled out, the results of the *in vitro* and *in vivo* assays described in this thesis indicate that other physicochemical properties of the tested NPs, including particle size, dissolution and chemical composition, are more important determinants of the investigated biological responses. Also for particle size, dissolution and chemical composition it is important to assess how they may change

over time depending on their surrounding environment. The results of our *in vitro* multi-omic study demonstrate the advantage of designing a toxicity assay in such a way that the influence of environmental conditions over time can be taken into account. By including ionic controls in the study design, measuring the molecular responses over time, and performing dissolution testing in cell culture medium, it was possible to investigate the influence of relevant environmental conditions on the dissolution of the Ag and ZnO NPs and the subsequent development and reversibility or persistence of the observed molecular responses. This shows that knowledge on changes within physicochemical properties of the NPs under the environmental conditions relevant for the toxicological assay is needed to evaluate the influence of the different physicochemical properties on the outcome of the toxicological assay. Consequently, variabilities in environmental conditions within the various toxicity assays used to investigate the potential toxicological effects of NPs often hampers comparisons between adverse effects of NPs with different characteristics across different studies. Hence, more systematic research and harmonization or standardization of the various *in vitro* and *in vivo* assays to evaluate the potential toxicity of NPs is needed.

Another challenge when investigating the influence of physicochemical properties on the biological responses of NPs is that there is usually more than one mechanistic pathway by which NPs can cause a specific biological response. This was demonstrated by the results of the *in vivo* study on the adjuvant activity and the *in vitro* studies on inflammasome activation and dendritic cell maturation. The adjuvant potency of the different NPs *in vivo* varied with the different immune responses and indicated that different immunological pathways are involved in the adjuvant activity of undoped and Zr-doped CeO₂ NPs compared to undoped and Fe-doped Co₃O₄ NPs. Lymphoid cell accumulation and formation of ectopic lymphoid tissues in the lungs only occurred after co-exposure to OVA and undoped or Fe-doped Co₃O₄ NPs. The outcomes of the *in vitro* studies indicated that undoped and Zr-doped CeO₂ NPs induced inflammasome activation, while several undoped and Fe-doped Co₃O₄ NPs induced dendritic cell maturation. The ranking of the various NPs with respect to their *in vitro* IL-12p40 response was similar to the ranking of their *in vivo* B-cell density in the lungs, indicating that the results of the dendritic cell maturation assay may be indicative for the potential of NPs to induce *in vivo* ectopic lymphoid tissues in lungs. However, the type of immune responses observed *in vivo* cannot be readily predicted using *in vitro* assays on dendritic cell maturation and inflammasome activation alone, since these assays only cover two of the key events in the AOP network on respiratory allergic responses.

The results of the research presented in this thesis provides more insight how some physicochemical properties and environmental conditions may influence various biological responses after exposure to NPs in the lung. The challenge for future research is to fill the remaining knowledge gaps on how the various physicochemical properties, environmental conditions and underlying mechanistic pathways are connected to each other.

Samenvatting

Nanotechnologie maakt het mogelijk om producten te ontwikkelen met uitzonderlijke kwaliteiten. Door de verschillende eigenschappen van nanomaterialen (NMs) te veranderen is het mogelijk om materialen te ontwikkelen met buitengewoon aantrekkelijke functionaliteiten. Er is nog veel onduidelijk over hoe deze veranderingen onze gezondheid mogelijk nadelig kunnen beïnvloeden. Meer kennis over de invloed van de verschillende fysisch-chemische eigenschappen op de mogelijke gezondheidseffecten zal het mogelijk maken om aantrekkelijke NMs te ontwikkelen zonder de risico's voor de gezondheid te vergroten.

Het belangrijkste doel van het onderzoek dat in dit proefschrift wordt beschreven is om te onderzoeken hoe de fysisch-chemische eigenschappen van NMs van invloed kunnen zijn op de veronderstelde toxicologische werkingsmechanismen van NMs na inhalatie. Hiervoor werd een zorgvuldig geselecteerde reeks *in vivo* en *in vitro* toxiciteitstesten gebruikt in combinatie met een zorgvuldig geselecteerde set van binnen het Europese NanoMILE-project gesynthetiseerd NMs met specifieke eigenschappen. Het doel en de aanpak van het onderzoek kunnen worden vertaald in de volgende onderzoeksdoelstellingen:

1. Het bepalen van de invloed van deeltjesgrootte en redoxactiviteit van ongedopeerde en zirkonium(Zr)gedopeerde ceriumdioxide (CeO_2) NMs op de long depositie, biodistributie en pulmonaire (en cardiovasculaire) effecten in muizen en ratten na inhalatie (hoofdstuk 2 en 3).
2. Het onderzoeken van de invloed van oplosbaarheid en redoxactiviteit van zilver (Ag), zinkoxide (ZnO) en ongedopeerde en Zr-gedopeerde CeO_2 NMs op de moleculaire mechanismen waarmee deze NMs *in vitro* toxiciteit induceren in A549-cellen (hoofdstuk 4).
3. Het evalueren van de invloed van de chemische samenstelling en redoxactiviteit van ongedopeerde en Zr-gedopeerde CeO_2 en ongedopeerde en ijzer(Fe)-gedopeerde kobaltoxide (Co_3O_4) NMs op de adjuverende werking *in vivo* (hoofdstuk 5).
4. Het bestuderen van de invloed van de chemische samenstelling en redoxactiviteit van ongedopeerde en Zr-gedopeerde CeO_2 en ongedopeerde en Fe-gedopeerde Co_3O_4 NMs op *in vitro* inflammasoom activatie en dendritische cel maturatie (hoofdstuk 6).

De centrale hypothese was dat redoxmodificatie (het veranderen van de mate waarin de NMs kunnen oxideren of reduceren) door Zr-dopering van CeO_2 en Fe-dopering van Co_3O_4 NMs zou leiden tot een afname van het vermogen van de NMs om reactieve zuurstofradicalen, oxidatieve stress en daaropvolgende *in vitro* en *in vivo* toxiciteit en *in vivo* adjuvantie te veroorzaken. Daarnaast wordt verwacht dat de toxicologische werkingsmechanismen van

Ag en ZnO NMs gerelateerd zijn aan hun oplosbaarheid en het vermogen om metaalionen af te geven.

***In vivo* biodistributie en toxiciteit na inademing**

De invloed van redoxactiviteit van CeO₂ NMs op de biodistributie, pulmonaire en cardiovasculaire effecten na inademing werd onderzocht door muizen aan CeO₂ NMs met wisselende hoeveelheden Zr-dopering (0%, 27% of 78% Zr) bloot te stellen (hoofdstuk 2). Gezonde muizen (C57BL/6), muizen die vatbaar zijn voor hart- en vaatziekten (ApoE^{-/-}, westerse voeding) en een muismodel van neurologische aandoeningen (5xFAD) werden gedurende een periode van vier weken blootgesteld via “nose only” inhalatie (4 mg/m³ gedurende 3 uur/dag, 5 dagen/week). De effecten werden vier weken na blootstelling bepaald.

In alle drie de muismodellen veroorzaakte blootstelling aan 4 mg CeO₂ NMs/m³ alleen minimale toxicologische effecten, waaronder enkele geringe ontstekingsreacties in de longen die niet gerelateerd waren aan de hoeveelheid Zr-dopering. In ApoE^{-/-} muizen veranderde CeO₂ NM-blootstelling de grootte van atherosclerotische plaques ten opzichte van niet blootgestelde dieren niet, maar was er wel een trend zichtbaar waarbij een verhoogd Zr-gehalte van de CeO₂ NMs tot een verhoogd gehalte aan ontstekingscellen in de plaques in de truncus branchiocephalicus leidde. Deze bevindingen geven aan dat redoxmodificatie van CeO₂ NMs via Zr-dopering weinig invloed heeft op de pulmonaire en cardiovasculaire toxiciteit na subchronische blootstelling. Omdat echter slechts minimale effecten werden waargenomen na blootstelling aan 4 mg/m³ CeO₂ NMs zonder Zr-dopering, was de veronderstelde vermindering van de toxiciteit als gevolg van de Zr-dopering mogelijk niet zichtbaar in deze studie.

In vergelijking met andere inhalatiestudies met CeO₂ NMs waren de waargenomen toxicologische effecten in onze studie inderdaad relatief mild. Een gedetailleerde analyse van de gegevens van verschillende inhalatiestudies met verschillende blootstellingsduur, diersoorten en typen CeO₂ NMs, gaf aan dat de verschillen in de waargenomen toxiciteit tussen deze studies verklaard kunnen worden doordat ratten over het algemeen gevoeliger zijn voor de effecten van blootstelling aan deeltjes dan muizen en door verschillen in kinetiek van de NMs (hoofdstuk 3). Verschillen in diersoort en kinetiek konden de verschillen in waargenomen toxiciteit in de geanalyseerde onderzoeken echter niet volledig verklaren, wat erop wijst dat pulmonaire reacties niet alleen afhangen van de diersoort en NM-eigenschappen die de kinetiek beïnvloeden, zoals de deeltjesgrootte, maar ook van andere fysisch-chemische eigenschappen van de NMs.

Moleculaire mechanismen van *in vitro* toxiciteit

De invloed van redoxmodificatie van CeO₂ NMs via Zr-dopering werd verder onderzocht door de moleculaire routes te onderzoeken waarmee ongedopeerde en Zr-gedopeerde CeO₂ NMs *in vitro* toxiciteit induceren in een multi-omics studie (hoofdstuk 4). Naast de invloed van redoxactiviteit van ongedopeerde en Zr-gedopeerde CeO₂ NMs, werd in deze studie ook de invloed van de oplosbaarheid of het vermogen om metaalionen af te geven op de moleculaire mechanismen van *in vitro* toxiciteit van Ag en ZnO NMs onderzocht. Humane longepitheel cellen (A549) werden gedurende 24 uur blootgesteld aan verschillende Ag, ZnO en CeO₂ NMs, Ag en ZnO microdeeltjes, Ag ionen (Ag⁺) en zink ionen (Zn²⁺). Moleculaire responses werden gekarakteriseerd bij blootstellingsniveaus die ~20% cytotoxiciteit veroorzaakten. Lipidomics en polaire metabolomics analyses werden uitgevoerd met behulp van directe infusie massaspectrometrie (DIMS) en transcriptomics analyses met behulp van RNA sequencing.

Blootstelling aan ongedopeerde en Zr-gedopeerde CeO₂ NMs vertoonde opmerkelijk minder cytotoxiciteit in vergelijking met de vorige *in vitro* studie met dezelfde NMs in hetzelfde celttype (A549) (hoofdstuk 2). Bovendien veroorzaakten CeO₂ NMs weinig moleculaire veranderingen, welke slechts een gering bewijs vormde voor het veroorzaken van oxidatieve stress voor slechts één van de vier geteste CeO₂ NMs. Deze resultaten geven aan dat de invloed van redoxactiviteit op het veronderstelde toxicologische werkingsmechanisme van oxidatieve stress van CeO₂ NMs zeer beperkt was.

Alle blootstellingen aan Ag, Zn en ZnO deeltjes en ionen resulteerden in significante metabole en transcriptionele responses. De meerderheid van deze moleculaire veranderingen waren kenmerkend voor blootstelling aan metaalionen en werden zowel na blootstelling aan ionen als aan NMs gevonden wat bevestigt dat de werkingsmechanismen van deze NMs grotendeels worden bepaald door opgeloste metaalionen in plaats van door de fysieke aspecten van de NMs. De moleculaire veranderingen waren tijdsafhankelijk, wat verklaard kan worden door verschillen in de opname- en oplossingssnelheden, waardoor verschillen in de concentraties van de metaalionen in de cel en de verschillende compartimenten van de cel ontstaan. De tijdsafhankelijkheid van de moleculaire veranderingen kan ook worden verklaard door adaptieve veranderingen, zoals inductie van metallothioneïnen die cellulaire schade verminderen door de metaalionen te binden.

Adjuverende werking *in vivo*

De invloed van redoxactiviteit op de adjuverende werking van NMs werd onderzocht in een muismodel voor allergische astma (hoofdstuk 5). Aangezien Zr-dopering van CeO₂ NMs een beperkt effect had op de ontstekingsreacties na inhalatie, werden additionele NMs in deze *in vivo* studie opgenomen. Hiervoor werden Fe-gedopeerde Co₃O₄ NMs geselecteerd omdat verwacht werd dat deze NMs een groter vermogen zouden hebben om zuurstofradicalen,

oxidatieve stress, ontstekingsreacties en adjuverende activiteit te induceren. Gelijktijdige blootstelling van BALB/c-muizen aan ovalbumine (OVA) en alle geteste NMs resulteerde in verhoogde immunoresponses als reactie op blootstelling aan OVA. De responses op blootstelling aan OVA in combinatie met verschillende NMs werden niet beïnvloed door de hoeveelheid dopering of de acellulaire redoxactiviteit van de NMs. Wel werd het type immunorespons beïnvloed door de chemische samenstelling van de NMs. De cytokineprofielen toonden aan dat gelijktijdige blootstelling aan OVA en ongedopeerde of Zr-gedopeerde CeO_2 NMs voornamelijk Th2-type responses induceerde. Gelijktijdige blootstelling aan OVA en ongedopeerde of Fe-gedopeerde Co_3O_4 NMs induceerde geen of minder duidelijke verhogingen van IgE-plasmaspiegels, BALF IL-4- en IL-5-concentraties en percentages eosinofielen in BALF, maar wel een meer uitgesproken stijging in de BALF IL-6-concentratie en het percentage lymfocyten in BALF. Daarnaast induceerde co-blootstelling aan OVA en Co_3O_4 NMs in tegenstelling tot CeO_2 NMs, ook accumulatie van lymfoïde cellen en ectopische lymfoïde structuren (ELS) in de longen, welke onder normale omstandigheden afwezig zijn bij muizen, maar geïnduceerd kunnen worden door ontstekingsprocessen en infecties.

***In vitro* inflammasoom activatie en dendritische cel maturatie**

De resultaten van de *in vitro* testen waarin THP-1-macrofagen werden blootgesteld aan verschillende NMs gaven aan dat ongedopeerde en Zr-gedopeerde CeO_2 NMs inflammasoom activatie induceerden, terwijl ongedopeerde en Fe-gedopeerde Co_3O_4 NMs dat niet deden (hoofdstuk 6). Een inflammasoom is een complex van eiwitten dat in macrofagen gevormd en geactiveerd kan worden in reactie op verschillende stimuli, zoals bacteriën, virussen, asbest of NMs. De activatie van een inflammasoom leidt tot de productie van pro-inflammatoire cytokines, waaronder IL-1 β .

Niet-gedopeerde Co_3O_4 -NMs verhoogden de productie van interleukine-12p40 (IL-12p40) door dendritische cellen, wat indicatief is voor dendritische cel maturatie, terwijl ongedopeerde en Zr-gedopeerde CeO_2 -NMs dat niet deden. Maturatie van dendritische cellen is de rijping van dendritische cellen, waardoor antigen presentatie en activatie van T-cellen plaats kan vinden. Het effect van Fe-dopering van Co_3O_4 -NMs op de IL-12p40-productie was niet eenduidig.

Vergelijkbaar met de resultaten van onze *in vivo* studie (hoofdstuk 5), geven de resultaten van deze *in vitro* testen aan dat het type immunorespons van de NMs primair gerelateerd is aan de chemische samenstelling en niet aan de deeltjesgrootte of de acellulaire redoxactiviteit van de NMs. Daarnaast leek een uitgesproken toename van IL-12p40 in dendritische cellen *in vitro* indicatief te zijn voor *in vivo* accumulatie van lymfoïde cellen in de longen. Er zijn echter aanvullende studies met NMs van verschillende chemische samenstellingen en *in*

in vitro testen die andere mechanismen omvatten nodig om de adjuverende werking van NMs *in vivo* nauwkeuriger te kunnen voorspellen.

Conclusies en toekomstperspectieven

Redoxmodificatie van CeO₂ NMs door Zr-dopering en van Co₃O₄ NMs door Fe-dopering verminderde de *in vitro* en *in vivo* toxiciteit en adjuverende werking deze NMs niet. De invloed van de redoxactiviteit van deze NMs op de onderzochte biologische processen was zeer beperkt en volgde geen consequente trend door toe- of af te nemen naarmate de redoxactiviteit toe nam. Het onderzoeken van de invloed van redoxactiviteit op biologische processen is echter gecompliceerd, aangezien het veranderen van de redoxactiviteit van NMs meestal ook andere eigenschappen verandert, zoals de chemische samenstelling. Dit maakt het moeilijk om het effect van redoxactiviteit te scheiden van dat van de andere NM-eigenschappen. Bovendien kan de redoxactiviteit van NMs in de loop van de tijd veranderen als gevolg van de interactie van de NMs met hun omgeving. De omgevingscondities, zoals de pH en de aanwezigheid van eiwitten en zouten, zijn verschillend in de verschillende *in vitro* en *in vivo* toxiciteitstesten en kunnen in het verloop van een test veranderen. Daarom is een combinatie van verschillende testen en omgevingsomstandigheden nodig om de invloed van de redoxactiviteit van een NM op de uitkomst van een toxiciteitstest te onderzoeken. De keuze van deze testen en omgevingscondities moet gebaseerd zijn op de chemische samenstelling van het onderzochte NM en de specifieke omgevingscondities die het NM naar verwachting zal tegenkomen in de toxiciteitstesten.

Hoewel niet kan worden uitgesloten dat redoxactiviteit een rol speelt in de toxiciteit van NMs, geven de resultaten van de *in vitro* en *in vivo* testen die in dit proefschrift worden beschreven aan dat andere eigenschappen van de geteste NMs, waaronder deeltjesgrootte, oplosbaarheid en chemische samenstelling, belangrijkere determinanten van de onderzochte biologische processen zijn. Ook voor deeltjesgrootte, oplosbaarheid en chemische samenstelling is het belangrijk om te beoordelen hoe deze eigenschappen in de loop van de tijd kunnen veranderen, afhankelijk van hun omgeving. De resultaten van de *in vitro* multi-omic studie (hoofdstuk 4) tonen het nut aan van een studieopzet waarbij rekening is gehouden met de invloed van omgevingsfactoren in de tijd. Door ionen controles mee te nemen, de moleculaire responses in de tijd te meten en oplosbaarheidstesten uit te voeren in celkweekmedium, was het mogelijk om de invloed van relevante omgevingscondities op de oplosbaarheid van de Ag en ZnO NMs en de daaropvolgende ontwikkeling en reversibiliteit van de waargenomen moleculaire responses te onderzoeken. Dit voorbeeld laat zien dat kennis over veranderingen in eigenschappen van de NMs onder voor de toxiciteitstest relevante omgevingscondities nodig is om de invloed van de verschillende fysisch-chemische eigenschappen op de uitkomst van de toxiciteitstest te evalueren. Nu worden vergelijkingen van de nadelige effecten van NMs met verschillende eigenschappen tussen verschillende onderzoeken vaak worden belemmerd door verschillen in de omgevingscondities die in de

verschillende toxiciteitstesten worden gebruikt. Daarom is meer systematisch onderzoek en harmonisatie of standaardisatie van de verschillende *in vitro* en *in vivo* testen nodig voor de evaluatie van de potentiële toxiciteit van NMs.

Een andere uitdaging bij het onderzoeken van de invloed van fysisch-chemische eigenschappen van NMs op de biologische reacties is dat er meestal meer dan één toxicologisch werkingsmechanisme is waarmee NMs een specifieke biologische reactie kunnen veroorzaken. Dit werd gedemonstreerd door de resultaten van de *in vivo* studie naar de adjuverende werking en de *in vitro* studies naar inflammasoom activatie en dendritische cel maturatie. De adjuverende activiteit van de verschillende NMs *in vivo* varieerde voor de verschillende immuunresponses wat aan geeft dat verschillende immunologische processen betrokken zijn bij de adjuverende werking van ongedopeerde en Zr-gedopeerde CeO₂ NMs in vergelijking met ongedopeerde en Fe-gedopeerde Co₃O₄ NMs. Accumulatie van lymfoïde cellen en vorming van ectopisch lymfoïde weefsels in de longen trad alleen op na gelijktijdige blootstelling aan OVA en ongedopeerde of Fe-gedopeerde Co₃O₄ NMs. De resultaten van de *in vitro* studies gaven aan dat ongedopeerde en Zr-gedopeerde CeO₂ NMs inflammasoom activatie induceerden, terwijl verschillende ongedopeerde en Fe-gedopeerde Co₃O₄ NMs dendritische cel maturatie induceerden. De ranking van de verschillende NMs met betrekking tot hun *in vitro* IL-12p40-respons was vergelijkbaar met de ranking van hun *in vivo* B-celdichtheid in de longen, wat aangeeft dat de resultaten van de dendritische cel maturatie test indicatief kunnen zijn voor de potentie van NMs om *in vivo* ectopisch lymfoïde weefsels in de longen te induceren. Het type immuunrespons dat *in vivo* wordt waargenomen kan echter niet gemakkelijk worden voorspeld met behulp van alleen *in vitro* testen voor inflammasoom activatie en dendritische cel maturatie, aangezien deze testen slechts twee belangrijke werkingsmechanismen in het AOP-netwerk voor respiratoire allergische reacties omvatten.

De uitkomsten van het onderzoek die in dit proefschrift worden beschreven, geven meer inzicht in hoe een aantal fysisch-chemische eigenschappen en omgevingsfactoren verschillende biologische reacties van NMs kunnen beïnvloeden. De uitdaging voor toekomstig onderzoek is om de resterende kennishiaten over hoe de verschillende fysisch-chemische eigenschappen en omgevingscondities elkaar en de onderliggende werkingsmechanismen kunnen beïnvloeden op te vullen.

Curriculum vitea

Susan Dekkers was born on May 5th 1975 in Utrecht. After graduating from her secondary school (VWO), she attended a one year exchange programme at a High School in the USA. In 1994 she started studying Health Sciences at the Maastricht University and received her BSc degree in 1995, followed by her MSc degree in Environmental Health Sciences in 2000. Before starting her PhD research, Susan worked for several years as a toxicological risk assessor first at TNO and later at RIVM. Within her job at RIVM she was given the opportunity to perform her PhD research. In January 2021, Susan returned to TNO to work on the development and application of innovative and *in silico* methods in the toxicological risk assessment.

List of publications

Gimeno-Benito I, Guisti A, Dekkers S, Haase A, Janer G. A review to support the derivation of a worst-case dermal penetration value for nanoparticles. *Regul Toxicol Pharmacol.* 2021 Feb;119:104836. doi: 10.1016/j.yrtph.2020.104836.

Dekkers S, Wijnhoven SWP, Braakhuis HM, Soeteman-Hernandez LG, Sips AJAM, Tavernaro I, Kraegeloh A, Noorlander CW. Safe-by-Design part I: Proposal for nanospecific human health safety aspects needed along the innovation process. *NanoImpact.* 2020; 18: 100227. doi.org/10.1016/j.impact.2020.100227.

Wahle T, Sofranko A, Dekkers S, Miller MR, Heusinkveld HJ, Albrecht C, Cassee FR, Schins RPF. Evaluation of neurological effects of cerium dioxide nanoparticles doped with different amounts of zirconium following inhalation exposure in mouse models of Alzheimer's and vascular disease. *Neurochem Int.* 2020 Sep;138:104755. doi:10.1016/j.neuint.2020.104755.

Stone V, Stefania Gottardo S, Bleeker EAJ, Braakhuis H, Dekkers S, Fernandes T, Haase A, Hunt N, Hristozov D, Jantunen P, Jeliaskova N, Johnston H, Lamon L, Murphy F, Rasmussen K, Rauscher H, Sánchez Jiménez A, Svendsen C, Spurgeon D, Vázquez-Campos S, Wohlleben W, Oomen AG. A framework for grouping and read-across of nanomaterials- supporting innovation and risk assessment. *Nano Today.* 2020; 35: 100941. doi.org/10.1016/j.nantod.2020.100941.

Nymark P, Bakker M, Dekkers S, Franken R, Fransman W, García-Bilbao A, Greco D, Gulumian M, Hadrup N, Halappanavar S, Hongisto V, Hougaard KS, Jensen KA, Kohonen P, Koivisto AJ, Dal Maso M, Oosterwijk T, Poikkimäki M, Rodriguez-Llopis I, Stierum R, Sørli JB, Grafström R. Toward Rigorous Materials Production: New Approach Methodologies Have Extensive Potential to Improve Current Safety Assessment Practices. *Small.* 2020 Feb;16(6):e1904749. doi: 10.1002/sml.201904749.

Soeteman-Hernández LG, Blab GA, Carattino A, Dekker F, Dekkers S, van der Linden M, van Silfhout A, Noorlander CW. Challenges of implementing nano-specific safety and safe-by-design principles in academia. *NanoImpact*. 2020; 19, 100243. doi.org/10.1016/j.impact.2020.100243.

Dekkers S, Wagner JG, Vandebriel RJ, Eldridge EA, Tang SVY, Miller MR, Römer I, de Jong WH, Harkema JR, Cassee FR. Role of chemical composition and redox modification of poorly soluble nanomaterials on their ability to enhance allergic airway sensitisation in mice. Part I. *Fibre Toxicol*. 2019 Oct 28;16(1):39. doi: 10.1186/s12989-019-0320-6.

Soeteman-Hernandez LG, Apostolova MD, Bekker C, Dekkers S, Grafström RC, Groenewold M, Handzhiyski Y, Herbeck-Engel P, Hoehener K, Karagkiozaki V, Kelly S, Kraegeloh A, Logothetidis S, Micheletti C, Nymark P, Oomen AG, Oosterwijk T, Rodríguez-Lopis I, Sabella S, Sanchez Jiménez A, Sips AJAM, Suarez- Merino B, Tavernaro I, van Engelen J, Wijnhoven SWP, Noorlander CW. Safe Innovation Approach: Towards an agile system for dealing with innovations. *Materials Today Communications*. 2019; 20:100548. doi: 10.1016/j.mtcomm.2019.100548.

Oomen AG, Steinhäuser KG, Bleeker EAJ, van Broekhuizen F, Sips A, Dekkers S, Wijnhoven SWP, Sayre PG. Risk assessment frameworks for nanomaterials: Scope, link to regulations, applicability, and outline for future directions in view of needed increase in efficiency. *NanoImpact*. 2018; 9: 1-13. doi.org/10.1016/j.impact.2017.09.001.

Dekkers S, Ma-Hock L, Lynch I, Russ M, Miller MR, Schins RPF, Keller J, Römer I, Küttler K, Strauss V, De Jong WH, Landsiedel R, Cassee FR. Differences in the Toxicity of Cerium Dioxide Nanomaterials after Inhalation can be explained by Lung Deposition. *Animal Species and Nanoforms. Inhalation Toxicology*, 2018; 30:7-8, 273-286, doi: 10.1080/08958378.2018.1516834.

Yang Y, Xu L, Dekkers S, Zhang LG, Cassee FR, Zuo YY. Aggregation State of Metal-Based Nanomaterials at the Pulmonary Surfactant Film Determines Biophysical Inhibition. *Environ Sci Technol*. 2018 Aug 7;52(15):8920-8929. doi: 10.1021/acs.est.8b02976.

Dekkers S, Williams TD, Zhang J, Zhou J, Vandebriel RJ, De La Fonteyne LJJ, Gremmer ER, He S, Guggenheim EJ, Lynch I, Cassee FR, De Jong WH, Viant MR. Multi-omics approaches confirm metal ions mediate the main toxicological pathways of metal-bearing nanoparticles in lung epithelial A549 cells. *Environ. Sci.: Nano*, 2018; 5, 1506. doi: 10.1039/c8en00071a.

Dekkers S, Miller MR, Schins RPF, Römer I, Russ M, Vandebriel RJ, Lynch I, Belinga-Desaunay M, Valsami-Jones E, Connell SP, Smith IP, Duffin R, Boere JAF, Heusinkveld HJ, Albrecht C, de Jong WH, Cassee FR. The effect of zirconium doping of cerium dioxide nanoparticles

on pulmonary and cardiovascular toxicity and biodistribution in mice after inhalation. *Nanotoxicology*. 2017 Aug;11(6):794-808. doi: 10.1080/17435390.2017.1357214.

Dekkers S, Oomen AG, Bleeker EA, Vandebriel RJ, Micheletti C, Cabellos J, Janer G, Fuentes N, Vázquez-Campos S, Borges T, Silva MJ, Prina-Mello A, Movia D, Nesslany F, Ribeiro AR, Leite PE, Groenewold M, Cassee FR, Sips AJ, Dijkzeul A, van Teunenbroek T, Wijnhoven SW. Towards a nanospecific approach for risk assessment. *Regul Toxicol Pharmacol*. 2016 May 30; 80:46-59. doi: 10.1016/j.yrtph.2016.05.037.

Vandebriel RJ, Dekkers S, de Jong WH, Cassee FR. An Update on NLRP3 Inflammasome Activation by Engineered Nanomaterials. *Current Bionanotechnology*, 2016; 2(1): 40-46. doi 10.2174/2213529402666160601122127.

van Kesteren PC, Cubadda F, Bouwmeester H, van Eijkeren JC, Dekkers S, de Jong WH, Oomen AG. Novel insights into the risk assessment of the nanomaterial synthetic amorphous silica, additive E551, in food. *Nanotoxicology*. 2015 May; 9(4):442-52. doi: 10.3109/17435390.2014.940408.

Dekkers S, Bouwmeester H, Bos P, Peters R, Rietveld A, Oomen A. Knowledge gaps in risk assessment of nanosilica in food: evaluation of the dissolution and toxicity of different forms of silica. *Nanotoxicology*. 2013 Jun; 7(4):367-77. doi: 10.3109/17435390.2012.662250.

Dekkers S, Krystek P, Peters RJ, Lankveld DP, Bokkers BG, van Hoeven-Arentzen PH, Bouwmeester H, Oomen AG. Presence and risks of nanosilica in food products. *Nanotoxicology*. 2011 Sep;5(3):393-405. doi: 10.3109/17435390.2010.519836.

Jeurissen SMF, Seyhan F, Kandhai MC, Dekkers S, Booij CJH, Bos PMJ, van der Fels-Klerx HJ. An indicator based 'traffic light' model to pro-actively assess the occurrence of mycotoxins in tree nuts. *World Mycotoxin J*. 2011; 494:405-12. doi.org/10.3920/WMJ2010.1278

van der Fels-Klerx HJ, Dekkers S, Kandhai MC, Jeurissen SMF, Booij CJH, de Heer C. Indicators for early identification of re-emerging mycotoxins. *NJAS Wag J Life Sci* 2010; 57(2):133-9. doi.org/10.1016/j.njas.2010.02.003

Wijnhoven SWP, Herberts C, Hagens WI, Oomen A, Heugens E, Roszek B, Bisschops J, Peijnenburg W, Gosens I, Van de Meent D, Dekkers S, De Heer C, Sips AJAM, De Jong W, Van Zijverden M, Geertsma R. Nano-silver, a review of available data and knowledge gaps in human and environmental risk assessment. *Nanotoxicology*, 2009 June; 3(2), 1-30 (2009). doi.org/10.1080/17435390902725914

Miraglia M, Marvin HJ, Kleter GA, Battilani P, Brera C, Coni E, Cubadda F, Croci L, De Santis B, Dekkers S, Filippi L, Hutjes RW, Noordam MY, Pisante M, Piva G, Prandini A, Toti L, van den Born GJ, Vespermann A. Climate change and food safety: an emerging issue with special focus on Europe. *Food Chem Toxicol*. 2009 May;47(5):1009-21. doi: 10.1016/j.fct.2009.02.005.

Bouwmeester H, Dekkers S, Noordam MY, Hagens WI, Bulder AS, de Heer C, ten Voorde SE, Wijnhoven SW, Marvin HJ, Sips AJ. Review of health safety aspects of nanotechnologies in food production. *Regul Toxicol Pharmacol*. 2009 Feb; 53(1):52-62. doi: 10.1016/j.yrtph.2008.10.008.

Marvin HJ, Kleter GA, Prandini A, Dekkers S, Bolton DJ. Early identification systems for emerging foodborne hazards. *Food Chem Toxicol*. 2009 May;47(5):915-26. doi: 10.1016/j.fct.2007.12.021.

Freidig AP, Dekkers S, Verwei M, Zvinavashe E, Bessems JG, van de Sandt JJ. Development of a QSAR for worst case estimates of acute toxicity of chemically reactive compounds. *Toxicol Lett*. 2007 May 15; 170(3):214-22. doi: 10.1016/j.toxlet.2007.03.008.

Dekkers S, Telman J, Rennen MA, Appel MJ, de Heer C. Within-animal variation as an indication of the minimal magnitude of the critical effect size for continuous toxicological parameters applicable in the benchmark dose approach. *Risk Anal*. 2006 Aug; 26(4):867-80. doi: 10.1111/j.1539-6924.2006.00784.x.

Goldbohm RA, Tielemans EL, Heederik D, Rubingh CM, Dekkers S, Willems MI, Dinant Kroese E. Risk estimation for carcinogens based on epidemiological data: a structured approach, illustrated by an example on chromium. *Regul Toxicol Pharmacol*. 2006 Apr; 44(3):294-310. doi: 10.1016/j.yrtph.2006.01.007.

Dekkers S, de Heer C, Rennen MA. Critical effect sizes in toxicological risk assessment: a comprehensive and critical evaluation. *Environ Toxicol Pharmacol*. 2001 Jun;10(1-2):33-52. doi:10.1016/s1382-6689(01)00068-0.

Dankwoord

Midden in de Corona lock-down kijk ik terug en realiseer ik me dat ik het heel erg getroffen heb met zoveel behulpzame, begripvolle en lieve begeleiders, collega's, vrienden en familieleden. Juist nu ik bijna alleen nog maar online contact met anderen heb, besef ik dat ik mijn waardering voor iedereen die aan de totstandkoming van dit proefschrift heeft bijgedragen veel te weinig heb laten blijken. Gelukkig heb ik vaak horen zeggen dat het dankwoord het meest gelezen hoofdstuk van menig proefschrift is, dus zie ik het als een kans om iedereen die mij bij deze klus geholpen en gesteund hebben hier alsnog (of nogmaals) te bedanken.

Allereerst wil ik natuurlijk mijn promotoren en co-promoteren bedanken. Flemming, bedankt voor de kans die jij mij gegeven hebt om te kunnen promoveren. Ik weet nog dat jij in de bus op weg naar een werkbezoek van de nanowerkgroep aan MESA+ vroeg of iemand misschien een geschikte kandidaat voor een PhD binnen het NANOMILE project wist. Toen ik eruit flapte dat mij dat zelf wel interessant leek, vroeg je gelijk of ik dat serieus meende en heb je me vervolgens geholpen om dit binnen mijn aanstelling bij het RIVM voor elkaar te krijgen. Bedankt ook voor je vertrouwen, steun, advies en kritische blik, maar vooral ook voor je onuitputtelijke optimisme en de vele introducties bij collega's binnen jouw netwerk. Jouw netwerk bleek voor mij een haast onuitputtelijke bron aan mogelijke samenwerkingen met veel verschillende instituten zowel binnen als buiten het NANOMILE consortium te zijn. Van het Nederlandse PamGene tot aan de Michigan State University. Helaas hebben niet al deze initiatieven ook tot wetenschappelijke publicaties geleid, maar dat lag vooral aan tijdgebrek vanuit mijn kant. Bert, bedankt voor je kritische en motiverende opmerkingen over de voortgang van mijn promotieonderzoek. Ondanks dat je inhoudelijk wat meer afstand tot dit onderzoek had, wist jij me in onze voortgangsgesprekken wel te motiveren om niet alleen aandacht en tijd aan de uitvoering, maar ook aan het schrijfwerk te besteden. Helaas, was deze motivatie alleen niet genoeg en bleek het in de praktijk toch lastig om het schrijven prioriteit te geven, waardoor dit langer duurde dan eigenlijk de bedoeling was. Rob en Wim bedankt voor jullie begeleiding. Omdat ik regelmatig drie tegenstrijdige adviezen van jullie en Flemming kreeg, heb ik heel veel van jullie geleerd en veel aan jullie kennis en expertise gehad. Daarnaast heb ik ook nog veel plezier met jullie beleefd tijdens de verschillende consortium meetings en andere internationale bijeenkomsten.

Daarnaast wil ik mijn collega's bij DMG bedanken. Daan, John en Paul bedankt voor het meedenken en uitvoeren van alle praktische, technische, analytische en logistieke uitdagingen in mijn eerste en gelijk ongekend ingewikkelde inhalatie studie met heel veel verschillende experimentele groepen, samples, tijdschema's, epjes en buizen. Jullie hebben me meerdere keren op de kast gekregen, maar daar zat ik graag om het overzicht te kunnen behouden. Harm, Ilse en Miriam, fijn dat ik jullie altijd even lastig kon vallen met een vraag

of voor de nodige afleiding tijdens de gezellige koffiepauzes of het saaie stickeren (wat een stuk sneller gaat onder begeleiding van motiverende Spaanse ska). Ilse en Harm, wat fijn dat jullie mijn paranimfen willen zijn. Elise, Arjen, Angelique, Ingrid en Kelly bedankt voor de gezelligheid, het aanhoren van mijn frustraties en de toren-C-momentjes op vrijdag. Elmer, Geert, Rory, Jason, Jia en Jasper bedankt voor jullie inzet en bijdrage aan het onderzoek tijdens jullie stage. Dank ook aan de collega's van Intravacc voor hun bijdrage aan de uitvoering van de *in vivo* studies. Verder wil ik ook een aantal collega's bij GZB bedanken. Jolanda, Liset en Eric bedankt voor jullie hulp bij het *in vitro* werk en met name Jolanda voor je hulp bij het begeleiden van de stagiaires. Liset, Bhawani, Piet, Eric, Jolanda en Christina bedankt voor de analyse van de samples uit de *in vivo* studies en de endotoxine bepalingen. Bedankt ook Cees, Theo, Elske en Jan van VSP voor de mogelijkheid die jullie me hebben gegeven om dit onderzoek binnen mijn RIVM aanstelling te kunnen uitvoeren. En natuurlijk ook alle collega's van de nanowerkgroep en VSP voor hun interesse en lef om ook lang na de afronding van het NanoMILE project nog te durven vragen hoe het met mijn promotieonderzoek ging.

Many thanks (in English) to all international colleagues that contributed to this research within and outside the NanoMILE project. Mark, Roel (although you are not really an international colleague), Catrin, Tina and Julia for the great collaboration and for making optimal use of all samples from my first inhalation study. Isabella, Marie-France, Emily, Iseult and Eva for your advice, the distribution and the characterization of the NPs. Mike and Selina for your advice and the synthesis of the NPs. Lan, Jana and Robert for performing and sharing the data from previous and newly performed CeO₂ inhalation studies. Tim, Jinkang, Albert, Shan and Mark for the omics analysis and for making it possible to include multi-omics approaches within my thesis. Jim, Jack and colleagues for the great collaboration, for conducting the *in vivo* study on the adjuvant activity and for the warm welcome when I visited Michigan State University during the snowy cold weather. Leigh-Ann thank you for the great times we had together and for the opportunity to share the ups and downs in our research. And also thanks to all nano colleagues from other projects, conferences and meetings who showed their interest. Although I sometimes warned you not to ask again, I do appreciate your interest in the progress of my PhD work.

Naast alle lieve collega's op het werk, waren er natuurlijk ook vele vrienden en familieleden die mij gesteund hebben. Soms door mij wat vaker te moeten missen "omdat ik weer zo nodig aan mijn boekje moest werken" en soms juist door mij daar even van weg te trekken voor de nodige ontspanning of sportieve inspanning. Voor al deze mensen en voor iedereen die ik nog niet genoemd heb, bedankt voor jullie steun, begrip en geduld.

Myra en Eldin, bedankt voor de tijd die jullie mij hebben gegeven. Volgens mij bedank ik jullie nog het meeste door hier nu straks ook echt letterlijk de laatste punt achter te zetten.

Want ja, als dit boekje eindelijk af is, heb ik inderdaad meer tijd voor jullie en zal ik me in de weekenden niet meer hele dagen terugtrekken achter mijn computer.

Mark, de belangrijkste heb ik inderdaad tot het laatste bewaard. Zonder jou (en mijn twee ogen) was dit me niet gelukt. Bedankt voor je steun, geduld, vertrouwen, opbeurde woorden en vooral ook voor de ruimte die je me gegeven hebt om dit te kunnen doen. Maar het meeste nog bedankt voor wie jij bent en dat je er ook voor mij bent.



